AUTOMATED BEHAVIOURAL TESTING AND DRUG TREATMENT IN MOUSE MODELS OF HUNTINGTON'S DISEASE

by

Cameron L. Woodard

B.A.&Sc., McGill University, 2012

A THESIS SUBMITTED IN PARTIAL FULFILLMENT OF

THE REQUIREMENTS FOR THE DEGREE OF

DOCTOR OF PHILOSOPHY

in

THE FACULTY OF GRADUATE AND POSTDOCTORAL STUDIES

(Neuroscience)

THE UNIVERSITY OF BRITISH COLUMBIA

(Vancouver)

December 2020

The following individuals certify that they have read, and recommend to the Faculty of Graduate and Postdoctoral Studies for acceptance, the dissertation entitled:

Automated behavioural testing and drug treatment in mouse models of Huntington's disease

submitted by Cameron L. Woodard in partial fulfillment of the requirements for

the degree of Doctor of Philosophy

in Neuroscience

Examining Committee:

Dr. Lynn Raymond, Psychiatry, University of British Columbia
Supervisor

Dr. Cheryl Wellington, Pathology and Laboratory Medicine, University of British Columbia
Supervisory Committee Member

Dr. Catharine Winstanley, Psychology, University of British Columbia
University Examiner

Dr. Mark Carpenter, Kinesiology, University of British Columbia
University Examiner

Additional Supervisory Committee Members:

Dr. Timothy Murphy, Psychiatry
Supervisory Committee Member

Dr. Anthony Phillips, Psychiatry
Supervisory Committee Member

Abstract

Rodent genetic models are a critical tool for understanding the pathogenesis of neurological disorders, and for evaluating the efficacy and safety of novel therapeutics. Unfortunately, behavioural studies of rodents can be vulnerable to false positives or negatives, as many behaviours have substantial inter-animal variability and are sensitive to environmental stressors (which in turn vary between facilities and experimenters). Developing tools to decrease the impact of these stressors and increase the throughput of pre-clinical research is an important area of focus to help deal with this problem. To this end, my thesis project is focused on the development and testing of two automated, self-directed behavioural testing systems that are accessible to mice from their home-cage and can be accessed at will, 24 hours per day. Animals are individually identified through radio-frequency identification (RFID) tagging, allowing for mice to be group-housed and tested alongside their littermates. This design eliminates the need for the animal to be exposed to novel environments, and minimizes experimenter interaction, significantly reducing two of the largest stressors associated with animal behaviour. These two systems can be used, respectively, to assess motor phenotypes via a forelimb lever-positioning task (PiPaw), and to treat animals with drug through their drinking water (PiDose). I applied these home-cage tools to two mouse models of Huntington's disease (HD), a genetic neurodegenerative disorder that causes debilitating motor dysfunction, in addition to cognitive and psychiatric symptoms. Using the PiPaw system, I found that young HD mice had impairments on a task that required them to hold a lever within a rewarded position range, but not when they had to make a short-duration pull to a defined target. Deficits in older HD mice were dependent on the specific genetic model, with the transgenic YAC128 model showing little to no impairment on the task but knock-in Q175-FDN mice showing substantial motor deficits.

We also observed altered patterns of task engagement and changes in the circadian activity patterns of both HD mouse models. These two home-cage systems are open-source, low-cost and built with easily obtainable parts, and should prove useful for experimenters performing basic and translational rodent research.

Lay Summary

In this thesis, I developed two automated systems for assessing the behaviour of mice within their home-cage, allowing these animals to be tested in a high-throughput and low-stress manner. The first of these (PiPaw) assesses motor skills, while the second (PiDose) administers precise dosages of drugs to mice through their drinking water. I used these systems to investigate the behaviour of mice that carry the genetic mutation that causes Huntington's disease (HD), a disorder that results in loss of motor control and affects approximately 1 in 10,000 Canadians. I found that these HD mice had distinct motor abnormalities at early and late stages in addition to altered patterns of task performance. This research contributes to the further development and automation of behavioural testing methods, increasing our ability to translate findings from basic research to the clinic.

Preface

All experiments in this thesis were carried out in accordance with the Canadian Council on Animal Care and approved by the University of British Columbia Committee on Animal Care (certificate numbers A15-0069 and A19-0076).

A version of Chapter 2 has been published: Woodard, C. L., Bolaños, F., Boyd, J. D., Silasi, G., Murphy, T. H., & Raymond, L. A. (2017). An automated home-cage system to assess learning and performance of a skilled motor task in a mouse model of Huntington's disease. *eNeuro, 4*(5). I designed the experiments with help from Lynn Raymond and Tim Murphy. The hardware and software of the original home-cage task (used in all experiments in this chapter) was developed by Federico Bolaños, Jamie Boyd and Greg Silasi. Jamie Boyd created software to extract and visualize data. The 3D-renderings in Figure 2.1 were created by Luis Bolaños and are used with permission. I performed all experiments, analyzed the data and wrote the manuscript. Lynn Raymond and Tim Murphy provided revisions to the manuscript.

The work in Chapter 3 has not been published. I designed the experiments with help from Lynn Raymond, Tim Murphy and Marja Sepers. I modified the hardware and software of the original home-cage task to create the PiPaw system; however, the software incorporates some code originally written by Federico Bolaños. The 3D-renderings in Figure 3.1 were created by Luis Bolaños and are used with permission. The lever position graphs in Figure 3.4a-b were created using software written by Jamie Boyd. The whole-cell patch clamp experiments in Figure 3.11 and 3.12 were performed and analyzed by Marja Sepers. I performed and analyzed data for all other experiments, including the field electrophysiology experiments in Figure 3.13.

A version of Chapter 4 has been published: Woodard, C. L., Nasrallah, W. B., Samiei, B. V., Murphy, T. H., & Raymond, L. A. (2020). PiDose: an open-source system for accurate and

automated oral drug administration to group-housed mice. *Scientific reports*, *10*(1). I designed the experiments with help from Lynn Raymond. I created the hardware and software for the PiDose system in collaboration with Bahram Samiei. Wissam Nasrallah and Lucas Murphy assisted with calibration experiments and monitoring the animals. The 3D-renderings in Figure 4.1 were created by Luis Bolaños and are used with permission. I performed all experiments, analyzed the data and wrote the manuscript. Lynn Raymond and Tim Murphy provided revisions to the manuscript.

Table of Contents

List of Tables

List of Figures

List of Abbreviations

A	ampere
ACC	anterior cingulate cortex
aCSF	artificial cerebrospinal fluid
AMPA	α-amino-3-hydroxy-5-methyl-4-isoxazolepropionic
AMPAR	AMPA receptor
ANOVA	analysis of variance
A2AR	A2A-type adenosine receptor
BAC	bacterial artificial chromosome
BACHD	a full-length transgenic mouse model of HD
BDNF	brain-derived neurotrophic factor
CAA	cytosine-adenine-adenine
CAG	cytosine-adenine-guanine
CAG140	a knock-in mouse model of HD
CB1	type-1 cannabinoid receptor
C57BL/6	a mouse genetic background
DA	dopamine
DARPP-32	dopamine- and cAMP-regulated neuronal phosphoprotein
deg	degrees
DLS	dorsolateral striatum
dMSN	direct pathway medium spiny neuron
DNA	deoxyribonucleic acid
D1R	D1-type dopamine receptor

D2R	D2-type dopamine receptor
EPSC	excitatory post-synaptic current
ER	endoplasmic reticulum
fEPSP	field excitatory postsynaptic potential
FST	forced swim test
FVB/N	an albino inbred mouse strain
g	gram
GABA	gamma-aminobutyric acid
GPe	external segment of the globus pallidus
GPi	internal segment of the globus pallidus
HD	Huntington’s disease
Hz	hertz (1/s)
HAP1	huntingtin-associated protein 1
HdhQ111	a knock-in mouse model of HD
HdHQ150	a knock-in mouse model of HD
HFS	high-frequency stimulation
HSP70	70-kilodalton heat shock protein
HTT	huntingtin (human)
Htt	huntingtin (mouse)
iMSN	indirect pathway medium spiny neuron
kb	kilobase
L	litre
LH	left hemisphere

LTD	long-term depression
LTP	long-term potentiation
m	meter
M	molar
mHTT	mutant huntingtin (human)
mHtt	mutant huntingtin (mouse)
mRNA	messenger ribonucleic acid
min	minute
MRI	magnetic resonance imaging
MSN	medium spiny neuron
MWM	Morris water maze
M1	primary motor cortex
NMDA	N-methyl-D-aspartate
NMDAR	NMDA receptor
ns	not significant
N171-82Q	an N-terminal fragment transgenic mouse model of HD
PCR	polymerase chain reaction
PGC-1α	peroxisome proliferator-activated receptor gamma coactivator 1-alpha
PPR	paired-pulse ratio
PRS	polygenic risk score
PVC	polyvinyl chloride
PWM	pulse-width modulation
Q175-FDN	a knock-in mouse model of HD

REST	repressor element-1 transcription factor
RFID	radio-frequency identification
RH	right hemisphere
RPM	revolutions per minute
R6/1	an N-terminal fragment transgenic mouse model of HD
R6/2	an N-terminal fragment transgenic mouse model of HD
s	second
sEPSC	spontaneous excitatory post-synaptic current
SHIRPA	battery of behavioural tests used for neurological assessment in mice
SMA	supplemental motor area
SNc	substantia nigra pars compacta
SNr	substantia nigra pars reticulata
SSH	secure shell
STN	subthalamic nucleus
TrkB	tropomyosin receptor kinase B
UHDRS	unified Huntington's disease rating scale
UPS	ubiquitin-proteasome system
WT	wildtype
YAC	yeast artificial chromosome
YAC128	a full-length transgenic mouse model of HD
zQ175	a knock-in mouse model of HD

Acknowledgements

The work in this dissertation would not have been possible without the help and support of many people, including friends, family, labmates and mentors. I would first like to give my deepest thanks to my wonderful supervisor Dr. Lynn Raymond, who has been a constant source of encouragement and guidance and has always given me the freedom to pursue my own research ideas, even if they didn't always work out. I could not have asked for a better or more supportive mentor. I also owe a large debt of gratitude to Dr. Tim Murphy for creating the original home-cage lever task and for providing an invaluable source of feedback throughout the project. In addition, I would like to thank the former and current members of my advisory committee, Dr. Tony Phillips, Dr. Cheryl Wellington and Dr. Austen Milnerwood, for their scientific input and advice throughout the past six years.

This project also would not have been possible without financial support from the Canadian Institutes of Health Research, both in the form of project grants to the lab and a personal CGS-D award. Thank you also to the University of British Columbia for supporting my research through a Four-Year Fellowship.

Many thanks go to my colleagues in the Raymond lab, including Marja, Wissam, Ellen, Daniel, James, Lily, Rujun, Sakthi, Caodu, Matt, Karolina and Leon, for their help and scientific input. In particular, I would like to thank Marja Sepers for her critical contributions to the PiPaw project and Lily Zhang for animal support and genotyping. Thanks also to Daniel Ramandi, Wissam Nasrallah and Rujun Kang for their contributions to the PiPaw and PiDose projects. I would also like to thank my two undergraduate summer students, Bahram Samiei and Lucas Murphy, who were critical in the development and testing of the PiDose system.

The success of this project is also due to contributions from various members of the Murphy lab. Thank you in particular to Federico Bolaños, who designed the hardware and software of the original home-cage lever task and who taught me a lot of the electronic and surgical skills I needed for this project. Thank you also to Jamie Boyd for frequent help with analysis and electronics, Greg Silasi for advice, and Luis Bolaños for creating several sets of excellent 3D-renderings of the home-cage systems. I would also like to thank Julian, Peter and all of the animal staff at the ARU for their help with animal husbandry.

Special thanks go to my fellow neuroscience grad students at UBC, especially Troy, Ally, Lily, Sarah, Stefano and Melissa, who have become great friends over the past six years and have always provided moral support and scientific advice. Thanks also to Harrison, Bryce, Chris, Vickar, Andrew and Kyle for their friendship and encouragement. Last, but certainly not least, thank you to my parents, Freda, Bob and David, and brother Luke for their continuous love and support. And thank you especially to Maya for being my biggest supporter and best friend.

Dedication

To my parents.

Chapter 1: Introduction

1.1 Huntington's disease (HD)

Huntington's disease (HD) is a hereditary neurodegenerative disorder characterized by motor dysfunction, cognitive impairment and neuropsychiatric symptoms (Bates et al., 2015). This 'triad' of symptoms most often emerges in middle-age and progressively worsens over the course of ~20 years, eventually resulting in severe disability and death (F. O. Walker, 2007). Several brain regions, most notably the striatum and the cortex, show striking neuronal loss over the course of the disease, with affected individuals losing up to 30% of their brain mass by the time they reach late-stage disease (Waldvogel et al., 2012). Although HD has a low prevalence in comparison to some related disorders (e.g. Parkinson's disease), it is the most common genetic neurodegenerative disorder in the world (Bates et al., 2015; Rawlins et al., 2016). In Canada, the prevalence is estimated at 13.7 per 100,000 in the general population, with approximately 4,700 individuals affected across the country (Fisher & Hayden, 2014). In addition to the mental and emotional toll of the disease, the monetary cost to families of caring for an individual with HD is substantial, with a recent study in the UK estimating this at £21,605 per year (Jones et al., 2016). Although some drugs are available to manage the motor and psychiatric symptoms of HD, no treatments have been developed that can slow or reverse the progression of the disease and it remains a terminal illness (Bates et al., 2015).

1.1.1 Genetics and etiology

HD is inherited in an autosomal dominant manner, with each offspring of an affected individual having a 50% chance of developing the disease themselves. This pattern of inheritance was noted in the first detailed description of the disease by George Huntington (Huntington,

1872), but it was not until 1983 that the disease-causing genetic mutation was mapped to human chromosome 4 (Gusella et al., 1983), and a further ten years before the gene associated with HD was identified (MacDonald et al., 1993). The *huntingtin* (*HTT*) gene is located at chromosome 4p16.3 and contains a polymorphic tract of repeated CAG codons (coding for the amino acid glutamine) in exon 1. In the healthy population, this trinucleotide tract is between 9 and 35 repeats in length, but it is expanded on one allele in individuals affected by HD. Expansions in the range of 36 to 39 repeats result in reduced penetrance of HD, with symptoms either not present or emerging very late in life (F. O. Walker, 2007). However, expansions of 40 or more repeats result in the fully penetrant disease, and longer expansions are associated with earlier age of onset and faster disease progression (Brandt et al., 1996; Brinkman et al., 1997; Langbehn et al., 2010). A juvenile form of HD, where symptom onset occurs before the age of 21, is associated with expansions of greater than 60 CAG repeats, and has unique clinical features (Nance & Myers, 2001). Although CAG-repeat length accounts for approximately 60% of the variability in the age at which symptoms first appear, additional genetic variants outside of the *HTT* gene have been identified which affect age of onset and disease progression (GeM-HD Consortium, 2015; Moss et al., 2017), and environmental factors may also play a role (Wexler, 2004).

In carriers of the expanded *HTT* gene, the CAG trinucleotide tract shows meiotic instability and is susceptible to further expansion when passed down to offspring (Wheeler et al., 2007). This instability is positively correlated with CAG-repeat length, with longer tracts being more prone to large expansions (Ranen et al., 1995). Interestingly, paternal transmission of the *HTT* allele is associated with a much higher probability of large CAG-repeat expansions, suggesting that instability occurs primarily in spermatogenesis rather than oogenesis (Ranen et

al., 1995; Wheeler et al., 2007). These inter-generational expansions result in the phenomenon of 'anticipation', whereby the onset of HD symptoms occurs earlier and earlier with each passing generation (Ranen et al., 1995). As continued expansion will eventually lead to juvenile HD patients who are unlikely to have children, it is perhaps surprising that the prevalence of HD has stayed relatively stable over time. One reason for this is the emergence of *de novo HTT* mutations, which were found to account for ~8% of diagnosed cases in one study (Almqvist et al., 2001). These *de novo* cases most likely arise from a small expansion passed down from a parent with a *HTT* allele in the 'borderline' CAG-repeat range (from 28 to 35 repeats). Indeed, the average length of the *HTT* CAG tract in healthy individuals of different ethnic backgrounds has been shown to be correlated with the prevalence of HD in that population, consistent with longer tracts experiencing a higher expansion rate and resulting in an increased number of *de novo* cases (Squitieri et al., 1994). In addition, the CAG-repeat region of the *HTT* gene can show somatic instability, with large CAG-repeat expansions observed in brain regions that show the greatest susceptibility to degeneration in HD, such as the striatum and cortex (Kennedy et al., 2003; Shelbourne et al., 2007; Telenius et al., 1994).

The *HTT* gene encodes huntingtin (HTT), a large 348-kDa protein that is well conserved across mammals and has no sequence homology with other proteins (Saudou & Humbert, 2016). Although HTT is found ubiquitously in mammalian tissue types, it is expressed most highly in the brain and is important for the normal development of the nervous system (DiFiglia et al., 1995; Dragatsis et al., 2000; Godin et al., 2010), although it may not be critical for neuronal function in the adult brain (Wang et al., 2016). Within the neuron it is distributed broadly, and can be found in the cytoplasm, the nucleus and at synapses where it associates with vesicular membranes (DiFiglia et al., 1995; Marques Sousa & Humbert, 2013; Trottier et al., 1995). HTT

has an extensive proteomic interactome in the brain (Shirasaki et al., 2012), and is thought to play a role in cellular dynamics, metabolism, and gene transcription (Ross & Tabrizi, 2011; Saudou & Humbert, 2016). In HD, affected individuals express a mutant form of the HTT protein (mHTT) containing an abnormally long polyglutamine sequence corresponding to the CAG-repeat expansion. Numerous lines of evidence point to this mHTT protein as conferring a toxic gain-of-function in HD patients, rather than the disease being due to haploinsufficiency of the WT protein (Ross & Tabrizi, 2011). Indeed, mHTT can perform some important roles of the normal protein, as *Htt* knockout mice are embryonic lethal while homozygous carriers of the HD mutation develop normally (Nasir et al., 1995; F. O. Walker, 2007). On the other hand, animals expressing only one copy of the *Htt* gene have some neuropathological and behavioural deficits in common with those observed in HD, suggesting that loss-of-function of the normal huntingtin protein may also play a role in disease pathogenesis (Nasir et al., 1995).

1.1.2 Clinical presentation and symptomatology

HD is characterized by a broad spectrum of symptoms including motor dysfunction, cognitive impairment, neuropsychiatric symptoms and behavioural difficulties. Despite having a single gene etiology, the extent to which an individual manifests these symptoms can show a high degree of variability (Waldvogel et al., 2012). Indeed, even identical twins can show substantial differences in the clinical expression of HD (Anca et al., 2004) and unlike age of onset, distinct symptom phenotypes are not correlated with CAG-repeat length (Waldvogel et al., 2012). HD is diagnosed based on familial history and the presence of characteristic motor symptoms as defined by the Unified HD Rating Scale (UHDRS) (Huntington Study Group, 1996; McColgan & Tabrizi, 2018). The advent of genetic testing for the HD mutation, however,

has allowed for the study of the disease at the 'pre-symptomatic' stage before the criteria for clinical diagnosis are met. These studies have revealed that carriers of the HD mutation can show a variety of more subtle motor, cognitive and psychiatric symptoms up to 15 years prior to the expected age of diagnosis (based on CAG-repeat length) (Paulsen et al., 2008; Stout et al., 2011). These symptoms typically show a curvilinear progression over the pre-symptomatic period, with slow symptomatic progression distant from disease onset and a more rapid progression in the years prior to diagnosis (Paulsen et al., 2008; Snowden et al., 2002). As a consequence, HD mutation carriers can suffer from significant functional declines and decreased quality of life many years before being formally diagnosed with the disease (Beglinger et al., 2010).

1.1.2.1 Motor symptoms

The most characteristic motor symptom of HD at diagnosis is chorea – an ongoing pattern of abrupt and non-stereotyped involuntary movements. This initial hyperkinetic phase often progresses into a more hypokinetic disorder, where chorea decreases and motor symptoms are dominated by slowing of voluntary movement (bradykinesia), rigidity and difficulties with balance and gait (Bates et al., 2015; McColgan & Tabrizi, 2018). Although chorea is the symptom most associated with HD, it is not seen in all patients and hypokinetic symptoms show a stronger correlation with disease duration and CAG-repeat length (Rosenblatt et al., 2006). Indeed, in patients with juvenile HD, chorea is comparatively rare, with dystonia, rigidity and gait disturbances instead being the most common motor symptoms (Fusilli et al., 2018; Nance & Myers, 2001). Another characteristic clinical feature of HD is motor impersistence – the inability to maintain a voluntary muscle contraction at a constant force. This symptom, sometimes called 'milkmaid's grip', can be measured through tests of grip force variability and shows steady

longitudinal change with disease progression making it a good marker of the severity of motor symptoms (Reilmann et al., 2001; Tabrizi et al., 2013).

In addition to these characteristic motor symptoms, individuals affected by HD have a variety of more subtle deficits in their ability to learn and control voluntary movements. Pre-symptomatic and symptomatic HD mutation carriers have impaired learning of motor sequence tasks (Feigin et al., 2006; Willingham & Koroshetz, 1993), and deficits are also seen in the precision and speed of finger movements up to 15 years prior to estimated disease diagnosis (Paulsen et al., 2008; Stout et al., 2011). In one large longitudinal study, speeded finger tapping was the only clinical measure to show reliable change over time in pre-symptomatic HD mutation-carriers far from diagnosis, suggesting that this may be a sensitive measure for disease progression (Tabrizi et al., 2013). Studies in HD patients have also found that voluntary arm movements, either in a naturalistic context (e.g. reaching for food) or in a laboratory task (e.g. manipulating a joystick towards a visual target), display jerkiness, impaired error correction and abnormal temporal sequencing of movements (Bonfiglioli et al., 1998; Klein et al., 2011; Shabbott et al., 2013; Smith et al., 2000). For example, one study looking at reaching movements found that the timing of accelerative and decelerative phases of the movement was altered in HD patients, and was not scaled proportionally when performing movements of different speeds (Bonfiglioli et al., 1998). In a study in which participants were required to make fast reaching movements towards a visual target, HD patients were unable to reduce the error of their movements over time to the same degree as control subjects (Shabbott et al., 2013). Another study by Smith et al. (2000) found that errors in the early part of a reaching movement were poorly compensated for in both HD patients and pre-symptomatic mutation-carriers, and the ability to correct for an externally generated force was limited. This could indicate that HD

causes deficits in adapting movements in response to real-time sensory feedback, a theory supported by other studies (Fellows et al., 1997; Smith & Shadmehr, 2005). As difficulties with learning and executing movements appear before the onset of overt motor dysfunction, they may serve as good markers of early HD progression and useful endpoints for clinical trials.

1.1.2.2 Cognitive, psychiatric and other symptoms

Cognitive dysfunction is seen in almost all cases of HD, and typically affects executive functions such as attention, planning, cognitive flexibility and working memory (A. K. Ho et al., 2003; Tabrizi et al., 2013). These impairments often appear prior to clinical diagnosis (Lawrence et al., 1998; Snowden et al., 2002; Stout et al., 2011) and progress over the course of the illness, leading to intellectual decline, memory loss and speech difficulties (Kirkwood et al., 2001). The extent of cognitive deficits in HD has been found to correlate with CAG-repeat length (Podvin et al., 2019), and was also recently shown to be inversely correlated with a polygenic risk score (PRS) for intelligence (Ellis et al., 2020). Neuropsychiatric symptoms also emerge early on and are pervasive in HD, with apathy, dysphoria, irritability and anxiety being among the most common (McColgan & Tabrizi, 2018; Paulsen et al., 2001). Moderate to severe depression is seen in ~13% of HD mutation carriers, and a similar proportion show obsessive behaviour, while psychotic symptoms are seen in ~1% of patients (Van Duijn et al., 2014). Although the severity of psychiatric symptoms was previously thought to remain stable in HD mutation carriers (Tabrizi et al., 2013), a recent large-scale study found that the majority of psychiatric measures show longitudinal increases in severity over the course of the pre-symptomatic period (Epping et al., 2016). Sleep disruptions are another commonly reported symptom of HD, and have been

suggested to exacerbate neurological deficits and influence disease progression (Maywood et al., 2010; Morton, 2013).

1.1.3 Human neuropathology

The symptoms of HD are thought to result largely from a distinct and specific pattern of neuronal dysfunction and degeneration, most prominently affecting the striatum. Comprised of the caudate nucleus and the putamen, the striatum is a key structure of the basal ganglia, a set of subcortical nuclei that are involved in motor function, action selection and reinforcement learning (Graybiel & Grafton, 2015; Klaus et al., 2019). The striatum is primarily made up of medium spiny neurons (MSNs) - a class of inhibitory GABAergic projection neurons named for the large number of spines on their dendrites. These cells make up 90-95% of striatal neurons, with the remainder comprised of several subtypes of GABAergic and cholinergic interneurons (Gittis & Kreitzer, 2012). Striatal MSNs receive glutamatergic projections from a wide range of cortical areas (Hintiryan et al., 2016) and the thalamus, as well as dopaminergic inputs from the substantia nigra pars compacta (SNc). The striatum can be broadly separated into two interdigitating compartments, the striosomes and matrix, which stain for distinct neurochemical markers and have substantially different gene expression profiles (Crittenden & Graybiel, 2011; Graybiel & Ragsdale Jr., 1978). While the matrix receives input preferentially from sensorimotor and associative cortical regions, striosomes receive connections predominantly from limbic cortical regions (e.g. orbitofrontal cortex) (Crittenden & Graybiel, 2011).

Striatal MSNs can be subdivided into two main subtypes based on their physiology, axonal projections and their expression of dopamine (DA) receptors. The direct pathway is so named because it projects directly to the internal segment of the globus pallidus (GPi) and the

substantia nigra pars reticulata (SNr), the main output structures of the basal ganglia. These direct pathway MSNs (dMSNs) express the peptides Substance P and dynorphin as well as D1-type DA receptors (D1Rs) and their activity is positively modulated by DA release. MSNs in the indirect pathway (iMSNs) form a multi-synaptic, indirect connection to basal ganglia output structures via the external segment of the globus pallidus (GPe) and the subthalamic nucleus (STN). iMSNs express enkephalin and D2-type DA receptors (D2Rs) and their activity is inhibited by DA (Eidelberg & Surmeier, 2011). The canonical view of the function of these two pathways is that they serve opposing roles in the execution of movements, with direct pathway MSNs promoting movement and the indirect pathway MSNs inhibiting it (Calabresi et al., 2014). Indeed, large-scale activation of D1-MSNs in mice is seen to increase movement, while activation of D2-MSNs reduces it (Kravitz et al., 2010). However, recent studies have found that movement initiation and execution are associated with the simultaneous activity of direct and indirect pathway neurons, prompting reconsideration of this view (G. Cui et al., 2014; Markowitz et al., 2018; Tecuapetla et al., 2016). One possible explanation for this is a 'support/suppress' model, where direct and indirect pathways act in concert to simultaneously promote performance of the desired movement, while also suppressing competing actions (Klaus et al., 2019), but other models have also been proposed.

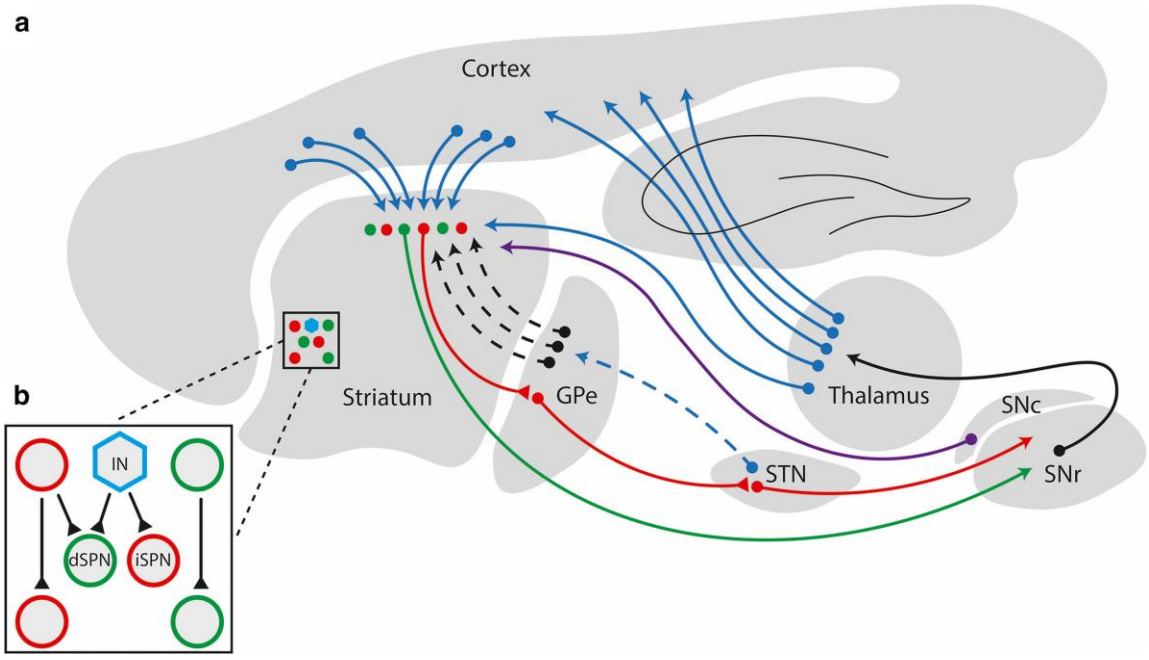

Figure 1.1 Input and output pathways of the mouse basal ganglia

(a) The striatum receives glutamatergic inputs (blue lines) from the cortex and thalamus, as well as dopaminergic input from the SNc (purple lines). Direct pathway MSNs (green lines) project directly to the SNr, whereas indirect pathway MSNs (red lines) form a multi-synaptic connection to the SNr via the GPe and STN. The SNr provides GABAergic input back to the thalamus (black lines). **(b)** Direct and indirect pathway SPNs form collateral connections and receive GABAergic input from striatal interneurons (IN). Reprinted with permission from: Peak, J., Hart, G., & Balleine, B. W. (2019). From learning to action: the integration of dorsal striatal input and output pathways in instrumental conditioning. European Journal of Neuroscience, 49(5), 658-671. © 2018 Federation of European Neuroscience Societies and John Wiley & Sons Ltd.

In HD patients, the Vonsattel grading system is used to classify the extent of striatal degeneration into five grades (0-4), and up to 95% of striatal MSNs can be lost in severe cases (grade 4) (Vonsattel et al., 1985). Striatal atrophy begins, on average, 9-11 years prior to disease onset (Aylward et al., 2004) and is the strongest predictor of symptom progression in pre-symptomatic patients (Paulsen et al., 2008). In the early stages of HD, iMSNs show substantially

more degeneration than dMSNs, resulting in an imbalance in direct vs. indirect pathway activation (Albin et al., 1992; Reiner et al., 1988). This imbalance is theorized to contribute to the chorea seen in HD, as the indirect pathway may become limited in its ability to suppress unwanted movements. In support of this, HD-associated chorea can be treated with the drug tetrabenazine which decreases striatal DA levels, thereby increasing the activity of iMSNs and inhibiting dMSNs (Eidelberg & Surmeier, 2011). In later stages of the disease, direct and indirect pathway MSNs are affected equally (Reiner et al., 1988), potentially explaining the shift in symptoms away from chorea and towards akinesia and rigidity. Interestingly, most subtypes of striatal interneurons are spared from degeneration in HD, with the exception of GABAergic interneurons expressing parvalbumin, which show substantial cell loss (Reiner & Deng, 2018). This gradual loss of parvalbumin-containing interneurons could be related to the onset of dystonia, as loss of these neurons has been seen to cause dystonia in animal models (Reiner et al., 2013).

Although not as extensive as the degeneration seen in the striatum, several other brain regions show substantial neuropathological changes in HD. This includes other basal ganglia nuclei, such as the STN, substantia nigra and globus pallidus, as well as the cerebral cortex and thalamus (de la Monte et al., 1988; Eidelberg & Surmeier, 2011). Next to the striatum, the cortex is earliest and most severely affected and decreases in cortical thickness of >30% can be found in some regions (Rosas et al., 2002, 2008). Cortical thinning can be seen in HD mutation carriers prior to diagnosis, and is correlated with performance on cognitive tests (Rosas et al., 2005; Tabrizi et al., 2013). In symptomatic HD patients, this degeneration occurs in several layers of the cortex including layers V and VI (Hedreen et al., 1991), and tends to affect sensorimotor regions most strongly (Rosas et al., 2002). A recent MRI study examined cortical degeneration in

HD patients longitudinally over the course of 10 years around the time of clinical onset and found substantial regional variation in the temporal pattern of progressive atrophy (Johnson et al., 2019). While fronto-occipital areas underwent a relatively steady rate of atrophy, sensory-motor cortex had a noticeable acceleration of degeneration in the years following HD diagnosis. As the cerebral cortex is extensively interconnected with the striatum, this degeneration could be directly influenced by the loss of striatal neurons, as caudate-putamen atrophy is correlated with cortical grey matter loss (Halliday et al., 1998). White matter connecting cortical and striatal areas also shows early and progressive microstructural changes, and this degeneration is associated with impaired cognitive and motor performance (Poudel et al., 2014, 2015). However, it remains unclear whether striatal degeneration directly causes cortical grey and white matter loss, if cortical changes contribute to striatal loss, or if these processes are simply correlated due to a common disease process.

In individuals with HD, there is substantial spatial and temporal heterogeneity in the pattern of neuropathology, and findings from a number of studies suggest that this variation may explain some of the heterogeneity observed in clinical symptoms. In the striatum, the extent of degeneration in striosome vs. matrix compartments can vary significantly between patients. Cases with profound degeneration in the striosomes are seen to have a much higher prevalence of mood symptoms, including anxiety and depression, as compared to those with a lower degree of striosomal cell loss (Tippett et al., 2007). This finding is consistent with the postulated role of limbic projections to the striosomes as being important for the modulation of mood and affect (Waldvogel et al., 2012). In the cortex, post-mortem HD brains have been found to have high variability in the level of neuronal loss in the primary motor cortex (0-51% loss) and the anterior cingulate cortex (ACC) (0-65% loss) (Thu et al., 2010). Cases with cell loss preferentially in the

ACC had increased mood symptoms, while cell loss in the primary motor cortex was associated with higher levels of motor dysfunction. Another study found that subjects with predominantly hypokinetic symptoms (e.g. bradykinesia, dystonia) had a higher degree of cortical thinning (measured by MRI) in pre-motor and supplementary motor areas (SMA) as compared to those with chorea, despite striatal volume being similar (Rosas et al., 2008). In a recent longitudinal MRI study, atrophy of the SMA and frontal gyrus was predictive of worsening motor deficits in HD patients (Johnson et al., 2019). This observed pathological heterogeneity is important to consider in the context of treatment, and also provides insights into the role of these regions in healthy brains.

On a cellular level, the hallmark pathological characteristic of HD is the presence of large protein aggregates in the nuclei of neurons, as well as in the cytoplasm and neuropil. These intranuclear and extranuclear inclusions are enriched with mHTT and N-terminal cleavage products of mHTT containing the expanded polyglutamine chain (DiFiglia et al., 1997). Inclusions can be seen decades before the expected age of onset, even in the absence of any cell loss (Gomez-Tortosa et al., 2001) and the number of these inclusions increases with increasing CAG repeat length (Bates et al., 2015). Interestingly, the striatum displays comparatively few of these aggregates as compared to the cortex, and so it is not clear that they are toxic to cells or directly lead to degeneration (Gutekunst et al., 1999). Indeed, research in a mouse model of HD has found that inclusions do not cause degeneration (Slow et al., 2005) and it has been suggested that they might actually protect the cell by aggregating soluble intermediate oligomers of mHTT, which have higher neurotoxicity (Ross & Tabrizi, 2011). HD is also associated with changes in the expression and distribution of several neurotransmitter receptors, including cannabinoid, dopamine, adenosine and GABA receptors (Glass et al., 2000). These changes are present prior

to the start of degeneration, but it's unclear whether they are pathological or represent compensatory responses to alterations in the basal activity and connectivity of neurons. Regardless, changes in the expression of certain receptor types that are important for the induction of synaptic plasticity, such as the type-1 cannabinoid receptor (CB1), are likely to affect learning and behaviour and contribute to symptom onset (Pacher et al., 2006).

1.1.4 Animal models of HD

Animal models are a critical tool for researchers attempting to understand and develop treatments for neurological disorders. In order to determine how closely an animal model approximates the human disease, it's useful to assess its validity in three broad categories. Construct validity describes how closely the pathogenic cause of the disease is replicated in the animal model (e.g. is a disease-causing genetic mutation expressed in the context of the human gene and under control of the gene's promoter). Face validity pertains to how closely the animal model replicates the phenotype of the human disease, both on a behavioural and pathophysiological level. Finally, the predictive validity of a model describes how well a successful therapeutic intervention in the model predicts therapeutic improvement in humans. In HD, an impressive variety of animal models have been generated in organisms varying from insects, to rodents, to non-human primates and other large animals (Pouladi et al., 2013; Rangel-Barajas & Rebec, 2018). As the majority of basic research in HD uses one or more of these, it's important to consider the characteristics of these animal models with these concepts of validity in mind.

Prior to the discovery of the *HTT* gene, HD was modelled by administering neurotoxins such as 3-nitroproprionic acid (systemic injection) (Borlongan et al., 1995) and quinolinic acid

(intra-striatal injection) (Beal et al., 1986) to rodents and non-human primates. These neurotoxins produce lesions that are histologically similar to what is seen in HD and cause motor dysfunction; however, these models lack construct validity, as the lesion is produced acutely and the pathogenic mechanisms that lead to degeneration in HD are not replicated. The first genetic models of HD were generated in mice within several years of the disease-causing mutation being discovered. Mice are useful animals for modelling human disease due to the ease of performing genetic manipulations and the practicality and low cost of maintaining large colonies. However, a clear limitation of mice with regards to modelling a progressive illness such as HD is their short lifespan – only around 2 years on average as compared to 70-80 years in humans. As a result, it has been necessary to express very long CAG-repeat expansions in mice (often >100 repeats) in order to see effects of the disease within the animal's lifetime. This CAG tract length is larger than what is typically seen even in juvenile cases and is an important caveat when considering the validity of these models. In addition, mouse models of HD do not show degeneration and atrophy to the extent that is observed in patients, and so the majority of models are more representative of an earlier disease stage rather than fully symptomatic HD. Mouse models of HD fall into three broad categories based on whether they express the full-length mutated *HTT* or a fragment of the gene, and whether the mutation is expressed transgenically or via knock-in into the endogenous murine *Htt* gene. A summary of some of the most popular models can be found in Table 1, with a more detailed description below.

Table 1.1 Characteristics of commonly used genetic mouse models of HD

	Trinucleotide repeat	Striatal volume reduction	Striatal intranuclear inclusions	Impaired motor coordination (rotarod test)	Earliest cognitive/psychiatric phenotype	Average lifespan
R6/1 (N-terminal transgenic)	~115 (pure CAG)	6.5 months (Harrison et al., 2013)	2 months (Hansson et al., 2001)	2 months (Hansson et al., 2001)	2 months (Water T-maze) (Harrison et al., 2013)	7 months (Mangiarini et al., 1996)
R6/2 (N-terminal transgenic)	~150 (pure CAG)	6 weeks (Samadi et al., 2013)	4.5 weeks (Davies et al., 1997)	5 weeks (Carter et al., 1999)	4 weeks (Morris water maze) (Lione et al., 1999)	3 months (Mangiarini et al., 1996)
YAC128 (Full-length transgenic)	125 (mixed CAG-CAA)	9 months (Slow et al., 2003)	12 months (Pouladi et al., 2012)	4 months (Pouladi et al., 2012)	3 months (Forced swim test) (Pouladi et al., 2009)	Normal
BACHD (Full-length transgenic)	97 (mixed CAG-CAA)	12 months (Gray et al., 2008)	Absent	2 months (Gray et al., 2008)	2 months (Forced swim test) (Hult Lundh et al., 2013)	Normal
Q175-FDN (Knock-in)	~200 (pure CAG)	6 months (Southwell et al., 2016)	6 months (Southwell et al., 2016)	8 months (Southwell et al., 2016)	6 months (Forced swim test) (Southwell et al., 2016)	13 months (Southwell et al., 2016)

1.1.4.1 N-terminal transgenic mouse models

The first mouse models of HD to be developed, and still among the most popular, are the R6/1 and R6/2 mice which express a truncated N-terminal fragment of the human *HTT* gene containing exon 1 (where the CAG tract is located) and 1 kilobase (kb) of the *HTT* promotor (Mangiarini et al., 1996). These lines originally contained 115-150 CAG repeats; however, due to somatic instability this expansion length can show substantial variability, influencing the onset and severity of symptoms (Morton et al., 2009). Both of these models express the transgene as a single copy integrant, but the R6/2 mouse has a substantially higher expression level of the transgene as compared to R6/1. Perhaps reflecting this, the R6/2 mice also have a more accelerated phenotype with symptom onset occurring at 1-2 months-old as compared to 4-5 months-old in R6/1. The phenotype in these mice is characterized by a pronounced neurological symptoms, including tremor, jerky movements similar to chorea, limb dyskinesia (manifested as clasping when held by the tail) and epileptic seizures, and lifespan is shortened to ~3 months in R6/2 and 8-9 months in R6/1 (Mangiarini et al., 1996). Prior to the emergence of this phenotype, mice display hypoactivity and progressive impairments in balance and coordination, gait, grip strength and sensorimotor gating (Carter et al., 1999; Hansson et al., 2001; Hodges et al., 2008; Menalled et al., 2009; Pallier et al., 2009). Cognitive deficits on a variety of procedural and spatial learning and memory tasks have been reported (Cayzac et al., 2011; Ciamei & Morton, 2009; Lione et al., 1999; Mazarakis et al., 2005), as well as depression and anxiety-related behaviours (Ciamei et al., 2015; Menalled et al., 2009; Pang et al., 2009) and circadian abnormalities (in R6/2 mice) (Maywood et al., 2010; Morton et al., 2005).

Fragment models, particularly R6/2 mice, have been used extensively in translational HD research as their shortened lifespan and aggressive phenotype provide clear endpoints for testing

novel therapeutics. Importantly, these models demonstrated that expressing just exon 1 of mHTT was sufficient to cause the neuropathological and behavioural hallmarks of HD (Mangiarini et al., 1996). Although these models have good face validity, it's important to note that they may not accurately reflect the full pathological processes underlying the development of HD due to the truncated nature of the expressed protein. Interestingly, a longer fragment model expressing both exons 1 and 2 of *HTT* with 120 repeats (the 'shortstop' mouse) was found to have no behavioural phenotype, despite high mRNA expression and an abundance of nuclear inclusions (Slow et al., 2005). This suggests that the exon 1 fragment is particularly pathogenic, a finding contributing to the accelerated progression of the R6 mice. Indeed, an endogenous splice variant of *HTT* very similar to the fragment expressed in these models is seen in brains of human HD patients, and this aberrant splicing has been suggested to be an important step in the pathogenesis of HD (Neueder et al., 2017; Sathasivam et al., 2013). An additional N-terminal fragment model, the N171-82Q, also expresses a longer amino-acid segment of *HTT* with 82 repeats but presents with similar behavioural and neuropathological phenotypes to the R6 mice (Schilling et al., 1999). However, this mouse has limited construct validity as expression of the transgene is under the control of a generic neuronal promotor.

1.1.4.2 Full-length transgenic mouse models

With the goal of increasing construct validity, several mice have been generated which carry the full length human *HTT* along with large upstream and downstream promotor and regulatory regions on a yeast or bacterial artificial chromosome (YAC and BAC respectively) (Gray et al., 2008; Hodgson et al., 1999; Slow et al., 2003). In contrast to the fragment models, these mice display a gradual phenotypic progression and have normal lifespan. The YAC128

mouse is the most widely used of these mice, and expresses the human mHTT protein with 125 glutamine repeats at a level comparable (~75%) to the endogenous mouse Htt (Slow et al., 2003). The trinucleotide tract in the YAC128 mouse is composed primarily of CAG codons, but with 9 CAA codons interspersed (Pouladi et al., 2012). These CAA codons also code for glutamine and are functionally equivalent at the protein sequence level, but confer stability to the CAG-tract and prevent somatic and germ-line instability (Menalled et al., 2014). The behavioural phenotype in these mice emerges around 2- to 4-months-old, with mice displaying subtle motor learning deficits and depressive-like behaviour (Pouladi et al., 2009; Van Raamsdonk et al., 2005). By 8 months-old, YAC128 mice are hypoactive and have procedural and reversal learning deficits (Van Raamsdonk et al., 2005). The first clear neuropathology in YAC128 mice is seen at 9-months-old, well after the onset of symptoms, when striatal volume and overall brain weight are decreased (Slow et al., 2003). By 12-months-old, decreased cortical volume is observed and cell death and aggregation of mHTT are visible in the striatum of animals (Pouladi et al., 2012; Slow et al., 2003). These phenotypes are dependent on background strain, and YAC128 mice on a C57BL/6 background show a slower and less severe phenotype (Brooks et al., 2012; Van Raamsdonk et al., 2007).

The BACHD mouse expresses *HTT* with a somewhat smaller upstream and downstream regulatory region as compared to YAC128, and with a mixed CAG-CAA trinucleotide repeat expansion encoding for 97 glutamine repeats (Gray et al., 2008). Despite expressing a higher level of mHTT protein as compared to the YAC128 mouse (1.5-2x the level of endogenous Htt), the BACHD mouse displays relatively little of the hallmark neuropathology associated with HD, including aggregation of mHtt or HD-associated gene transcription changes (Pouladi et al., 2012). Similarly, striatal and cortical atrophy in this model is more variable and may be

dependent on genetic background (Gray et al., 2008; Mantovani et al., 2016; Pouladi et al., 2012). Interestingly, BACHD mice show progressive and robust deficits on a variety of motor, cognitive and mood-related tests (Abada et al., 2013; Gray et al., 2008; Menalled et al., 2009; Pouladi et al., 2012). This disconnect between neuropathology and behavioural phenotype provides support for the idea that behavioural phenotypes in transgenic models are largely driven by synaptic and circuit-level dysfunction rather than by cell loss or degeneration.

An important caveat with these two models is that due to their transgenic nature, they express both copies of the native murine *Htt* in addition to the human *mHTT,* and as such have relative overexpression of the huntingtin protein. This huntingtin overexpression may protect neurons from loss-of-function effects associated with HD, and has also been shown to cause the increased bodyweight observed in YAC128 and BACHD models via modulation of the insulin-like growth factor 1 pathway (IGF-1) (Pouladi et al., 2010). This increased bodyweight presents a confound for the assessment of some motor tasks, and reducing weight via food restriction has been found to improve performance on a test of motor coordination in BACHD (Kudwa et al., 2013) and YAC128 mice (Moreno et al., 2016). In addition, these mice are typically bred on the FVB/N background which carries a gene mutation causing retinal degeneration and blindness from ~2 months-old (Farley et al., 2011). As a result, they cannot be reliably tested on behavioural tasks that rely on visual cues, somewhat limiting their usefulness.

1.1.4.3 Knock-in mouse models

Knock-in models of HD have been generated by introducing a specified number of CAG-repeats directly into the mouse *Htt* gene. Heterozygous mice express one copy of the wildtype *Htt* gene and one copy of mutant *Htt* under control of the endogenous murine *Htt* promoter,

better replicating the genetics of HD in humans. Several different allelic series of knock-in mice have been created, varying in their CAG-repeat length from 48 to over 300; the most commonly used animals are the HdhQ111 (Wheeler et al., 1999), HdhQ150 (Lin et al., 2001), CAG140 (Menalled et al., 2003) and zQ175 models (Menalled et al., 2012). Despite having arguably the best construct validity of any of the mouse models, these animals are slowest to develop the symptoms and neuropathology of HD and have normal lifespan (with the exception of homozygous zQ175 mice). The severity of the behavioural phenotype in these models is generally correlated with CAG length, with HdhQ111 displaying mainly cognitive and mood-related deficits (Orvoen et al., 2012; Yhnell et al., 2016a) and minimal motor abnormalities even at 24-months-old (Menalled et al., 2009), while zQ175 mice display deficits in motor function from around 7-months-old (Menalled et al., 2012). Regional-specific changes in brain volume and mHtt aggregates are seen in all models, although the severity of this pathology again seems to correlate with CAG-length (Kovalenko et al., 2018; Rangel-Barajas & Rebec, 2018). In order to hasten the phenotypic progression in these mice, experimenters sometimes use homozygotes, which express two expanded *Htt* alleles; however, these animals lack wtHtt and are less similar to the genetics typically observed in HD patients.

In an effort to create a heterozygous knock-in mouse model with increased phenotypic severity, the zQ175 mouse has recently been backcrossed onto the FVB/N background which is known to have increased susceptibility to neurodegeneration (Southwell et al., 2016). This heterozygous Q175-FDN mouse has an expanded *Htt* gene on one allele with approximately 200 CAG-repeats, and mHtt protein is expressed at about 55% of the level of the endogenous wtHtt. The behavioural phenotype of these mice is relatively normal until around 6-months-old, when mild motor coordination and recognition memory deficits begin to emerge, as well as depressive-

like behaviour. By 8- to 9-months-old, motor and cognitive impairments are more obvious, including decreased grip strength and a deficit in behavioural flexibility. Q175-FDN mice show ataxia and weight loss starting at around 12-months-old and have reduced survival beyond 13-months-old. Neuropathological changes are seen around the time of symptom onset, with decreased striatal volume, decreased forebrain weight and mHtt inclusions observed at 6-months-old. As is observed in pre-symptomatic HD mutation carriers, Q175-FDN mice also have decreased expression of genes including DARPP-32 and CB1 from 3-months-old, prior to the onset of any symptoms. Altogether, these mice appear to have the best face validity of the heterozygous knock-in models generated to date, although the expression of such a long CAG-repeat is an important caveat.

1.1.5 Mechanisms of HD pathogenesis

1.1.5.1 Cell autonomous effects of mHTT

Huntington's disease is associated with a multifaceted cascade of pathogenic events spread out over decades. Although a huge body of research has focused on determining the order and progression of these events, much remains unknown about the pathogenesis of HD. At the root of the disease is the *mHTT* gene and its protein products, which includes both the full-length protein and smaller protein fragments generated at a transcriptional and a post-translational level. These small fragments of mHTT, which contain the expanded polyglutamine region, are highly toxic and are thought to contribute substantially to the pathogenesis of HD (Bates et al., 2015). The first mechanism by which these protein fragments are generated is via alternative splicing of HTT mRNA (Hughes et al., 2014; Labadorf & Myers, 2015). Aberrant splicing of the mHTT transcript can lead to the generation of a short exon-1 mRNA, the level of which is proportional

to CAG-repeat length (Sathasivam et al., 2013). The resultant exon-1 protein has been shown to be the most pathogenic of the identified protein fragments, causing cell death in *Drosophila* and mouse models (Barbaro et al., 2015; Mangiarini et al., 1996). At a post-translational level, cleavage of the mHTT protein by caspases and calpains also leads to the creation of short N-terminal protein fragments, and inhibiting this cleavage has been shown to reduce mHTT toxicity (Gafni et al., 2004; Wellington et al., 2000). In particular, caspase-6-mediated cleavage of mHTT at amino acid 586 seems to be a particularly important pathogenic event, as a YAC mouse expressing a form of mHTT resistant to cleavage at this site did not show the striatal degeneration or increased susceptibility to excitotoxic damage typically seen in HD mice (Graham et al., 2006). Post-translational modifications can also modulate the toxicity of mHTT protein products. For example, inducing phosphorylation at a specific site in the N-terminal region has been shown to eliminate motor dysfunction in a mouse model of HD, even after the onset of symptoms (Di Pardo et al., 2012).

As a direct consequence of the expression of these mHTT protein products, the proteostasis network, which is responsible for folding, transporting and degrading proteins, quickly becomes overwhelmed (Labbadia & Morimoto, 2013). Chaperone proteins, which are the main effectors of the proteostasis network, are recruited to deal with misfolded and aggregated mHTT, reducing the ability of the system to fold and process other proteins (Hipp et al., 2012; Soares et al., 2019; Yu et al., 2014). In addition, chaperone proteins such as HSP70 are downregulated in HD models (Yamanaka et al., 2008), and chaperones themselves can become sequestered into mHTT aggregates (S. H. Park et al., 2013; Yu et al., 2014), further reducing the capacity of the system. When proteins cannot be recovered from their aggregated or misfolded state, they are directed for degradation to proteasomes via the ubiquitin-proteasome system

(UPS) or to lysosomes via autophagy pathways (Labbadia & Morimoto, 2015). Huntingtin aggregates found in the brains of HD patients contain ubiquitin, the marker of proteins tagged for degradation by the UPS (DiFiglia et al., 1997). This suggests that the UPS is unable to effectively deal with the volume of proteins tagged for degradation, causing them to aggregate. Mutant HTT has also been shown to impair the initiation of autophagy and recognition of cargo in autophagosomes, and may disrupt the hypothesized role of wildtype HTT as an autophagy-promoting scaffold (Cortes & La Spada, 2014; Soares et al., 2019). Together, these chronic disruptions of the proteostasis network significantly impair the normal functioning of neurons, allowing mHTT to aggregate and mediate other toxic interactions.

The expression of mHTT and the inability of the proteostasis network to effectively deal with these proteins leads to dysfunction in a wide variety of downstream cellular processes. Some of these effects are caused by direct and inappropriate interactions of the mHTT protein itself, while others are an indirect result of protein aggregation or partial loss of function of wildtype HTT. For example, wildtype HTT regulates the transcription of brain-derived neurotrophic factor (BDNF) and other neuronal genes by sequestering the repressor element-1 transcription factor (REST) in the cytoplasm and preventing its inhibitory action (Zuccato et al., 2001, 2003). In contrast, mHTT is impaired in its ability to perform this regulatory role, resulting in accumulation of REST in the nucleus and decreased BDNF transcription (Zuccato et al., 2003). Striatal MSNs depend on BDNF secreted by cortical neurons for trophic support, and this disruption of BDNF transcription may contribute to the selective vulnerability of MSNs in HD (Plotkin & Surmeier, 2015). Another domain in which mHTT mediates cellular dysfunction is intracellular trafficking. Wild-type huntingtin plays a role in intracellular trafficking via formation of a protein complex with huntingtin-associated protein-1 (HAP1) and a subunit of the

dynactin motor complex, thereby increasing the efficiency of microtubule-based transport (Gauthier et al., 2004; X.-J. Li et al., 1995). However, when mHTT is recruited to this complex, it inhibits the binding of dynactin to microtubules, impairing intracellular transport (Gauthier et al., 2004). In addition, components of vesicular trafficking machinery can be found in mHTT-aggregates in brain tissue from HD patients, suggesting a multifaceted inhibition of intracellular trafficking pathways by mHTT (Trushina et al., 2004).

In addition to its cytoplasmic effects, mHTT is transported into the nucleus and can cause cellular dysfunction either by indirectly sequestering transcription factors into intranuclear inclusions, or by directly disrupting gene transcription. In one study, mHTT was shown to directly inhibit expression of the transcriptional co-activator PGC-1α by associating with its promotor, thereby disrupting PGC-1α's important role in regulating mitochondrial biogenesis (L. Cui et al., 2006). In addition to this transcriptional dysregulation, the function, transport and degradation of mitochondria are disrupted by mHTT through various other mechanisms, leading to metabolic dysfunction and cellular energy deficits (Chang et al., 2006; Gu et al., 1996; Guedes-Dias et al., 2016; Khalil et al., 2015). Mutant HTT has also been implicated in the dysregulation of intracellular calcium, which acts as an important second messenger in many cellular signaling pathways. For example, the function of receptors involved in controlling intracellular calcium release from the endoplasmic reticulum (ER) is disturbed in HD, leading to cellular dysfunction and engagement of cell death pathways (Raymond, 2017).

1.1.5.2 Cortico-striatal synaptic alterations

Despite a multitude of cellular processes going awry in HD, neurons are able to largely overcome these disruptions for many years before finally degenerating. However, research in

animal models has revealed significant dysfunction at a synaptic and circuit level prior to the onset of degeneration, particularly at the cortico-striatal synapse (Plotkin & Surmeier, 2015; Raymond et al., 2011). This includes both basal changes in neurotransmitter release and signaling, as well as altered activity-induced plasticity (Smith-Dijak et al., 2019). Cortico-striatal plasticity is associated with a variety of learning processes, including acquisition of motor skills, habit learning, decision making and behavioural flexibility (Graybiel & Grafton, 2015; A. M. Lee et al., 2015; Packard & Knowlton, 2002). In addition, cortico-striatal circuits play an important role in movement initiation, action selection and kinematic aspects of movement execution (Dudman & Krakauer, 2016; Klaus et al., 2019). As a result, changes in intercellular communication and the altered ability of circuits to enhance or inhibit their activity are likely to contribute to early motor and cognitive symptoms in HD mutation carriers and in mouse models of HD. Indeed, as HD mice have comparatively minimal neuronal degeneration overall, behavioural phenotypes in these mice may be primarily due to synaptic and circuit level dysfunction.

Striatal MSNs receive synaptic input primarily of three different kinds: glutamatergic projections from the cortex and thalamus, dopaminergic projections from the SNc, and GABAergic input from striatal interneurons and other MSNs. Early in HD, an increase in spontaneous glutamatergic activity has been seen in MSNs of several HD model mice (André, Cepeda, et al., 2011; André, Fisher, et al., 2011; Cepeda et al., 2003; Joshi et al., 2009). This has been attributed both to a greater number of postsynaptic AMPA receptors (Joshi et al., 2009) as well as a dMSN-specific increase in presynaptic glutamate release probability (André, Cepeda, et al., 2011; André, Fisher, et al., 2011). Interestingly, evoked glutamatergic responses are normal in dMSNs, but enhanced in iMSNs (André, Cepeda, et al., 2011), suggesting a postsynaptic

mechanism in indirect pathway neurons. Increased glutamatergic transmission is accompanied by an early and progressive increase in inhibitory GABAergic input to MSNs, which is reported to occur first in dMSNs (André, Fisher, et al., 2011; Cepeda et al., 2004). A variety of studies in both animal models and humans have also found increased levels of dopamine and dopamine release, but decreased levels of D1 and D2 receptors early in HD (Koch & Raymond, 2019). These changes likely contribute to the failure of dopamine agonists to modulate the activity of MSNs in both the direct and indirect pathway in HD mice (André, Cepeda, et al., 2011). As dopamine receptor activation is a critical modulator of dMSN and iMSN firing, this change in dopaminergic tone may directly result in observed changes in firing and spontaneous activity of these neurons.

Following the onset of symptoms, there is evidence for a progressive disconnection between the cortex and striatum in HD mice. Spontaneous and evoked glutamatergic input to MSNs is progressively decreased in mouse models of HD (Cepeda et al., 2003; Joshi et al., 2009; Kolodziejczyk & Raymond, 2016), with dMSNs more affected than iMSNs (André, Cepeda, et al., 2011). This decrease is associated with a loss of cortical and thalamic input to the striatum, as well as reductions in striatal MSN dendritic complexity and synapse density (Buren et al., 2016; Deng et al., 2013, 2014; Joshi et al., 2009). Lowered excitatory input is accompanied by an increase in inhibitory input to MSNs (Cepeda et al., 2004), although in contrast to what is seen early in HD, this increased inhibition is specific to iMSNs (André, Fisher, et al., 2011; Cepeda et al., 2013). One study found that increased GABAergic input was mediated specifically by feedforward projections from a ‘fast-spiking’ subtype of inhibitory interneuron, while collateral connections between MSNs were reduced (Cepeda et al., 2013). In contrast to what is seen early in HD, dopamine release is decreased in later-stage HD patients and aged HD models (Koch &

Raymond, 2019). Although the level of DA receptors remains low in HD mice (Ariano et al., 2002), the ability of dopaminergic drugs to modulate activity is restored in direct, but not indirect pathway MSNs (André, Cepeda, et al., 2011). This suggests that the reduced ability of dMSNs to be modulated by DA in young HD mice is primarily caused by increased dopaminergic tone, and less so by decreased receptor levels. The gradual weakening of cortico-striatal connections is also directly related to behavioural phenotypes, as a recent study found that repeated stimulation of projections from the secondary motor cortex to the DLS was able to rescue motor deficits in HD mice (Fernandez-Garcia et al., 2020).

In addition to baseline changes in the strength of glutamatergic inputs to striatal MSNs, several studies have found alterations in the ability of these synapses to change their strength in response to stimulation. In order to assess activity-dependent plasticity in MSNs, trains of stimulation at varying frequencies can be applied to mouse acute brain slices. Depending on the stimulation parameters, these protocols can result in pre- and post-synaptic forms of long-term potentiation (LTP) or long-term depression (LTD) (Cerovic et al., 2013). Long-term potentiation of MSNs induced via high-frequency (100 Hz) stimulation (HFS) of cortical inputs is dependent on NMDAR and D1R activation and BDNF signaling through the TrkB receptor, and is impaired in both R6/2 and BACHD mouse models (Kung et al., 2007; Plotkin et al., 2014). In BACHD mice, this deficit was rescued by inhibiting signaling pathways downstream of the p75 neurotrophin receptor and was linked to an attenuation of BDNF signaling through TrkB specifically in iMSNs (Plotkin et al., 2014). A postsynaptic, NMDAR-dependent LTD can be induced in MSNs by extended low-frequency (1-4 Hz) stimulation (LFS) of glutamatergic inputs. This type of LTD is unimpaired in R6/2 mice using electrical stimulation of cortical afferents (Kung et al., 2007), but was found to be enhanced in YAC128 mice using optogenetic

stimulation of motor cortex inputs, and was linked to an increase in GluN2B-containing NMDARs (Glangetas et al., 2020).

HFS protocols can also be used to induce a presynaptic form of LTD that is dependent on postsynaptic endocannabinoid synthesis and activation of presynaptic CB1 receptors (Lovinger, 2010). This form of HFS-LTD was found to be impaired from an early, pre-symptomatic stage in YAC128 and Q175-FDN mice (Sepers et al., 2018). In YAC128 mice, this impairment was seen specifically in indirect pathway MSNs, and could be normalized by increasing levels of the endocannabinoid 2-AG (Sepers et al., 2018) Although this deficit was related to endocannabinoid production rather than receptor-signalling, CB1 receptor expression is also affected in HD, with decreases found in both patients (Glass et al., 2000) and in mouse models (Chiodi et al., 2012; Dowie et al., 2009; Pouladi et al., 2012). Interestingly, downregulation of CB1 is specific to MSNs and does not affect receptor levels at cortical terminals at least in early stage disease (Chiarlone et al., 2014; Chiodi et al., 2012), and so this downregulation likely does not directly impact cortico-striatal endocannabinoid-mediated LTD. It was also found that rescuing MSN expression of CB1Rs in R6/2 mice ameliorated some cellular phenotypes of HD but was not able to reverse motor deficits (Naydenov et al., 2014), suggesting that altered CB1R expression in striatal MSNs does not trigger the onset of behavioural phenotypes.

In summary, diverse changes are observed in the presynaptic input and postsynaptic receptor distribution in HD mouse models and these synaptic phenotypes change substantially as symptoms progress. Although certain forms of stimulation-induced cortico-striatal plasticity are consistently impaired, others show no change or are pathway specific. As there have been comparatively few studies examining changes in activity-dependent plasticity in HD mice, more investigation is warranted. Although changes in plasticity have most frequently been studied at

the cortico-striatal synapse, deficits in activity-dependent plasticity have been found in other regions, including the cortex (Cummings et al., 2007) and hippocampus (Gibson et al., 2005).

1.2 Assessing behaviour in mouse models of Huntington's disease

Behavioural testing is an important step in determining the manifestation and progression of functional deficits in animal models of HD and can provide clues towards the underlying neuropathology. In addition, behavioural tests provide a functional readout of the effects of therapeutic interventions, and so are an important outcome measure for drug treatment studies. As HD is associated with a diverse set of symptoms that can present differently between patients, a wide variety of behavioural tests have been employed in rodent models. These vary from observational studies of naturalistic behaviour to standardized cognitive tasks with complex learning rules. The choice of a behavioural test is very important, as even a model with high face validity may present with a phenotype that is difficult to interpret if the wrong test is selected or the test is not optimized (Schellinck et al., 2010). Furthermore, an effective treatment may not result in the reversal of a behavioural impairment if the test lacks sensitivity or is biased by systematic error. One approach to testing animal models is to try to directly translate tasks that are used in humans (and which HD patients show deficits on) for use in mice (Haaker et al., 2019). However, the repertoire of natural behaviours is quite different in rodents and humans, and they rely heavily on different senses (primarily olfaction and whisker touch as opposed to vision) (Rosser, 2011). In addition, certain behavioural tests have been shown to have very strong predictive validity (e.g. the forced swim test for depression) and yet have minimal construct validity and are not directly comparable to assessments used in humans (Petit-Demouliere et al., 2005). To address these concerns, the benefits and disadvantages of different

behavioural methods must be carefully considered before commencing a course of research (Schellinck et al., 2010).

All commonly used rodent models of HD show changes in their behaviour from WT animals on a variety of tests, although the specific pattern of these changes and the age at which they emerge varies from model to model (Abada & Ellenbroek, 2016). As a result, it often makes sense to test mice at multiple timepoints to determine both when a phenotype emerges and how it progresses over time. Many of the behavioural deficits observed in mice progressively worsen with age, although some do not (Ciamei et al., 2015; Menalled et al., 2009; Pouladi et al., 2009; Trueman et al., 2008), similar to what is observed for certain symptoms in HD patients (A. K. Ho et al., 2003). As HD features prominent motor dysfunction, the most frequently used behavioural tests are those measuring motor coordination (e.g. rotarod) or locomotor activity (e.g. open field). However, tests of cognition (e.g. T-maze) and affective phenotypes (e.g. forced swim test) are also frequently performed. Effects of sex and time of day of testing (e.g. light vs. dark phase) have been found for some behavioural tests (Menalled et al., 2009, 2012; Orvoen et al., 2012) and are important to consider when designing experiments. Furthermore, control animals (preferably littermates) of the same background strain should be used, as different genetic strains can show substantial variability in their performance on behavioural tests (Brooks et al., 2004; McFadyen et al., 2003). In this section, I will review some of the behavioural assessments most frequently employed in HD mice, and discuss some caveats associated with their use.

1.2.1 Physiological and observational measures

At a basic level, measures of lifespan, bodyweight and general health (e.g. piloerection, body tone) can provide important information about disease progression in HD mice. Lifespan is

significantly shortened in the fragment models of HD, with R6/1 mice showing increased mortality from ~30 weeks-old (Harrison et al., 2013; Mangiarini et al., 1996) and R6/2 mice from ~10 weeks-old (Mangiarini et al., 1996; Menalled et al., 2009). However, the majority of full-length transgenic and knock-in animals show normal lifespan, with the exception of homozygous zQ175 mice (Menalled et al., 2012) and Q175-FDN mice (both heterozygous and homozygous) (Southwell et al., 2016). Bodyweight is frequently altered in mouse models of HD, and the fragment and knock-in models generally show decreased weight as compared to WT mice (Carter et al., 1999; Fowler & Muma, 2015; Harrison et al., 2013; Heikkinen et al., 2012; Rattray et al., 2017; Southwell et al., 2016), replicating the weight loss seen in HD patients. Weight loss seems to be modulated by mHtt dosage, as homozygous knock-in mice are seen to lose weight earlier than heterozygotes (Heikkinen et al., 2012; Menalled et al., 2012). In contrast, both the YAC128 and BACHD transgenic models show increased body weight as compared to WT littermates. This paradoxical finding was shown to be related to a modulation of the IGF-1 pathway caused by HTT overexpression (Pouladi et al., 2010; Van Raamsdonk, Gibson, et al., 2006). Interestingly, this HTT-mediated weight gain was dependent on strain and was not observed in a YAC128 model on the 129 genetic background (Van Raamsdonk et al., 2007).

Naturalistic observation aims to quantify the behaviour (e.g. spontaneous activity, grooming) of mice in their home-cage or a test arena without intervention from the experimenter. Although these types of assessments have not been extensively studied in mouse models of HD, abnormal whisker movements (Garland et al., 2018) and nest building (Estrada-Sanchez et al., 2015) have been reported. In addition, several studies have performed automated measurement and classification of naturalistic behaviours in the home-cage (further discussed in Chapter 1.3) (Alexandrov et al., 2016; Rudenko et al., 2009). Basic measures of motor function can be

assessed in HD mice through the use of behavioural screening batteries such as the SHIRPA which incorporate observational health measures as well as other tests of neurological symptoms (Brooks, 2011). Although the full test battery is sometimes used in HD mice (Lawhorn et al., 2008; Woodman et al., 2007), specific neurological symptoms such as tremor and feet clasping when held by the tail are more commonly assessed. Feet clasping behaviour is thought to be a manifestation of limb dyskinesia and is commonly observed in the more severe N-terminal fragment models of HD, including the R6/1 (Mangiarini et al., 1996; Naver et al., 2003), R6/2 (Mangiarini et al., 1996) and N171-82Q mice (Schilling et al., 1999; Southwell et al., 2009), but not typically in full-length transgenic or knock-in mice. Tremor has also been observed in some models (Mangiarini et al., 1996; Schilling et al., 1999) and was quantified in aged CAG140 mice with the use of a force-sensing actometer (Fowler & Muma, 2015). Despite being the most characteristic motor symptom of HD in patients, chorea (or a behaviour resembling it) is only seen in the fragment models of HD (Mangiarini et al., 1996), although whether these jerky movements are directly analogous to chorea is debateable.

1.2.2 Locomotor activity levels

Changes in locomotor activity levels have been observed in many mouse models of HD, with mice often displaying a hypoactive phenotype at older ages. This hypoactivity has been reported in fragment models (Dunnett et al., 1998; Naver et al., 2003), full-length transgenic models (Menalled et al., 2009; Slow et al., 2003) and knock-in models of HD (Fowler & Muma, 2015; Menalled et al., 2012; Rattray et al., 2017; Southwell et al., 2016). In addition, an early hyperactive stage has been reported for the YAC128 (Slow et al., 2003), HdhQ111 (Menalled et al., 2009) and CAG140 models (Menalled et al., 2003), with analogies drawn to hyperkinetic

movement symptoms in humans. However, conflicting results have been reported for several models, including YAC128 (Lawhorn et al., 2008; Menalled et al., 2009). Although factors such as time of day of testing may play a role (Menalled et al., 2009, 2012; Robinson et al., 2018), the main contributor to this inconsistency seems to be the choice of behavioural test and the specific parameters of test administration.

By far the most common method of assessing locomotor activity is the open field test, where the mouse is placed in an open arena for a set period of time and movement parameters are quantified through the use of either video recording or an infrared photocell array (Brooks & Dunnett, 2009). In addition to total distance travelled, measures such as velocity of movements, rearing and other behaviours can be extracted from open field data. An important issue, however, is that decreased exploration due to anxiety associated with novel open environments can be confounded with hypoactivity. This is a significant caveat in testing genetic models of HD, as several lines have been found to show increased (Abada et al., 2013; Orvoen et al., 2012) or decreased (File et al., 1998; Naver et al., 2003) anxiety-like behaviour on other tests. Indeed, time spent in the center of the open field is often used as a measure of anxiety in mice (see Chapter 1.2.5). Factors such as bright lighting and short testing duration can increase the influence of anxiety-like behaviours, as anxiety tends to reduce as the animal habituates to the test arena. Open field activity has been assessed for as little as 3-minutes in some studies (Mazarakis et al., 2005), and as long as 60-minutes in others (Woodman et al., 2007), likely contributing to inter-study variability.

A preferred option is to use systems that can track the activity of animals in their home environment over long periods (i.e. 24 hours or more), as these provide a measure of activity level that is less likely to be affected by acute factors such as anxiety. Within-study comparisons

of home-cage and open field movement have found conflicting results in the R6/1 (Hodges et al., 2008) and YAC128 models (Slow et al., 2003), with alterations of activity levels found to be more subtle or even non-existent with home-cage based analysis. An additional advantage of using longer-term home-cage based tracking is the ability to analyze circadian patterns of rest and activity. HD patients often suffer from sleep disorders and disruptions of circadian rhythms (Arnulf et al., 2008; Morton et al., 2005) and these symptoms have been replicated in R6/2 (Maywood et al., 2010; Morton et al., 2005) and BACHD (Oakeshott et al., 2011) mice using home-cage activity tracking. Automated measurements of wheel running in the home-cage can also be used to measure circadian activity patterns, and have revealed abnormalities in R6/2 (Kudo et al., 2011; Morton et al., 2005), BACHD (Kudo et al., 2011) and zQ175 mice (Loh et al., 2013). More generally, wheel running can be used to measure locomotor activity levels and this method has replicated the finding of hypoactivity in zQ175 (Loh et al., 2013) and R6/1 (Harrison et al., 2013) mice using the open field test. However, it's important to note that long-term exposure to a running wheel has been found to delay onset of certain motor and cognitive phenotypes and attenuate neuropathology in HD mice (Harrison et al., 2013; van Dellen et al., 2008), so caution is warranted when using this technique.

1.2.3 Motor function

1.2.3.1 Rotarod test

The rotarod is an apparatus used to measure motor coordination and balance in rodents and is likely the most widely used assessment of motor function in HD mice. This test measures the ability of mice to walk or run on top of a narrow horizontal rotating rod in order to prevent themselves from falling off (Brooks & Dunnett, 2009). Task learning and performance can be

assessed using either using a series of fixed-speed tests (the rod rotates at a constant speed through the trial), or an accelerating test (rotation speed smoothly accelerates over the course of the trial). Although using the same apparatus, these two tests measure somewhat different aspects of motor coordination and may differ in their sensitivity, as the accelerating task requires animals to continuously adapt their gait in response to the changing speed (Pallier et al., 2009; Van Raamsdonk et al., 2005). Rotarod deficits are consistently observed in fragment and full-length transgenic models, and are usually first seen around 4- to 6-months-old (Hodges et al., 2008; Menalled et al., 2009), although much earlier (5-6 weeks-old) in R6/2 mice (Carter et al., 1999). Knock-in models with long CAG expansions (e.g. zQ175, Q175-FDN) also have impaired rotarod performance at around 8- to 9- months-old (Menalled et al., 2012; Southwell et al., 2016), but deficits are inconsistently seen in other knock-in models and generally only past one-year of age (Menalled et al., 2009; Rattray et al., 2017; Rising et al., 2011). Paradoxically, HdhQ150 and HdhQ111 were both seen to have improved rotarod performance as compared to WT mice at certain timepoints, although these improvements were not consistent (Menalled et al., 2009; Rattray et al., 2017). Although some models display a progressive impairment of rotarod performance, other show a more stable deficit that does not worsen over time (Menalled et al., 2009).

The rotarod test is easy to perform and sensitive to a variety of neurological insults, however there are some important confounds to consider. Increased bodyweight, as is seen in both YAC128 and BACHD models of HD, is known to impair performance on the rotarod (McFadyen et al., 2003). Interestingly, restoring normal body weight with dietary restriction resulted in either partial or full rescue of rotarod performance deficits in full-length transgenic animals (Kudwa et al., 2013; Moreno et al., 2016). However, dietary restriction also results in

diverse transcriptional and epigenetic changes that are likely mediating this rescue (Moreno et al., 2016), rather than normalization of bodyweight alone. A second confound concerns the motivation of mice to comply with task requirements and remain on the rod as it spins. If a mouse does not find the punishment of falling to be particularly aversive, they may willingly fall off. Indeed, some mice seem to learn that there is a beneficial consequence of falling off prematurely (i.e. being returned to their cage), and so do not make an effort to stay on (Brooks et al., 2004). Considering apathy and motivational impairments are commonly seen in both HD patients (Tabrizi et al., 2013) and animal models (Oakeshott et al., 2012), this may be of particular concern. Other phenotypes frequently observed in HD mice, such as locomotor hypoactivity and anxiety-like behaviour, could also theoretically impair rotarod performance leading to misinterpretation of deficits. Fatigue is also a concern, especially in accelerating rotarod protocols which can be 5-minutes or longer. As a result, use of the rotarod should be carefully considered and is best when accompanied by other behavioural tests as part of a test battery.

1.2.3.2 Balance beam test

Although not as popular as the rotarod, the balance beam test is sometimes used as an assessment of motor coordination and balance in HD mice. In this test, animals are placed at one end of an elevated beam and have to traverse to the opposite side in order to reach a ‘safe’ platform or enclosed area (Brooks & Dunnett, 2009). A variety of output measures can be quantified, including time to cross the beam and the number of forepaw and hindpaw slips, with the latter suggested to be the most sensitive measure of motor dysfunction (Brooks, 2011). Balance beam deficits have been reported in all models that consistently show rotarod deficits

(Carter et al., 1999; Harrison et al., 2013; Lawhorn et al., 2008; Loh et al., 2013; Southwell et al., 2016), however the age of onset of these deficits is often later than for rotarod. However, despite this reduced sensitivity, balance beam deficits are more progressive than rotarod in some models and may be better suited for longitudinal analysis of motor function (Brooks, Jones, et al., 2012a). As with the rotarod, both non-compliance with the task requirements and increased body weight can be confounds for this test (Brooks, 2011).

1.2.3.3 Analysis of gait

Gait abnormalities are characteristic of many neurological disorders including HD (Hausdorff et al., 1998). As locomotion is a natural behaviour shared between mice and humans, gait analysis has good validity as a behavioural measure, and can be measured in mice using several different methods. However, gait abnormalities are not as consistently observed in mouse models of HD and tend to be seen at an older age than rotarod or balance beam deficits, reducing the usefulness of gait as a measure of motor dysfunction (Menalled et al., 2009). The most frequently used assessment of gait is the 'footprint' test, where the fore- and hindpaws are covered with paint and the mouse is encouraged to walk in a straight line over paper (Brooks & Dunnett, 2009). Automated alternatives based on video capture of mouse footfalls have been developed, such as the Digigait treadmill task (Mouse Specifics Inc.) and the Catwalk system (Noldus IT) which allow for assessment of animal speed and a larger variety of gait parameters (Abada & Ellenbroek, 2016). Because the detection of gait abnormalities may be dependent on the way in which it is measured, the literature regarding gait in mouse models of HD is somewhat inconsistent. For example, BACHD mice were found to have gait abnormalities at 9-10 months-old using the Catwalk system (Abada et al., 2013), but not up to 1-year-old using the

footprint test (Menalled et al., 2009). In contrast, the footprint test is quite sensitive to gait deficits in R6/2 mice (Carter et al., 1999; Pallier et al., 2009) whereas no abnormalities were seen even in late-stage mice using the Digigait test (Pallier et al., 2009). Furthermore, many aspects of locomotion have been found to vary consistently with speed and bodyweight (Batka et al., 2014; Machado et al., 2015), clear confounds for research with HD mice.

1.2.3.4 Skilled forelimb use

Although assessments of full body motor coordination have shown sensitivity for detecting motor dysfunction in mouse models of HD, an appealing alternative involves assessing finer aspects of motor skill. Given the confounds discussed above, tasks involving manual dexterity or manipulation of an object could be a less biased way to test motor function in HD mice. Several assessments of skilled forelimb use are available in rodents, but the most popular is undoubtedly the skilled reaching task, where the animal reaches through a narrow opening in order to grasp and retrieve small pellets of food (Klein et al., 2012). Skilled reaching has good validity as a behavioural task, as manipulation of food is an ethologically relevant behaviour and the general features of reaching movements are relatively similar between humans and rodents (Alaverdashvili & Whishaw, 2013; Sacrey et al., 2009). Furthermore, deficits in tasks involving reaching or skilled hand movements have been observed in both pre-symptomatic HD mutation carriers and HD patients (Bonfiglioli et al., 1998; Klein et al., 2011; Smith et al., 2000). Skilled reaching has been relatively unexplored in genetic models of HD, although deficits have been found in rat neurotoxin models (Fricker-Gates et al., 2003; Whishaw et al., 2007) that mimic the deficits seen in HD patients. In addition, a recent study in homozygous YAC128 mice found a deficit in the frequency of successful attempts on a skilled reaching task, however this was only

observed after a break in training (Glangetas et al., 2020). Considering the presence of early deficits on similar tasks in HD patients, the face and construct validity, and the comparative lack of confounds, further investigation of skilled forelimb behaviours is warranted in HD mice.

1.2.3.5 Other assessments

Several other tests have less frequently been used to measure aspects of motor function in HD mice. In a form of the climbing test, mice are placed in a cylinder with wire mesh covering the walls, and the latency to begin climbing as well as total time spent climbing are assessed over 5-minutes (Southwell et al., 2009). This test provides a general measure of motor function, and impairments have been observed in a variety of HD mice (Menalled et al., 2009, 2012; Southwell et al., 2009, 2016). However, similar to the open field, this test depends on the animal's exploratory drive which may vary between genotypes. Simple tests of swimming speed and coordination provide a sensitive measure of overall motor function and coordination, and deficits in swimming are among the earliest motor phenotypes reported in R6/2 mice (Carter et al., 1999). However, exposure to water is a significant stressor for mice (Contet et al., 2006), decreasing the appeal of this test in comparison to less stressful alternatives. Furthermore, both the climbing and swimming tests provide a relatively coarse and non-specific measure of motor function, giving few clues as to the nature of the underlying deficit. In contrast, the grip strength test measures a single well-defined aspect of motor function (Brooks & Dunnett, 2009), and forelimb/hindlimb grip strength is seen to be decreased in fragment and knock-in models (Menalled et al., 2009, 2012; Rattray et al., 2017; Southwell et al., 2016; Woodman et al., 2007), though not in full-length transgenic models. However, decreased grip strength is generally, although not always (Woodman et al., 2007), seen after the onset of other motor deficits.

1.2.4 Cognitive tasks

Given that impairments of executive function are an early symptom observed in HD mutation carriers, a number of studies have investigated the presence of cognitive phenotypes in mouse models of HD. In some models, such as the HdhQ150 mouse, cognitive phenotypes have an earlier age of onset than impairments on motor tasks (Brooks et al., 2012). In others, however, they appear at approximately the same age (e.g. R6/2, YAC128, Q175-FDN) (Carter et al., 1999; Lione et al., 1999; Southwell et al., 2016; Van Raamsdonk et al., 2005). In studies where cognitive phenotypes are assessed after the onset of motor symptoms, it's important to consider that motor function could be impacting the ability of the animal to perform the task. In addition, many cognitive tasks require intact visual function, and so cannot be accurately assessed in mice on the FVB/N genetic background (e.g. YAC128, BACHD, Q175-FDN) who suffer from retinal degeneration (Farley et al., 2011). Still, tests of cognitive and executive function can be useful, especially for slowly progressing models such as the HdhQ111 mouse that have no clear deficits on motor tasks.

1.2.4.1 Object and spatial learning

A basic test of object recognition memory can be performed in mice by measuring the amount of time they spend investigating a novel object versus one that they have already been exposed to when placed in an open field. Decreased time investigating the novel object, indicating an impairment in recognition memory, has been observed in a number of mouse models of HD (Giralt et al., 2011; Hodges et al., 2008; Southwell et al., 2009, 2016). However, impairments have generally been reported only at an age at which rotarod or other motor deficits are already present. Spatial learning tasks, on the other hand, have been found to be much more

sensitive to cognitive dysfunction early in HD mice. Spatial learning and memory are commonly assessed using the Morris water maze (MWM) task, in which mice learn to swim to a hidden platform with the guidance of visual cues displayed around the swim tank. In R6/2 mice, a deficit on this task is one of the earliest behavioural symptoms that can be detected, with impairments seen as early as 4-weeks-old (Lione et al., 1999; K. P. S. J. Murphy et al., 2000). In addition, a deficit on this task was seen in HdhQ150 mice at 4-months-old, substantially earlier than other cognitive or motor phenotypes (Brooks et al., 2012). These findings are interesting, given that spatial navigation is thought to largely depend on the hippocampus, an area which is not as severely affected in HD. Interestingly, carriers of the HD mutation were also found to have impaired performance on a virtual reality version of the MWM adapted for humans, even prior to clinical diagnosis (Begeti et al., 2016). This observation of similar deficits on a task translated for use in humans supports further use of the MWM for testing HD mice. The main disadvantage of this task in mice, as mentioned above, is the inability to test HD model mice bred on the FVB/N background, somewhat limiting its utility.

1.2.4.2 Behavioural flexibility

Behavioural flexibility and strategy shifting have been well-studied in humans and rodents and are thought to specifically involve projections from prefrontal cortical regions to the dorsal striatum (Ragozzino & Baker, 2016). Considering the prominent cortico-striatal pathology of HD, it's perhaps not surprising that impairments in tasks involving behavioural flexibility are seen early in HD, and can occur before clinical diagnosis (Lawrence et al., 1998; Paulsen et al., 2013). Behavioural flexibility, or more specifically reversal learning, is often assessed in mice using a swimming T-maze paradigm. In this task, mice first learn to swim to an escape platform

placed in one arm of a T-shaped maze over the course of several days. In the reversal phase, the platform is switched to the opposite arm, and the ability of animals to inhibit the previously learned strategy and acquire the new platform location is measured. Acquisition and reversal learning of the T-maze task has been performed in HD mice, with deficits on the reversal phase seen in some models (Brooks et al., 2012; Harrison et al., 2013; Southwell et al., 2016; Van Raamsdonk et al., 2005), but not others (Rattray et al., 2017). Reversal learning deficits in HD mice have also been found using the MWM (Lione et al., 1999) and operant tasks (Brooks et al., 2006).

1.2.5 Anxiety and depressive-like behaviours

Neuropsychiatric symptoms, including anxiety and depression, are common in HD patients (Paulsen et al., 2001). Although there are inherent difficulties in measuring psychiatric features of disease in mice, certain tasks have been developed that can measure aspects of behaviour that are thought to be related to anxiety and affective symptoms. Studying these behaviours has enabled a better understanding of the phenotype of HD mice, and can provide insight into the neuropathology underlying neuropsychiatric symptoms in HD.

Anxiety-like behaviours can be assessed with a variety of tests in mice, most of which take advantage of the 'approach-avoidance' conflict between wanting to engage in exploratory activity versus the perceived danger of brightly lit, open or elevated areas. Generally, mice who show increased exploration even in the face of these naturally aversive environments are taken to be less anxious, while those who show decreased exploration are more anxious. The simplest test of anxiety levels in mice is the amount of time an animal spends in the central zone of the test arena during an open field test. Decreased center time has been seen in several lines of HD mice

(Orvoen et al., 2012; Southwell et al., 2009, 2016); however, significant doubts have been cast about the reliability and reproducibility of the open field test as a measure of anxiety, especially with short testing durations (Fonio et al., 2012). An alternative is the elevated-plus or elevated-zero mazes, which measure the amount of time an animal spends in open versus closed sections of a narrow platform elevated off the ground. Decreased open-arm time has been seen in BACHD and YAC128 mice (Abada et al., 2013; Glangetas et al., 2020), however increased open-arm time (indicating lower anxiety) has also been seen in R6/1 and R6/2 models (File et al., 1998; Naver et al., 2003). Confusingly, R6/2 mice were seen to spend more time in the dark area during the light/dark test of anxiety, indicating increased anxiety as compared to WT mice (Menalled et al., 2009). These conflicting findings highlight the protocol-dependence of anxiety-related phenotypes and underscore the need for caution in interpreting the results of any one test. It should also be noted that animals who show strongly reduced baseline locomotor activity and exploration may not be appropriate for anxiety tests based on exploratory behaviour, as hypoactivity could confound these measures.

Depressive-like behaviour in HD mice is usually measured using the forced-swim test (FST). In this test, an animal is placed inside a glass cylinder partially filled with water from which they can't escape and left for a set period of time (usually 5 minutes) (Petit-Demouliere et al., 2005). An increase in time spent floating (immobility time) as opposed to actively swimming or trying to escape is taken as an indication of depressive-like behaviour. A variety of HD mice have been found to have increased immobility on the FST, including fragment (Ciamei et al., 2015; Pang et al., 2009), full-length transgenic (Pouladi et al., 2009, 2012) and knock-in models (Ciamei et al., 2015; Orvoen et al., 2012; Southwell et al., 2016), although in some models this phenotype was sex-specific (Orvoen et al., 2012). Interestingly, the FST phenotype in mouse

models of HD does not worsen with age. Although floating behaviour was stable in YAC128 mice (Pouladi et al., 2009), it was seen to decrease in aged R6/2 and Hdh250 knock-in mice to a level below that of WT animals (Ciamei et al., 2015). Given this, depressive behaviour may not be the best functional indicator of disease progression in HD mice.

1.3 Automated home-cage behavioural testing of rodents

The non-reproducibility of certain research findings has garnered significant attention in recent years. With regards to behavioural testing, one contributor to this replicability crisis is the low construct validity of many commonly used behavioural tests, which leads to the desired output measure (e.g. locomotor activity) being confounded by other factors (e.g. anxiety, neophobia) (Fonio et al., 2012). Another issue is the lack of standardization of behavioural tools and protocols, which can result in a behavioural test having significantly different parameters across different studies (Walsh & Cummins, 1976). However, even with rigorous standardization, several studies have found systematic differences in behavioural measures between laboratories (Crabbe et al., 1999; Mandillo et al., 2008). This suggests that a contributor to inter-laboratory variability may in fact be the experimenter themselves and the way in which they interact with the animal. For example, animal handling and olfactory exposure to male experimenters have both been shown to cause significant stress in mice, and these effects can last for an extended period (Balcombe et al., 2004; Sorge et al., 2014). Although a certain amount of interaction with the animal is inevitable in the course of rodent research, when this handling comes immediately prior to the start of a behavioural test, it could influence the outcomes of this test in ways that are difficult to predict.

An alternative approach that minimizes the impact of 'the experimenter' as a confound is to assess the behaviour of rodents within their own home-cage. Home-cage behavioural testing encompasses two complementary strategies. The first is to record and quantify the activity and spontaneous behaviours of animals in their home-cage, typically by using video recording and computer vision techniques (Bains et al., 2016; de Chaumont et al., 2019; Goulding et al., 2008; Hong et al., 2015; Jhuang et al., 2010; Weissbrod et al., 2013). Rather than administering a standardized test, this observational approach takes advantage of the rich behavioural repertoire of mice to identify traits that vary across genotypes or treatments. The second approach is to integrate an automated behavioural test, typically an operant learning paradigm, directly into the animal's home-cage (Francis & Kanold, 2017; Kaupert et al., 2017; J. H. Lee et al., 2020; Poddar et al., 2013; Remmelink et al., 2017; Rivalan et al., 2017; Silasi et al., 2018). These two forms of home-cage testing address a number of the confounds of traditional behavioural testing paradigms. Animals are allowed to behave in a self-directed and spontaneous manner and are free to interact with the task whenever they are motivated to do so. In addition, behaviours can be measured without the experimenter ever having to directly handle the animal, or even enter the room (other than to perform standard animal husbandry). Another advantage is that of increased throughput, as the number of animals that can be tested is limited mostly by the equipment available for testing rather than by the time of the experimenter. Mice can also be tested for extended periods of time with relatively minimal intervention, allowing for the collection of large longitudinal behavioural datasets. These benefits have led to a growth in the popularity of home-cage behaviour in the past ten years, and a variety of commercial and open-source tools have been developed to facilitate these experiments.

1.3.1 Methods of home-cage testing

One of the earliest commercial options for home-cage testing, and still among the most popular, is the Intellicage (TSE Systems). This large home-cage system can house up to 16 mice at a time and animals are differentiated in the cage through the use of subcutaneously implanted radio-frequency identification (RFID) microchips. At each corner of the cage, mice can interact with an operant conditioning wall containing two nose poke ports, an array of lights and a door that opens to provide access to a water bottle (Kiryk et al., 2020). Using these operant corners, a variety of tasks can be assessed, including place learning, reversal learning, and more complex rule-based paradigms. Although this system doesn't directly measure the movement of animals, the timing and frequency of corner visits has been shown to provide an effective proxy measure of locomotor activity (Robinson & Riedel, 2014). In addition to the Intellicage, there are several other commercial options to perform home-cage activity monitoring of mice, including the PhenoTyper (Noldus IT) and PhenoMaster (TSE Systems) systems. Although developed primarily for activity tracking, these systems also have a number of add-ons that allow for assessment of operant and stimulus-response learning. In support of the use of these systems, several studies have demonstrated high inter-laboratory reliability of both the Intellicage (Krackow et al., 2010) and the PhenoTyper (Robinson et al., 2018), with different laboratories finding similar behavioural differences among commonly used inbred mouse strains. Unfortunately, many commercial systems (aside from the Intellicage) are limited to testing single-housed animals, an important caveat for their use.

Due to the high-cost of commercial systems, a number of research groups have developed open-source tools to monitor the home-cage activity and behaviours of mice. Some of these are designed specifically as an open-source alternative to commercial activity monitors, and provide

basic measures of locomotor activity in single-housed mice using either video (Singh et al., 2019), microwave-based motion detection (Genewsky et al., 2017) or passive infrared (Matikainen-Ankney et al., 2019). Others have used computer-vision techniques to automatically segment and classify a range of spontaneous behaviours in either single (Jhuang et al., 2010) or group-housed mice (Hong et al., 2015). For analyzing social behaviours in group-housed animals, video-tracking is often combined with detection of implanted RFID capsules (Bains et al., 2016; Weissbrod et al., 2013) to periodically confirm animal identity. More recently, depth-sensing cameras have been employed to provide an even more detailed and accurate characterization of home-cage spontaneous behaviour in group-housed animals (de Chaumont et al., 2019). Other home-cage tools have focused not on locomotor activity or social behaviour, but on physiological measures such as body weight (Noorshams et al., 2017) and food/water consumption (Ahloy-Dallaire et al., 2019; Godynyuk et al., 2019; Nguyen et al., 2016). Aside from tracking naturalistic behaviours, a number of studies have integrated behavioural tests directly into the rodent home-cage. Most often this is an operant task, in which the mouse has to perform successful trials in order to receive water (Francis & Kanold, 2017) or food (Remmelink et al., 2017). Although this is often done with single housing (Bollu et al., 2019; J. H. Lee et al., 2020; Poddar et al., 2013; Remmelink et al., 2017) or by combining data from all animals (Francis & Kanold, 2017), other groups have used an automated sorting system to segregate individual animals from their cage-mates (Kaupert et al., 2017; Rivalan et al., 2017), or have used implanted RFID capsules to identify animals (Silasi et al., 2018). Notably, several studies have integrated skilled forelimb tasks into the home-cages of mice and rats. These have included an automated single-pellet reaching training system (Fenrich et al., 2015), as well as joystick (Bollu et al., 2019; Poddar et al., 2013) and lever tasks (Silasi et al., 2018).

1.3.2 Home-cage testing in mouse models of HD

Home-cage behavioural testing has been used to assess HD mice in a number of studies and has often proved to be sensitive at detecting early phenotypes in these animals. As discussed previously, commercial activity tracking systems using either photobeam arrays or video-tracking have been used to measure locomotor activity in HD mice (Hodges et al., 2008; Slow et al., 2003). These systems have also proved very useful for longer term (weeks to months) studies analyzing circadian activity patterns, sometimes in conjunction with activity-tracking running wheels (Kudo et al., 2011; Loh et al., 2013; Maywood et al., 2010; Morton et al., 2005; Pallier et al., 2007). To collect a more detailed characterization of home-cage behaviours in HD mice, a few different approaches have been used. The first of these is the LABORAS system, which uses a force-sensing plate underneath the cage to automatically detect and classify behaviours including locomotor activity, grooming, eating, drinking and climbing (Van De Weerd et al., 2001). This was used in several studies that focused on food and water consumption in R6/2 mice, finding that these animals spent substantially more time eating and drinking than wildtype mice, despite being hypoactive overall (van der Burg et al., 2008; Wood et al., 2008). A more common approach in recent years has been to use computer vision techniques to automatically segment and identify behaviours from video data. One of the first papers to use this approach quantified the home-cage behaviour of R6/2 mice longitudinally, finding significant alterations in a number of features (e.g. grooming, rest, awakening from rest) from a young age (Steele et al., 2007). The authors also performed a multi-feature analysis that was able to reliably distinguish R6/2 mice as young as 7-weeks-old from WT animals. A subsequent paper using a similar, but open-source, methodology replicated some of these results, finding significant

alterations in the home-cage behavioural patterns of R6/2 mice from around 6-7 weeks-old (Zarringhalam et al., 2012).

A number of studies have also assessed HD mice on operant tasks in the home-cage, typically using an Intellicage or similar system. In one study, R6/2 mice were group-housed in the Intellicage for 8 weeks and a series of behavioural assessments were administered, including spatial learning and spatial alternation (rewarded corner switches between two locations) (Rudenko et al., 2009). They found that HD mice had significantly decreased exploratory behaviour even when first introduced to the cage at 4.5 weeks, and subsequently had deficits in performing the alternation task. In a more recent series of studies, spontaneous and learned behaviours of BACHD and R6/2 mice were investigated using a modified Intellicage unit (the 'PhenoCube') (Balci et al., 2013; Oakeshott et al., 2011). In addition to the Intellicage operant corners, the PhenoCube system included a top-down camera to track locomotion, immobility and rearing in animals. Both R6/2 and BACHD mice were found to have increased immobility and reduced exploration; however, consistent operant learning and spatial alternation deficits were found only in the R6/2 model (Balci et al., 2013). These results were extended to an allelic series of knock-in HD mice in a study which used the PhenoCube along with two additional computer-vision-based tools to collect several thousand behavioural traits for each animal (Alexandrov et al., 2016). Using machine-learning analysis, the authors extracted higher level behavioural features that varied predictably with age and CAG-length, allowing them to predict CAG-length from behavioural data with a good degree of accuracy. This study is a significant advance in the phenomic analysis of HD mice, but is unfortunately limited by the lack of transparency concerning the specific measures collected and the way in which their home-cage system

functioned. Skilled motor learning has not been investigated in HD mice in the home-cage, as no commercial (and few open-source) systems have been available to do so.

1.4 Dissertation overview and research aims

As discussed previously, HD mutation carriers have diverse impairments in learning and controlling voluntary arm and hand movements, some of which appear long before the onset of over motor dysfunction (Bonfiglioli et al., 1998; Feigin et al., 2006; Klein et al., 2011; Paulsen et al., 2008; Shabbott et al., 2013; Smith et al., 2000; Stout et al., 2011; Tabrizi et al., 2013; Willingham & Koroshetz, 1993). Despite tests of skilled forelimb use in rodents having good face and construct validity for the functional assessment of striatal pathology (Karl & Whishaw, 2011; Klein et al., 2012), they have seen limited use in mouse models of HD. Furthermore, home-cage-based testing offers a novel method of assessing behaviour in mice that increases throughput and reduces stressors that could lead to inter-study variability (Hånell & Marklund, 2014; Richter, 2020; Robinson et al., 2018; Spruijt & DeVisser, 2006). Given this, **we hypothesized that a home-cage based forelimb motor learning task would be of substantial use for the assessment of behavioural phenotypes in mouse models of Huntington's disease.** Furthermore, such a system could provide a sensitive platform for assessing the functional effects of novel therapeutics in these animals. Pursuant to this hypothesis, I have undertaken a course of research encompassing three main sections:

AIM I (Chapter 2): Assessing the feasibility of using a prototype home-cage lever-positioning task in HD mice, and investigating whether YAC128 HD mice have motor deficits on this task at pre- and early symptomatic timepoints.

AIM II (Chapter 3): Developing this home-cage task into a more standardized behavioural testing system (‘PiPaw’) and investigating motor phenotypes and training-associated striatal plasticity in HD mice.

AIM III (Chapter 4): Developing a new home-cage based system for automated drug administration to rodents (‘PiDose’) and assessing the ability of this system to treat mice with a drug over an extended period.

Chapter 2: YAC128 HD mice have deficits at early symptomatic timepoints in a home-cage lever-positioning task

2.1 Introduction

As discussed in the previous chapter, animal models of HD are a critical tool for elucidating the underlying mechanisms of the disease, as well as for the pre-clinical screening of potential therapies. To date, over twenty mouse models of HD have been developed (Menalled et al., 2014; Pouladi et al., 2013) and behavioural testing is an important step in determining how closely aligned each model's phenotype is with the disease symptoms in human (i.e. its face validity). Motor behaviour is most commonly assessed in these mice using tests of balance and motor coordination such as the rotarod and balance beam, as well as gait assessments, and measures of overall activity level. Although HD patients have difficulties with balance and gait, the earliest motor deficits observed in carriers of the HD mutation actually do not involve full body coordinated movement, but rather precision movements. For example, pre-symptomatic carriers of HD have impaired performance of timed finger movements (Paulsen et al., 2008; Tabrizi et al., 2013), and learned motor sequences (Feigin et al., 2006; Ghilardi et al., 2008). Reaching movements have also been observed to have increased jerkiness and impaired movement termination in pre-symptomatic HD (Smith et al., 2000). Consequently, tests of full body coordination such as the rotarod may not detect certain motor phenotypes relevant to HD in mice. Despite this, skilled motor tasks have rarely been used in the assessment of mouse models of HD.

YAC128 HD mice have been well established to show many of the features of the human disease, including striatal and cortical degeneration and progressive behavioural changes. Among

the models that express the full-length *HTT* gene, they are among the first (along with the BACHD model) to show motor abnormalities, with rotarod deficits emerging around 4- to 6-months-old (Pouladi et al., 2012; Slow et al., 2003). However, conflicting results have been reported concerning the time frame, severity and progression of these motor abnormalities (Menalled et al., 2009; Van Raamsdonk et al., 2005). Differences in methodology and apparatus may be contributing to this (Mandillo et al., 2008), as well as the use of underpowered experimental groups. In addition, YAC128 mice have increased bodyweight as compared to their WT littermates, a known confound for tests of full body motor function such as the rotarod (McFadyen et al., 2003; Moreno et al., 2016). To address these issues, importance must be placed on finding novel ways to assess behaviour that reduce confounding factors and increase throughput. In recent years, several systems have become commercially available which increase the automation of behavioural testing and analysis by assessing animals within their home-cage (e.g. Intellicage). These systems have the combined benefits of increasing the throughput of behavioural phenotyping, eliminating the subjectivity associated with manual scoring, increasing the length of the testing period and reducing the amount of animal-experimenter interaction (Hånell & Marklund, 2014). However, as of yet, systems for the home-cage assessment of an operant motor learning task are not widely available and have not been applied to the study of HD.

In this chapter, I employed an automated home-cage behavioural testing system first developed in Dr. Tim Murphy's laboratory (Silasi et al., 2018). This task integrates a skilled lever-positioning task into the animal's home-cage and is accessible by group-housed mice full-time over several weeks of testing. Following an initial training period, the demands of the task change dynamically in order to probe learning and motor control. Mice are differentiated through

the use of implanted RFID capsules, and individually progress through phases of the task in a self-directed manner. Using this system, I aimed to study the emergence and progression of motor deficits at early symptomatic timepoints in the YAC128 model. I also sought to use this task to assess overall activity levels and circadian activity patterns to determine if these were altered in YAC128 mice.

2.2 Methods

2.2.1 Animals

A colony of heterozygous YAC128 mice on the FVB/N background (YAC128 line 53; Slow et al., 2003) was maintained by breeding with wildtype FVB/N animals. Animals were housed in cages of two to five male littermates on a 12/12 h light/dark cycle in a temperature- and humidity-controlled room. All animals were male, and separate cohorts of naïve animals began the testing protocol at 2-months-old (60 ± 5 days), 4-months-old (120 ± 5 days), or 6-months-old (180 ± 5 days). Initially, 41 mice (20 WT/21 YAC128) began the testing protocol at 2-months-old, 38 mice (19 WT/ 19 YAC128) at 4-months-old and 44 mice (25 WT/19 YAC128) at 6-months-old, for a total of 123 animals. All procedures were carried out in accordance with the Canadian Council on Animal Care and approved by the University of British Columbia Committee on Animal Care. Mice were provided with free access to chow and standard environmental enrichment within the cage (bedding, hut, PVC tube) throughout testing. Animal tissue was collected via ear clipping at weaning, and DNA extraction and PCR analysis was subsequently used to determine genotype, as previously described (Slow et al., 2003).

2.2.2 RFID capsule implantation

To enable identification of group-housed mice, animals were implanted with glass RFID capsules (Sparkfun SEN-09416) prior to the start of testing as previously described (Bolaños et al., 2017). Animals were anesthetized with isoflurane (4% initially, then maintained at 1.5%) and given buprenorphine via subcutaneous injection (0.05 mg/kg) for analgesia. Betadine was applied to disinfect the incision site, and a small incision was made in the upper thoracic torso. A sterile injector (Fofia ZS006) was then used to insert the RFID capsule subcutaneously below the nape of the neck. The incision was sutured, and the animal was removed from anesthesia, allowed to recover, and then returned to its home-cage. Animals were monitored for the following 3 days to ensure healthy recovery and proper placement of the RFID capsule. Animals were given at minimum five days to recover following surgery before being used for any experiments.

2.2.3 Hardware and software

All experiments were performed in a modified mouse home-cage with a custom designed Plexiglas chamber (the ‘testing module’) attached to one side (Fig. 2.1a-b). This testing module was enclosed on all sides (except for an entrance leading into the cage) and sized such that only one mouse could enter at a time (2.5×2.5×9.5cm). A cylindrical steel rod (2mm thick) extended 1 cm into the module through a small opening along the bottom of the right wall at the end opposite the entrance. This rod was moveable on a horizontal axis, restricted to a range of 24° by two metal posts (Fig. 2.1c), and held in its ‘start’ position by a 1.5 g counterweight. The lever was coupled to a rotary encoder (Phidgets ISC3004) in order to measure and record all movements. Adjacent to the lever, a spout dispensed water drops using a gravity-fed valve-based

system (Gems Sensors MB202-VB30-L203) (T. H. Murphy et al., 2016). An RFID antenna and reader (Sparkfun SEN-11828) was inset into the ceiling of the module in order to individually identify RFID-tagged animals (Bolaños et al., 2017)**.** All components were controlled by custom software written in Python running on a Raspberry Pi B+ running the Raspbian operating system. The program ran continuously for the duration that animals were housed in the testing cage. Three of these cages were constructed and used to perform the described experiments.

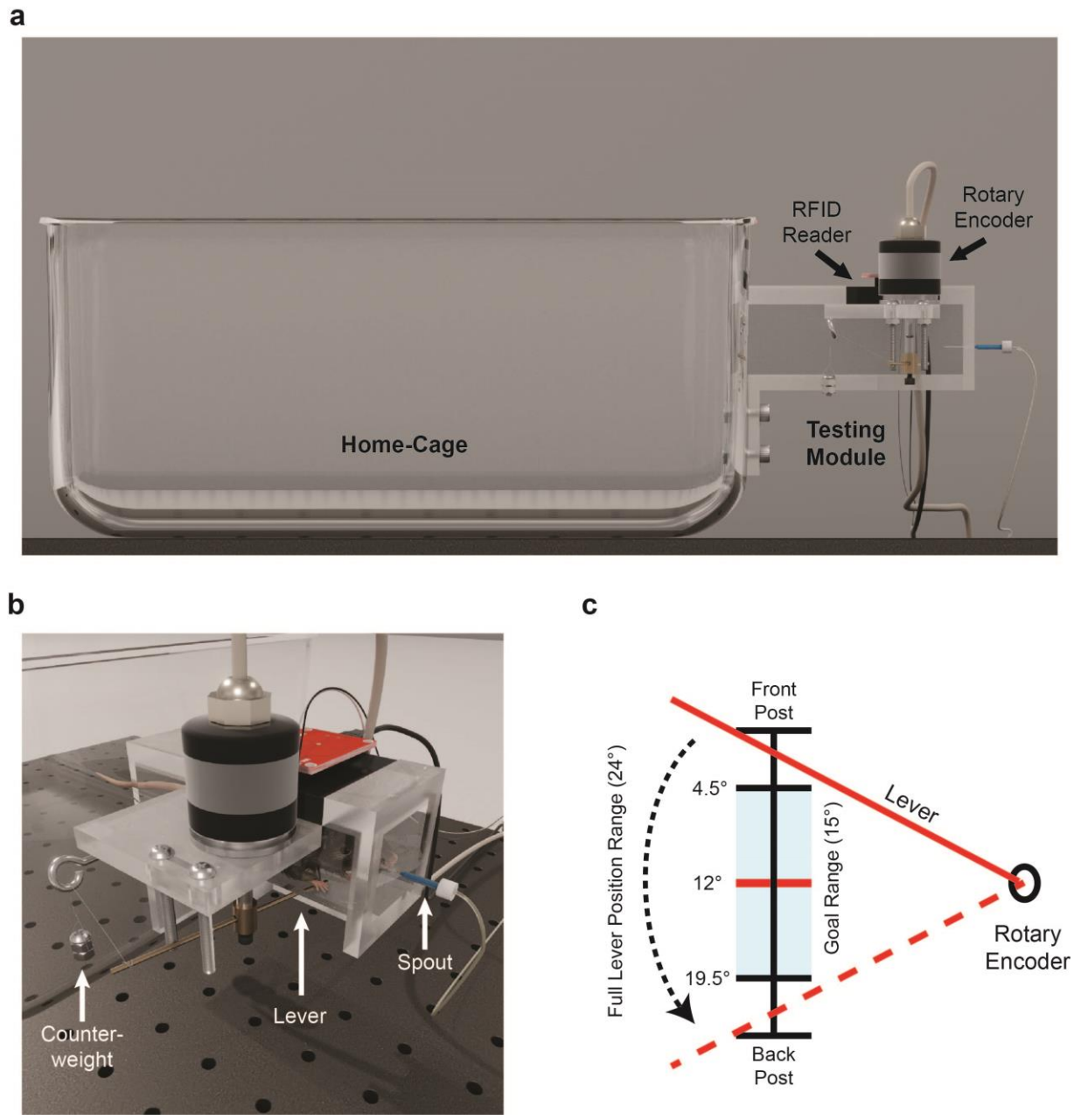

Figure 2.1 System for home-cage assessment of skilled motor learning

(a-b) A small opening on one side of the home-cage allows 24-hour access to a testing module containing a metal lever and water spout. RFID-tagged animals are identified by an RFID reader upon entrance into the module, allowing for individual tracking and assessment of group-housed animals. The lever is restricted in its horizontal movement by two metal posts and held in starting position by a small counterweight. In the training phase, the mouse must pull the lever backwards 12° from its starting position in order to receive a water drop. **(c)** A top-down view of the lever position range. In the main

testing phase, the mouse must first pull the lever back to the center (red line), and then hold it within a central goal position range (shaded area) in order to receive a water drop. The length of time the lever must be held for changes dynamically based on the individual animal's success rate.

2.2.4 Testing methodology

In the initial phase of testing ('training phase'), small groups of littermate mice were introduced to the cage. The number of animals in each cage was between two and five and was determined by the number of littermates of the same sex at birth (and restricted by the maximum permitted cage size of five mice). This was done so that as many available animals as possible could be used for testing (i.e. so that animals did not have to be removed from cages, or certain cages excluded because they didn't contain the same number of mice). Animals were tested alongside the littermates that they had been housed with since weaning. Genotype was mixed in the majority of testing cages, although some cohorts of animals contained only WT or YAC128 mice (25% of cages). Upon transfer to the testing cage, *ad libitum* water bottle access was removed, so that water could only be retrieved by entering the testing module. When a mouse entered the module, it was detected by the RFID reader and a small water drop (5 µL) was delivered from the reward spout, up to a maximum of 200 drops per day (1 mL). Additional water drops (10 µL) could be obtained by pulling the lever backwards past the center of its position range (12° from starting position). The testing module was accessible to animals 24 hours/day and the timing of each entrance, exit and trial were automatically collected and saved. Additionally, the position of the lever during each trial was recorded at 200 Hz. This initial training period lasted from 3 to 8 days, depending on how quickly all animals in the cage learned to perform the operant response. Animals were not disturbed once placed in the cage except for weighing (twice per week) and bedding changes. Animals that did not perform at least 200 trials

during this initial acquisition period were removed from the cage and not used for further testing (see Fig. 2.2a). In total, four 2-month-old-mice (0 WT / 4 YAC128), four 4-month-old mice (2 WT / 2 YAC128) and five 6-month-old mice (1 WT/ 4 YAC128) did not progress past this training phase. Additionally, one 6-month-old YAC128 mouse lost >15% body weight during this initial training phase and was removed from the cage and not used for analysis.

Following acquisition of the basic task, animals were moved to a second phase ('testing phase') where the criteria to receive a water drop changed. As before, the animal was required to displace the lever to the center of the position range. However instead of immediately receiving a drop, the lever then had to be held in a central 'goal range' (between 4.5° and 19.5° from start position) for a set target duration before a drop was dispensed (Fig. 2.1c). If the lever was not held in the range for the required duration the trial was failed, and no water was dispensed. Initially this hold duration was set to 100 ms for all animals, but this could increase based on the animal's performance of the task. Every 25 trials, a ratio of successful to failed trials was calculated for that animal; if the animal had a greater than 75% success rate over this block, the required hold duration increased by 100 ms to a maximum of 800 ms (an end goal that the large majority of animals were able to achieve in pilot experiments). If the animal was less than 10% successful, the required hold duration decreased by 100 ms. Otherwise, the hold duration remained the same for the subsequent block of trials. Animals remained in this testing phase for a minimum of seven days, after which testing was terminated and animals were returned to their regular home-cage. Only five animals did not reach the maximum hold duration within the seven days.

2.2.5 Data analysis and statistics

All task performance data were automatically recorded into text files by the testing software and was subsequently extracted and analyzed by customized scripts using Igor (Wavemetrics). For analysis of kinematic measures in the testing phase, all successful trials at the maximum hold duration (800 ms) were averaged to determine mean maximum displacement, speed, and slope of trajectory for each animal. Only animals with a minimum of 200 eligible trials before the end of testing were used in order to obtain a representative average and reduce the effect of inter-trial variability. During the course of testing, some cohorts of animals were excluded from analysis at intermediary stages because of system crashes that resulted in interruption of task access, and several other animals were excluded because of faulty data collection or program errors that led to non-standard task advancement. In total, twelve mice (7 WT / 5 YAC128) were removed at 2-months-old, eight mice (5 WT / 3 YAC128) at 4-months-old and fourteen mice at 6-months-old (9 WT / 5 YAC128). Numbers of animals used for each analysis are indicated in the results text and figure legends.

All statistical analyses were performed using GraphPad Prism 6.01 (GraphPad Software). Data are expressed as mean ± SEM unless otherwise specified. Alpha level for all tests was $p = 0.05$. For most datasets, regular or repeated measures two-way ANOVA (as appropriate) with Bonferroni post-tests was used for statistical analysis of main/interaction effects. For the analysis of trials performed per day, a log transformation was used to normalize the data to allow for the use of two-way ANOVA, as several of the groups had a strong right skew in their distribution. For the analysis of time spent in the testing module, a significantly non-Gaussian distribution was seen in many of the groups, limiting the use of two-way ANOVA. Paired comparisons between genotypes at each age group using either Student's t-tests or Mann-Whitney tests was

performed, in addition to Kruskal-Wallis tests with Dunn's post-tests to analyze age effects in each genotype group. Fisher's exact test was used to compare the proportion of animals that reached criteria in the training phase and reached the maximum hold duration in the testing phase.

2.3 Results

2.3.1 WT and YAC128 mice rapidly acquire a home-cage lever positioning task

The large majority of WT (n = 64) and YAC128 (n = 59) animals (~90%) tested in all age groups successfully acquired the basic operant lever task and reached the performance criteria of 200 trials in the training phase. There was no difference in the proportion of animals that acquired the task between age groups or between genotypes within each age group, but there was an overall greater proportion of YAC128 animals that failed to reach the performance criteria within the training phase as compared to WT (p = 0.0386) (Fig. 2.2a). During the first few days in the cage, some animals (especially at 6-months-old) dropped in weight in response to the removal of *ad libitum* water. However, all but one animal recovered to within 10% of baseline weight after one week, and 2-month-old WT mice gained weight over this period (p = 0.0485). 2-month-old mice, as well as 4-month-old YAC128 mice, gained weight overall by the end of testing (2-month WT: p = 0.0001; 2-month YAC128: p = 0.0004; 4-month YAC128: p = 0.0211), whereas 4-month-old WT mice and 6-month-old mice showed no change (Fig. 2.2b).

A substantial amount of inter-animal variability was observed in the frequency of task performance among WT and YAC128 mice, with mice typically performing an average of 300 to 500 trials per day (Fig. 2.2c). An overall age effect was seen on trial performance rate, with younger mice tending to have more trials per day, but no genotype differences were observed

(Age: $F_{2, 84} = 4.803$, $p = 0.0106$; Genotype: $F_{1, 84} = 0.1089$, $p = 0.7422$; Interaction: $F_{2, 84} = 0.5332$, $p = 0.5887$). A significant age effect was also seen in the amount of time spent in the testing module per day for both WT ($H = 15.22$, $p = 0.0005$) and YAC128 ($H = 13.50$, $p = 0.0012$) mice, with 2-month-old animals higher on this measure than older animals (Fig. 2.2d). While some mice developed a relatively consistent strategy by the fifth day of testing, others were more variable in their performance, although no consistent genotype differences were observed (Fig. 2.2e-f).

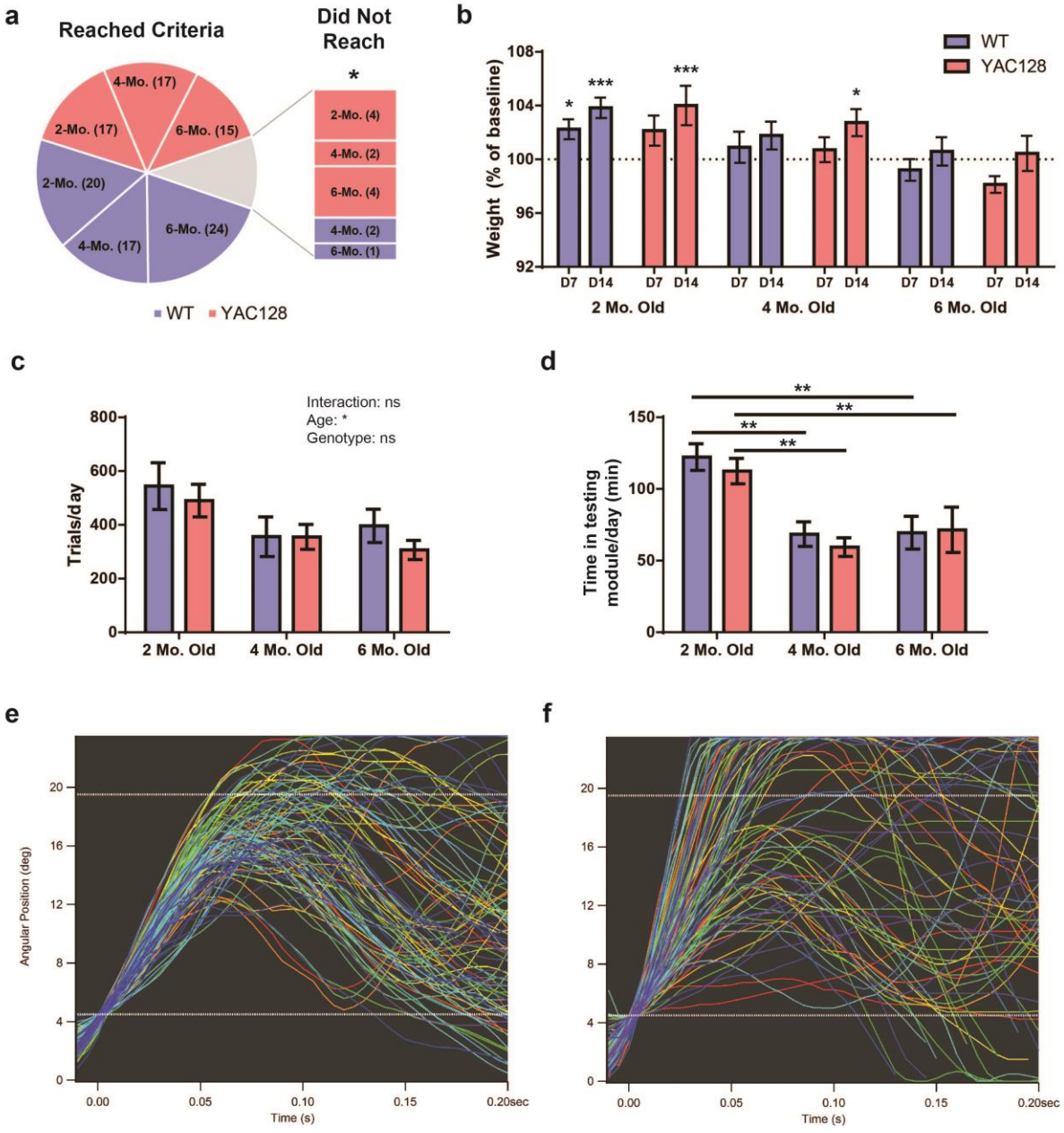

Figure 2.2 WT and YAC128 mice learn a home-cage lever positioning task

(a) Number of animals to reach the performance criteria of 200 trials performed in the training phase. An overall lower proportion of YAC128 animals acquired the task as assessed by this cut-off. **(b)** Average weight over the course of testing as a percentage of baseline. Although 6-month-old animals remained at their baseline weight, 2-month-old WT and YAC128 animals and 4-month-old YAC128 animals gained weight over 14 days in the lever-cage (asterisks indicate significant increase as compared to baseline weight). **(c)** No significant differences between WT and YAC128 were seen in the number of trials

performed per day, however animals in both genotypes performed fewer daily trials with increasing age. **(d)** Time spent in the testing module per day was also not significantly different between genotypes, however both WT and YAC128 animals were much higher on this measure at 2-months-old than at other ages. **(e-f)** Sample lever position traces from two 4-month-old animals (WT and YAC128 respectively) in the training phase. Each line represents one trial. Numbers of animals (WT/YAC128) used for weight, trial frequency and time in testing module analysis are n = 17/13 at 2-months-old, n = 14/16 at 4-months-old and n = 18/12 at 6-months-old. *: $p < 0.5$; **: $p < 0.01$; ***: $p < 0.001$; ns: not significant.

2.3.2 YAC128 mice display abnormal circadian activity patterns

Performance of the task was distributed throughout the day for individual animals, but an increase in activity was almost always observed during the first 6 hours of the dark phase (Fig. 2.3a). Interestingly, when the overall proportion of light versus dark phase trials was analyzed, YAC128 mice were found to have a significantly higher light phase activity than WT mice overall (Age: $F_{2, 84} = 2.945$, $p = 0.0580$; Genotype: $F_{1, 84} = 4.772$, $p = 0.0317$; Interaction: $F_{2, 84} = 0.2492$, $p = 0.7800$) (Fig. 2.3b). To more closely examine this, we binned each animal's trials by hour of day, and compared the average trial distribution for WT and YAC128 mice. While 2-month-old YAC128 animals had a normal circadian trial distribution (Hour: $F_{23, 644} = 86.51$, $p < 0.0001$; Genotype: $F_{1, 28} = -0.3218$, $p > 0.9999$; Interaction: $F_{23, 644} = 0.7632$, $p = 0.7788$; n = 17 WT, 13 YAC128), there was a strong interaction between genotype and the timing of trials throughout the day in 4-month-old (Hour: $F_{23, 598} = 56.36$, $p < 0.0001$; Genotype: $F_{1, 26} = 0.0$, $p > 0.9999$; Interaction: $F_{23, 598} = 2.296$, $p = 0.0006$; n = 14 WT, 16 YAC128) and 6-month-old mice (Hour: $F_{23, 644} = 43.87$, $p < 0.0001$; Genotype: $F_{1, 28} = 0.8750$, $p = 0.3576$; Interaction: $F_{23, 644} = 1.911$, $p = 0.0066$; n = 18 WT, 12 YAC128) (Fig. 2.3c-e). YAC128 mice at these ages tended to increase their trial performance in the last three hours of the light phase, and then drop steeply 2

hours after the start of the dark phase, whereas WT mice maintained a higher trial performance rate through the first 6 hours of the dark phase.

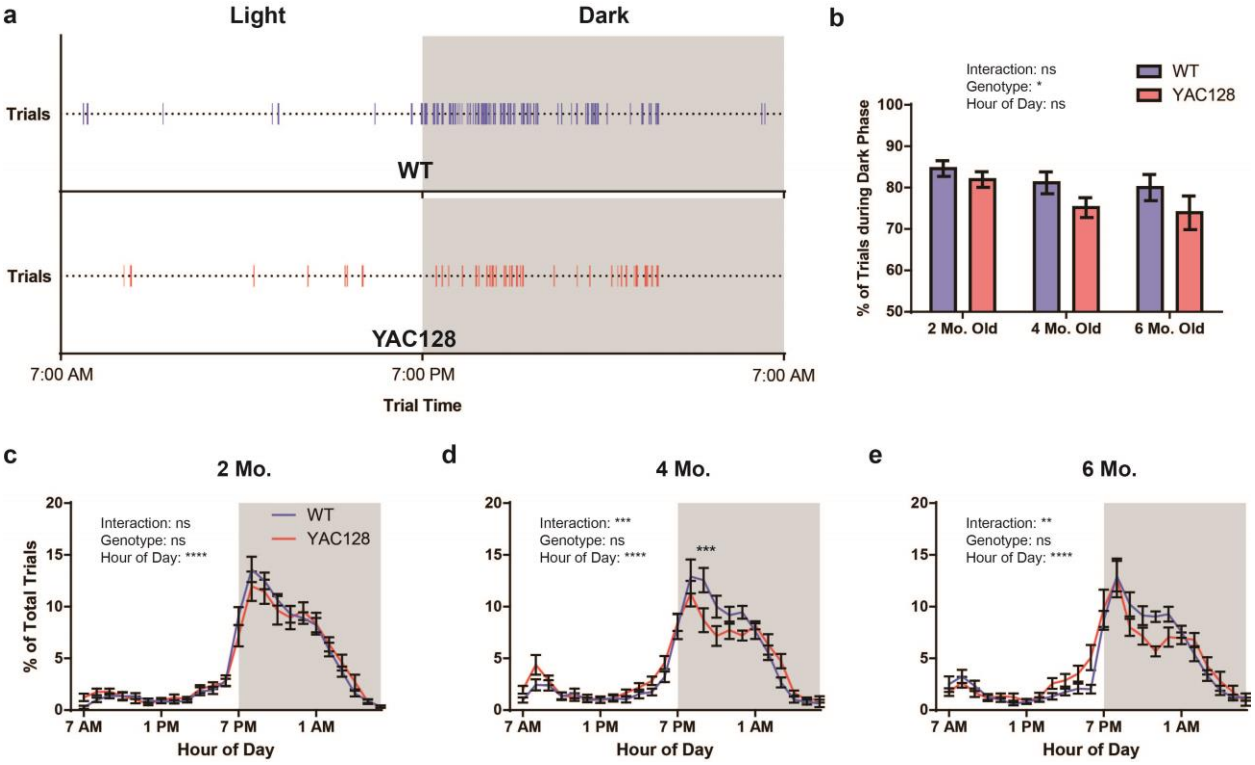

Figure 2.3 YAC128 mice have an altered circadian distribution of trials

(a) Raster plots show the distribution of trials through the day for representative 4-month-old WT and YAC128 animals on the fifth day of testing (each line represents one trial). **(b)** The average percentage of all trials performed during the dark phase of testing was significantly higher in WT than in YAC128 mice, suggesting a disruption of normal circadian activity patterns in these animals. **(c-e)** Trials were split into one-hour bins for each animal and the percentage of trials occurring in each bin is shown for 2-, 4- and 6-month-old age groups. A significant interaction between genotype and the hour of day was observed for 4-month-old and 6-month-old, but not 2-month-old animals. Numbers of animals (WT/YAC128) used for analysis are n = 17/13 at 2-months-old, n = 14/16 at 4-months-old and n = 18/12 at 6-months-old. *: $p <$ 0.5; **: $p < 0.01$; ***: $p < 0.001$; ****: $p < 0.0001$; ns: not significant.

2.3.3 2-month-old YAC128 mice are impaired at adapting their motor response to changes in task demands

In the main testing phase, animals were required to hold the lever for progressively longer within a designated position range in order to continue to receive water rewards. The way in which they progressed was based on their success rate at the current required hold duration, such that if over 75% of their trials in a 25-trial bin were held for the required length of time, the hold duration increased incrementally by 100 ms. Animals that were more successful at adapting to these changing demands had a higher success rate and consequently a faster progression to the maximum hold duration (800 ms). Conversely, animals that continued to perform their trials as in Phase 1 did not advance.

While 4- and 6-month-old YAC128 animals showed an equivalent progression through the task to their WT counterparts (4-month-old: Trial: $F_{20, 460} = 115.8$, $p < 0.0001$; Genotype: $F_{1, 23} = 0.029$, $p = 0.866$; Interaction: $F_{20, 460} = 0.674$, $p = 0.853$; $n = 14$ WT, 16 YAC128; 6-month-old: Trial: $F_{20, 520} = 115.7$, $p < 0.0001$; Genotype: $F_{1, 26} = 0.274$, $p = 0.605$; Interaction: $F_{20, 520} = 1.336$, $p = 0.15$; $n = 18$ WT, 12 YAC128), 2-month-old YAC128 mice showed a markedly slower progression, remaining at a lower required hold duration for longer on average before advancing (Trial: $F_{20, 500} = 70.42$, $p < 0.0001$; Genotype: $F_{1, 25} = 6.367$, $p = 0.0184$; Interaction: $F_{20, 500} = 5.321$, $p < 0.0001$; $n = 17$ WT, 13 YAC128) (Fig. 2.4a-c). However, despite this slower progression, there were no genotype differences in the percentage of animals that eventually reached the maximum hold duration ($p = 0.7292$) suggesting that this was not a problem with meeting the physical demands of the task (Fig. 2.4d). This deficit in 2-month-old YAC128 animals is also reflected in the overall success rate of these animals over the first 500 pulls of Phase 2 (Fig. 2.4e). This group had a lower average success rate as compared to all other WT

and YAC128 groups, although this difference was not significant (Age: $F_{2, 74} = 2.753$, $p = 0.0703$; Genotype: $F_{1, 74} = 2.002$, $p = 0.1613$; Interaction: $F_{2, 74} = 1.504$, $p = 0.2290$).

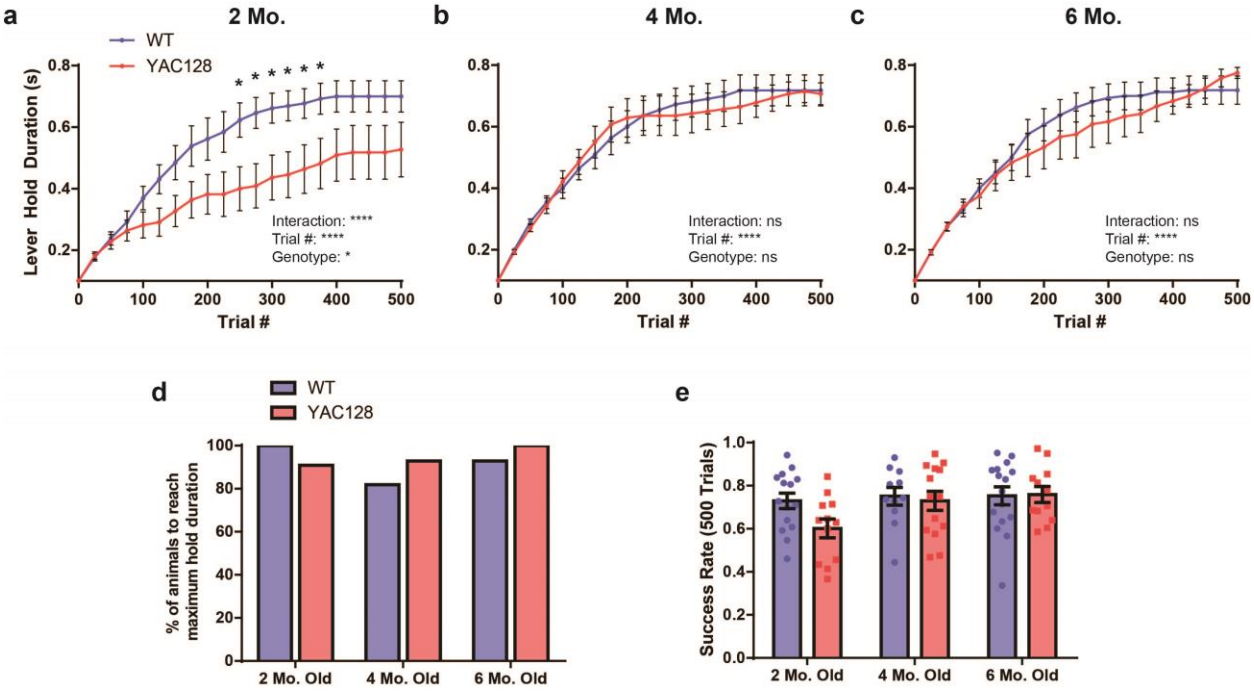

Figure 2.4 2-month-old mice show impaired motor learning on this task

(a-c) Progression to the maximum required hold duration over the first 500 trials of the main testing phase is plotted for 2-, 4-, and 6-month-old age groups. At the end of each 25-trial bin, success rate was calculated over these trials to determine whether the animal met the threshold for their required hold duration to increase. Data are plotted as the required lever hold duration reached at the end of each 25-trial bin. YAC128 mice at 2-months-old, but not other ages, had a significantly slower progression over the first 500 trials as compared to WT controls. **(d)** The majority of animals reached the maximum hold duration within one week, and no significant differences were observed between genotypes. **(e)** Success rate of animals over the first 500 trials of the testing phase is plotted for each age group. 2-month-old YAC128 animals had the lowest average success rate over this period, although no significant main or interaction effects were found. Numbers of animals (WT/YAC128) used for analysis are $n = 15/12$ at 2-months-old, $n = 11/14$ at 4-months-old and $n = 16/12$ at 6-months-old. *: $p < 0.5$; **: $p < 0.01$; ***: $p < 0.001$; ****: $p < 0.0001$; ns: not significant.

2.3.4 6-month-old YAC128 mice have kinematic differences in pull strategy when required to hold the lever for longer

The change in performance of the task from the training phase can be seen when looking at lever position traces of trials from WT and YAC128 animals that have reached the maximum hold duration (Fig. 2.5a-b). Instead of rapidly pulling back and then releasing, animals held the lever within the goal range for the designated amount of time, as was required to receive a reward. However, the specific strategy used to achieve this goal differs, and several systematic differences between WT and YAC128 animals were observed in the 6-month-old group. Analysis of averaged traces revealed that WT animals at this age typically displace the lever to a point just past the center of the goal range and hold it steady within this range until the end of the trial (Fig. 2.5c). In contrast, many 6-month-old YAC128 mice pull the lever straight through the goal range, and then slowly allow it to return to its start position (Fig. 2.5d).

To quantify this, we took averages of several kinematic measures for each animal's successful trials at the maximum required hold duration. The first of these was the amplitude of the pull (i.e. the distance the lever is pulled backwards). A larger average pull amplitude was seen with increasing age (Age: $F_{2, 64} = 3.193$, $p = 0.0477$; Genotype: $F_{1, 64} = 2.798$, $p = 0.0993$; Interaction: $F_{2, 64} = 2.522$, $p = 0.0883$) with this effect largely driven by an age-related increase in the YAC128 mice (Fig. 2.5e). Post-hoc comparisons revealed a significant difference between WT and YAC128 mice in the 6-month-old ($p = 0.0418$; $n = 14$ WT, 9 YAC128), but not other age groups. During the subsequent 800 ms lever hold period, 6-month-old animals had a greater negative slope of their lever trajectory on average ($p = 0.0330$; $n = 14$ WT, 9 YAC128), reflecting a progressive release of the lever during the hold period (Age: $F_{2, 64} = 0.8329$, $p = 0.4395$; Genotype: $F_{1, 64} = 3.837$, $p = 0.0545$; Interaction: $F_{2, 64} = 6.309$, $p = 0.0032$) (Fig. 2.5f).

An interaction between age and genotype was also found in the average movement speed (Age: $F_{2, 64} = 1.188$, $p = 0.3113$; Genotype: $F_{1, 64} = 2.193$, $p = 0.1435$; Interaction: $F_{2, 64} = 3.381$, $p = 0.0402$) due to a WT-specific decrease in this measure across ages, however this was not significantly different in any individual age group (Fig. 2.5g).

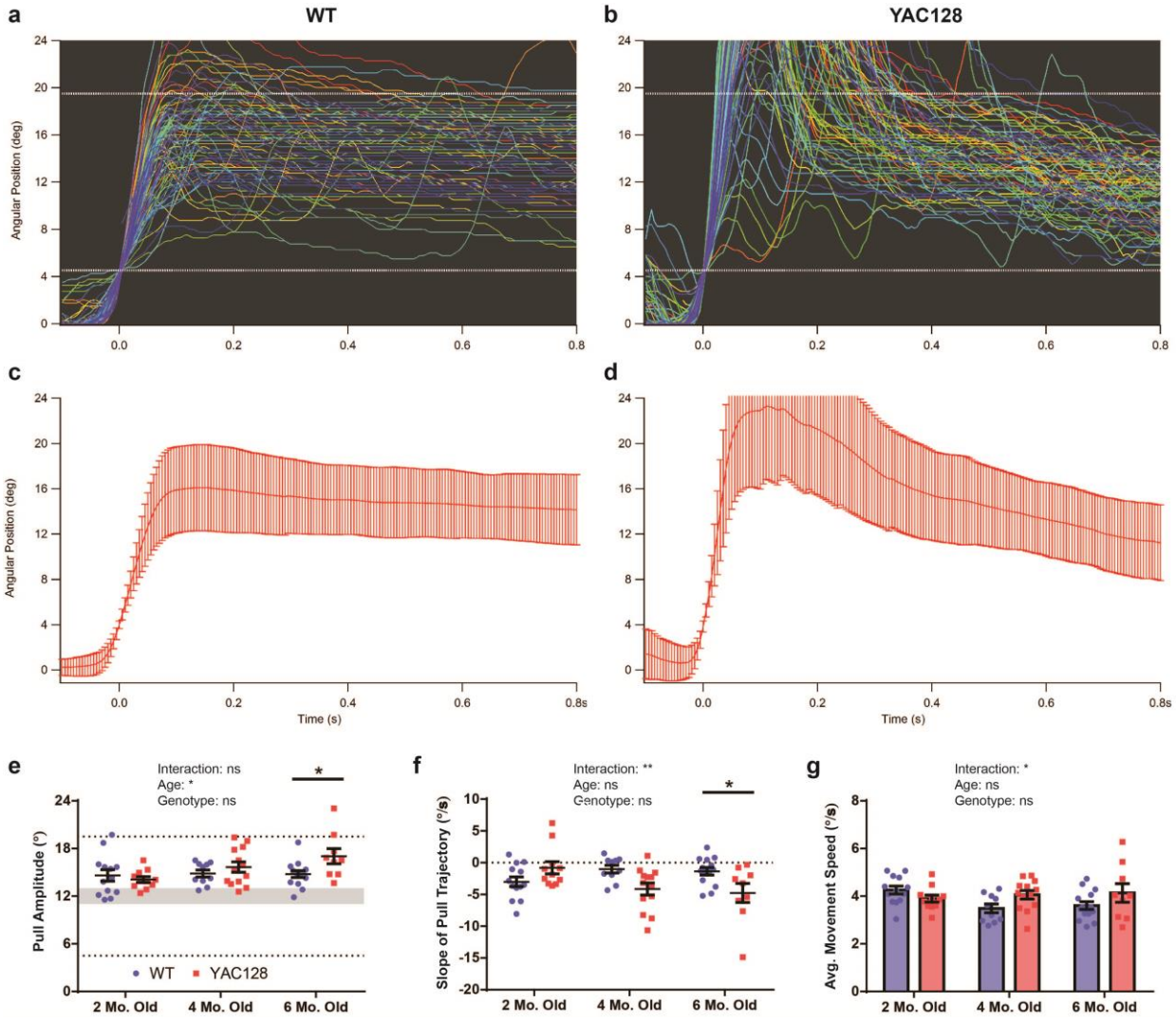

Figure 2.5 6-month-old YAC128 mice have kinematic differences from WT mice

(a-b) Lever position traces of 100 successful trials are shown for representative 6-month-old WT and YAC128 mice who reached the maximum required lever hold duration. A tendency to overshoot the goal zone (dotted white lines) is seen in this YAC128 animal. **(c-d)** Averaged lever position traces for the same

two animals (error bars represent standard deviation). **(e)** Average pull amplitude for all trials at the 800 ms hold duration is shown for WT and YAC128 animals. The shaded region represents the point at which a trial is initiated when pulled backwards (12° ± 1° from starting position), and the dotted lines represent the range it must be held within in order to receive a reward. 6-month-old YAC128 mice have a larger pull amplitude than WT animals of the same age, but no differences were seen at 2- and 4-months-old. **(f)** The average slope of the lever position trace from 200 to 800 ms after trial initiation was also calculated. An interaction between age and genotype was observed, and 6-month-old YAC128 animals had a larger negative slope on average, indicating a progressive release of their hold on the lever. **(g)** The average movement speed over all trials at maximum hold duration. Although a significant interaction effect was seen, post-hoc testing found no genotype differences in any of the age groups. Numbers of animals (WT/YAC128) used for analysis are n = 13/11 at 2-months-old, n = 10/13 at 4-months-old and n = 14/9 at 6-months-old. *: $p < 0.5$; **: $p < 0.01$; ns: not significant.

2.4 Discussion

In this chapter, I made use of a fully automated home-cage behavioural testing system to investigate motor learning and movement kinematics in a transgenic mouse model of Huntington's disease. I found that YAC128 HD mice display circadian and motor abnormalities at different time points, although interestingly, some of these deficits did not progress with age as expected.

The first of these observed differences was that a larger proportion of YAC128 animals overall failed to reach the task performance criteria in our first phase of testing. One possibility is that this genotype difference is due to a failure to learn the association between the lever and water reward. Several papers have reported operant learning deficits in both YAC128 (Brooks, Jones, et al., 2012b) and knock-in mouse models of HD (Trueman et al., 2007, 2008; Yhnell et al., 2016b), supporting this theory. However, the majority of these deficits were related to accuracy and reaction time and impaired task acquisition was generally not observed, making this somewhat less likely. A second possibility is that these animals were capable of learning the

response-outcome contingency but had reduced motivation to work for access to water. Animals tested in the lever-cage received a minimal amount of water (approximately 1 mL per day) simply by entering the testing module. However, this is much less than the ~3 mL per day that wildtype FVB/N and YAC128 mice consume when allowed *ad libitum* water access (Pouladi et al., 2009), and is equivalent to what is typically given on a water restriction protocol (Guo et al., 2014). A depressive phenotype has previously been reported in YAC128 animals when tested on forced swim and sucrose preference tests (Pouladi et al., 2009, 2012), and so the failure of some animals to perform the task could be a reflection of these affective changes. This would be supported by the lack of age-related effects on this measure, as depressive and anhedonic phenotypes were not found to be progressive in these previous reports. Additionally, apathy, lack of motivation and depression are commonly reported in HD patients, and can occur long before the onset of motor symptoms (Kirkwood et al., 2001; Paulsen et al., 2001).

Weight fluctuations were observed in some animals during the first week of testing, especially in the 6-month-old group. However, all animals (with the exception of one 6-month-old YAC128 mouse) adapted to the restriction in water access and returned to within 5% of baseline weight by the end of testing (at minimum), suggesting that the change in *ad libitum* water access was well tolerated. The observed weight loss in older animals may reflect this group having the highest baseline weight, and consequently highest dietary requirements for weight maintenance. In contrast, 2-month-old mice, and 4-month-old YAC128 mice, continued to grow during the testing period. Younger animals also tended to perform more trials, and consequently received more water, in comparison to older animals. As 2-month-old mice have a higher growth rate as compared to older animals, the increased task performance observed at this age may

reflect a higher level of motivation for water as compared to the older group (The Jackson Laboratory, n.d.).

Differences were also observed between YAC128 and WT mice in the circadian distribution of trials. YAC128 mice performed more of their trials during the light phase overall, and subdividing trials into one-hour bins revealed distinct circadian irregularities specifically in the 4- and 6-month-old mice. While WT mice at these time points tended to have a very low percentage of their trials in the hours leading up to the start of the dark phase, YAC128 mice began to increase their performance of the task three to four hours before this point. Furthermore, WT animals maintained a high performance rate over the first six hours of the dark phase, whereas YAC128 mice began to decrease in their performance rate in the third hour. Circadian disruptions have been reported in HD patients (Morton et al., 2005), as well as in several mouse models of HD, including R6/2, BACHD and Q175 (Kudo et al., 2011; Loh et al., 2013; Morton et al., 2005; Oakeshott et al., 2011). However, similar changes in circadian activity patterns have not previously been reported for YAC128 mice. Similar to results published with other genetic lines, this appears to be a progressive phenotype and was not observed in the 2-month-old animals. Although our task does not give a direct measure of overall activity level or locomotion, trial distribution through the day seems to provide a good proxy measure for this, and further confirms the disruptions observed in other genetic models.

In the testing phase, the success requirements of the task changed incrementally, and animals were required to modify their motor response. The majority of animals were able to adapt to these changes in task requirements and progressed quickly to the maximum required lever hold duration. However, 2-month-old YAC128 mice had a slower average progression through the levels of the task as compared to WT mice. This was not due to difficulties with the

physical demands of the task, as these 2-month-old animals showed no kinematic abnormalities and a similar percentage of them reached the maximum hold duration. Rather, this deficit may reflect a persistence in using the previously learned strategy instead of adapting their behaviour to meet the new requirements. The observation of a motor learning deficit is not surprising in itself, as YAC128 mice as young as 2-months-old have previously been found to have slower learning on a fixed speed rotarod task (Van Raamsdonk et al., 2005). A mild reversal learning deficit was also seen at 2-months-old in the water T-maze, with more robust effects seen in animals at 8.5-months-old and older (Brooks et al., 2012; Van Raamsdonk et al., 2005), and our results could also be a reflection of impaired behavioural flexibility. However, what is more surprising is that the 4- and 6-month-old YAC128 mice did not show a similar impairment. One possibility is that this effect was driven by variance between cohorts of mice, and the animals we used for testing at 2-months-old had a stronger behavioural phenotype due to environmental or epigenetic factors. However, given that all mice used for testing were bred and aged in an ongoing manner and did not come from separate starting pools of animals, this seems less likely. In addition, the data for 2-month-old animals was acquired over an extended period (~18 months) and deficits were observed in animals tested both early and late in testing. Still, given that these results are unexpected in the context of the existing literature, it would be worthwhile to repeat this study with an additional cohort of 2-month-old animals to confirm this finding.

Interestingly, several other phenotypes reported in young YAC128 mice have been seen to normalize to WT levels at later time points. For example, YAC128 animals display an early hyperkinetic phenotype in locomotor activity at 3-months-old, before later decreasing in their open field activity to WT levels by 6-months-old (Slow et al., 2003). At a physiological level, an early increase in the frequency of spontaneous excitatory post-synaptic currents (sEPSCs) has

been reported in dopamine D1R-expressing MSNs of YAC128 mice at 1.5 months of age, however this is reduced to WT levels in 6-month-old animals (André, Cepeda, et al., 2011). Furthermore, modulation of spontaneous activity by D1R activation was found to be lost in acute striatal slices from YAC128 mice at 1.5 months-old but restored at 6-months-old (André, Cepeda, et al., 2011). D1R function in direct pathway MSNs is an important regulator of synaptic plasticity (Kreitzer & Malenka, 2008), and it's possible that the motor learning deficit we observe is linked to over-activation and loss of synaptic plasticity at these striatal inputs. The presence of these early and transient phenotypes in HD mice suggests that multiple parallel pathophysiological processes may underlie the progression of motor phenotypes in HD. One possibility is that the behavioural changes observed in young HD mice are a direct effect of the huntingtin mutation which is later compensated for during the early disease progression. Alternatively, behavioural phenotypes might be caused by an early compensatory process, and failure of compensation at later stages results in apparent normalization of the behaviour. In either case, this suggests that separate and independent processes, as well as eventual neurodegeneration, may cause the slower and progressive development of cognitive and motor phenotypes observed in older (>4-months-old) YAC128 mice.

In addition to assessing motor learning, a second objective was to investigate the possibility of task-related kinematic abnormalities in YAC128 mice. Mild motor deficits have previously been observed in 5- to 6-month-old YAC128 mice on the rotarod, horizontal ladder and narrow beam tests (Di Pardo et al., 2012; Van Raamsdonk et al., 2005). However, assessments of skilled motor performance, such as reach-to-grasp and lever-pulling tests, have been infrequently used in genetic models of neurodegenerative disorders. Kinematic analysis of HD models has been primarily focused on gait abnormalities, although these are subtle in the

YAC128 model and have only been observed in animals over 1-year-old (Chen et al., 2011). In our task, we found that 6-month-old YAC128 animals displayed several irregularities as compared to WT animals in the testing phase. Specifically, many animals used a distinctive 'overshoot and release' strategy in order to meet the task requirements. It seems possible from this behaviour that these animals are compensating for a lack of control, and have difficulty stopping their movement and holding the lever steady within the required region. This phenotype may reflect motor impersistence, a common movement abnormality seen in patients with HD which is characterized by an inability to maintain a constant strength during muscle contractions (F. O. Walker, 2007). Motor impersistence is seen in nearly all HD patients, and unlike other primary motor symptoms (such as chorea) it is typically linearly progressive with the disease course (Reilmann et al., 2001). The observed 'overshooting' may also reflect an impaired ability to terminating movements at the appropriate time, comparable to reaching deficits observed in pre-symptomatic HD patients (Smith et al., 2000).

In summary, I found that young YAC128 HD mice had abnormalities in the learning and performance of a task that required them to pull and hold a lever in a certain position range in order to receive water drops. I also analyzed patterns of task engagement through the light/dark cycle and found progressive circadian abnormalities in YAC128 mice, a phenotype seen in other mouse models of HD as well as in patients. These results lend support to the usefulness of a home-cage based behavioural task for the high-throughput identification of phenotypes in mouse models of HD.

Chapter 3: Q175-FDN HD mice have impaired motor learning and altered training-associated striatal plasticity in the PiPaw home-cage task

3.1 Introduction

As demonstrated in Chapter 2, home-cage testing systems can offer a number of benefits over traditional behavioural paradigms used in disease research. By assessing mice on a self-paced task within their own home environment, the exposure of mice to handling and other stressors is significantly reduced, and animals are given a greater deal of control over their interactions with the task. This allows learning to progress in a more naturalistic and self-directed fashion and facilitates the collection of detailed longitudinal datasets about the refinement of task performance over time. In addition, home-cage testing permits the assessment of more difficult tasks than would be possible if the animal was only given a short amount of time each day to practice.

Despite these benefits, however, interpreting the results of the previous study was sometimes difficult. For example, many 6-month-old YAC128 mice were seen to overshoot the goal range and then slowly move the lever back towards the start position in order to reach the required hold duration. One interpretation of this finding is that these mice had difficulty terminating their pull at the appropriate time, comparable to difficulties with terminating reaching movements observed in pre-symptomatic HD patients (Smith et al., 2000). Another possibility is that mice were overshooting in order to compensate for an inability to hold the lever steady within the hold-range. However, regardless of the reason, these animals displayed normal motor learning as the parameters of the task were permissive to this strategy. If these overshot trials had not been rewarded, it is unclear whether the YAC128 mice would have

adjusted their strategy appropriately or if a motor deficit would have prevented them from doing so. As such, it's difficult to know whether this reflects a motor control deficit *per se*, or simply an alternative strategy employed by some animals.

In young (2-month-old) animals, YAC128 mice were slower to increase their hold duration and advance through the task as compared to WT littermates but did not have any kinematic differences at the maximum hold-duration. This may reflect a deficit in responding to changes in reward contingency (i.e. related to behavioural flexibility and motor learning) but could perhaps also indicate that the animals developed a different strategy in training (e.g. shorter duration pulls) that was more difficult to adjust in the second phase of testing. As this deficit was transient, it's also not clear that this would be a relevant phenotype for use as an outcome measure in drug treatment studies. Another difficulty in comparing the performance of animals was related to the progressive nature of the task. Cross-sectional comparisons of success rate and kinematics were difficult to perform, as animals often had different hold-duration requirements from each other on any given day. This could limit the design of drug treatment studies using this system, as there are few discrete outcome measures that could be consistently compared between animals at specific time-points. Furthermore, without a clear understanding of what the observed deficits indicate with regards to motor function, the reversal of a specific impairment with a drug treatment might be difficult to interpret and lack predictive validity.

To address these concerns, I sought to both improve the design of the home-cage system and to create a new testing methodology that would provide a simpler assessment of motor learning and forelimb kinematics in mouse models of HD. Several additions were made to the system, including a nose-poke port to ensure that trials were performed consistently with the forelimb, as well as a piezo buzzer to provide auditory stimuli and a camera to film trials. The

lever was also coupled to a motor in order to provide a constant level of resistance during lever-pull trials and enforce a time-out period between trials. The testing methodology was altered such that mice no longer had to hold the lever for an increasing amount of time, but rather had to pull the lever back with a specific amplitude in order to receive water drop rewards. Once each mouse had started the main phase of testing, the success requirements stayed constant and ability to learn and perform the task was assessed.

Once developed and tested, I used this improved home-cage system ('PiPaw') to investigate motor phenotypes in the YAC128 transgenic mouse, as well as the Q175-FDN knock-in model of HD. The Q175-FDN mouse is a full-length knock-in model with high face validity that displays a neuropathological and symptomatic progression very similar to what is seen in human HD patients (Southwell et al., 2016). Of the knock-in models, it also has the earliest onset of motor symptoms (~8 months-old), increasing its usefulness for pre-clinical studies. In addition to studying forelimb motor learning in WT and HD mice, I also wanted to determine if training on the task resulted in changes in the activity or plasticity of striatal MSNs. Previous studies have found that motor learning is associated with changes in the activity of both cortical inputs to the DLS (Kupferschmidt et al., 2017) and DLS-MSNs themselves (Giordano et al., 2018; Koralek et al., 2013; Santos et al., 2015; Yin et al., 2009), and requires the expression of NMDA receptors at cortico-striatal synapses (Lambot et al., 2016). Given that altered plasticity of striatal MSNs has been reported in both YAC128 and Q175-FDN mice (Glangetas et al., 2020; Sepers et al., 2018), observed motor learning deficits in these models may be related to deficits in the ability of cortico-striatal connections to change their synaptic strength.

3.2 Methods

3.2.1 Animals

All experiments were conducted using heterozygous YAC128 line 53 transgenic mice (Slow et al., 2003) and heterozygous Q175-FDN knock-in mice (Southwell et al., 2016), both on the FVB/N genetic background. All mice were male, and wildtype littermates of these animals were used as controls. Initially, both male and female mice were planned for use in these experiments; however, as we only had a small room to house the PiPaw cages and were concerned about behavioural testing and housing of male and female mice in close proximity, we decided to use only male mice for this phase of the project. YAC128 mice were assessed in the PiPaw task beginning at either 2-months-old (60 ± 10 days) or 10-months-old (300 ± 10 days). Q175-FDN mice were assessed in the PiPaw task beginning at 10- to 11-months-old (310 ± 20 days). Additional cohorts of YAC128 and Q175-FDN mice were used at 10- to 11-months-old (310 ± 20 days) for rotarod and open field testing. For the sake of simplicity, mice tested between 10- and 11-months old will be referred to as ’10-months-old’ in this chapter. A total of 99 YAC128 mice and 66 Q175-FDN mice were used for experiments, including WT littermates. Animals were housed on a 12/12 h light/dark cycle in a temperature and humidity-controlled room. Mice were provided with free access to chow and standard environmental enrichment within the cage (bedding, hut, PVC tube) throughout testing. Mice were handled by the experimenter on at least two occasions for 2-3 minutes per animal prior to any surgery or behavioural testing. Animal tissue was collected via ear clipping at weaning, and DNA extraction and PCR analysis was subsequently used to determine genotype. All procedures were carried out in accordance with the Canadian Council on Animal Care and approved by the University of British Columbia Committee on Animal Care.

3.2.2 RFID capsule implantation

RFID capsule implantation was performed as described in Chapter 2.2.2. Animals were allowed to recover for a minimum of one week following surgery before behavioural testing.

3.2.3 PiPaw testing

3.2.3.1 Hardware and software

The PiPaw system was developed based on the design of the original home-cage behavioural testing system described in Chapter 2 and retained a similar general design but with a number of important changes. An opening was created on one side of a regular mouse home-cage to allow mice to access a separate enclosed chamber (the 'testing module') (Fig. 3.1a-b). This module was 3D-printed from black PLA filament (MakerBot MP05775), apart from the floor which was made from a separate glass piece. At the opposite end of the module from the entrance, a nose-poke port accessed a water spout, which delivered drops using the same valve-based system described in Chapter 2.2.3. An infrared break-beam sensor (Adafruit 2168) was positioned adjacent to the port to detect nose-pokes. The ceiling at this end of the chamber was raised to allow mice to sit back on their hind-legs and more easily reach the nose-poke port (which was also slightly elevated). An RFID antenna and reader (Sparkfun SEN-11828) were inset into the ceiling in order to detect and identify animals, as in the previous system. On the right wall of the chamber adjacent to and slightly below the nose poke port, a lever extended ~1cm into the chamber. This lever was moveable on a horizontal axis with a range of 30° and was positioned such that the mouse's right forelimb would naturally rest on it when nose-poking.

On the left side of the chamber opposite the lever, a small ledge allowed the mouse to support themselves on their left forelimb while nose-poking and grasping the lever.

a

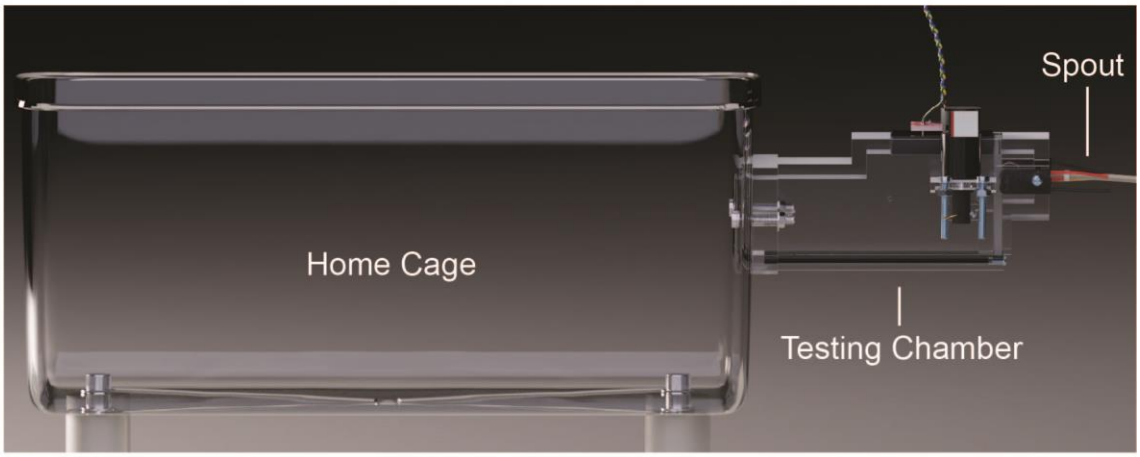

b

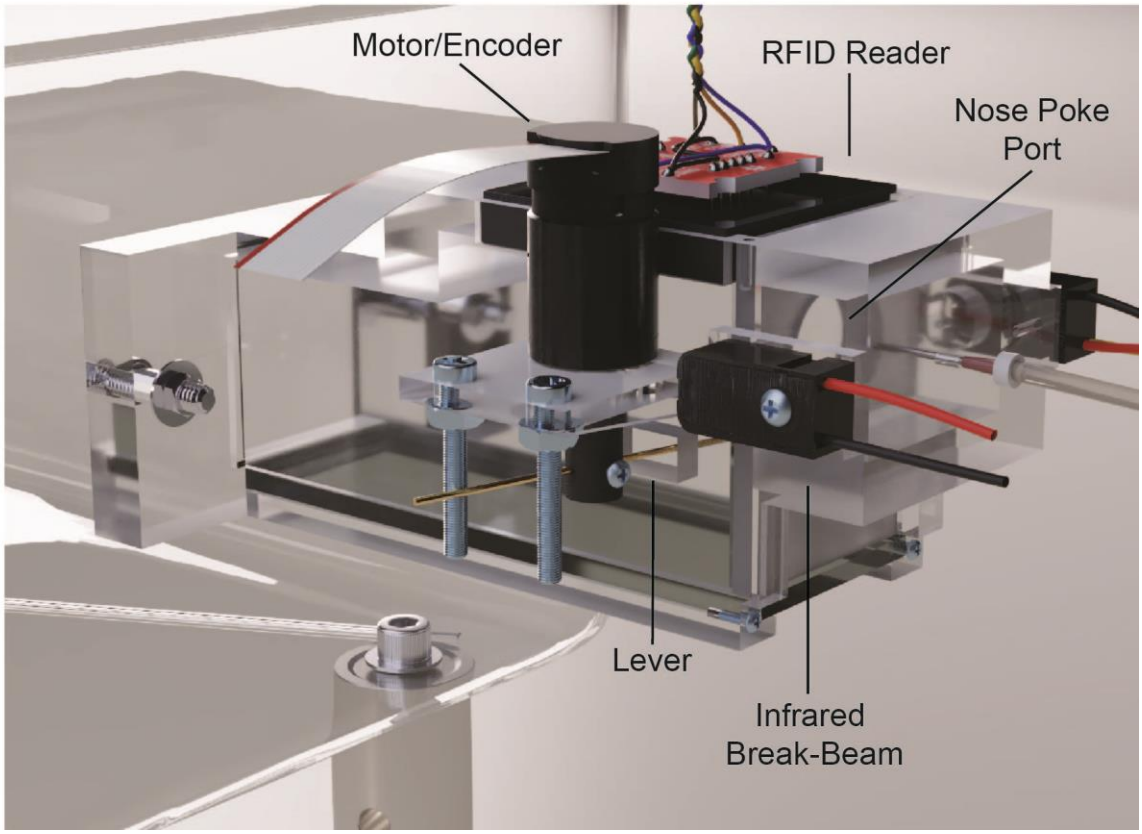

Figure 3.1 The PiPaw home-cage system

(a-b) A small testing chamber was accessible from the mouse home-cage containing a nose-poke port and spout which delivered water drop rewards. An RFID reader would detect and identify animals upon entrance into the chamber and load the appropriate testing parameters. A lever extended into the chamber which was moveable on a horizontal axis within a position range of 30°. This lever was coupled to a combined motor/encoder in order to provide a constant force on the lever and to measure lever position during trials. In order to perform a trial, the mouse first had to nose-poke and then pull the lever back to a specific position range using their right forelimb.

Instead of the counterweight used in the previous system, the lever was coupled to a DC micro-motor, providing much better control over the resistance applied to the lever. This motor was controlled by a motor control board (Maxon 466023) running in current control mode. This control setting maintains a fixed torque regardless of any external force applied to the rotor, meaning that the force required to move the lever remained steady as it was pulled backwards. The torque was controlled via a pulse-width modulation (PWM) signal and was set to one of two levels: a 'low-force' condition when a mouse was performing a trial, and a 'high-force' condition at all other times (e.g. during the time-out between trials). The torque applied during the low-force condition was extremely low – essentially the minimum required to overcome the friction of the rotor and return the lever back to its start position after it was pulled backwards. In contrast, the 'high-force' condition was strong enough to prevent the mice from pulling the lever with their forelimb before the next trial was permitted to begin.

Initially, a 15mm micro-motor (Faulhaber 1524T012SR) was used for experiments. However, this was later replaced by a 22mm motor (Faulhaber 2224U012SR), as the larger motor had a higher rated torque and was better able to hold the lever in place between trials (i.e. in the high-force condition). In the low-force condition, the torque was identical for both motors,

ensuring that the required pull force during trials was the same. One consequence of using the larger motor was that it had to be mounted slightly further away from the testing module, and consequently there was a greater distance from the end of the lever to the coupler. As a result, the absolute size of each degree of rotation at the end of the lever was larger with the large motor as compared to the small motor. In order to compensate for this and maintain the same arc length of lever movement between the two motors, the size of the lever range was decreased to 24° from 30° for all cages tested with the large motor (all sub-ranges were scaled proportionately as well). During analysis, all lever position data for animals tested with the large motor was scaled by a factor of 1.25× in order to normalize the data to the 30° range used with the small motor. No differences in pull kinematics or learning were seen between cohorts tested in cages with the two different motors.

The motor was coupled to a high resolution (4096 lines per revolution) incremental encoder (Faulhaber IEH2-4096) to allow for accurate measurement and recording of all lever movements. Lever positions during each trial were collected at 200 Hz and recorded to text files for each mouse. In addition, a camera (Waveshare 10299) was mounted below the chamber and recorded a bottom-up video of each trial through the glass floor. A piezo buzzer (Adafruit 1739) was attached to one side of the chamber and delivered auditory stimuli to indicate trial initiation, success and failure. The cage and attached testing module were attached to aluminum spacers (Siskiyou AS-2.00) mounted on a polycarbonate sheet. All components were connected to a breakout board and controlled by custom software running on a Raspberry Pi 3B micro-computer. This software was written in Python 3 and ran continuously during testing. Eight PiPaw systems were constructed and used to perform the experiments in this chapter.

3.2.3.2 Behavioural methodology

Small groups of littermate mice (1-4 animals) were introduced to the cage and allowed to explore and discover the attached testing module. As in Aim 1, the number of animals tested in each cage was determined by litter size at birth. Cages were typically mixed genotype, although a small number contained only WT or HD mice. *Ad libitum* water bottle access was removed, so that water could only be retrieved by interacting with the behavioural task. Upon entering the module, the mouse was detected by the RFID reader and the motor switched to the high-force condition in order to hold the lever in the 'start position' until the trial was allowed to begin. In order to initiate a trial, the mouse had to nose-poke at the port and remain in position for a short waiting period (1 s). Following this, the motor switched to the low-force condition and a short tone was played (1200 Hz, 0.1 s) to signal that a trial could begin. The mouse could then initiate a trial by pulling the lever backwards out of the 'threshold' position range (0° to 3°). If the mouse removed their head prior to initiating a trial, the motor would switch back to the high-force condition and the trial would be cancelled. Once a trial was initiated, it could end in one of two ways – either the lever would be returned back to the start position, or the trial time limit of 2 s would be reached. After the trial was ended, the motor would return to the high torque condition and a 5 s timeout would begin until the mouse was permitted to perform another trial. If the trial was successful, a 20 µL water drop would be delivered by the spout and two high tones would play (2400 Hz, 2×0.2 s). If the trial was failed, no water would be delivered, and two low tones would play (400 Hz 2×0.2 s).

Testing was split into three phases which each mouse completed sequentially, each animal advancing at their own pace. The rewarded lever position range in each of these phases was different, becoming progressively more difficult as the animal learned the task. In the first

phase (Training 1) the mouse acquired the simple operant behaviour of nose-poking and simultaneously pulling the lever with their right forelimb. In this phase, mice could receive a water drop on a fixed-interval 10-minute schedule simply for nose-poking (i.e. maximum one water drop every 10 minutes). To receive additional drops, they had to pull the lever past the threshold range and return it to the start position (either intentionally or simply by letting go of it) within the 2 s trial time limit (Fig. 3.2a). A trial could only be failed by holding the lever too long, encouraging mice to perform short movements. Once a mouse reached 100 successful trials in this phase, they were advanced to Training 2. In this phase, mice no longer received water drops simply for nose poking, and had to pull the lever past the 8° mark in order to meet the task success requirements (Fig. 3.2b). After 100 successful trials in this phase, mice were moved on to the main Testing phase.

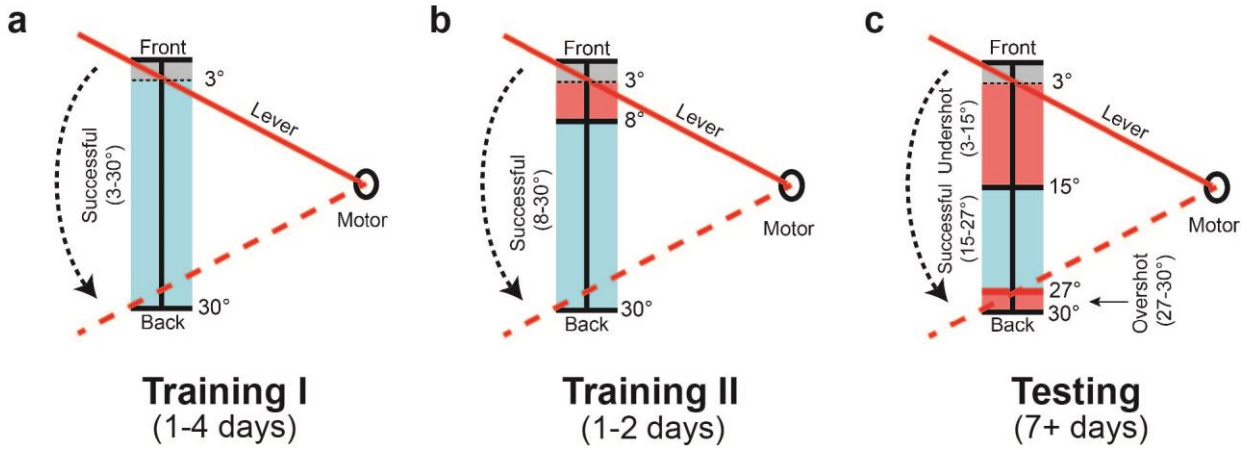

Figure 3.2 Rewarded lever position ranges during the three phases of PiPaw testing
(a) The lever is held in its starting position at the front of the lever position range by the motor until a trial is initiated. In all testing phases, the mouse initiates a trial by pulling the lever backwards out of the threshold range (0-3°, shown in grey). In the first Training phase, a water drop is given for all trials, regardless of pull amplitude, as long as the lever is returned back to the start position within the trial time limit (2 s). **(b)** In the second Training phase, the rewarded lever position range narrows slightly to

between 8° and 30°. If the amplitude of the pull (i.e. maximum position of the lever during the trial) is less than 8°, the trial is not rewarded. **(c)** In the main Testing phase, the rewarded lever position range narrows to between 15° and 27° (shown in blue). If the amplitude of the pull is less than 15° (undershot) or greater than 27° (overshot), the trial is not rewarded.

In the Testing phase, the rewarded position range was narrowed to between 15° and 27° of the full 30° lever position range (Fig. 3.2c). In order for a trial to be successful, the amplitude of the pull (i.e. the maximum position of the lever during the trial) had to fall within this success range. If the lever went past 27°, the trial was 'overshot' and if the lever did not reach 15° it was 'undershot'. In both cases, the trial was considered failed and no water was delivered. As in Training 1 and 2, if the lever was held for longer than 2 s, the trial was also failed. This task remained the same for the remainder of the Testing period, and the ability to learn to pull the lever to this sub-range was assessed. Mice remained in the Testing phase for a variable amount of time, but all animals used for analysis were assessed for at least one week. In all phases, when the lever entered the 'success range' (i.e. when it passed 3° in Training 1, 8° in Training 2 or 15° in Testing), a short high tone was played (2400 Hz, 0.1 s). In the Testing phase, if the mouse pulled the lever all the way back past the far end of the success range (27°) into the overshot range, a short low tone was played (400 Hz, 0.1s). These tones served to reinforce the location of the success range within the full lever position range.

3.2.3.3 Data analysis

All data were automatically recorded to text files by the PiPaw software and was extracted and analyzed using custom scripts written in Python 3. Prior to analysis, lever position data were 'cleaned' in order to remove trials with abnormally high timestamps, low lever

position readings or trials with 2 or fewer total position readings. This cleaning resulted in the removal of only a very small number of trials (~0.1%). In order to perform daily analysis of performance and kinematic measures in the first week, trials were grouped into 24-hour bins from the time that the animal was switched to the main Testing phase. These bins were used to calculate mean values for kinematic measures, as well as inter-trial variability of those kinematic measures.

In order to define 'bouts' of trials, an average trial rate was calculated second-to-second with a 3-minute sliding window across the full period of testing for all animals. When this average trial rate went above 1.333 trials/min (corresponding to >4 trials in the 3-minute window), all trials in the window were grouped into a bout and the bout continued for as long as the trial rate stayed above this value. This threshold value of 1.333 trials/min was calculated by determining the trial rate at every second of testing for all WT mice at either 2-months-old or 10-months-old and taking the 95^{th} percentile value of these trial rates. This value was determined to be the same for mice in the two age groups. Average values for trials and bouts (e.g. trials per day, trials per bout) were assessed over the first full week in the main Testing phase. To calculate average trial-wise success rate over the bout, all bouts with at least 12 trials were collected for each animal and first averaged for each trial position within animals, and then averaged across animals. Circadian activity levels were assessed over the full period of testing (including Training and Testing phases) for all animals.

Two main exclusion criteria were used to remove animals from analysis. The first was the removal of animals that used a non-standard pull strategy (i.e. did not pull consistently with their right forelimb), as the use of a different strategy could be a confounding factor for kinematic analysis. In order to assess this, 50 videos were randomly selected from all trial videos

for each animal and manually scored to determine if the mouse had pulled the lever with their right forelimb, left forelimb, both forelimbs, or undetermined. Mice that had greater than 3/50 videos scored as left or both forelimbs were excluded from analysis. No significant genotype differences were seen in the number of animals using a non-standard pull strategy. In the 2-month-old group, seven animals (3 WT / 4 YAC128) were removed, while in the 10-month-old group, thirteen mice were removed (4 WT / 3 YAC128 / 6 Q175-FDN) due to a non-standard pull strategy. Animals were also removed if they did not have seven full days of assessment in the main Testing phase (4 animals total between all groups). In addition, one mouse could not be properly genotyped and was excluded. For 10-month-old animals, WT controls from the YAC128 and Q175-FDN experiments were combined together for all analyses, as these mice are from the same genetic background and displayed similar learning and performance of the task. In total, 27 mice were used for PiPaw analysis at 2-months-old (13 WT / 14 YAC128) and 56 mice at 10-months-old (27 WT / 15 YAC128 / 14 Q175-FDN).

3.2.4 Accelerating rotarod test

In the rotarod test, a mouse is placed on a rotating rod and must balance themselves and run on top of the rod in order to prevent themselves from falling. On each trial, the rotarod (Ugo Basile, Italy) accelerated from 5 to 40 RPM over the course of 300 s, and the latency for each mouse to fall from the rotarod was noted. If the mouse performed a complete rotation holding onto the rod, this was also treated as a fall and the trial was ended. If the mouse reached the maximum allowed time, the trial was ended and scored as 300 s. The rotarod was wiped with ethanol between each mouse. Testing was performed at the same time on each day during the light phase of the light/dark cycle. Each mouse performed 3 trials per day on each of 4

consecutive days, with a one-hour inter-trial interval. Latency to fall off the rotarod on the three trials each day was averaged for each mouse to obtain a daily average.

3.2.5 Open field test

Mice were placed one at a time in the corner of an open-top clear acrylic box (48 × 38 cm) under bright lighting and were allowed to explore for 10 minutes. The box was wiped down with ethanol between animals. Testing was performed during the light phase of the light/dark cycle. Open field activity was recorded by a camera mounted above the box and distance travelled was analyzed using Ethowatcher (Crispim Junior et al., 2012).

3.2.6 Electrophysiology

Slice electrophysiology experiments were performed on YAC128 and Q175-FDN mice as well as wildtype littermates. Animals were split into two cohorts on the basis of whether they had been tested in the PiPaw system or not – a 'trained' group and a 'naïve' group. Animals in the naïve group had been previously used for rotarod and open field behavioural testing but had not undergone testing on the PiPaw task. Animals in the trained group were used for slice experiments immediately following the end of PiPaw testing.

3.2.6.1 Slice preparation

Animals were anesthetized with isoflurane and decapitated. The brain was rapidly removed and bisected along the midline, separating the two hemispheres. Acute left- and right-hemisphere sagittal slices (250-300 μm) containing the dorsal striatum were cut using a vibratome (Leica VT1000) in ice-cold artificial cerebrospinal fluid (aCSF), before being

transferred to a holding chamber containing aCSF at 37° for 30 minutes. Slices were then maintained in aCSF at room temperature for at least 30 minutes for whole-cell experiments, or 1 hour for extracellular experiments. All aCSF contained the following (in mM): 125 NaCl, 2.5 KCl, 25 $NaHCO_3$, 1.25 NaH_2PO_4 and 10 glucose. In addition, aCSF used for cutting slices contained 0.5mM $CaCl_2$ and 2.5mM $MgCl_2$, while all other aCSF contained 2mM $CaCl_2$ and 1mM $MgCl_2$. The pH of aCSF was 7.3-7.4 and osmolarity was 310 (±3) Osm/L. aCSF was continuously oxygenated with carbogen (95% O_2/5% CO_2) during slicing, recovery and all experiments. Once transferred to the recording chamber, slices were continuously superfused with room temperature aCSF containing picrotoxin (50µM; Tocris Bioscience) to block $GABA_A$ receptors and minimize inhibitory responses. Slices were allowed to equilibrate in the recording chamber for at least 20 minutes before the start of recording.

3.2.6.2 Extracellular recordings

To record field excitatory postsynaptic potentials (fEPSPs), a glass recording micropipette electrode filled with aCSF was placed in the dorsolateral striatum and a second glass micropipette stimulating electrode was placed 300-500 µm dorsal to this. This pipette delivered test stimuli every 15 seconds and stimulation intensity was set at a level to evoke a robust sub-maximal response at the recording pipette (60-300 µA for 100 µs duration). Each run included two stimuli separated by 50 ms so that paired-pulse ratio (PPR) could be assessed. Data were acquired with a Multiclamp900 amplifier and Clampex 11.1 (Molecular Devices) software, sampled at 100 kHz and filtered at 1 kHz. Responses were recorded for at least 10 minutes to ensure that the fEPSP amplitude was stable before applying a high-frequency stimulation (HFS) protocol to evoke depression or potentiation of fEPSPs. This HFS consisted of four 100 Hz

stimulation trains of 1 second each, separated by a 10 second interval. The stimulation intensity during these trains was the same as used for the test stimuli. fEPSPs were recorded for 40 minutes following HFS to determine the response of striatal field responses to this stimulation protocol. The amplitude of fEPSPs during the 5 minutes prior to HFS were averaged to obtain a baseline response size and this was compared to fEPSP amplitude in the response period. Average response to HFS was calculated as the average of responses in the time period 30-35 minutes after the application of HFS. PPR was calculated as the ratio of the amplitude of the second pulse to the first pulse on each run, and was averaged over the 5 minutes prior to HFS, and 30-35 minutes post-HFS and compared.

3.2.6.3 Whole-cell voltage-clamp

Intracellular recordings were made using a whole-cell patch clamp technique and were acquired with an Axopatch-700A amplifier and pClamp 11 software, digitized at 20kHz and filtered at 1 kHz. Pipettes (3-5Ω) were pulled from borosilicate glass capillaries using a micropipette puller (Narishige International). The intracellular solution was cesium-based and contained the following in mM: 130 cesium methanesulfonate, 5 CsCl, 4 NaCl, 1 $MgCl_2$, 5 EGTA, 10 HEPES, 5 QX-314 chloride, 5 MgATP, 0.5 MgGTP and 10 sodium phosphocreatine. The pH of intracellular solution was 7.2-7.3 and the osmolarity was 290 (±3) mOsm/L. Cells were rejected and not recorded if series resistance was >17 MΩ. To record spontaneous excitatory post-synaptic currents (sEPSCs), cells were voltage-clamped at -70 mV. To record PPR, a glass micropipette electrode filled with aCSF was positioned ~200 µm dorsal to the recording site. The cell was voltage clamped at -70 mV with a 50 ms step to -80 mV every 30 s, and activity was elicited by injecting current through the stimulating electrode. Two pulses (100

μs duration) were administered with an inter-pulse interval of either 50, 100, 150, 200, 250, 300, 350 or 400 ms. Three runs were performed at each interval length and averaged, and the PPR at each interval was calculated as the ratio of the average response amplitude of the second pulse to the average response amplitude of the first pulse. Analysis of electrophysiology data was performed using Clampfit 10.7 (Molecular Devices).

3.2.7 Statistics

All statistical testing was performed with Prism 8 (GraphPad Software). Data are expressed as mean ± SEM unless otherwise specified. Alpha level for all tests was $p = 0.05$. For electrophysiology experiments, n = the number of slices (extracellular experiments) or neurons (whole-cell experiments) and the number of animals is given in brackets. For all other experiments, n = the number of animals. Repeated measures data with group comparisons (e.g. success rate over seven days for WT vs. YAC128) was analyzed with repeated measures two-way ANOVA to assess overall main and interaction effects. Sidak's multiple comparisons test was then used to compare between groups at each time-point (e.g. comparing success rate on D3 between WT and YAC128). Repeated measures data for a single group (e.g. comparing success rate across 7 days of testing for WT mice) was analyzed using repeated measures one-way ANOVA, or Friedman's test in the case of non-normally distributed data. Dunnett's test (or Dunn's test for non-normal data) was used following one-way or two-way ANOVA to compare within-group data on the first day to each subsequent day (e.g. comparing success rate on D1 vs. D7 for WT mice). To compare non-repeated measures data across three or more groups (e.g. open field distance travelled in WT/YAC128/Q175-FDN), one-way ANOVA was performed, followed by Tukey's test to compare pairs of groups to each other. To compare two groups on a

single measure, unpaired two-tailed t-tests were used when groups were normally distributed and had equal variances. If groups were found to have unequal variances using the F-test of equality of variances, Welch's t-test was used instead. If one or both groups was found to have a non-normal distribution using the D'Agostino & Pearson test, the Mann-Whitney test, a non-parametric alternative, was used. To compare paired data (e.g. success rate in bouts vs. non-bout trials), paired two-tailed t-tests were used.

3.3 Results

3.3.1 Mice learn the PiPaw task and organize their activity into short bouts of high task engagement

A cohort of mice (n = 13) were tested using the PiPaw system at 2-months-old in order to validate the new behavioural methodology and assess the ability of mice to acquire the task and improve over time. The majority of mice (~75%) successfully acquired the basic lever-pull response and progressed through the two Training phases and onto the Testing phase. In the Testing phase, the average success rate was initially quite low (19.0% ± 3.7% on day 1), but improved significantly over the course of one week, reaching 50.0% ± 2.6% by day 7 ($F_{6, 72}$ = 25.57, $p < 0.0001$) (Fig. 3.3a). This increase in success rate was associated with a concurrent decrease in the number of 'overshot' trials that were pulled past the far end of the success range ($F_{6, 72}$ = 7.204, $p < 0.0001$) as well as a decrease in the number of trials held for longer than the trial time limit of 2 seconds (χ^2 = 47.68, $p < 0.0001$) (Fig. 3.3a). In contrast, the number of 'undershot' trials where the lever failed to reach the success range did not change significantly over one week of testing ($F_{6, 72}$ = 1.186, p = 0.323), accounting for the largest proportion of failed trials across all days (Fig. 3.3a).

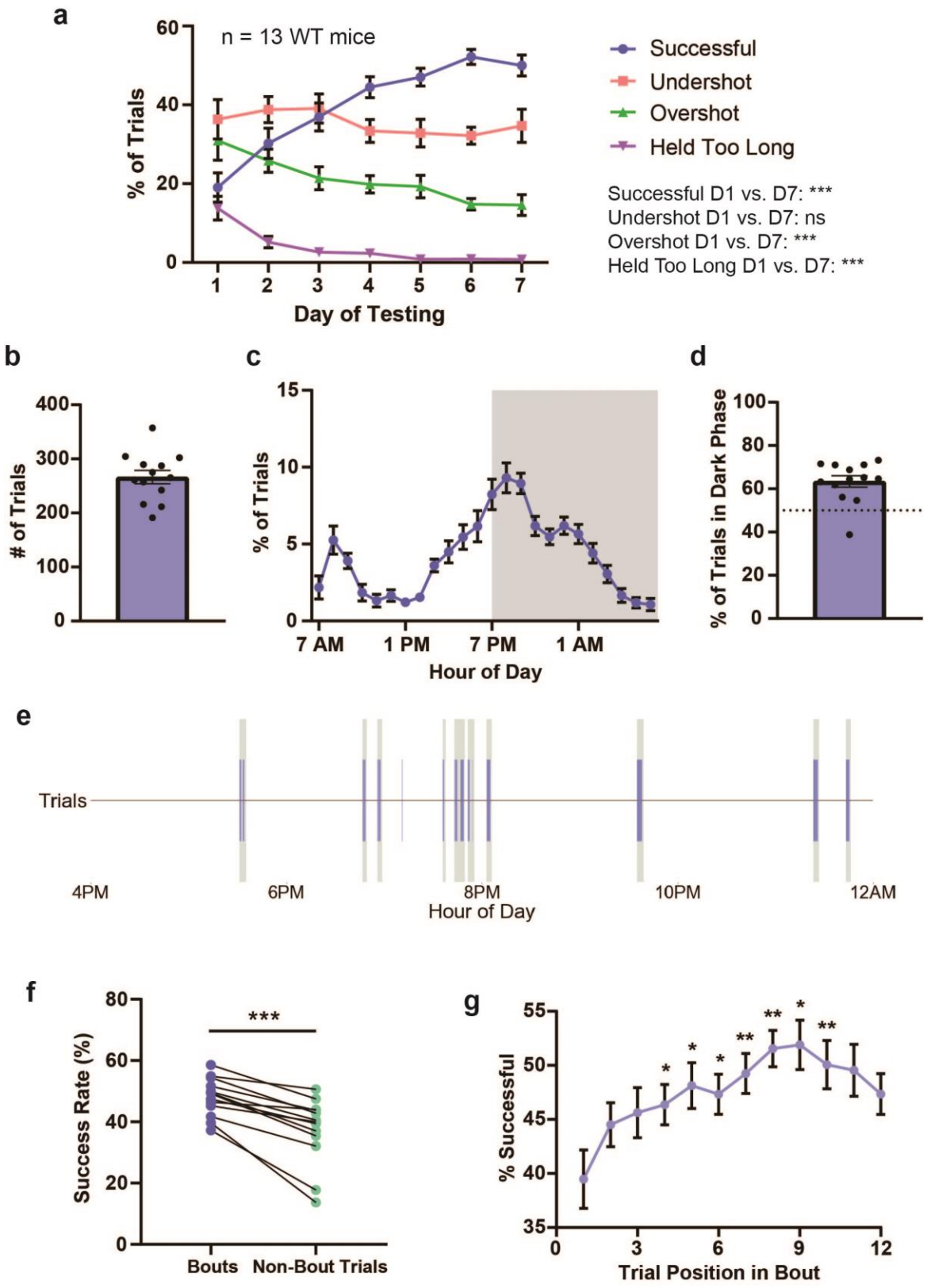
a
n = 13 WT mice
% of Trials
Day of Testing
Successful
Undershot
Overshot
Held Too Long
Successful D1 vs. D7: ***
Undershot D1 vs. D7: ns
Overshot D1 vs. D7: ***
Held Too Long D1 vs. D7: ***
b
# of Trials
c
% of Trials
7 AM
1 PM
7 PM
1 AM
Hour of Day
d
% of Trials in Dark Phase
e
Trials
4PM
6PM
8PM
10PM
12AM
Hour of Day
f
Success Rate (%)
***
Bouts
Non-Bout Trials
g
% Successful
Trial Position in Bout

Figure 3.3 WT mice improve their performance of the PiPaw task over time and cluster their trials into short bouts of high task engagement

(a) Over the course of one week in the Testing phase, WT mice increase their proportion of successful trials and decrease their proportion of overshot and held too long trials, while the proportion of undershot trials stay relatively stable. **(b)** Average number of trials performed by each mouse over the Testing phase. **(c)** Average circadian distribution of trials (hourly bins), with the grey-shaded region indicating the dark phase of the light cycle (7 PM – 7 AM). **(d)** Percentage of trials performed by each mouse during the dark phase of the light cycle. **(e)** Trials (blue lines) for a representative mouse are shown over the course of 8-hours on one day of testing. The large majority of trials occur in 'bouts' (grey-shaded regions) of high task engagement (>4 trials within a 3-minute window). **(f)** Success rate is higher for trials occurring within bouts as compared to non-bout trials (lines indicate paired values for each mouse). **(g)** Average success rate by trial position in the bout for all bouts with at least 12 trials. Asterisks indicate a significant increase as compared to the first trial in the bout. n = 13 2-month-old WT mice for all analyses. *: $p<0.5$; **: $p<0.01$; ***: $p<0.001$; ns: not significant.

On average, mice performed 266.1 ± 12.4 trials and received 2.34 ± 0.08 mL of water per day during the Testing phase (Fig. 3.3b). However, these trials were not evenly distributed throughout the day – mice tended to increase their activity beginning in the late afternoon, with task engagement peaking between 7 and 9 PM (Fig. 3.3c). Overall, mice typically performed the majority of their trials during the dark phase of the light cycle between 7 PM and 7 AM (63.4% ± 2.6% of trials in the dark phase), although some had a more evenly divided light/dark phase trial distribution and one showed a preference for the light phase (Fig. 3.3d). When mice interacted with the task, they tended to cluster their trials into short (<10 minutes) 'bouts' of high task engagement, rather than distributing them more evenly over time. To identify and segregate these trial bouts, we determined the average trial rate in a three-minute sliding window over the full Testing phase for each mouse, and clustered trials together when the rate went above a certain value (>1.333 trials/minute). Using this method, we found that 92.3% ± 0.9% of each

mouse's trials occurred in these periods of high task engagement, with the remainder showing a sparser distribution (Fig. 3.3e). Mice performed an average of 18.2 ± 0.9 bouts per day, with each bout containing an average of 14.8 ± 0.6 trials.

Interestingly, the success rate in trials occurring within bouts was found to be much higher than the success rate in non-bout trials ($t_{12} = 6.16$, $p < 0.0001$), suggesting that this clustering served a functional role with regards to learning (Fig. 3.3f). In further support of this, we found a relationship between the position of a trial within a bout and the success rate on that trial, such that trials later in the bout had a higher success rate than those at the beginning ($F_{11, 132} = 6.02$, $p < 0.0001$). In bouts with at least 12 trials, the average success rate increased from 39.5% ± 2.7% in the first trial to 51.9% ± 2.3% in the ninth trial before decreasing slightly (Fig. 3.3g). This demonstrates that mice show substantial within-bout motor learning, although fatigue may play a role in decreasing average success rate after a certain number of trials.

3.3.2 Performance improvement on the PiPaw task is associated with reductions in trial-to-trial variability in pull amplitude and duration

To further examine how mice improve their performance of the task over time, kinematic features of lever-pull trials were measured over the course of one week in the Testing phase. Initially, trials were characterized by substantial heterogeneity of kinematic measures (e.g. amplitude, tortuosity) and were often held for one second or more before being returned to the start position (Fig. 3.4a). However, by day 7, mice performed trials with a more stereotyped movement, typically pulling the lever backwards in a single motion and then returning it to the start position within 0.5 s (Fig. 3.4b). As pull amplitude is the feature of the trial most relevant to task success, the distribution of these amplitudes was seen to change substantially from day 1 to

day 7 as mice improved their performance of the task (Fig. 3.4c-d). Interestingly, average pull amplitude was within the rewarded range even on the first day of testing and did not change significantly over seven days, despite the 2.5-fold increase in success rate ($F_{6, 72} = 1.742$, $p = 0.124$) (Fig. 3.4e). To better quantify the shift in the distribution of pull amplitude towards the rewarded range, the inter-trial variability (quantified as variance) of pull amplitude was measured over all trials on each day of testing (Fig. 3.4f). This variability decreased by over 40% over the course of one week ($F_{6, 72} = 17.01$, $p < 0.0001$), providing a robust measure of the progression of motor learning over this period.

In addition to pull amplitude, pull duration is another parameter that directly influences success on the task, as trials held away from the start position for longer than 2 s are automatically failed. Paralleling the decrease observed in 'held too long' trials (Fig. 3.3a), trial duration decreased significantly over the course of testing ($F_{6, 72} = 15.5$, $p < 0.0001$) (Fig. 3.4g). The inter-trial variability of pull duration also decreased over this period ($\chi^2 = 47.74$, $p < 0.0001$) (Fig. 3.4h). This is perhaps unsurprising, as the mean values of trial duration are also decreasing, and variance tends to be smaller for smaller means. However, even when mean duration was controlled for by calculating the Fano factor ($\frac{\sigma^2}{\mu}$) of trial duration for each animal on each day, a strong decrease was still observed over one week of testing ($F_{6, 72} = 13.92$, $p < 0.0001$). These decreases in the inter-trial variability of pull amplitude and trial duration, distinct from changes in the means of these values, reflect the refinement of task performance over the course of one week that allows for the concurrent increase in success rate.

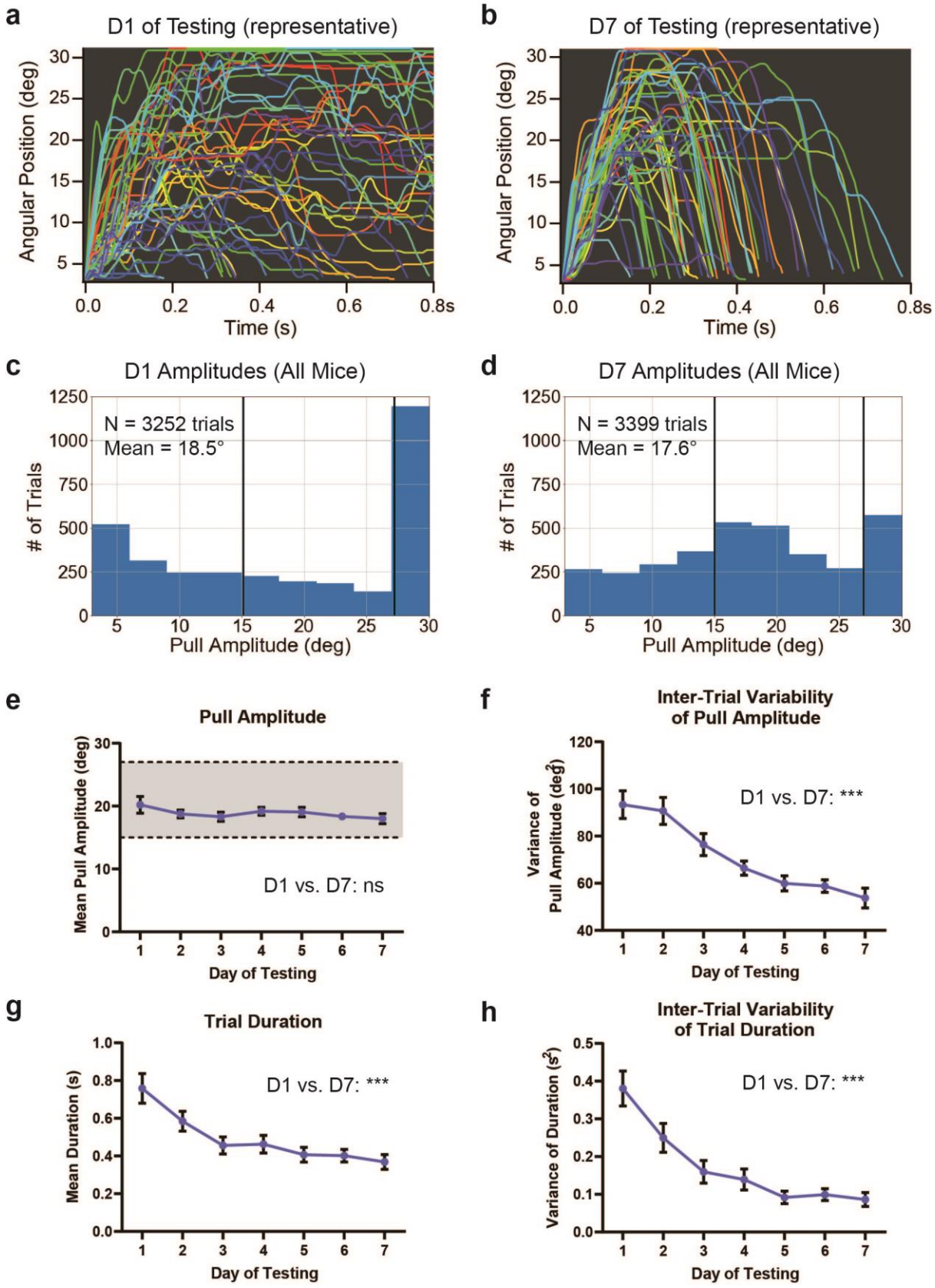
a
D1 of Testing (representative)
Angular Position (deg)
Time (s)
b
D7 of Testing (representative)
Angular Position (deg)
Time (s)
c
D1 Amplitudes (All Mice)
N = 3252 trials
Mean = 18.5°
# of Trials
Pull Amplitude (deg)
d
D7 Amplitudes (All Mice)
N = 3399 trials
Mean = 17.6°
# of Trials
Pull Amplitude (deg)
e
Pull Amplitude
Mean Pull Amplitude (deg)
D1 vs. D7: ns
Day of Testing
f
Inter-Trial Variability of Pull Amplitude
Variance of Pull Amplitude (deg²)
D1 vs. D7: ***
Day of Testing
g
Trial Duration
Mean Duration (s)
D1 vs. D7: ***
Day of Testing
h
Inter-Trial Variability of Trial Duration
Variance of Duration (s²)
D1 vs. D7: ***
Day of Testing

Figure 3.4 Increased success rate is driven by decreased inter-trial variability of task-relevant kinematic parameters

(a) Representative lever position vs. time traces (n = 50 trials) for a representative WT mouse on the first day of the Testing phase. Each line represents the lever position over the course of a single trial. **(b)** Lever position traces (n = 50) for the same mouse on the seventh day of the Testing phase show a shorter duration and more stereotyped movement **(c)** Histogram of pull amplitude (i.e. maximum lever position) of every trial for all mice on D1 of the Testing phase. Only ~23% of trials have an amplitude falling within the rewarded position range (indicated by black lines). **(d)** Histogram of pull amplitude of every trial for all mice on D7 of the Testing phase, showing that ~49% of trials now have an amplitude in the rewarded range **(e)** The average pull amplitude of all trials over seven days of testing does not change significantly. The grey shaded region indicates the rewarded position range. **(f)** The inter-trial variance of pull amplitude shows a strong decrease over testing. **(g-h)** Mean trial duration and the variance of trial duration both show significant decreases over seven days in the Testing phase. n = 13 2-month-old WT mice for all analyses.

3.3.3 2-month-old and 10-month-old YAC128 mice have normal motor learning on the PiPaw task

I next assessed the performance of heterozygous YAC128 mice on the PiPaw task at both an early, pre-symptomatic timepoint (2-months-old) and a later, symptomatic timepoint (10-months-old). In 2-month-old animals, no significant differences were seen between WT (n = 13) and YAC128 mice (n = 14) in learning of the task (Fig 3.5a), with both groups improving their success rate over one week of testing (Day: $F_{6, 150} = 34.1$, $p < 0.0001$; Genotype: $F_{1, 25} = 0.1171$, $p = 0.735$; Interaction: $F_{6, 150} = 1.02$, $p = 0.415$). Although no significant main or interaction effects were seen for the proportion of undershot trials in WT and YAC128 mice over testing (Day: $F_{6, 150} = 1.832$, $p = 0.097$; Genotype: $F_{1, 25} = 0.007$, $p = 0.935$; Interaction: $F_{6, 150} = 1.978$, $p = 0.072$), post-hoc tests revealed a significant decrease in undershot trials on D7 as compared to D1 in YAC128 mice ($p = 0.0018$) but not WT mice (Fig. 3.5b). In contrast, an overall effect of

day was seen in the proportion of overshot trials over testing (Day: $F_{6, 150} = 6.2$, $p < 0.0001$; Genotype: $F_{1, 25} = 0.131$, $p = 0.721$; Interaction: $F_{6, 150} = 1.298$, $p = 0.262$) but this was primarily driven by a decrease in WT mice (D1 vs. D7: $p = 0.0001$), and post-hoc tests found no significant change in YAC128 mice on any day as compared to D1 (Fig. 3.5c). A significant interaction was observed between day of testing and genotype in the proportion of 'held too long' trials, with WT mice initially higher on this measure (D1 WT vs. YAC128: $p = 0.048$), but both genotypes decreased to the same level after one week of testing (Day: $F_{6, 150} = 23.2$, $p < 0.0001$; Genotype: $F_{1, 25} = 0.010$, $p = 0.920$; Interaction: $F_{6, 150} = 3.085$, $p = 0.007$) (Fig. 3.5d).

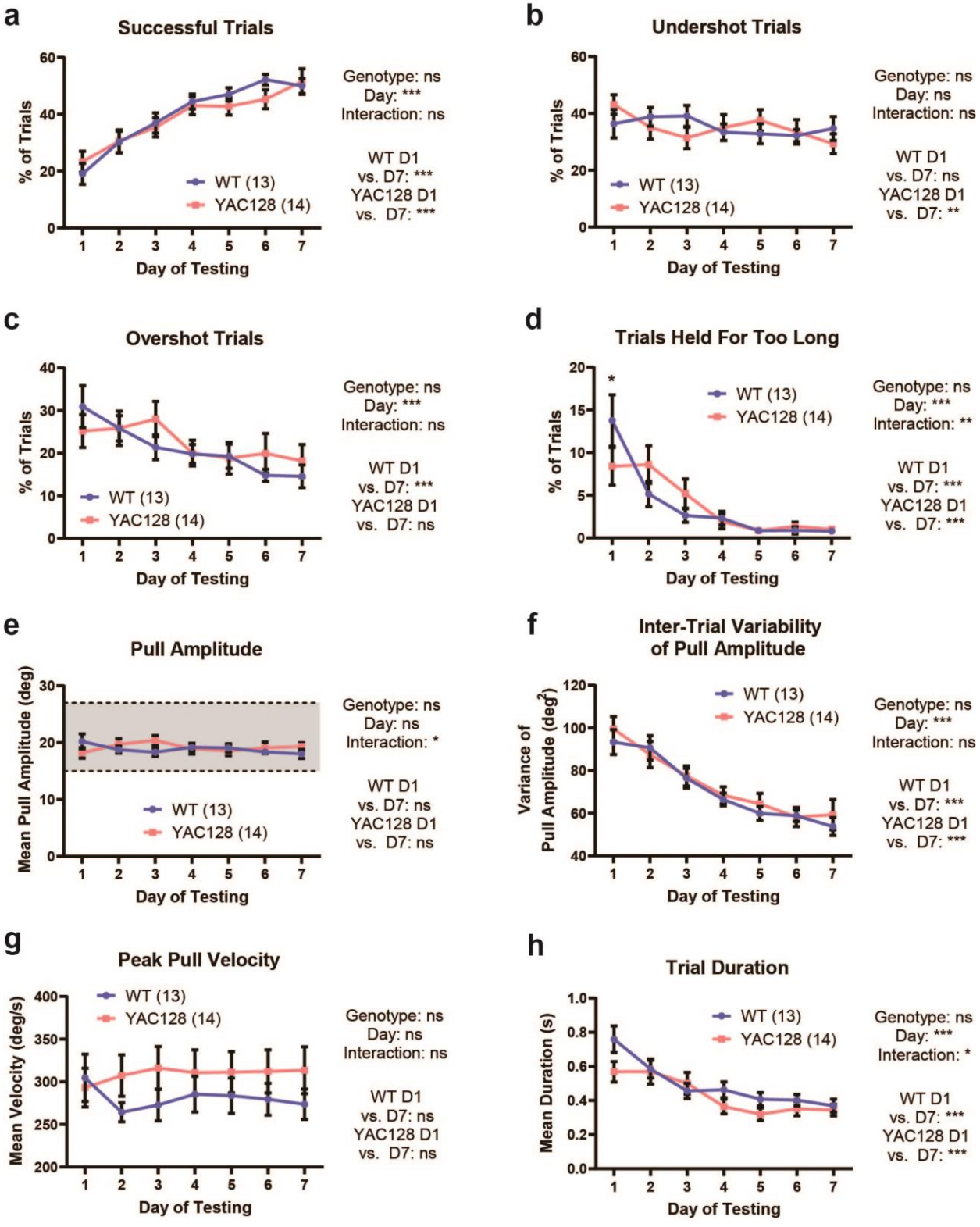
a
Successful Trials
% of Trials
Day of Testing
WT (13)
YAC128 (14)
Genotype: ns
Day: ***
Interaction: ns
WT D1
vs. D7: ***
YAC128 D1
vs. D7: ***
b
Undershot Trials
% of Trials
Day of Testing
WT (13)
YAC128 (14)
Genotype: ns
Day: ns
Interaction: ns
WT D1
vs. D7: ns
YAC128 D1
vs. D7: **
c
Overshot Trials
% of Trials
Day of Testing
WT (13)
YAC128 (14)
Genotype: ns
Day: ***
Interaction: ns
WT D1
vs. D7: ***
YAC128 D1
vs. D7: ns
d
Trials Held For Too Long
*
% of Trials
Day of Testing
WT (13)
YAC128 (14)
Genotype: ns
Day: ***
Interaction: **
WT D1
vs. D7: ***
YAC128 D1
vs. D7: ***
e
Pull Amplitude
Mean Pull Amplitude (deg)
Day of Testing
WT (13)
YAC128 (14)
Genotype: ns
Day: ns
Interaction: *
WT D1
vs. D7: ns
YAC128 D1
vs. D7: ns
f
Inter-Trial Variability
of Pull Amplitude
Variance of
Pull Amplitude (deg²)
Day of Testing
WT (13)
YAC128 (14)
Genotype: ns
Day: ***
Interaction: ns
WT D1
vs. D7: ***
YAC128 D1
vs. D7: ***
g
Peak Pull Velocity
Mean Velocity (deg/s)
Day of Testing
WT (13)
YAC128 (14)
Genotype: ns
Day: ns
Interaction: ns
WT D1
vs. D7: ns
YAC128 D1
vs. D7: ns
h
Trial Duration
Mean Duration (s)
Day of Testing
WT (13)
YAC128 (14)
Genotype: ns
Day: ***
Interaction: *
WT D1
vs. D7: ***
YAC128 D1
vs. D7: ***

Figure 3.5 2-month-old YAC128 mice have normal motor learning on the PiPaw task
(a) The proportion of successful trials increases to a similar extent over 7 days of testing between 2-month-old WT and YAC128 mice. (**b)** Undershot trials are significantly decreased on D7 as compared to D1 for YAC128, but not WT mice. However, no overall main or interaction effects are observed. **(c)** An overall effect of day on the proportion of overshot trials is driven largely by a decrease in these trials in WT, but not YAC128 mice. **(d)** WT mice initially have a higher proportion of trials held past the time limit of 2 s, but both genotypes decrease to a similar level by D7. **(e)** An overall interaction is observed between genotype and day for average pull amplitude, but no significant differences were seen on any specific day and amplitude does not change over time for either genotype. **(f)** WT and YAC128 mice decrease the inter-trial variance of pull amplitude to a similar extent over 7 days of testing. **(g)** Average peak velocity of pulls is similar between genotypes and does not change over testing. **(h)** An overall interaction is seen between genotype and day for average trial duration, but the genotype difference is not significant on any day and both genotypes decrease mean trial duration to a similar extent over testing. Data shown for WT animals is the same as shown in Fig. 3.3 and 3.4. n = 13 WT, 14 YAC128 for all analyses. *: p<0.5; **: p<0.01; ***: p<0.001; ns: not significant.

Kinematic measures of lever-pull trials were also found to be similar between 2-month-old WT and YAC128 mice. Although an interaction was observed between genotype and day in average pull amplitude (Day: $F_{6, 150} = 0.404$, $p = 0.876$; Genotype: $F_{1, 25} = 0.121$, $p = 0.731$; Interaction: $F_{6, 150} = 2.456$, $p = 0.027$), this was not significant between genotypes on any day of testing and average amplitude did not change significantly over time for either genotype (Fig. 3.5e). YAC128 mice decreased the inter-trial variability of pull amplitude to a similar extent to WT mice over the course of testing (Day: $F_{6, 150} = 29.41$, $p < 0.0001$; Genotype: $F_{1, 25} = 0.237$, $p = 0.631$; Interaction: $F_{6, 150} = 0.355$, $p = 0.906$), providing further support for normal motor learning in these mice (Fig. 3.5f). Peak velocity of the lever during the trial was also not significantly different between genotypes and did not change over seven days of testing (Day: $F_{6, 150} = 0.227$, $p = 0.968$; Genotype: $F_{1, 25} = 1.075$, $p = 0.310$; Interaction: $F_{6, 150} = 1.060$, $p = 0.389$)

(Fig. 3.5g). Paralleling the early increase in 'held too long' trials in WT mice, trial duration tended to be longer for WT animals on D1 of testing as compared to YAC128 contributing to an overall interaction between genotype and day of testing (Day: $F_{6, 150} = 23.34$, $p < 0.0001$; Genotype: $F_{1, 25} = 1.13$, $p = 0.298$; Interaction: $F_{6, 150} = 2.284$, $p = 0.039$) (Fig. 3.5h). However, this was not significantly different between genotypes on any day of testing, and both genotypes decreased the average duration of trials to a similar extent over seven days.

A cohort of 10-month-old heterozygous YAC128 mice was next assessed using PiPaw. At this age, YAC128 mice are reported to be hypoactive in the open field, have a strong motor learning and coordination deficit on the rotarod, and display mild cognitive deficits (Van Raamsdonk et al., 2005). Surprisingly, we found that YAC128 mice at this age ($n = 15$) learned the PiPaw task just as well as WT mice ($n = 27$), showing a similar increase in success rate over 7 days of testing (Day: $F_{6, 240} = 55.86$, $p < 0.0001$; Genotype: $F_{1, 40} = 0.033$, $p = 0.856$; Interaction: $F_{6, 240} = 0.295$, $p = 0.939$) (Fig. 3.6a). Both WT and YAC128 mice had a significant decrease in their proportion of undershot trials over 7 days of testing (Day: $F_{6, 240} = 9.907$, $p < 0.0001$; Genotype: $F_{1, 40} = 0.001$, $p = 0.974$; Interaction: $F_{6, 240} = 0.745$, $p = 0.614$), in contrast to the results at 2-months-old where no significant main effect of day of testing was observed (Fig. 3.6b). Although an overall effect of day of testing was seen for the proportion of overshot trials (Day: $F_{6, 240} = 3.425$, $p = 0.003$; Genotype: $F_{1, 40} = 0.207$, $p = 0.652$; Interaction: $F_{6, 240} = 0.561$, $p = 0.761$), a significant decrease was only observed in WT mice (D1 vs. D7: $p = 0.0002$), mirroring results at 2-months-old (Fig. 3.6c). Still, no genotype or interaction effects were found in the proportion of these trials, nor in the number of 'held too long' trials, which decreased similarly over testing for both genotypes (Day: $F_{6, 240} = 14.95$, $p < 0.0001$; Genotype: $F_{1, 40} = 0.502$, $p = 0.483$; Interaction: $F_{6, 240} = 0.789$, $p = 0.58$) (Fig. 3.6d).

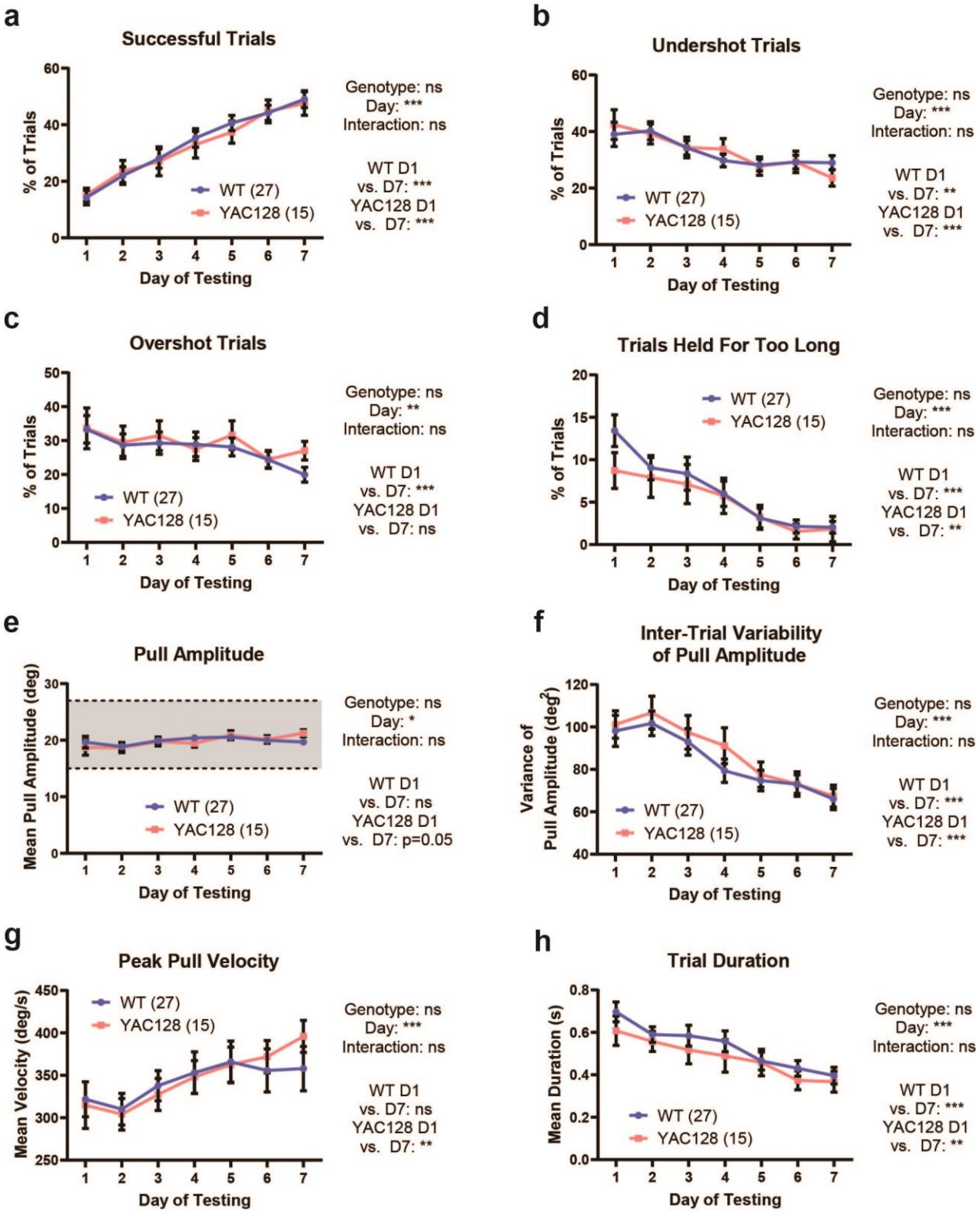
a
Successful Trials
% of Trials
Day of Testing
WT (27)
YAC128 (15)
Genotype: ns
Day: ***
Interaction: ns
WT D1
vs. D7: ***
YAC128 D1
vs. D7: ***
b
Undershot Trials
% of Trials
Day of Testing
WT (27)
YAC128 (15)
Genotype: ns
Day: ***
Interaction: ns
WT D1
vs. D7: **
YAC128 D1
vs. D7: ***
c
Overshot Trials
% of Trials
Day of Testing
WT (27)
YAC128 (15)
Genotype: ns
Day: **
Interaction: ns
WT D1
vs. D7: ***
YAC128 D1
vs. D7: ns
d
Trials Held For Too Long
% of Trials
Day of Testing
WT (27)
YAC128 (15)
Genotype: ns
Day: ***
Interaction: ns
WT D1
vs. D7: ***
YAC128 D1
vs. D7: **
e
Pull Amplitude
Mean Pull Amplitude (deg)
Day of Testing
WT (27)
YAC128 (15)
Genotype: ns
Day: *
Interaction: ns
WT D1
vs. D7: ns
YAC128 D1
vs. D7: p=0.05
f
Inter-Trial Variability
of Pull Amplitude
Variance of
Pull Amplitude (deg²)
Day of Testing
WT (27)
YAC128 (15)
Genotype: ns
Day: ***
Interaction: ns
WT D1
vs. D7: ***
YAC128 D1
vs. D7: ***
g
Peak Pull Velocity
Mean Velocity (deg/s)
Day of Testing
WT (27)
YAC128 (15)
Genotype: ns
Day: ***
Interaction: ns
WT D1
vs. D7: ns
YAC128 D1
vs. D7: **
h
Trial Duration
Mean Duration (s)
Day of Testing
WT (27)
YAC128 (15)
Genotype: ns
Day: ***
Interaction: ns
WT D1
vs. D7: ***
YAC128 D1
vs. D7: **

Figure 3.6 10-month-old YAC128 mice display normal motor learning on the PiPaw task
(a) Symptomatic YAC128 mice have normal learning on the PiPaw task over 7 days of testing. **(b)** WT and YAC128 mice show a similar decrease in the proportion of undershot trials over testing. **(c)** WT, but not YAC128 mice have a significant decrease in the proportion of overshot trials from day 1 to day 7 of testing. **(d)** Trials held for too long (i.e. past the trial time limit) decrease in both genotypes over testing. **(e)** Average pull amplitude is similar for both genotypes; however, an overall main effect of day was observed, most likely caused by a tendency for amplitude to increase in YAC128 mice. **(f)** WT and YAC128 mice decrease the inter-trial variability of pull amplitude to a similar extent over testing. **(g)** YAC128 mice tend to increase the peak velocity of lever-pull trials over the course of testing, while this measure stays comparatively stable for WT mice. **(h)** Average trial duration decreases in both genotypes over the course of testing. n = 27 WT, 15 YAC128 for all analyses. *: p<0.5; **: p<0.01; ***: p<0.001; ns: not significant.

Forelimb kinematics during lever-pull trials were also, for the most part, similar in WT and YAC128 mice at 10-months-old. Average pull amplitude was not different between WT and YAC128 mice (Day: $F_{6, 240} = 2.517$, $p = 0.022$; Genotype: $F_{1, 40} = 0.001$, $p = 0.973$; Interaction: $F_{6, 240} = 0.953$, $p = 0.458$) (Fig. 3.6e), and both genotypes had a similar decrease in the inter-trial variability of pull amplitude over 7 days (Day: $F_{6, 240} = 19.74$, $p < 0.0001$; Genotype: $F_{1, 40} = 0.34$, $p = 0.563$; Interaction: $F_{6, 240} = 0.344$, $p = 0.913$) (Fig. 3.6f). YAC128 mice tended to increase the peak velocity of their pulls over testing (YAC128 D1 vs. D7: $p = 0.0075$) contributing to an overall effect of day (Day: $F_{6, 240} = 5.564$, $p < 0.0001$; Genotype: $F_{1, 40} = 0.014$, $p = 0.907$; Interaction: $F_{6, 240} = 0.634$, $p = 0.703$), whereas peak velocity was not different on any day in WT mice as compared to D1 (Fig. 3.6g). However, an overall genotype or interaction effect was not seen for this measure. Average trial duration decreased similarly for both genotypes over 7 days of testing (Day: $F_{6, 240} = 11.59$, $p < 0.0001$; Genotype: $F_{1, 40} = 0.947$, $p = 0.336$; Interaction: $F_{6, 240} = 0.248$, $p = 0.96$) (Fig. 3.6h), as was been seen in 2-month-old

mice. These results demonstrate that YAC128 mice at both early and later stages have an intact ability to learn and refine their performance of a skilled motor task.

3.3.4 YAC128 mice show opposing age-related alterations of their activity patterns

I next investigated whether patterns of task engagement and circadian activity levels were different in YAC128 as compared to WT animals. An altered circadian pattern of task engagement had previously been found in 4- and 6-month-old YAC128 mice, but not 2-month-old animals (Fig. 2.3c-e), suggesting that this phenotype may progressively worsen over time. Further supporting this, a significant interaction between genotype and hour of day was not seen when the average circadian distribution of PiPaw trials was compared in 2-month-old animals (Hour: $F_{23, 575} = 29.35$, $p < 0.0001$; Genotype: $F_{1, 25} = 3.947$, $p = 0.058$; Interaction: $F_{23, 575} = 1.324$, $p = 0.144$) (Fig. 3.7a). In contrast, 10-month-old YAC128 mice showed a significantly altered circadian distribution of their trials as compared to WT mice (Hour: $F_{23, 920} = 52.53$, $p < 0.0001$; Genotype: $F_{1, 40} = 2.933$, $p = 0.095$; Interaction: $F_{23, 920} = 2.043$, $p = 0.0027$) (Fig. 3.7b). Although the difference in trial distribution was relatively subtle, trials tended to be more concentrated in YAC128 mice at this age, especially in the first two hours of the dark phase (7-9 PM).

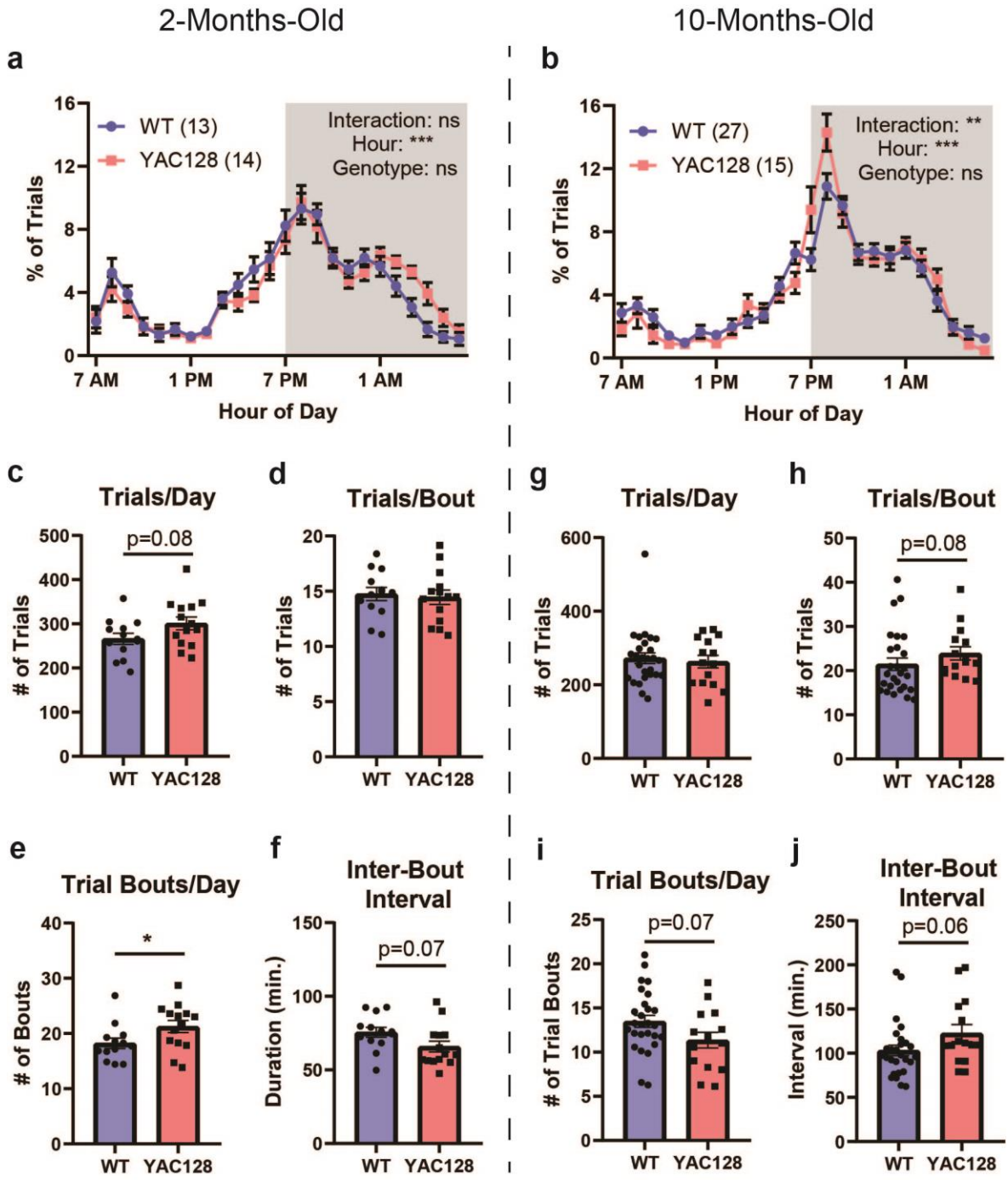

Figure 3.7 YAC128 mice show age-dependent alterations in their patterns of task engagement

(a) Proportion of PiPaw trials occurring in each hour are shown for 2-month-old WT and YAC128 mice. No differences in the circadian distribution of trials are seen at this age. **(b)** 10-month-old YAC128 mice show an altered circadian trial distribution as compared to WT controls, as indicated by a significant interaction between genotype and hour of day. **(c)** 2-month-old YAC128 mice tend to perform more trials

per day over one week of testing as compared to WT littermates. **(d)** Average number of trials per bout are similar between genotypes for 2-month-old animals. **(e)** 2-month-old YAC128 mice have significantly more trial bouts per day as compared to WT littermates. **(f)** A trend for decreased inter-bout interval is seen in YAC128 mice. **(g)** 10-month-old WT and YAC128 mice perform a similar number of trials each day. **(h)** A trend is seen for an increased number of trials in each bout in YAC128 mice as compared to WT at 10-months-old. **(i)** 10-month-old YAC182 mice tend to perform fewer trial bouts than WT controls each day. **(j)** A trend is also seen for an increased inter-bout interval in 10-month-old YAC128 mice as compared to WT littermates. n = 13 WT, 14 YAC128 for 2-month-old animals and n = 27 WT, 15 YAC128 for 10-month-old animals. *: p<0.5; **: p<0.01; ***: p<0.001; ns: not significant.

Although they did not display any circadian abnormalities, 2-month-old YAC128 mice were different from WT mice in their pattern of task engagement. These mice tended to perform more trials each day than their WT littermates (t_{25} = 1.808, p = 0.083), possibly reflecting a hyperactive phenotype (Fig. 3.7c). Interestingly, this increased trial rate did not manifest as an increase in the average number of trials in each bout (t_{25} = 0.337, p = 0.739) (Fig. 3.7d), but rather as an increase in the number of bouts performed each day (t_{25} = 2.077, p = 0.048) (Fig. 3.7e). This was also associated with a trend for a decreased inter-bout interval in 2-month-old YAC128 mice as compared to WT mice (t_{25} = 1.919, p = 0.066) (Fig. 3.7f). In contrast, 10-month-old YAC128 mice had the same number of trials per day as their WT littermates on average (U = 198, p = 0.917) (Fig. 3.7g) but tended to perform more trials in each bout (U = 135, p = 0.079) (Fig. 3.7h). A trend for a decreased number of trial bouts each day (t_{40} = 1.884, p = 0.067) (Fig. 3.7i) and an increased inter-bout interval (U = 130, p = 0.058) (Fig. 3.7j) were also observed in older YAC128 mice. These results point to a bidirectional age-related modulation of task engagement in YAC128 mice, with young and old animals tending to interact with the task more and less frequently respectively.

3.3.5 10-month-old Q175-FDN mice have robust motor learning deficits and altered circadian activity levels

Given the surprising finding that YAC128 mice display normal motor learning on the PiPaw task even at an advanced symptomatic stage, I next assessed the performance of a different model of HD, the Q175-FDN mouse. The heterozygous Q175-FDN mouse is a knock-in model of HD expressing one copy of an expanded *Htt* gene (~200 CAG-repeats) on an FVB/N genetic background (the same as the YAC128 model) (Southwell et al., 2016). Although these mice show behavioural and neuropathological symptoms at an earlier age than most other knock-in models, this model still has a comparatively slow phenotypic progression and mice do not have a significant motor coordination deficit on the rotarod until 8-months-old (as compared to ~4-months-old in YAC128 mice).

In 10-month-old Q175-FDN mice (n = 14), a striking motor learning deficit was observed as compared to WT mice (n = 27) (Fig. 3.8a). Although both genotypes had a similar success rate on day 1 of the Testing phase, Q175-FDN mice had a much slower rate of improvement on the task, and were significantly worse than WT mice by D3 of testing (Day: $F_{6, 234} = 31.04$, $p < 0.0001$; Genotype: $F_{1, 39} = 22.83$, $p < 0.0001$; Interaction: $F_{6, 234} = 9.272$, $p < 0.0001$). Contributing to this low success rate, Q175-FDN mice had a higher proportion of undershot trials across testing as compared to WT mice (Day: $F_{6, 234} = 9.471$, $p < 0.0001$; Genotype: $F_{1, 39} = 8.585$, $p = 0.006$; Interaction: $F_{6, 234} = 0.349$, $p = 0.91$), although the prevalence of these trials decreased to a similar extent in both genotypes (Fig. 3.8b). The proportion of overshot trials was initially similar between genotypes, but while WT mice had a significant decrease in the number of these trials across testing, Q175-FDN mice did not (Day: $F_{6, 234} = 0.831$, $p = 0.547$; Genotype: $F_{1, 39} = 0.614$, $p = 0.438$; Interaction: $F_{6, 234} = 3.575$, $p =$

0.002) (Fig. 3.8c). Similarly, a large decrease was seen in the proportion of 'held too long' trials across testing for WT mice, but no such change was seen Q175-FDN animals (Day: $F_{6, 234}$ = 7.576, $p < 0.0001$; Genotype: $F_{1, 39} = 0.71$, $p = 0.404$; Interaction: $F_{6, 234} = 3.794$, $p = 0.001$) (Fig. 3.8d). In sum, Q175-FDN mice had an altered categorical distribution of their failed trials initially, and an inability to reduce the proportion of certain types of failed trials over time.

Despite having a larger proportion of undershot trials, average pull amplitude was relatively normal in Q175-FDN mice (Day: $F_{6, 234} = 3.993$, $p = 0.0008$; Genotype: $F_{1, 39} = 2.526$, $p = 0.12$; Interaction: $F_{6, 234} = 1.338$, $p = 0.241$), although it increased significantly over 7 days of testing (D1 vs. D7: $p = 0.015$) (Fig. 3.8e). The ability of Q175-FDN mice to reduce the trial-to-trial variability of pull amplitude, however, was significantly impaired (Day: $F_{6, 234} = 8.611$, $p < 0.0001$; Genotype: $F_{1, 39} = 5.487$, $p = 0.024$; Interaction: $F_{6, 234} = 1.788$, $p = 0.102$) (Fig. 3.8f). In contrast to WT mice, Q175-FDN mice did not show a significant reduction in the inter-trial variability of pull amplitude between day 1 and day 7 ($p = 0.657$), reflecting an inability to refine the kinematics of their pulls in order to improve performance. Peak velocity of pulls was not different between genotypes, although an overall effect of day was observed (Day: $F_{6, 234}$ = 4.865, $p = 0.0001$; Genotype: $F_{1, 39} = 0.777$, $p = 0.386$; Interaction: $F_{6, 234} = 0.384$, $p = 0.889$) and Q175-FDN mice had an increased average peak velocity on D7 as compared to D1 ($p = 0.033$) (Fig. 3.8g). Interestingly, while WT mice had a significant decrease in average trial duration (D1 vs. D7: $p < 0.0001$), YAC128 mice had no such decrease, paralleling the failure of these mice to decrease their proportion of 'held too long' trials (Day: $F_{6, 234} = 4.613$, $p = 0.0002$; Genotype: $F_{1, 39} = 0.6$, $p = 0.443$; Interaction: $F_{6, 234} = 2.71$, $p = 0.015$) (Fig. 3.8h).

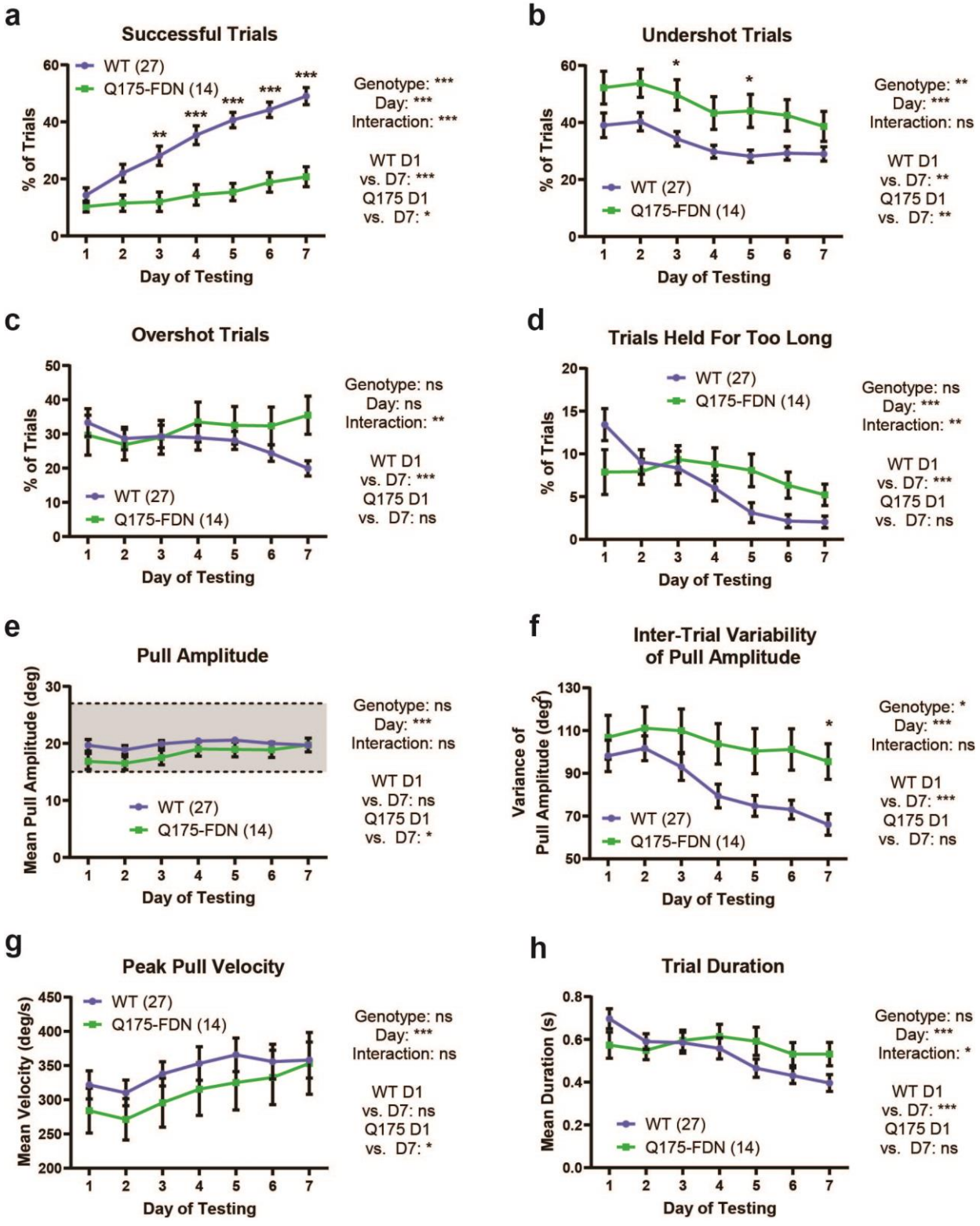
a
Successful Trials
WT (27)
Q175-FDN (14)
% of Trials
Day of Testing
Genotype: ***
Day: ***
Interaction: ***
WT D1 vs. D7: ***
Q175 D1 vs. D7: *
b
Undershot Trials
Genotype: **
Day: ***
Interaction: ns
WT D1 vs. D7: **
Q175 D1 vs. D7: **
c
Overshot Trials
Genotype: ns
Day: ns
Interaction: **
WT D1 vs. D7: ***
Q175 D1 vs. D7: ns
d
Trials Held For Too Long
Genotype: ns
Day: ***
Interaction: **
WT D1 vs. D7: ***
Q175 D1 vs. D7: ns
e
Pull Amplitude
Mean Pull Amplitude (deg)
Genotype: ns
Day: ***
Interaction: ns
WT D1 vs. D7: ns
Q175 D1 vs. D7: *
f
Inter-Trial Variability of Pull Amplitude
Variance of Pull Amplitude (deg²)
Genotype: *
Day: ***
Interaction: ns
WT D1 vs. D7: ***
Q175 D1 vs. D7: ns
g
Peak Pull Velocity
Mean Velocity (deg/s)
Genotype: ns
Day: ***
Interaction: ns
WT D1 vs. D7: ns
Q175 D1 vs. D7: *
h
Trial Duration
Mean Duration (s)
Genotype: ns
Day: ***
Interaction: *
WT D1 vs. D7: ***
Q175 D1 vs. D7: ns

Figure 3.8 Q175-FDN mice have a motor learning deficit on the PiPaw task at 10-months-old
(a) Motor learning is significantly impaired in Q175-FDN mice as compared to WT mice. Asterisks indicate a significant post-hoc test (WT vs. Q175-FDN) on a particular day. (**b)** Q175-FDN mice have significantly more undershot trials than WT mice across testing (main effect of genotype), although both genotypes have a decreased proportion of these trials over time. **(c)** The proportion of overshot trials is initially similar between genotypes, but Q175-FDN mice do not have a decreased number of these trials across testing. **(d)** Q175-FDN mice also do not decrease the proportion of trials held longer than the trial time limit of 2 s across testing, whereas WT mice do. **(e)** Average pull amplitude is similar between genotypes and tends to increase slightly over time, especially in Q175-FDN mice. Grey-shaded region indicates the rewarded pull amplitude position range. **(f)** Q175-FDN mice decrease the inter-trial variability of pull amplitude to a much lesser extent than WT littermates and have significantly higher inter-trial variability than WT by D7. **(g)** The peak velocity of pulls is similar between genotypes and increases slightly across testing. **(h)** Average trial duration decreases in WT mice across 7 days of testing but does not change in Q175-FDN mice. n = 27 WT, 14 Q175-FDN for all analyses. *: p<0.5; **: p<0.01; ***: p<0.001; ns: not significant.

Similar to the YAC128 animals, the circadian trial distribution of Q175-FDN mice was also significantly altered as compared to their WT littermates (Hour: $F_{23, 897} = 41.26$, $p < 0.0001$; Genotype: $F_{1, 39} = 0.042$, $p = 0.839$; Interaction: $F_{23, 897} = 5.306$, $p < 0.0001$) (Fig. 3.9a). However, this altered activity pattern was quite different as compared to what had been seen in YAC128 mice. Specifically, Q175-FDN mice had a lower proportion of trials in the light phase of the light/dark cycle (especially from 5-7 PM) and a greater number of trials in the second half of the dark phase (2-4 AM). As they had a much lower trial success rate overall, Q175-FDN mice also tended to perform more trials each day, although this was not significant ($U = 132$, $p = 0.121$) (Fig. 3.9b). Although average bout length was not different in Q175-FDN mice ($U = 181$, $p = 0.839$) (Fig. 3.9c), they performed a greater number of bouts per day ($t_{17.69} = 2.558$, p = 0.02) (Fig. 3.9d), the opposite of the pattern observed in YAC128 mice at the same age. The average

inter-bout interval in Q175-FDN mice was also significantly lower than WT mice (U = 113, p = 0.037) (Fig. 3.9e).

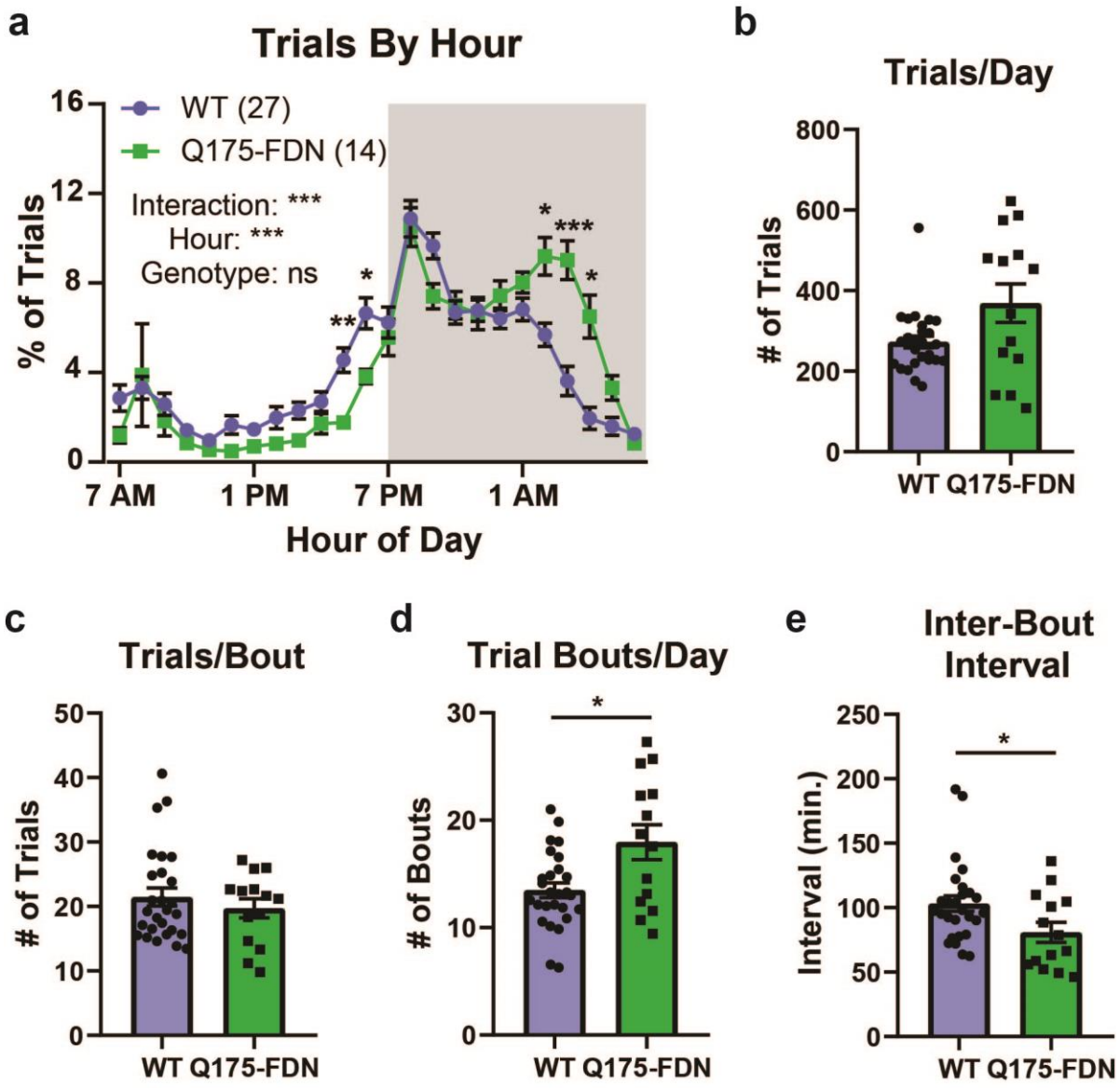

Figure 3.9 10-month-old Q175-FDN mice have altered patterns of task engagement

(a) The circadian distribution of PiPaw trials is significantly different in Q175-FDN mice as compared to WT littermates. Q175-FDN mice have a lower proportion of trials in the last two hours of the light phase and a higher proportion of trials in the second half of the dark phase. **(b)** Q175-FDN mice tend to have more trials per day through one week of testing, although this was not significant. **(c)** No significant

genotype difference was seen in the average number of trials per bout of task engagement. **(d)** Q175-FDN have significantly more trial bouts per day that WT littermates through one week of testing. **(e)** The average interval between trial bouts is lower in Q175-FDN than in WT mice. n = 27 WT, 14 Q175-FDN for all analyses. *: p<0.5; **: p<0.01; ***: p<0.001; ns: not significant.

3.3.6 10-month-old YAC128 and Q175-FDN mice display motor phenotypes in rotarod and open field test

The lack of any significant deficit in motor learning on the PiPaw task in 10-month-old YAC128 mice was surprising given the previous reports of robust deficits at this age on tests of full body motor coordination, such as the rotarod (Lawhorn et al., 2008; Pouladi et al., 2012; Van Raamsdonk et al., 2005). To confirm that our colony of YAC128 mice replicated these previous findings, I next assessed 10-month-old YAC128 and Q175-FDN mice on an accelerating rotarod test for four consecutive days (three trials per day). Both YAC128 (n = 11) and Q175-FDN mice (n = 10) had a significant deficit in motor learning on the rotarod task as compared to WT mice (n = 11) (Day: $F_{3, 87} = 24.79$, $p < 0.0001$; Genotype: $F_{2, 29} = 9.416$, $p = 0.0007$; Interaction: $F_{6, 87} = 2.594$, $p = 0.023$) (Fig. 3.10a). Although neither genotype was significantly worse than WT on day 1 (D1 WT vs. YAC128: $p = 0.089$; D1 WT vs. Q175-FDN: $p = 0.16$), latency to fall was significantly lower by day 2 (D2 WT vs. YAC128: $p = 0.002$; D2 WT vs. Q175-FDN: $p = 0.021$) and in subsequent days. Interestingly, YAC128 mice performed, if anything, somewhat worse than Q175-FDN mice, showing only a trend for improved task performance from D1 to D4 ($p = 0.055$), whereas Q175-FDN mice had a significant improvement over four days of testing ($p = 0.0005$). However, the two HD models were not significantly different from each other overall (WT vs. Q175-FDN: $p = 0.6$).

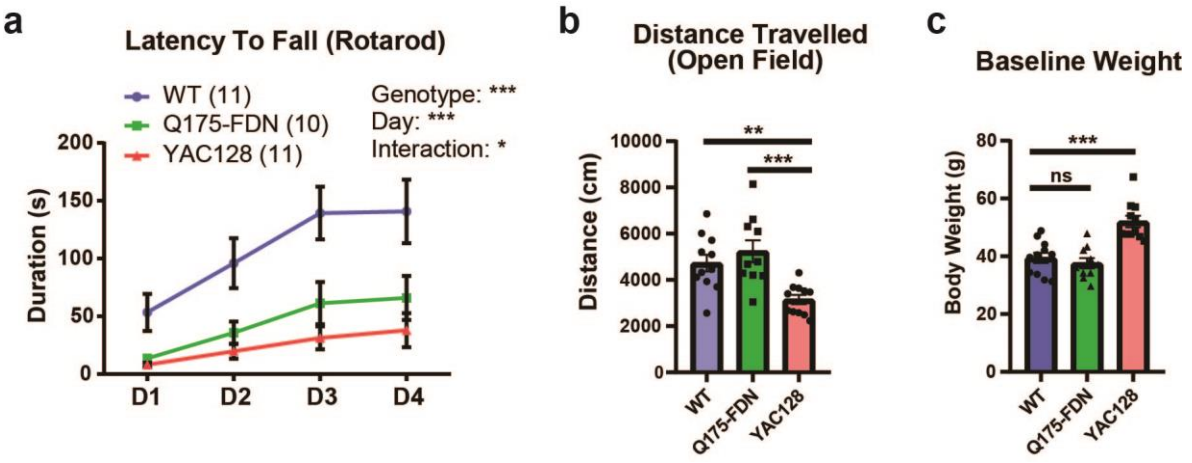

Figure 3.10 Motor coordination, locomotor activity and body weight are altered in HD mice
(a) 10-month-old YAC128 and Q175-FDN mice show a similarly strong impairment in motor coordination on the accelerating rotarod task over four days of assessment. **(b)** YAC128 mice, but not Q175-FDN mice, show pronounced hypoactivity in the open field test over a 10-minute exploration period. **(c)** Baseline bodyweight is increased in YAC128 mice as compared to both WT and Q175-FDN mice. *n* = 11 WT, 11 YAC128 and 10 Q175-FDN for all analyses. *: p<0.5; **: p<0.01; ***: p<0.001; ns: not significant.

The overall activity level of 10-month-old HD mice was also assessed by measuring the total distance that mice travelled during a 10-minute open field exploration. A significant effect of genotype was found ($F_{2, 29} = 9.316$, $p = 0.0008$), with YAC128 mice having a much lower activity level than both WT ($p = 0.0096$) and Q175-FDN ($p = 0.0009$) mice (Fig. 3.10b). In contrast, Q175-FDN mice had the same level of open field activity as WT mice ($p = 0.581$). YAC128 mice were also found to have much higher bodyweight than other animals ($F_{2, 29} = 17.92$, $p < 0.0001$), weighing over 30% more than WT mice on average ($p = 0.0001$) (Fig. 3.10c). Q175-FDN mice also weighed significantly less than YAC128s ($p < 0.0001$), but no difference was seen between WT and Q175-FDN ($p = 0.764$).

3.3.7 Q175-FDN mice have altered learning-associated changes in dorsolateral striatum MSN activity and plasticity

Motor learning and task-related refinement of kinematic variability are known to be associated with plasticity of cortico-striatal circuits (Barnes et al., 2005; Koralek et al., 2013; Santos et al., 2015; Yin et al., 2009). As previous studies have reported altered activity and plasticity of striatal MSNs in Q175-FDN mice (Sepers et al., 2018; Southwell et al., 2016), one possibility is that the motor learning deficits observed in this model are related to dysfunctional cortico-striatal plasticity. To investigate this, we next used acute slice electrophysiology to measure the spontaneous activity of dorsolateral striatum MSNs in animals who were either task-naïve or had been tested in the PiPaw system. Given that training on this task is unilateral (i.e. only the right forelimb performs the task), learning-associated changes are likely to be hemisphere-specific. For this reason, we first sought to determine if there were baseline differences between the right and left hemisphere in the properties of spontaneous excitatory postsynaptic currents (sEPSCs). Spontaneous EPSCs are a measure of the frequency and amplitude of glutamatergic excitatory input received by a neuron. A higher sEPSC frequency indicates either a greater number of excitatory synapses, or an increased frequency of glutamate release from presynaptic terminals. In contrast, an increase in sEPSC amplitude indicates a higher concentration of postsynaptic glutamate receptors. In 10-month-old task-naïve mice, no hemispheric differences were seen in DLS-MSN sEPSC frequency; however, frequency was much higher in WT than Q175-FDN mice (Hemisphere: $F_{1, 49} = 0.111$, $p = 0.74$; Genotype: $F_{1, 49} = 23.19$, $p < 0.0001$; Interaction: $F_{1, 49} = 0.0059$, $p = 0.939$) (Fig. 3.11a). In contrast, no hemispheric or genotype differences were observed for sEPSC amplitude (Hemisphere: $F_{1, 49} =$

0.0052, $p = 0.943$; Genotype: $F_{1, 49} = 1.17$, $p = 0.285$; Interaction: $F_{1, 49} = 2.24$, $p = 0.141$) (Fig. 3.11b).

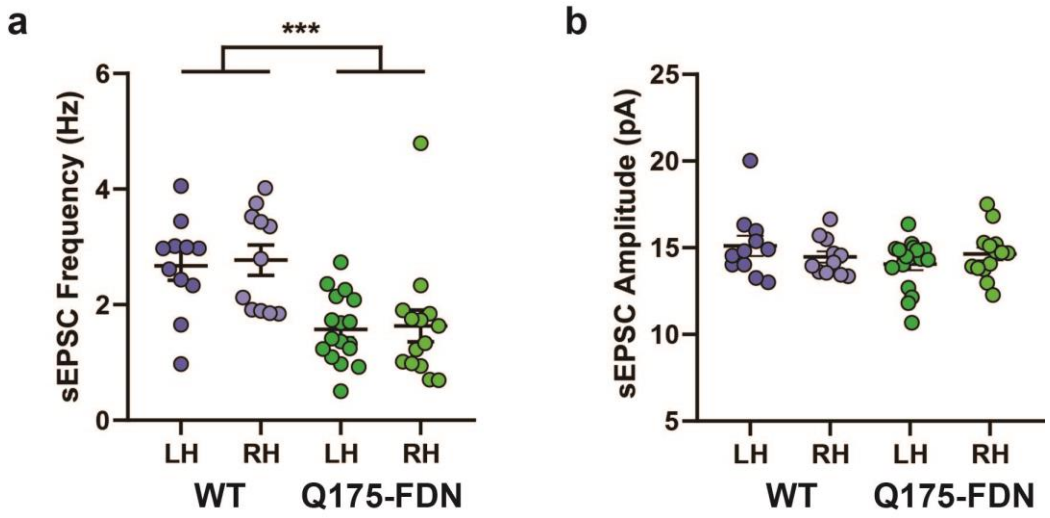

Figure 3.11 DLS-MSN spontaneous activity in 10-month-old WT and Q175-FDN mice
(a) Spontaneous EPSC frequency recorded from left and right-hemisphere (LH and RH) dorsolateral striatum MSNs in 10-month-old WT and Q175-FDN mice. No hemispheric differences are seen, but sEPSC frequency is strongly reduced in Q175-FDN cells. **(b)** Spontaneous EPSC amplitude is similar between hemispheres and genotypes in 10-month-old animals. *n* = 11(4) WT-LH, 11(4) WT-RH, 17(5) Q175-LH and 14(5) Q175-RH, with n=number of cells and numbers in brackets indicating the number of animals. ***: p<0.001.

We next performed acute slice electrophysiology in 10-month-old WT and Q175-FDN mice immediately after the end of PiPaw testing. Interestingly, a genotype difference was no longer observed in the frequency of DLS-MSN sEPSCs in trained animals (Hemisphere: $F_{1, 82} = 0.056$, $p = 0.813$; Genotype: $F_{1, 82} = 0.482$, $p = 0.489$; Interaction: $F_{1, 82} = 3.412$, $p = 0.068$) (Fig. 3.12a-b). The primary reason for this was a bilateral decrease in sEPSC frequency in trained WT mice as compared to task-naïve animals ($t_{64} = 2.082$, $p = 0.041$) (Fig. 3.12c). In contrast,

frequency was not significantly different in trained Q175-FDN mice as compared to naïve animals (U = 509.5, p = 0.115) (Fig. 3.12d).

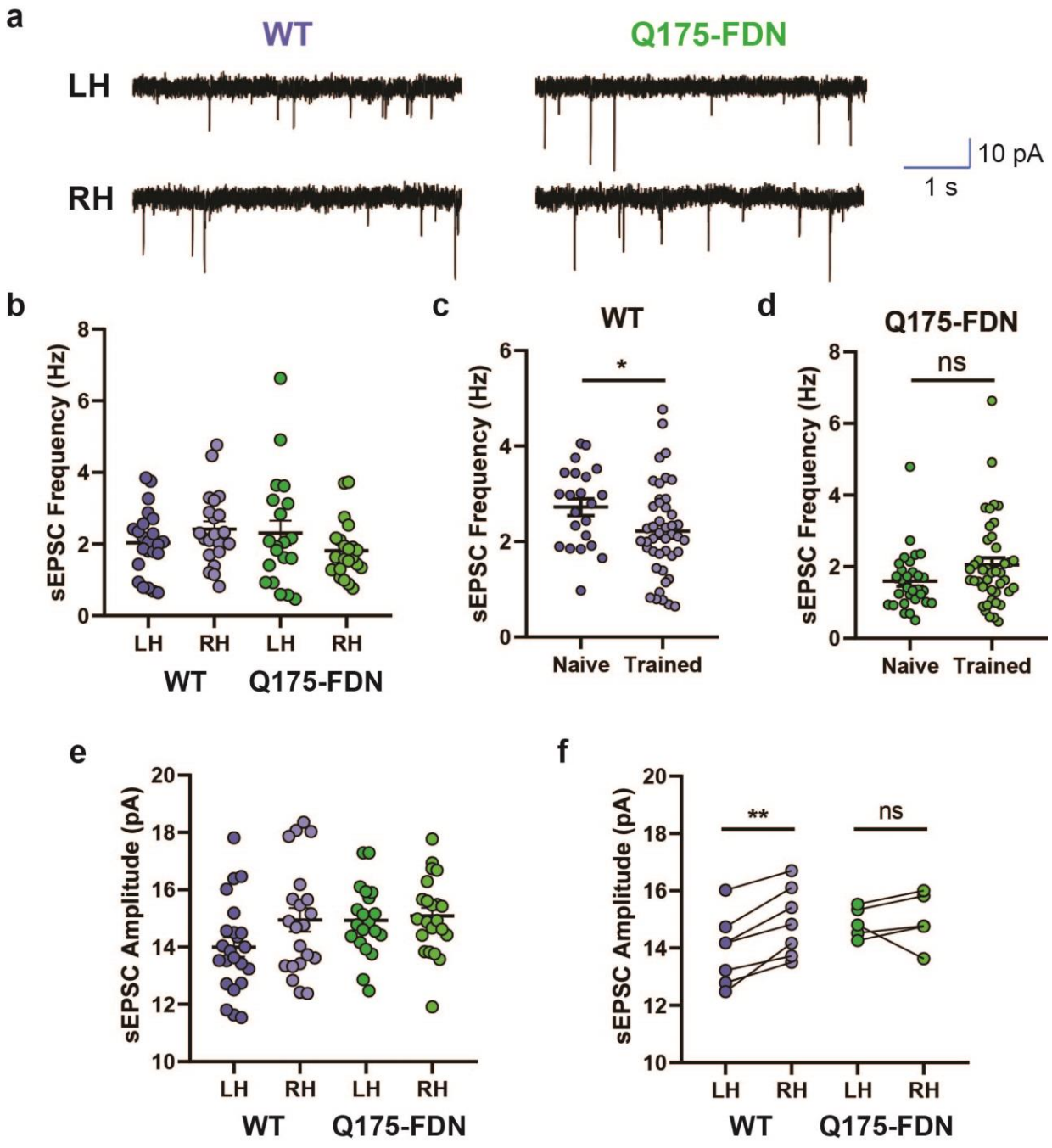

Figure 3.12 DLS-MSN spontaneous activity after PiPaw testing in 10-month-old WT and Q175-FDN mice

(a) Representative sEPSCs recorded from either left hemisphere (LH) or right hemisphere (RH) DLS-MSNs of 10-month-old WT and Q175-FDN mice immediately after the end of PiPaw testing (right forelimb trained). **(b)** The frequency of sEPSCs in DLS-MSNs was not significantly different between left and right hemisphere in either genotype. sEPSC frequency was also similar between genotypes, in contrast to naïve animals. **(c)** PiPaw-trained WT mice had a significantly lower sEPSC frequency as compared to naïve WT mice (hemispheres combined). **(d)** sEPSC frequency was not different between PiPaw-trained and naïve Q175-FDN mice. **(e)** Average sEPSC amplitude was not different between genotypes or hemispheres when all cells were compared, although a trend was seen for decreased amplitude in the LH as compared to RH in WT mice ($p = 0.09$). **(f)** Within-animal comparisons of the average sEPSC amplitude in the left versus right hemisphere (lines indicate the same animal). sEPSC amplitude was consistently lower in the LH (contralateral to the trained forelimb) as compared to the RH in WT animals, but no hemispheric differences were seen in Q175-FDN mice. $n = 23(7)$ WT-LH, 21(7) WT-RH, 20(5) Q175-LH and 22(5) Q175-RH, with numbers in brackets indicating the number of animals. All mice had been tested for 3-4 weeks in the PiPaw task up to the day of experiments. *: $p<0.5$; **: $p<0.01$; ns: not significant.

Similar to what was seen in naïve mice, no significant effects were observed when comparing the sEPSC amplitude between genotypes in MSNs from PiPaw-trained animals (Hemisphere: $F_{1, 82} = 2.762$, $p = 0.1$; Genotype: $F_{1, 82} = 2.589$, $p = 0.112$; Interaction: $F_{1, 82} = 1.439$, $p = 0.234$) (Fig. 3.12e). However, when average sEPSC amplitude in the left and right hemisphere was compared within-animal, a significant effect of hemisphere and an interaction between genotype and hemisphere were observed (Hemisphere: $F_{1, 10} = 10.32$, $p = 0.009$; Genotype: $F_{1, 10} = 0.72$, $p = 0.416$; Interaction: $F_{1, 10} = 6.72$, $p = 0.027$) (Fig. 3.12f). In WT mice, sEPSC amplitude was consistently lower in the LH (contralateral to the trained forelimb) as compared to the RH ($p = 0.0023$). In contrast, no hemispheric difference was seen in sEPSC amplitude in PiPaw-trained Q175-FDN mice ($p = 0.906$). The observed difference in WT mice

was due more so to a decrease in amplitude in the left hemisphere (WT-LH Naïve vs. Trained: $U = 80$, $p = 0.091$) as opposed to an increase in the right hemisphere (WT-RH Naïve vs. Trained: $t_{30} = 0.774$, $p = 0.45$), although neither difference was significant when comparing naïve to trained animals. Overall, these results indicate that WT mice display both bilateral and hemisphere-specific changes in DLS-MSN glutamatergic synapses in response to training in the PiPaw task, whereas no such changes are seen in Q175-FDN mice.

We next investigated whether forelimb motor learning influences the magnitude or direction of synaptic plasticity evoked in dorsolateral striatum neurons in response to a stimulation protocol. For these experiments, extracellular field potentials (fEPSPs) were recorded in the DLS of 10-month-old WT and Q175-FDN mice immediately after testing in the PiPaw system. Field potentials were evoked every 15 seconds by stimulating in an area of the DLS dorsal to the recording site, and $GABA_A$ receptors were blocked with an antagonist (50 µM picrotoxin) in order to minimize inhibitory responses. To elicit plasticity, a high-frequency stimulation (HFS) protocol was applied (100 Hz for 1 s, repeated 4 times with a 10 s interval). This protocol typically causes an endocannabinoid-mediated long-term depression (LTD) in wildtype striatal neurons (Sepers et al., 2018), although it has also been reported to cause a post-synaptic NMDA receptor-dependent LTP, depending on the recording conditions (Kung et al., 2007; H. Park et al., 2014).

In the left hemisphere, contralateral to the trained forelimb, a modest decrease in fEPSP amplitude was seen in response to HFS in WT animals, with responses decreasing to 90.1% (± 5.7%) of baseline 30 minutes after administration of the protocol (Fig. 3.13a-b). In contrast, Q175-FDN striatal field responses showed an increase in amplitude that lasted until the end of the 40-minute recording period (Time: $F_{49, 637} = 2.104$, $p < 0.0001$; Genotype: $F_{1, 13} = 14.2$, $p =$

0.0023; Interaction: $F_{49, 637} = 3.969$, $p < 0.0001$) (Fig. 3.13a). The average response amplitude of Q175-FDN field responses was 112.9% (±1.8%) of baseline 30 minutes after HFS, significantly different from WT mice ($t_{7.203} = 3.779$, $p = 0.0065$). Surprisingly, no change in the amplitude of fEPSPs was seen in the right hemisphere following HFS in either WT or Q175-FDN mice, (Time: $F_{49, 637} = 3.839$, $p < 0.0001$; Genotype: $F_{1, 13} = 1.432$, $p = 0.253$; Interaction: $F_{49, 637} = 1.469$, $p = 0.023$) (Fig. 3.13c). WT and Q175-FDN striatal field responses were similar 30 minutes following right hemisphere HFS (98.1% ± 3.8% and 104.4% ± 1.9% respectively) and no genotype difference was observed ($t_{13} = 1.521$, $p = 0.152$) (Fig. 3.13d).

The paired-pulse ratio of fEPSPs (50 ms interval) was measured prior to and 30 minutes after HFS in order to identify any changes in the presynaptic probability of glutamate release. At baseline, no significant effect of hemisphere or genotype was observed, although a slight trend was seen towards an overall increase in PPR in the RH as compared to LH (Hemisphere: $F_{1, 26} = 2.874$, $p = 0.102$; Genotype: $F_{1, 26} = 2.622$, $p = 0.118$; Interaction: $F_{1, 26} = 0.017$, $p = 0.897$). Following HFS, a significant increase in PPR was seen in the left hemisphere of WT animals ($t_6 = 3.927$, $p = 0.0077$), supporting a presynaptic mechanism of HFS-induced LTD (Fig. 3.13e). In Q175-FDN, however, a significant decrease in PPR was observed ($t_7 = 2.655$, $p = 0.033$), suggesting that probability of glutamate release increased in response to HFS (Fig. 3.13e). In the right hemisphere, no significant changes in PPR were observed following HFS in either WT ($t_6 = 0.547$, $p = 0.604$) or Q175-FDN ($t_7 = 0.211$, $p = 0.839$) (Fig. 3.13f). These results indicate that the response to a plasticity-inducing stimulation protocol is altered in the DLS of Q175-FDN mice following training on a forelimb motor task. Specifically, this difference in the direction of plasticity was restricted to the hemisphere contralateral to the trained forelimb, whereas response to HFS in the ipsilateral DLS was similar to WT.

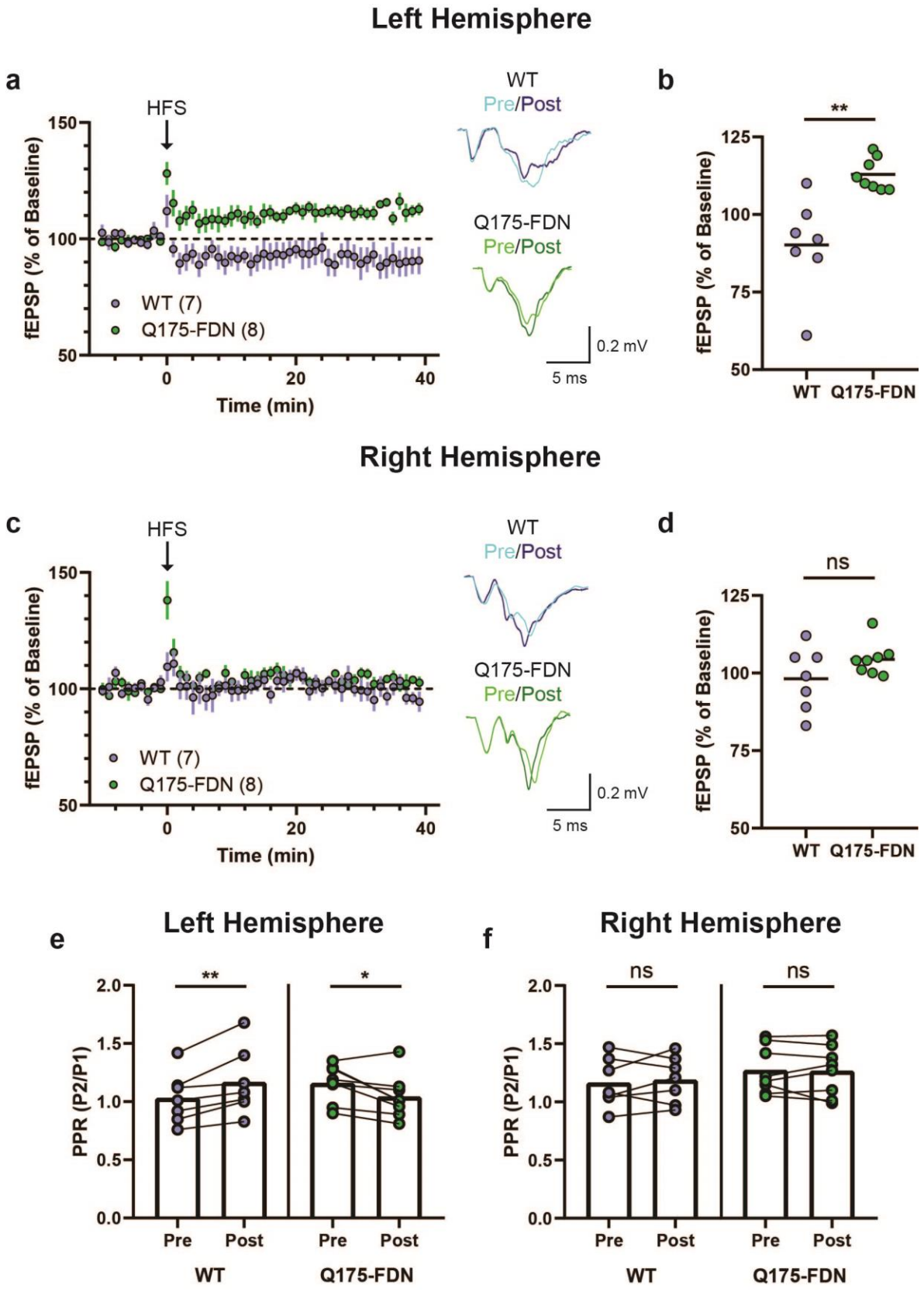
Left Hemisphere
a
HFS
fEPSP (% of Baseline)
150
100
50
0
20
40
Time (min)
WT (7)
Q175-FDN (8)
WT
Pre/Post
Q175-FDN
Pre/Post
0.2 mV
5 ms
b
**
125
100
75
50
WT
Q175-FDN
Right Hemisphere
c
HFS
WT (7)
Q175-FDN (8)
WT
Pre/Post
Q175-FDN
Pre/Post
0.2 mV
5 ms
d
ns
e
Left Hemisphere
**
*
PPR (P2/P1)
2.0
1.5
1.0
0.5
0.0
Pre
Post
WT
Q175-FDN
f
Right Hemisphere
ns
ns

Figure 3.13 Hemisphere and genotype-specific HFS-induced plasticity following PiPaw testing **(a)** Averaged time course of fEPSP amplitude in the LH-DLS before and after application of an intrastriatal HFS protocol (time 0). fEPSPs were recorded every 15 s and each circle represents the average of four responses normalized to the average of the baseline period (5 min period before HFS). Experiments were performed in acute slices taken from 10-month-old WT and Q175-FDN mice immediately after the end of PiPaw testing (right forelimb trained). While the amplitude of WT fEPSPs in the LH are depressed in response to HFS, Q175-FDN responses are potentiated. Traces show average response in baseline versus 30-35 minutes post-HFS for a representative experiment (stimulation artifact removed for clarity). **(b)** The average LH-DLS fEPSP amplitude 30-35 minutes post-HFS is higher in Q175-FDN than WT. **(c)** Averaged time course of fEPSP amplitude in the RH-DLS shows no significant potentiation or depression of responses in either WT or Q175-FDN. **(d)** The average amplitude of RH-DLS fEPSPs compared to baseline is similar in the two genotypes 30-35 minutes post-HFS. **(e)** Paired-pulse ratio of LH-DLS fEPSPs was averaged in the 5 min period before HFS ('Pre') and from 30-35 minutes after HFS ('Post'). PPR increases in WT and decreases in Q175-FDN following HFS. **(f)** In the right hemisphere, no changes are seen in PPR of DLS fEPSPs following HFS for either WT or Q175-FDN mice. *n* = 7(4) RH WT, 7(4) LH WT, 8(5) RH Q175-FDN and 8(5) LH Q175-FDN, with n=number of slices and numbers in brackets indicating the number of animals. All mice had been tested for 3-4 weeks in the PiPaw task up to the day of experiments. *: $p<0.5$; **: $p<0.01$; ns: not significant.

3.4 Discussion

Expanding on the study presented in Chapter 2, the work in this chapter had several distinct goals. The first was to develop a standardized and open-source tool that could be used to assess forelimb motor learning and kinematics within the mouse home-cage. To this end, I made several important modifications to the original home-cage system in order to ensure mice performed the task in a consistent manner and individual trials were structured and discrete. In addition I designed a behavioural methodology that would assess a specific aspect of motor learning and control, namely the ability to accurately terminate a backwards forelimb movement within a specific position range. In order to achieve high rates of task acquisition, I implemented

a multi-phase shaping paradigm where animals first learned to nose-poke, and then nose-poke while simultaneously pulling the lever further and further backwards. This enabled successful training of animals from a wide range of ages (2- to 11-months-old) and genotypes, including symptomatic HD mice.

In order to ensure that learning ability was not confounded by fatigue or differences in strength between animals, the force required to pull the lever was set at a very low level (~15 mN). In addition, the range of motion required to perform successful trials was relatively small (~1 cm), and attainable regardless of body size. As an indication of this, learning of the task was strikingly similar in 2- and 10-month-old WT mice, including a similar proportion of undershot and overshot trials across training, despite significant differences in body weight and size. Although the PiPaw module was designed in such a way that mice would naturally grasp the lever with their right forelimb, a small number of animals (7 of 47 WT mice) pulled the lever with either both forelimbs or with their left forelimb alone on a proportion of trials. In order to reduce variability in our data set due to these differences in task strategy, these mice were removed from analysis. One adaptation that could be made in a future version of the system, however, would be to incorporate a touch-sensing fixed-position post for the animal's left forelimb to grasp, as was used in a similar system (Bollu et al., 2019). In addition to nose-poking, the mouse would be required to contact the post with their left forelimb before a trial could be initiated, ensuring more consistent and standardized task performance.

Over the course of one week of PiPaw testing, WT mice increased their proportion of successful trials by 2.5× on average, although individual learning trajectories varied substantially. Unexpectedly, the mean values of certain task execution parameters (e.g. pull amplitude, peak velocity) did not change across testing despite clear performance improvements.

For example, average pull amplitude, which was the main determinant of trial success, was only ~2° different on D7 as compared to D1. In contrast, the inter-trial variability of certain kinematic parameters was strongly reduced across testing. In reinforcement learning, variability during early stages is advantageous as exploration is necessary in order to determine execution parameters that will lead to reward (Dhawale et al., 2017; Van Mastrigt et al., 2020). However, as information about the outcomes of different movements becomes available, variability is reduced in order to improve performance (Dhawale et al., 2019; Pekny et al., 2015; Todorov & Jordan, 2002). As movement execution is inherently noisy and it is not possible to decrease variability universally, an optimal solution is to reduce variability specifically on those parameters that are relevant to task success (Santos et al., 2015; Todorov & Jordan, 2002). In this case, the inter-trial variability of pull amplitude, the parameter most relevant to success, decreased by 42% on average from D1 to D7. Trial duration was another reward-related parameter, as trials that were held for longer than two seconds were automatically failed. Consistent with this, the inter-trial variability of trial duration decreased by over 75% from D1 to D7. This reduction of inter-trial variability in specific kinematic parameters provides a direct measure of motor learning on the task and correlates with improved success rate.

One of the most compelling benefits of studying behaviour in a home-cage system is the opportunity to examine the structure of self-paced learning and task performance. In this regard, we found that mice consistently clustered their trials into short bouts of high task engagement, followed by longer breaks where no trials were performed. The large majority of trials occurred in such bouts, with less than 10% of trials being classified as non-bout trials. On one hand, this structure is likely related to the natural circadian pattern of eating and drinking displayed by mice (Godynyuk et al., 2019; A. Ho & Chin, 1988) and the volume of water required to sate the

animals thirst. However, there also appeared to be a more functional purpose of clustering trials into short bouts. Animals displayed significant within-bout learning, with a greater than 10% increase in average success rate from the first trial of a bout to the eighth trial. Reflecting this, the average success rate for all trials occurring within bouts was substantially greater than that for non-bout trials. This short-term motor learning is often seen in motor tasks and tends to be most prominent in early stages of learning (Buitrago, Ringer, et al., 2004; Buitrago, Schulz, et al., 2004). Interestingly, average success rate tended to decrease towards the end of the bout, possibly indicating an effect of task-related fatigue on motor performance. In addition to these factors, competition between animals for access to the testing module could lead mice to perform longer, but less frequent, bouts in order to exploit their access to the task during periods when it's available. Competition could also provide an explanation for the comparative lack of circadian rhythmicity of task performance seen in some animals. However, considering the relatively short amount of time that mice spend in the testing module per day (<1 hour on average), the contribution of this factor is most likely modest.

The second goal of this chapter was to use the PiPaw task to characterize motor learning and forelimb kinematics in mouse models of Huntington's disease. Given reported deficits in the termination of arm movements in HD patients (Klein et al., 2011; Smith et al., 2000) and the 'overshooting' behaviour displayed by some YAC128 mice in the original home-cage lever task (Fig. 2.5), the PiPaw methodology was expected to show good sensitivity to motor phenotypes in HD mice. Surprisingly, YAC128 at both early (2-month-old) and symptomatic (10-month-old) stages showed intact motor learning and refinement of kinematic variability on the PiPaw task. In contrast, Q175-FDN knock in HD mice had robust motor learning deficits on this task at 10-months-old. The divergent phenotype between these two models was surprising given that

YAC128 mice manifest motor abnormalities several months earlier than Q175-FDNs (Slow et al., 2003; Southwell et al., 2016), and show certain motor deficits (e.g. open field hypoactivity) that are not observed in Q175-FDN mice at any age. Indeed, YAC128 mice have been reported to show a mild motor learning deficit on the rotarod as early as 2-months-old (Van Raamsdonk et al., 2005), a full 8-months earlier than the age at which mice were assessed here. To confirm the presence of abnormalities on other behavioural tests in our colony of YAC128 mice, we performed rotarod and open field testing. This testing replicated previously reported results, with significant rotarod deficits and hypoactivity seen in YAC128 mice at this age. In fact, YAC128 mice had a somewhat worse performance on the rotarod than Q175-FDN, although this was not significant. Thus, the reason for comparatively normal learning of the PiPaw task is not immediately clear.

In this regard, one possibility is that YAC128 and Q175-FDN mice simply have different manifestations of HD-related pathology, just as humans with HD have substantial symptomatic heterogeneity (Waldvogel et al., 2012). In YAC128 mice, the functional consequences of mHTT expression may manifest as early and non-progressive deficits in full body motor coordination (Menalled et al., 2009), in addition to locomotor hypoactivity (Slow et al., 2003), but less so as a universal impairment in motor learning. In contrast, Q175-FDN mice may have a later, but progressive, onset of motor dysfunction that manifests more uniformly as impaired motor learning, balance and coordination (Southwell et al., 2016). Another factor to consider is the way in which motor symptoms have traditionally been assessed in HD mice. The rotarod test has several confounds, including bodyweight and task non-compliance (as discussed in Chapter 1.2.3.1). Considering the significant weight gain seen in YAC128 mice and the fact that rotarod deficits in this model can be rescued with dietary restriction (Moreno et al., 2016), it seems likely

that rotarod testing may overestimate the severity of the motor phenotype in these mice. Still, the absence of any obvious motor phenotype on this lever-pulling task is surprising, and it must also be considered that this specific methodology may simply not be particularly sensitive to HD-related motor phenotypes. However, the poor performance of Q175-FDN mice makes this less likely. In fact, considering the severity of the deficit in these mice it's possible that this impairment actually emerges prior to a rotarod deficit (8-months-old), although further testing would be necessary to confirm this.

Although these two HD mouse models have the same genetic background, a variety of factors could contribute to the observed divergence in phenotypes, the most obvious of which is the way in which the expanded huntingtin gene is expressed. In YAC128 mice, the full human *mHTT* gene with large upstream and downstream regulatory regions is inserted as a transgene on the long arm of chromosome 3, and is expressed under the control of the human *HTT* promotor (Pouladi et al., 2012; Slow et al., 2003). The precise insertion location, and whether this affects the expression of any endogenous genes, is not known, and may be a relevant concern considering reports of altered gene expression due to transgene insertion in the R6/2 mouse (Jacobsen et al., 2017). YAC128 mice also express both copies of the endogenous *Htt* gene in addition to the transgene, resulting in substantial overexpression of huntingtin protein. The contribution of this overexpression is not fully known, although the results from one study suggest that it has a negligible effect on motor phenotypes but may improve striatal neuropathology (Van Raamsdonk, Pearson, et al., 2006).

In contrast, heterozygous Q175-FDN mice express one copy of a chimeric *mHtt* gene with the endogenous mouse exon-1 replaced by an expanded human exon-1 containing ~200 CAG repeats (Southwell et al., 2016). As a result, the mHtt protein is expressed under the mouse

promotor, which may result in differential regulation of protein expression as compared to what is seen in humans. However, from a perspective of total protein level, this strategy recapitulates HD much more closely – one wtHtt allele expressed at a normal level, and one mHtt allele expressed at ~55% of the normal level, resulting in an underexpression of total huntingtin protein (about 73% of the normal level overall) (Southwell et al., 2016). In contrast, the YAC128 mouse expresses mHtt at 75% of the endogenous level for both gene copies (Slow et al., 2003). As a result, there is almost three times as much mHtt protein expressed in YAC128 as in Q175-FDN. Although this should lead to a substantial increase in pathogenicity in YAC128 mice, the length of the polyglutamine tract must be considered as well. At face value, the polyglutamine expansion in Q175-FDN mice (~200 repeats) is substantially longer than in YAC128 mice (125 repeats), perhaps counteracting some of the expression-related differences. However, these models also differ in the nature of the trinucleotide repeat coding for glutamine. In the Q175-FDN model, this trinucleotide expansion is a pure CAG-tract, identical to what is typically seen in patients. As a result, this region is prone to repeat-length instability, both between generations and somatically (Wheeler et al., 2007). In contrast, the expanded tract in YAC128 mice has 9 CAA codons (which also code for glutamine) interspersed to confer stability (Pouladi et al., 2012). This could have significant implications for disease pathogenesis in this model, as two recent studies have found that interrupting CAA codons in HD patients are protective, and it is the pure CAG-tract length, rather than polyglutamine length, that correlates with HD age of onset (GeM-HD Consortium, 2019; Wright et al., 2019). As age of onset is also correlated with polymorphic variation at certain DNA maintenance genes, it's likely that this CAG-dependence is related to somatic expansion of *mHTT*, a process which would not occur in YAC128 mice (GeM-HD Consortium, 2019). These differences in polyglutamine length, protein level,

promoter region and presence of interrupting CAA codons are certain to influence the pathogenesis of HD models, and may contribute to the divergent behavioural phenotype seen in this study.

Although the specific task methodology was different, these results are also in contrast with the previously presented finding of impaired motor learning in young YAC128 mice (Fig. 2.4a; Woodard et al., 2017). One possibility is that the deficit observed in Chapter 2 was caused by impaired behavioural flexibility and was not seen in PiPaw testing because the success requirements did not change. This would be supported by the observation of a mild abnormality in the reversal phase of the T-maze in 2-month-old YAC128s (increased arm entries on the first trial of reversal) (Van Raamsdonk et al., 2005). However, the fact that no such deficit was seen in 4- and 6-month-old mice (Fig. 2.4b/c), and the absence of any other cognitive deficits in YAC128 mice until around 6-months-old (Southwell et al., 2009) makes this somewhat doubtful. Another possibility is that 2-month-old WT mice in the original home-cage task tended to have a longer hold duration to begin with, and consequently did not have to adapt their behaviour substantially to progress through the task. This is supported by the finding that 2-month-old YAC128 mice in the PiPaw task had a significantly lower proportion of held-too-long trials on the first day of testing as compared to WT mice, and average trial duration tended to be longer in WT mice as well ($p = 0.07$). If this is a manifestation of an early hyperactive phenotype that later normalizes, it would explain the normal motor learning of older mice on the original home-cage task. Indeed, the tendency for decreased trial duration and 'held too long' trials was not seen in 10-month-old YAC128 mice, supporting this possibility.

One interesting observation was that although HD mice did not have an increased proportion of overshot trials overall, they did not decrease the proportion of these trials over one

week of testing, whereas WT mice did. This was seen in both young and symptomatic YAC128 mice as well as in symptomatic Q175-FDN mice and could be reflection of impaired movement termination. This is also consistent with the kinematic abnormalities seen in 6-month-old YAC128 mice in Chapter 2 (Fig. 2.5), although it was not observed in younger animals using that methodology. Differences in the patterns of PiPaw task engagement were also observed in young and old YAC128 mice. Two-month-old mice had a significant increase in the number of trial bouts they performed per day that could not be explained by a difference in task success rate. One possibility is that this is related to hyperactivity that has been reported in young YAC128 mice (Slow et al., 2003), however other factors such as motivation for water can't be ruled out. In contrast, 10-month-old YAC128 mice showed a trend towards a decreased number of trial bouts per day. As we also observed significant open field hypoactivity in these mice, it's likely that this is related to this phenotype. Although an increase in the number of trial bouts per day was also seen in Q175-FDN mice, this result is somewhat more difficult to interpret given that these animals had a much lower success rate and consequently performed a greater number of trials per day on average. The altered circadian distribution of trials seen in these animals must also be interpreted in this context, as this could have been influenced by increased task engagement.

The third goal of the research in this chapter was to investigate whether PiPaw testing was associated with changes in the spontaneous activity and plasticity of dorsolateral striatum MSNs, and whether this was altered in Q175-FDN mice. As the PiPaw task involves motor learning specifically in the right forelimb, any task-related electrophysiological changes are likely to be different between the two hemispheres. Thus, we first investigated whether there were hemispheric differences in the properties of DLS-MSNs in animals that hadn't been

exposed to the task. Consistent with a previous study (Southwell et al., 2016), we found an overall decrease in the frequency of spontaneous EPSCs in Q175-FDN MSNs as compared to WT, but sEPSC amplitude was unchanged. Following PiPaw testing, a bilateral decrease in sEPSC frequency was observed in WT DLS-MSNs, however no change was seen in Q175-FDN cells. This decrease in WT mice suggests either a lower presynaptic probability of release at glutamatergic inputs to MSNs or a decreased number of synapses onto MSNs (or a combination of these factors). However, as this decrease was not hemisphere-specific, it's difficult to say whether this change is specifically related to forelimb motor learning, or rather to another aspect of the behavioural testing. Regardless, presynaptic input was not altered in DLS-MSNs recorded from Q175-FDN animals following PiPaw testing. As sEPSC frequency was already quite low in these animals, one possibility is that the capacity for a further decrease was occluded. In addition, the ability for synaptic inputs to show presynaptic depression may have been limited, given previously reported deficits in the ability of Q175-FDN DLS-MSNs to undergo stimulation-dependent presynaptic LTD (Sepers et al., 2018).

In contrast to the bilateral decrease in sEPSC frequency observed in WT mice, the effect of PiPaw testing on sEPSC amplitude was hemisphere-specific. Average sEPSC amplitude was consistently lower in the LH of trained WT mice as compared to the RH, suggesting that forelimb training was associated with a postsynaptic depression of responses specifically in the DLS contralateral to the trained forelimb. Interestingly, a recent study found that ipsilateral projections from the primary motor cortex to the DLS (e.g. left M1 to left DLS) were biased towards LTD in response to a theta-burst stimulation protocol, while contralateral projections (e.g. left M1 to right DLS) were biased towards LTP. This opposing plasticity was explained by an increase in GluN2B-containing NMDARs on contralateral projections (W. Li & Pozzo-Miller,

2019). Given that the left motor cortex is primarily responsible for controlling the trained right forelimb, these findings coincide with our observations regarding training-associated plasticity. In addition, it has been found that habitual learning on an operant lever-press task in mice causes a decrease in sEPSC amplitude in DLS-MSNs, however this change was reportedly specific to indirect pathway neurons (Shan et al., 2015). Unfortunately, we were not able to differentiate between direct and indirect pathway neurons in our experiments, but it's possible that the effect we observed in the LH was primarily driven by a decrease in iMSNs. In contrast to what was seen in WT mice, no hemispheric differences were observed in Q175-FDN mice following PiPaw-training. One reasonable explanation is that these mice have a deficit in training-associated plasticity, and that this deficit is directly related to their impaired learning and performance of the task. However, it's also possible that this difference from WT animals is related to Q175-FDN mice being at a different stage of learning (i.e. early vs. late motor learning). Changes in the activity, plasticity and input to MSNs at different stages of learning on motor tasks have been investigated in mice using *in vivo* and *ex vivo* methodologies (Giordano et al., 2018; Kupferschmidt et al., 2017; Yin et al., 2009). However, typically learning-associated changes in MSN activity are greater during the early as opposed to late learning phases, making this hypothesis less likely.

In addition to changes in the spontaneous activity of DLS-MSNs, PiPaw-trained animals also exhibited hemisphere and genotype-specific plasticity of striatal neuronal population responses in response to HFS. In the left hemisphere, WT field responses showed a presynaptic depression of fEPSPs in response to HFS, as indicated by a modest decrease in peak amplitude and an increase in PPR. In contrast, Q175-FDN LH striatal neurons showed a significant potentiation of field responses following HFS. The opposing direction of this plasticity is similar

to what is seen in early vs. late rotarod learning, with early learning being associated with a metaplastic shift from LTD to LTP (Giordano et al., 2018). This implies that the ability to undergo HFS-LTP, which is NMDAR-dependent, is intact in Q175-FDN mice at this age and suggests that animals may be still in an 'early' learning phase, even after 3-4 weeks of testing. In the right hemisphere, no significant plasticity of field responses was observed in response to HFS in either genotype. The reason for a lack of HFS-LTD in the right hemisphere of WT animals is not clear; however, if a large number of neurons had already undergone substantial presynaptic LTD (as suggested by reduced sEPSC frequency), it may have occluded any further depression. In addition, PPR tended to be higher in the RH as opposed to the LH at baseline, again suggesting that glutamatergic inputs were already inhibited prior to HFS. Interestingly, right hemisphere WT fEPSPs showed a relatively wide spread of responses following HFS, with two of seven slices showing LTD (>10% decrease in fEPSP peak), but one slice also showing LTP (>10% increase). In contrast, only one of eight right hemisphere Q175-FDN slices showed any plasticity (LTP in this case) in response to HFS. In fact none of the sixteen Q175-FDN slices across both hemispheres displayed any depression of fEPSP amplitude in response to HFS, consistent with a reported impairment in presynaptic depression in these mice (Sepers et al., 2018).

In summary, the PiPaw system provides a novel and high-throughput method for assessing motor learning and kinematic measures of task execution in wildtype and transgenic animals. Using this tool, I investigated how variability is refined over time on a precision lever pulling task in order to increase success and maximize rewards. In addition, I examined how self-directed task performance is structured over long periods by animals tested in this system. Importantly, I also applied this to two separate mouse models of HD, finding that these models

strongly diverged in their ability to perform this particular task. These results suggest that motor deficits in the YAC128 mice may not be as universal as previously thought and encourage future elucidation of the motor phenotype in these mice. In addition, I found that the failure to effectively perform the task in Q175-FDN mice is associated with an absence of synaptic plasticity in dorsolateral striatum MSNs in response to training, and differences in the direction of HFS-induced plasticity as compared to WT animals. These results further validate the use of home-cage tools for behavioural assessment in genetic models of Huntington's disease and other neurological disorders.

Chapter 4: Development and testing of the PiDose home-cage drug administration system

4.1 Introduction

Behavioural testing is an important step in determining the validity of rodent models of disease and in establishing the response of these animals to a therapeutic intervention. However, before the behavioural response to a drug treatment can be assessed, a treatment protocol and route of administration must be selected and applied to the animals. A variety of routes of administration are used in drug treatment studies, with the goal to optimize delivery of the agent while reducing the potential for injury and procedure-associated stress. Parenteral administration via subcutaneous or intraperitoneal injection is often used due to the high bioavailability of injected drugs; however, repeated restraint and injection causes stress and puts the animal at risk of physical complications (Meijer et al., 2006; Turner et al., 2011; Vinkers et al., 2009). These stress responses are particularly undesirable in behavioural studies, as chronic stress affects a variety of behaviours and may mask treatment affects and increase the risk of Type I/II errors (Elizalde et al., 2008; Mineur et al., 2006).

An alternative to injection is oral administration, which is often useful in a pre-clinical context as oral drug treatment is the most common and convenient route of administration in humans. Unfortunately, oral gavage presents the same problems as injection regarding treatment stress and the potential for injury (Turner et al., 2011; M. K. Walker et al., 2012). To avoid this, several studies have provided methods for the voluntary feeding of drugs to animals in a palatable form (e.g. sucrose water, peanut butter) (Atcha et al., 2010; Corbett et al., 2012; Dhawan et al., 2018; Doenni et al., 2016). This avoids some of the side effects associated with

injection and gavage, but is time-consuming for chronic experiments and involves extensive experimenter interaction, which in itself may be enough to increase animal stress (Sorge et al., 2014). To circumvent the need for manual administration, other studies have mixed the drug with the animal's drinking water (Dau et al., 2014; Gordon et al., 2018; Kim et al., 2014; Vetere et al., 2017). However, this method typically estimates drug dosage based on the average bodyweight and water consumption for all mice in a cage. This relies on the assumption that mice are drinking an amount of water that is directly proportional to their bodyweight, for which there is not clear support.

As previously discussed, the approach of automating experimental procedures using devices that the animal can freely access from within their home-cage has gained popularity in recent years. These systems provide the combined benefits of increasing the throughput of experiments and volume of data that can be collected, while also decreasing experimenter interaction and animal stress. Open-source tools that enable the home-cage monitoring of feeding and drinking (Godynyuk et al., 2019; Nguyen et al., 2016), bodyweight (Ahloy-Dallaire et al., 2019; Noorshams et al., 2017) and activity levels (Genewsky et al., 2017; Matikainen-Ankney et al., 2019) have all been published in the past five years. In addition, the automation of more complex operant tasks, such as those presented in Chapters 2 and 3, is becoming more and more popular (Bollu et al., 2019; Francis & Kanold, 2017; O'Leary et al., 2018; Silasi et al., 2018). In one notable home-cage study, the authors developed a proprietary methodology to automatically dose group-housed mice with the synthetic nucleoside BrdU over several days (Santoso et al., 2006). This system used an RFID detector to individually identify transponder-tagged mice and dispense drug solution to them through a liquid port. Dosage of drug could be individually specified for different mice, however animals had to be manually weighed in order to set drug

dose, and the accuracy of drug delivery was not directly assessed. Aside from this study, the potential for long-term home-cage drug administration in experimental rodents has not been explored.

To address the lack of such an option, I developed PiDose – an open-source tool for home-cage oral drug administration. PiDose allows mice to freely access a chamber (the 'dosing module') from their home-cage where they are automatically weighed and lick a spout to obtain drops of drug solution. This design ensures that mice consistently ingest the drug, as liquid is delivered directly into the mouth in response to licking. Mice are RFID-tagged to discriminate group-housed animals, and the drug volume each mouse receives can be individually customized based on their dosing condition and current bodyweight. Once they have received the required dose of drug for each day, they receive only water from the spout. This system allows for accurate dosing to be maintained over long periods (weeks to months) with minimal experimenter interaction. It is low-cost (~400 CAD) and built with 3D-printed parts and electronic components that can be easily obtained. In this chapter, I provide a description of the PiDose system and a demonstration of its accuracy and function in treating mice with drugs.

4.2 Methods

4.2.1 Hardware

The PiDose system consisted of a modified mouse home-cage with an opening to allow animals to freely access a linked 3D-printed dosing module (Fig. 4.1). The module was supported by a free-floating 0.78kg load cell (Phidgets 3132) mounted on a separate post that did not contact the cage, similar to the configuration described in Noorshams et al. (2017). A 3D-printed entranceway was attached to the cage, framing the chamber opening and allowing the

mouse to more easily enter the dosing module. At the opposite end of the dosing module from the entrance, a nose-poke port accessed a spout which dispensed drops from two separate liquid reservoirs. This spout was wired to a capacitive touch sensor controller (Adafruit 1982) to detect individual licks. Adjacent to the nose-poke port, an RFID reader (Sparkfun SEN-11828) was inset into the ceiling of the dosing module to identify transponder-tagged animals as described in Bolaños et al. (2017). A camera (Waveshare 10299) was positioned to one side of the dosing module in order to capture images of mice during drop delivery. The cage, dosing module, and camera were all attached to aluminum spacers (Siskiyou AS-2.00) mounted on a polycarbonate sheet. Four PiDose cages were built and used to perform the described experiments. The total cost for one system was ~300 USD and full instructions for constructing and wiring a PiDose cage can be found online (https://osf.io/rpyfm/).

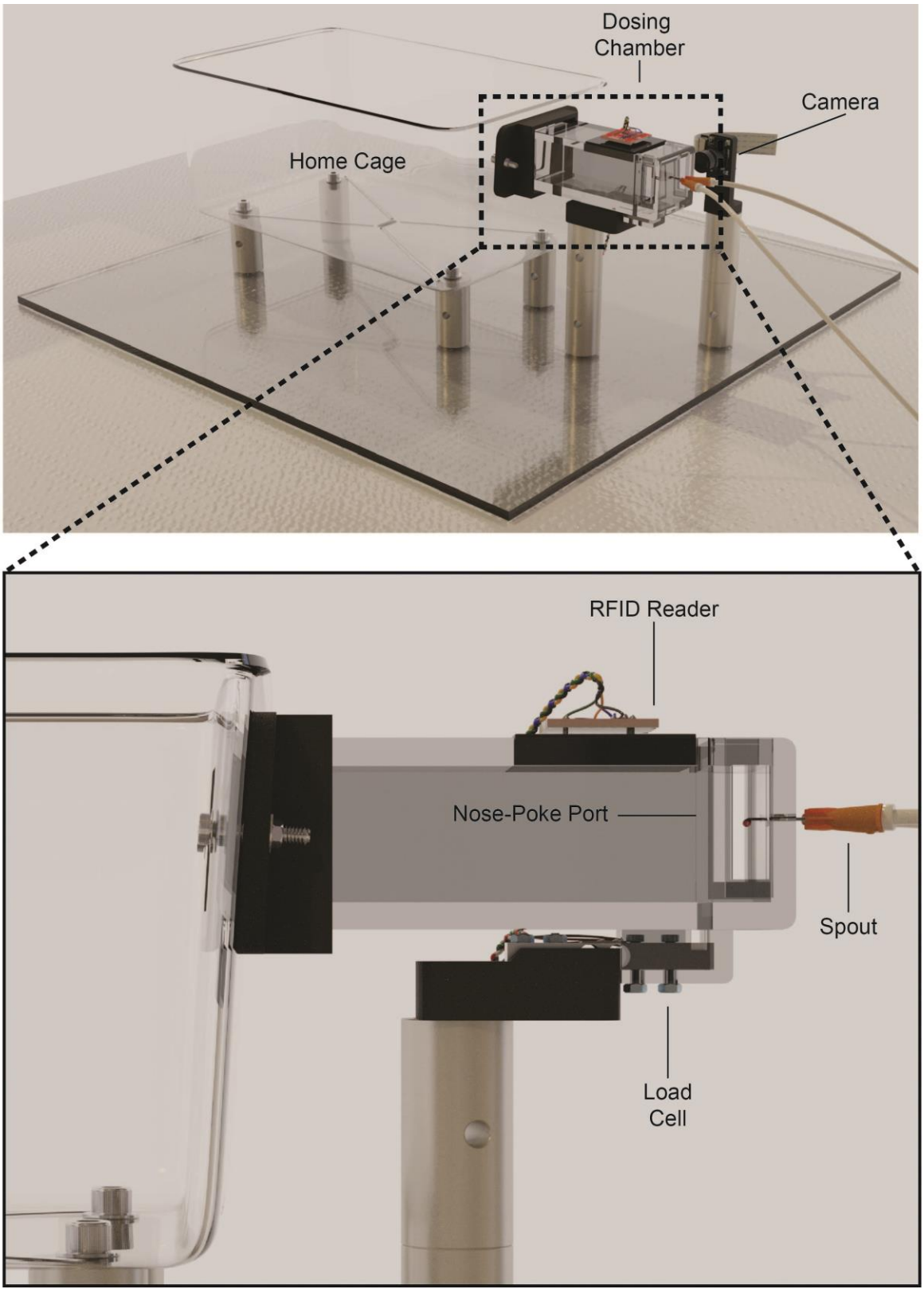
Dosing
Chamber
Camera
Home Cage
RFID Reader
Nose-Poke Port
Spout
Load
Cell

Figure 4.1 The PiDose home-cage drug administration system

PiDose consists of a dosing module mounted adjacent to a standard mouse shoebox home-cage. An entranceway allows animals to freely access the dosing module, where they can obtain both water and drug solution drops from a spout. An adjacent camera captures photos of drop delivery. The dosing module is mounted on a load cell which collects bodyweight measurements from mice. Transponder-tagged mice are identified by an RFID reader and can access the spout through a nose-poke port. Drop delivery is triggered by licking at the spout.

In order to dispense liquid from two sources with minimal dead volume and cross-contamination, a double-spout was constructed from two parallel and attached 18G gauge needles. To dispense drops from the double-spout, two complementary approaches were employed. Regular water drops were dispensed from a reservoir using a gravity-fed valve-based system, as in the original home-cage task and the PiPaw system (see Chapter 2.2.3). This method of water delivery was reliable; however, the drops varied somewhat in size over time due to changes in the level of the water reservoir or changes in resistance. As a result, the valve opening time had to be recalibrated every few days to ensure consistency. For dispensing drops of drug solution, I used a published open-source syringe pump design (Wijnen et al., 2014) which provides consistent and accurate liquid displacement over long periods. This syringe pump was constructed primarily from 3D-printed parts and used a NEMA17 stepper motor (Sparkfun ROB-09238) and threaded steel rod to move the plunger of a syringe. Through calibration of these pumps, it was determined that 57 steps were required to reliably give a drop of 10 µL from a 30mL syringe. To assess the accuracy of the syringe pumps, one hundred 10 µL drops were dispensed into a dish and weighed (repeated 8-10 times for each pump). Full instructions and parts required to construct this syringe pump can be found online (https://hackaday.io/project/27046-open-source-syringe-pump).

4.2.2 Software and dosing methodology

All PiDose components were connected to and controlled by custom software running on a Raspberry Pi 3B+ micro-computer running the Raspbian operating system. The software controlling the PiDose components and recording data was written in Python 3 and is available online (https://github.com/cameron-woodard/PiDose). The program ran continuously while animals were housed in the cage. When a mouse entered the dosing module, it was detected by the RFID reader and the program would load the relevant parameters and daily stats for the mouse. The size and shape of the chamber ensured that only one mouse could fully enter the dosing module and be detected by the reader at a time, however mice frequently went in and out of the chamber in quick succession. To ensure that the correct mouse was identified, the PiDose program continually monitored a 'tag-in-range' logic signal that indicated whether an RFID was currently in range of the reader. Every time a tag went in and out of range of the reader (even momentarily), a new read of the RFID was triggered to confirm whether it was the same or a different mouse. If the RFID was not recognized by the reader, possibly due to an incomplete read, the program would simply wait until the mouse left the chamber and attempt to read their ID again when they re-entered. If this happened too many times, however, a reboot of the Raspberry Pi would be automatically triggered.

For the duration the mouse was in the module, weight readings were collected from the load cell at 5 Hz and the capacitive sensor was activated on the spout. A lick at the spout would trigger the subsequent delivery of a water or drug drop depending on the mouse's treatment condition, and the number of drops they had received so far that day. Mice received drug drops starting at midnight until they have received the required number for the day, and then received water drops for the remainder of the 24-hour cycle. Immediately following drop delivery, an

image was taken by the camera which could then be used to validate that the animal had their mouth on the spout and the drop was not delivered in error. A 10-second timeout followed before the mouse was able to trigger delivery of another drop, in order to ensure that they fully ingested the liquid. After the mouse exited the dosing module, the capacitive trigger was deactivated, weight collection stopped, and a 30-second waiting period was triggered. If no mouse was detected before the end of this wait period, a sample of 20 readings was collected from the load-cell. If none of these readings were further than 0.1g away from the mean of the readings, the load-cell was tared.

Based on values collected from the load cell, an average daily weight was calculated for each mouse at midnight by rounding all values collected in the previous 24 hours to one decimal point, removing outliers and taking the mode of these values (i.e. the most commonly occurring weight). This was then used to determine the number of drug drops that the mouse received the following day. All events (e.g. entrance, lick, drop delivery) were recorded to a text file for that mouse with an event code and timestamp. Timestamped weights were recorded into a separate daily weight text file for each mouse, and a new file was created at midnight on each day. A summary file recorded the number of daily water and drug drops received, and the weight for the mouse on each day of treatment.

4.2.3 Animals

A total of 8 wildtype FVB/N mice and 10 YAC128 HD mice (FVB/N background, line 55) were used in experiments. All animals were male and were housed and treated in groups of 3-4 littermates in a temperature and humidity-controlled room on a 12/12 h light/dark cycle

(lights on at 6AM). All procedures were conducted in accordance with the Canadian Council on Animal Care and approved by the University of British Columbia Committee on Animal Care.

4.2.4 RFID capsule implantation

RFID capsule implantation was performed as described in Chapter 2.2.2. Animals were allowed to recover for a minimum of one week following surgery before behavioural testing.

4.2.5 Drug treatment

For drug treatment experiments, memantine hydrochloride (Tocris 0773) was dissolved in water at a concentration of 50 µg/mL. Three groups of YAC128 mice (54-71 days old) were randomly assigned to treatment (n = 6) and control (n = 4) conditions and housed in the PiDose cages. Parameters in the PiDose program were set such that mice in the treatment cohort received two 10 µL drops of memantine solution per gram of bodyweight per day, resulting in a dose of 1 mg/kg of bodyweight per day. Mice in the control group received only water drops. During the first day in the cage, no drug drops were delivered in order to determine a baseline weight for the mice and ensure that mice acquired the operant licking response. Mice remained in the PiDose cages for between 58 and 64 days.

4.2.6 Statistics

All data analysis and statistics were performed using Python (Python Software Foundation, version 3.7) and Prism 8 (GraphPad Software). Data are expressed as mean ± SEM. Alpha level for all tests was p = 0.05. Pearson correlation coefficients were calculated to measure the linear correlation between PiDose bodyweights and manual bodyweights, and between

bodyweight and water consumption. Paired two-tailed t-tests were used to compare total water and memantine consumption between start and end of treatment in the memantine study.

4.3 Results

4.3.1 PiDose accurately weighs and delivers liquids to group-housed mice

In order to assess the accuracy and functioning of different components of PiDose, two cages of wildtype mice (n = 8) were used to test the system. Following RFID capsule implantation, mice were placed in the PiDose cages and allowed free access to the dosing module for a 14-day period. For this initial group, no drug treatment was used, and mice obtained only water from the spout. Within 24 hours, all animals learned to lick the spout to trigger water delivery, receiving an average of 1.68 mL of water (± 0.06, n = 112 mouse-days) per day over the test period. An average of 8820 weight readings (± 612, n = 112), corresponding to ~30 minutes in the dosing module, were obtained per mouse per day. Based on these load-cell measurements, an average daily weight for each mouse was calculated by PiDose **(**Fig. 4.2a**)**. In order to determine the accuracy of these bodyweights, animals were also manually weighed daily at midday. There was a high correlation between the PiDose-calculated daily bodyweights and manually obtained bodyweights (R^2 = 0.989, p < 0.0001, n = 112) (Fig. 4.2b), and the average absolute discrepancy between the two weighing methods was 0.292 grams (± 0.025, n = 112). Expressed as a percentage of bodyweight for each mouse, this translates to an average weighing error of less than one percent (0.853% ± 0.077, n = 112), and is smaller than the average day-to-day change in bodyweight observed over this same period (1.414% ± 0.112, n = 104) (Fig. 4.2c).

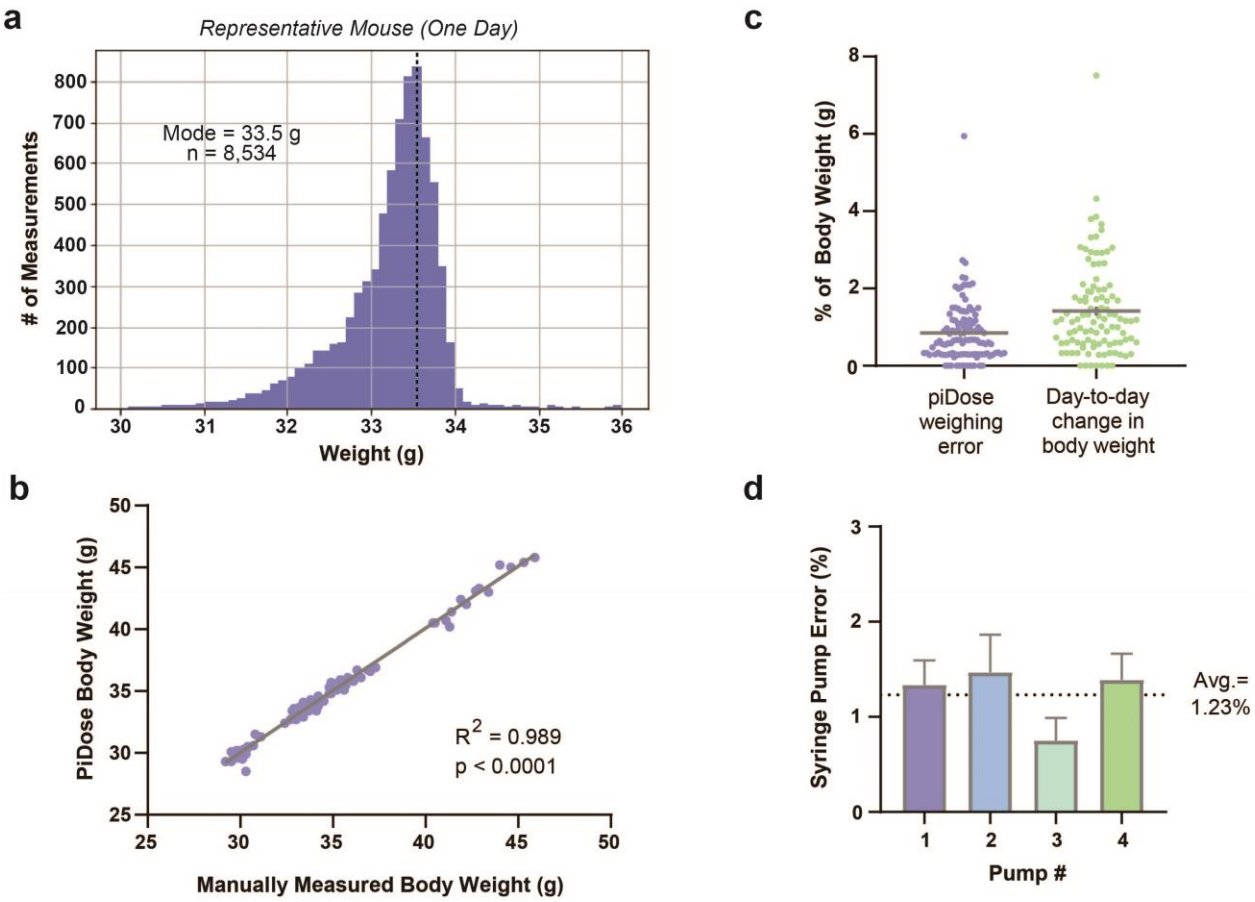

Figure 4.2 PiDose reliably weighs and administers solutions to group-housed mice

(a) Histogram of rounded bodyweight measurements collected for a representative animal over the course of one day. The average bodyweight for the mouse is determined by taking the mode of these values. **(b)** Average daily bodyweights calculated by PiDose are highly correlated with manually measured bodyweights (n = 112). **(c)** The average absolute discrepancy between the PiDose bodyweight and the manual bodyweight (i.e. the weighing error) (n = 112) is smaller than the average day-to-day change in bodyweight (n = 104) for the same animals. **(d)** Average error for each of the four syringe pumps constructed to administer drug-solutions to mice in PiDose expressed as a percentage of the desired drop volume (10 µL). Error bars represent SEM.

As it is critical that the volumes of drug delivered using PiDose are accurate and consistent, we used 3D-printed syringe pumps for each cage based on the design described by Wijnen et al. (2014). After determining the number of motor steps required to deliver a drop of

approximately 10 µL from a 30 mL syringe, we assessed the accuracy of test drops delivered by these pumps. The average drop size across the four pumps was 9.994 µL (range = 9.723–10.30, *n* = 36 tests), with an average absolute error of only 0.123 µL (± 0.015, *n* = 36), or 1.23% of the drop volume (Fig. 4.2d). Together, these results indicate that PiDose is capable of accurately weighing and delivering solutions to group-housed mice.

4.3.2 PiDose maintains stable drug treatment over long periods despite day-to-day changes in bodyweight and water consumption

We next assessed the ability of this system to treat mice with a fixed drug dosage over an extended period. Memantine is a low-affinity uncompetitive NMDA receptor antagonist that has shown potential as a treatment for HD both in animal models (Dau et al., 2014; Milnerwood et al., 2010) and patients (Ondo et al., 2007). YAC128 HD mice were assigned to either control or treatment groups and housed in the PiDose cages for two months beginning at 2-months-old. Treatment group mice received 1 mg/kg memantine per day, while control mice received only water. As with wildtype animals, YAC128 mice quickly learned to lick the spout to obtain water and drug solution. The timing of all dosing module entrances, licks and drop deliveries was automatically tracked and recorded by PiDose, allowing for detailed temporal analysis of water and drug consumption (Fig. 4.3a). Drug administration began at midnight each day and would continue until the mouse had received the required amount of memantine, typically by mid-morning. Overall, a clear circadian rhythmicity was observed, with mice drinking predominantly in the dark phase of the light cycle (73.9% of drops; ± 3.5, *n* = 10 mice) (Fig. 4.3b). The average duration of the daily dosing period (i.e. the time from first to last drug solution drop each day) was 10.31 hours (± 0.34, *n* = 375 mouse-days). To confirm that mice were consuming the

delivered water and drug solution drops, we positioned a camera adjacent to the spout to take images immediately following drop delivery. Over 30,000 images were taken from the PiDose cages and manually analyzed to assess whether the animal's mouth was on the spout at the time the drop was dispensed. We found that in 96.8% of images, the animal's mouth was on the spout immediately following drop delivery, while in the remaining 3.2% the mouse was either not in frame, or in frame but not licking the spout (n = 31,605 total photos) (Fig. 4.3c).

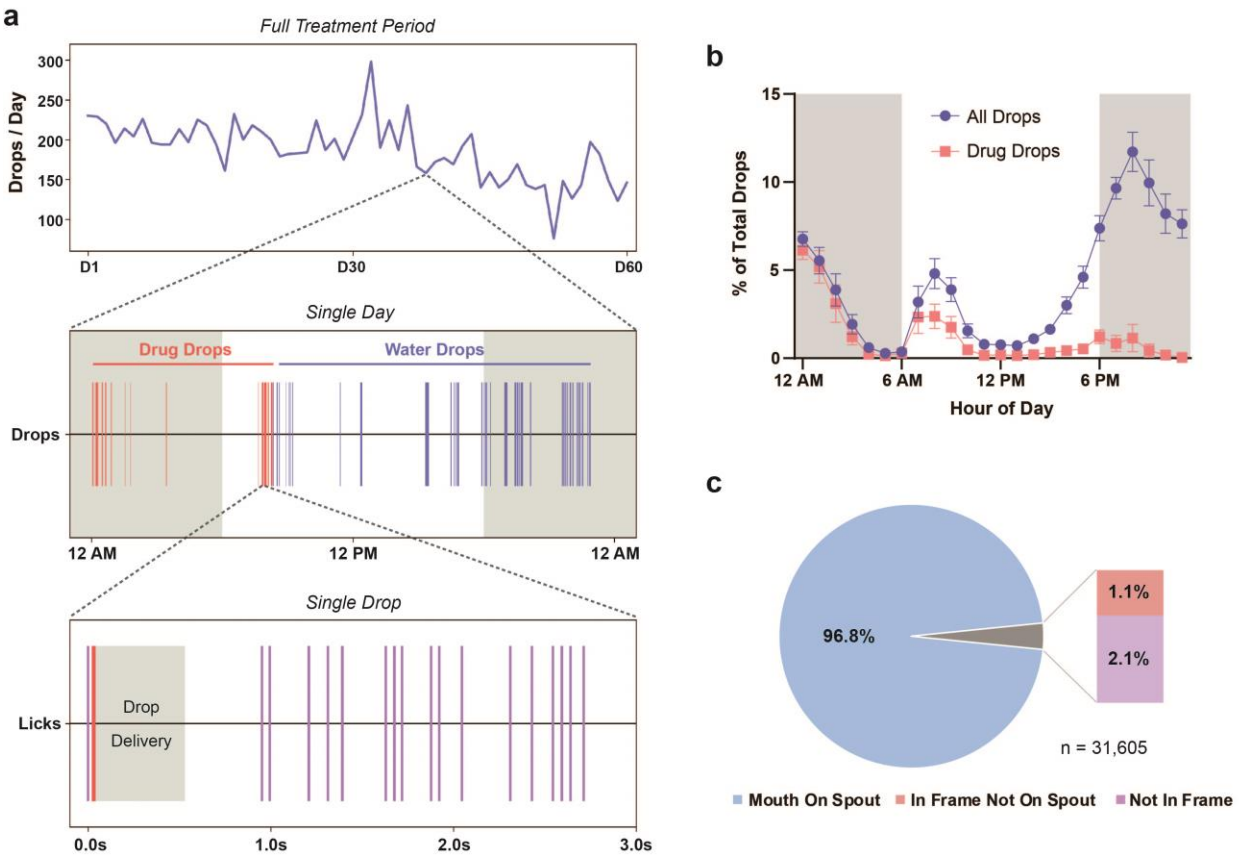

Figure 4.3 PiDose effectively administers drug to mice over a two-month period

(a) Analysis of the temporal structure of water and drug consumption is shown at several timescales for a representative YAC128 mouse. **(b)** Average total water (n = 10 mice) and memantine solution (n = 6 mice) consumed per hour throughout the treatment period. Memantine solution is dispensed beginning at midnight, and animals typically consumed the required dosage by 12 PM. Mice show clear circadian

rhythmicity in drinking behaviour, with most drops dispensed during the dark phase of the light cycle (grey-shaded regions). Error bars represent SEM. **(c)** Analysis of pictures taken immediately after drop delivery confirm that mice are properly triggering and ingesting water and drug solution on the large majority of trials.

Across treatment and control groups, YAC128 mice drank an average of 2.26 mL of liquid (water and drug solution) per day (± 0.10 mL, n = 10 mice), significantly greater than the amount WT mice drank on average during the initial testing of the cage (t_{16} = 3.15, p = 0.006, n = 8 WT, 10 YAC128). Interestingly, total liquid consumption in the control YAC128 group (2.5 ± 0.19, n = 4 mice) was slightly, but significantly, greater than consumption in the treatment group (2.09 ± 0.06, n = 6 mice) (t_8 = 2.42, p = 0.042). Over the course of the treatment period mice gradually gained weight, with a ~20% increase in bodyweight observed on average (5.12 ± 0.80 grams, n = 10 mice) (Fig. 4.4a). To ensure consistent dosing, PiDose automatically adjusted the amount of memantine dispensed each day, with mice receiving an additional 10 µL drop of memantine solution for every 0.5 g increase in bodyweight (Fig. 4.4b). In contrast to bodyweight, which changed gradually, the total drops consumed by each mouse varied substantially from day-to-day (Fig. 4.4c). Interestingly, mice drank less on average by the end of treatment as compared to the beginning despite their increased bodyweight (Week 1 vs. Week 8: t_9 = 5.888, p = 0.0002, n = 10). However, the total number of drops consumed remained consistently higher than the amount needed to receive the required dosage of memantine. As the decrease in water consumption could indicate an effect of PiDose on normal drinking behaviour, we compared daily bodyweight and water consumption in the first week to determine if these measures were correlated at the start of treatment. A positive correlation was observed (R^2 =

0.064, $p = 0.035$, $n = 70$ mouse-days) (Fig. 4.4d), however the relationship between the two variables was not proportional and the variability was very high.

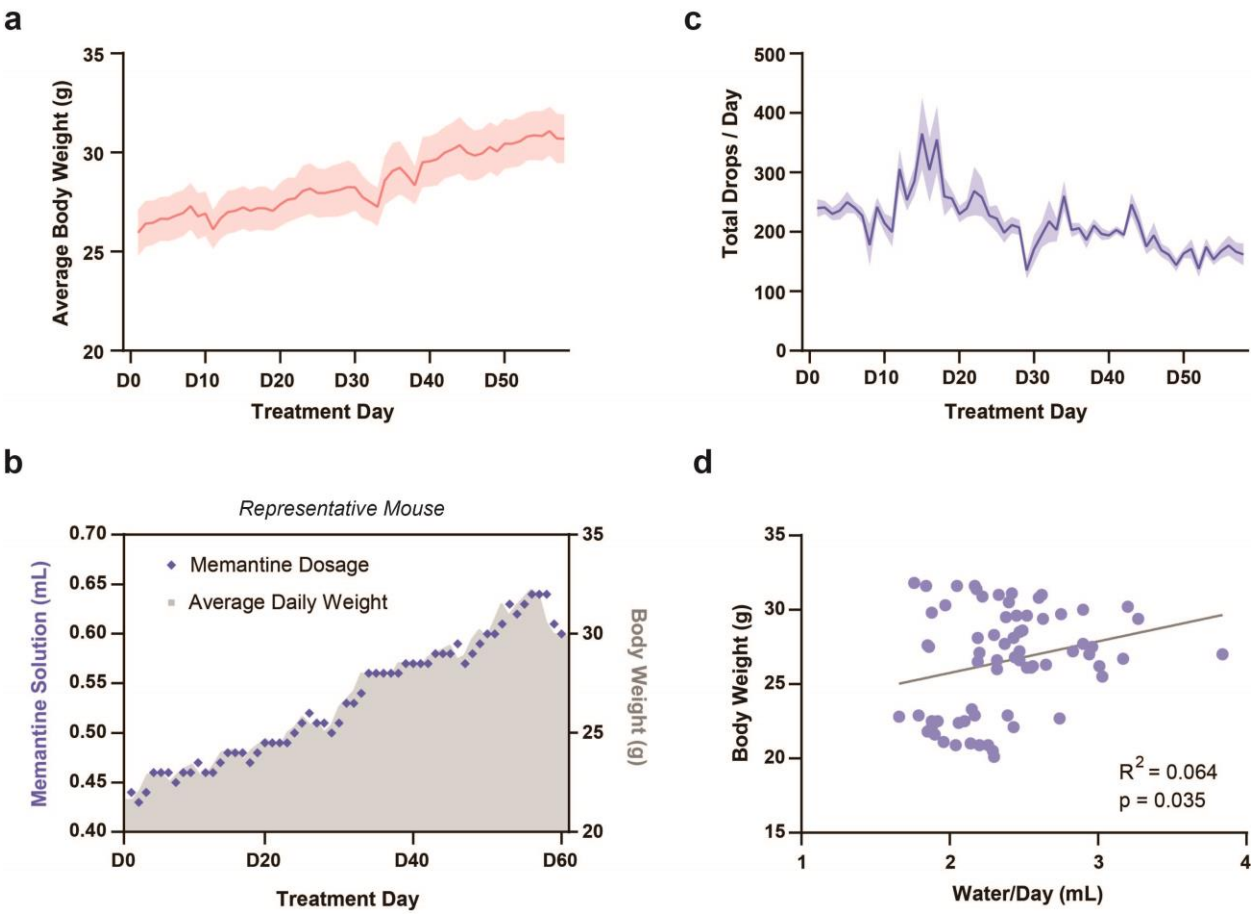

Figure 4.4 PiDose maintains stable drug treatment despite day-to-day changes in bodyweight and water consumption

(a) Mice ($n = 10$) show gradual and consistent weight gain over the course of two-months of memantine treatment. Data presented as daily mean (red line) ± SEM (red-shaded region). **(b)** The volume of memantine solution dispensed to a representative mouse is automatically adjusted over the course of two months to match changes in bodyweight and ensure consistent dosage. **(c)** Mice ($n = 10$) show substantial day-to-day variability in task engagement and total consumption of drops delivered by PiDose. Data presented as daily mean (blue line) ± SEM (blue-shaded region). **(d)** Daily water consumption during the first week of treatment is positively correlated with daily bodyweight ($n = 70$), although variability is high.

4.4 Discussion

Reliable drug administration requires that the weight of the animal and the amount of drug being delivered are known with high accuracy. As demonstrated in this chapter, PiDose meets these criteria, exhibiting low weighing error and high delivery accuracy both in terms of measurement of the drug volume and ingestion of the drug. All mice quickly learned to obtain water from the spout, and by training animals to perform an operant response that was identical to and continuous with the act needed to consume the reward, high delivery accuracy was achieved. Although drug delivery could not be confirmed on a small percentage (~3%) of trials, when combined with the measurement error of the syringe pump this level of precision is comparable to that of manual injection from a 1 mL syringe (tolerance of 5% or more) (International Organization for Standardization, 2017). The ability of PiDose to effectively automate long-term drug treatment was also demonstrated. PiDose requires minimal experimenter intervention once running, and the total time required to maintain each system is less than one hour per week. Furthermore, animals can be monitored without the need to enter the facility by connecting to the Raspberry Pi over a secure shell (SSH) network connection and running the system in a compact "headless" configuration without a monitor or keyboard.

In addition to the time-saving benefits of automation, PiDose offers several advantages over existing options in regard to improving the reproducibility of pre-clinical research. First, PiDose involves no handling or direct interaction with animals beyond what is typically required in an animal research facility (e.g. cage cleaning). In contrast, traditional drug administration paradigms often require daily handling and restraint of mice, procedures which are known to cause stress (Balcombe et al., 2004; Meijer et al., 2006). This procedure-associated stress is reported to cause various changes in animal behaviour and physiology, potentially masking or

enhancing the effects of drug treatment. For example, handling and/or injection stress has been shown to alter the behavioural response to anxiogenic drugs (Andrews & File, 1993), increase immobility time in the forced-swim test (Aydin et al., 2015), activate immediate early gene transcription in stress-responsive brain regions (Ryabinin et al., 1999) and alter immune function (Moynihan et al., 1990). Furthermore, the response to treatment-associated stress may vary between genotypes, further complicating the interpretation of results. YAC128 mice, for instance, show a depressive phenotype (Pouladi et al., 2009) and may consequently be more sensitive to the chronic stress of repeated injections (Aydin et al., 2015). Confounds such as this could introduce systematic error to the outcome measures of drug experiments and obscure treatment effects.

A second advantage of PiDose with regards to reproducibility is that of improved dosing accuracy and consistency when compared to other home-cage methods. Indeed, these results suggest several issues with the commonly used strategy of mixing a drug in directly with the animals' home-cage drinking water. Although an overall correlation between bodyweight and water consumption was observed in PiDose, the relationship was not proportional (i.e. a 40-gram mouse did not drink twice as much as a 20-gram mouse). As a result, when the 'drinking water' strategy is used in group-housed mice, it is likely that heavier mice in the cage receive a lower dosage on average than lighter mice. This could be especially problematic in mixed genotype cages where average bodyweight, and consequently average drug dosage, varies by genotype. Indeed, this is reported to be the case with heterozygous YAC128 mice who weigh more on average than their wildtype littermates (Slow et al., 2003; Van Raamsdonk, Gibson, et al., 2006). In addition, water consumption in PiDose varied by as much as 30-40% from day-to-day, while bodyweight changed comparatively slowly. As a result, even if mice are single-housed, day-to-

day dosage cannot be properly controlled by mixing the drug in directly with the mouse's drinking water. These inconsistencies could result in substantial differences in the effective dose received by each animal over the course of the treatment period, increasing the inter-animal variability of treatment outcome measures and consequently the risk of Type I and II errors. This dosing error also complicates any conclusions regarding the drug's dose-response relationship and increases the risk that the treatment will fail to translate to human use.

Although PiDose presents many advantages over alternative methodologies, there are also some important limitations to consider. First, its use is restricted to drugs that can be dissolved in water, are stable in solution and can be kept at room temperature. In addition, the specific timing of drug treatment each day cannot be precisely controlled, as mice have free access to the spout and consume the drug solution in a self-directed manner. For this reason, PiDose may not be appropriate for studies where the drug must be given at a precise time every day, or at specific intervals throughout the day. Nevertheless, the temporal pattern of drug administration can be broadly set by adjusting certain parameters within the software, and by changing the concentration of drug solution. For example, a high drug concentration could be used to shorten the average length of the dosing window and approximate an acute treatment method like oral gavage. This may be useful for treatments where a higher blood concentration of the drug is required in order to elicit effects. However, it would be important to ensure that the concentration of drug used was not unpalatable in order to ensure that mice were willing to voluntarily self-administer the solution. On the other hand, for rapidly metabolized compounds, it might be preferable to administer the drug throughout the day. For this purpose, a parameter in the PiDose program can be set so that the system dispenses a drug drop only once every two or three drops. With some minor modifications, it should even be possible to calculate a theoretical

blood concentration of the drug for each animal at any given time based on their bodyweight, the number and timing of previous drops, and known metabolic characteristics of the drug. This information could then be used to determine whether to deliver a drug or water drop in response to a lick, with the goal to keep the blood concentration of the drug within a target range.

Interestingly, YAC128 mice consumed more water on average than WT animals in the PiDose system, in contrast with a previous report which found no genotype differences in consumption from an *ad libitum* water bottle (Pouladi et al., 2009). As the water consumed by the original WT test group over 2-weeks was somewhat lower than reported in this previous study, one explanation for this discrepancy could be that these mice took some time to adjust to drinking from the PiDose cage, and consequently consumed less than they would typically. This would be less of a factor for the YAC128 mice, who were assessed for two months and had a longer period to adjust to the PiDose system. We also found that memantine-treated YAC128 mice consumed less liquid overall (water and memantine solution) than control mice. Although the reason for this difference is not clear, it is unlikely to be the result of the drug solution being unpalatable, as drug drops were administered first during each day and mice were subsequently free to drink as much regular water as desired. Indeed, if mice were failing to consume the drug solution (e.g. spitting it out), they would most likely consume a larger amount following the switch to regular water drops. Furthermore, we have previously reported that mice willingly drank 10 mg/kg memantine when administered in their drinking water (Dau et al., 2014), a dosage 10× greater than that given in this study. Although we collected strong evidence to suggest that mice were consuming the drugs administered via PiDose, it's important to note that we did not directly confirm the effectiveness of this system by assessing blood or plasma concentrations of memantine following administration. In future studies, measurements of blood

concentration of drug would be warranted to further confirm that the system is operating as intended. This could also be used to better determine the pharmacokinetics of drug administration via PiDose and compare this to existing methods of drug administration.

The use of PiDose described here was restricted to FVB/N strain male mice of two- to four-months-old; however, it's reasonable to expect that both male and female mice of a range of ages and different strains could be treated using this system. For the treatment of very small or very large animals, some modifications to the dimensions of the dosing module may be necessary to ensure that only one mouse can enter at a time. Nevertheless, I found that this configuration worked well for mice varying in bodyweight from 20 to 45 grams. The load cell used with PiDose has a maximum capacity of 780 grams (including the weight of the dosing module), which should be more than sufficient for any mouse applications and could even work in a modified system for treating larger rodents (e.g. rats). The load cell was able to maintain accurate bodyweight measurements across the range of animal sizes without the need for recalibration, and all other sensors and electronic components should be compatible with physical modifications of the dosing module. In order to facilitate any adjustments that other users may want to make, I have provided the original design files for all 3D parts online (https://osf.io/rpyfm/).

The potential of open-source tools in biological research has gathered attention as of late (White et al., 2019), and it is my hope that by making the code and design files for PiDose open-source and freely accessible, others will adapt and improve it as necessary for their use. Given the now well-established concerns regarding the reproducibility of many pre-clinical studies (Freedman et al., 2015; Scannell & Bosley, 2016), the need for a tool that can increase the accuracy of drug dosing while also decreasing the exposure of animals to stressful stimuli is

critical. PiDose holds promise in this regard and should prove useful for both basic and pre-clinical biological research.

Chapter 5: Conclusions

5.1 Summary of findings

In this thesis, I investigated the behaviour of wildtype and HD model mice on an operant task in which they had to precisely manipulate a lever with their forelimb in order to receive water rewards. This lever task was incorporated into the mouse home-cage, allowing for automated and high-throughput assessment of motor learning and kinematic parameters of task execution. To differentiate group-housed animals, an RFID capsule was subcutaneously implanted into each mouse prior to the start of testing, and parameters for that animal were loaded each time they entered the testing module. This task was available 24-hours per day, and learning was completely self-directed and could be initiated by the animal as desired.

In the first version of this task (Chapter 2), the lever had to be pulled backwards into a central position range and held for a certain duration. This duration increased as the mouse improved, with each animal advancing through the hold-duration 'levels' at their own pace. Young (2-month-old) YAC128 HD mice had a slower progression through these levels of task difficulty, suggesting an impairment in adapting their movements in response to changes in task requirements. Interestingly, this was a transient phenotype and was not observed in older YAC128 animals. However, despite having a similar success rate to WT animals, older (6-month-old) YAC128 mice differed from WT animals on certain kinematic features of their trials. Specifically, they tended to overshoot the target position range initially and then slowly release their hold on the lever to move it back through the target range and reach the required hold-duration. In addition to these motor phenotypes, we observed an altered circadian distribution of trials in 4- and 6-month-old YAC128 mice, but not 2-month-old animals.

In the second version of the task (Chapter 3), mice were tested in an updated home-cage system (PiPaw), and the testing methodology changed substantially. Mice were not required to hold the lever for a specific length of time but rather perform a short duration pull that ended within a defined target position range. If the amplitude of the pull (i.e. the maximum position) was in this target range, the trial was rewarded. WT mice steadily improved their success rate on this task over one week by performing progressively more accurate and consistent movements, as indicated by decreased inter-trial variability of pull amplitude and trial duration. In contrast, Q175-FDN HD mice had a much slower learning of the task and never achieved the performance level of WT mice. This impaired learning was associated with a failure to decrease the inter-trial variability of kinematic parameters over testing, suggesting an impairment both in motor learning and motor control. In contrast, YAC128 mice at both 2- and 10-months-old had no learning impairment on this task and performed comparably to WT animals. Despite this, 10-month-old YAC128 and Q175-FDN mice were equally impaired at performing the rotarod task and YAC128 mice showed significant open-field hypoactivity.

When the pattern of PiPaw task performance over the course of the day was analyzed, I found that animals tended to cluster their activity into short bouts of high task engagement separated by longer periods when no trials were performed. While young YAC128 mice performed more of these bouts per day as compared to their WT littermates, old YAC128 mice tended to perform fewer bouts, perhaps reflecting reported bidirectional age-related effects on activity level. Both YAC128 and Q175-FDN mice at 10 months of age had an altered circadian distribution of their trials, although the pattern of these changes was not consistent across genotypes. Acute slice electrophysiology experiments revealed that the DLS-MSNs of wildtype animals that had undergone PiPaw testing had altered spontaneous excitatory activity as

compared to MSNs from animals that had not been tested on the task. The frequency of sEPSCs was decreased in both hemispheres, while the amplitude of these currents was decreased selectively in the left hemisphere. In Q175-FDN mice, however, no significant changes were seen following PiPaw testing, suggesting that motor deficits may have been related to aberrant synaptic plasticity in these neurons. In further support of this, striatal neurons from PiPaw-trained Q175-FDN showed consistent LTP in striatal neuronal responses to a high-frequency stimulation protocol, whereas WT neuronal responses showed LTD.

The results from these chapters are significant for several reasons. First, they suggest that motor impairment in YAC128 mice may be much more localized than previously thought. The finding of completely normal learning and performance of a skilled forelimb task in aged YAC128 animals is very much at odds with the established symptomatic progression of these animals and emphasizes the importance of using tests that assess a variety of aspects of motor function. However, these results also add additional evidence that there is an early phenotype in these mice characterized by elevated activity levels and perhaps an impairment in motor learning (although this was task-dependent). In addition, this work suggests that YAC128 and Q175-FDN mice have altered circadian activity levels, a phenotype that has been seen in other mouse models and in HD patients. This work also adds significantly to the relatively small literature on the Q175-FDN mouse, demonstrating that they have robust forelimb motor impairments and associated deficits in striatal plasticity, and encourages further use of these animals. Aside from a study published this year (Glangetas et al., 2020), this research is the first to assess a skilled forelimb task in a genetic mouse model of HD.

5.2 Methodological developments

An additional goal of this thesis was the development of novel home-cage-based tools for *in vivo* rodent research. Although home-cage systems for assessing skilled forelimb tasks have been published in mice (Bollu et al., 2019) and rats (Fenrich et al., 2016; Poddar et al., 2013), the PiPaw system (Chapter 3), and the original home-cage task on which it is based (Chapter 2), are the first to incorporate group housing of animals and individual identification via RFID tagging. In this respect, these paradigms represent a significant step forward, as single housing is a stressor in rodents and could alter behaviour. Another advantage of group housing is that heterozygous transgenic or knock-in mice can be tested alongside their WT littermates, providing within-cage control of environmental factors. The PiPaw system exhibited a high success rate in training both young and aged mice and animals generally responded well to the shaping paradigm and changes in task success requirements. In addition, kinematic parameters of task execution were recorded with extremely high resolution – specifically, the temporal resolution of our lever position recording was on the level of 5 ms (positions recorded at 200 Hz) and positional resolution was on the level of ~50 µm. Although we implemented a task that rewarded pulls of a specific amplitude, the PiPaw system should be compatible with a range of other testing methodologies to target specific behaviours. A final important point is that PiPaw is relatively affordable (~700 CAD) and can be built with easy to acquire parts, facilitating the use of this system in other labs.

The PiDose cage (Chapter 4) also represents a significant methodological advancement, as there are currently no open-source or off-the-shelf commercial alternatives for performing automated home-cage drug administration. Although one paper had been published describing a comparable system in 2006 (Santoso et al., 2006), the topic has received little to no attention in

the intervening years despite the clear utility of such a system. As discussed above, extended drug treatment protocols often suffer from being stressful to animals (due to repeated injections or gavage), overly time-consuming (hand feeding methods) or inaccurate (dissolving drugs in the home-cage water bottle). PiDose is able to address these issues, and showed good accuracy, both in automated weighing of animals and in delivering drops of drug solution. As with the PiPaw system, PiDose is affordable (~400 CAD) and relatively straightforward to build with commercially available parts. Furthermore, a full build guide and code for the PiDose system has been posted online in order to facilitate the use of the system in other labs. Together, these two systems represent an important methodological contribution, and should be useful for basic and translational research with a variety of applications.

5.3 Limitations of this work

Perhaps the clearest limitation regarding the PiPaw task is that this test was not able to differentiate YAC128 mice from their WT littermates, even at an advanced age. As previously discussed, the disparity in performance between this and other motor tests may be partially accounted for by an exaggeration of YAC128 dysfunction on tests of full body coordination due to increased bodyweight. However, it's also important to note that a skilled reaching deficit has been reported in YAC128 mice at 3-4 months-old, although this was only seen after animals were given a two-day break in testing (Glangetas et al., 2020). In addition, a slower task progression was found in young YAC128 animals using the original home-cage task (Chapter 2). Thus, it seems likely that the task methodology used in Chapter 3 lacks sensitivity and could be improved by adjusting certain parameters. Although the reason for this lower sensitivity is not completely clear, it could be related to the short duration of the required movements. While one

study in pre-symptomatic HD mutation carriers found an impairment in correcting self-generated errors while performing a reaching task, a second paper by the same group found that performance was not impaired as long as the movement was <300 ms and didn't require the participant to react to real-time sensory input (Smith & Shadmehr, 2005). This ability to respond to real-time proprioceptive feedback was not a requirement for accurate performance in the PiPaw task, although it may have been necessary for the original home-cage task given the longer duration for which the lever had to be held. Thus, despite Q175-FDN mice showing significant deficits on the PiPaw task, the lack of cross-model validation for this specific testing methodology may limit its use. That said, alternative testing methodologies that might exhibit increased sensitivity should be relatively straightforward to implement using the PiPaw system and this would be a priority for future research.

A further limitation of both the original home-cage task and the PiPaw task is related to the use of water as a reward. Although mice were generally able to retrieve enough water to maintain their body weight, animals occasionally had to be given extra water, especially early in testing when success rates were very low. This meant that animals had to be monitored and weighed daily during initial task performance (although once the task had been acquired monitoring was reduced to every 2-3 days). Water restriction is well tolerated in mice and seems to have relatively few effects on behaviour or plasma corticosterone levels as compared to food restriction (Bekkevold et al., 2013; Tucci et al., 2006). However, thirst can modulate the activity of neurons in diverse brain areas, including the striatum, and may have influenced the electrophysiological changes we observed (e.g. reduced sEPSC frequency) (Allen et al., 2019). Furthermore, HD patients have been reported to have increased thirst and increased water consumption has been seen in R6/2 mice (Wood et al., 2008), complicating the use of water as a

reward. Normal water consumption has been reported in YAC128 mice (Pouladi et al., 2009); however, we observed that YAC128 mice in the PiDose cage drank more than WT animals. Q175-FDN mice have not been assessed for baseline water consumption, and so it is unknown if this could contribute to motivational differences in this genotype. An alternative would be to allow animals *ad libitum* access to water containing 2% citric acid, which makes water taste sour and is slightly aversive, but allows mice to maintain healthy bodyweight (Urai et al., 2020). Water given as a reward for the task could then be sweetened slightly with saccharine in order to increase animal's motivation to perform the task. However, considering anhedonia has been reported in HD mice (Pouladi et al., 2009), this strategy could result in fewer trials in HD animals and would have to be carefully tested.

Another factor that was not controlled for in the PiPaw experiments was paw preference, which can vary between mice, and typically leads animals to perform skilled reaching tasks primarily with one forelimb or the other (Karl & Whishaw, 2011). Due to the design of the PiPaw system, performance of the task was restricted to the right forelimb. In order to allow for performance with either forelimb, the full lever control apparatus would have to be duplicated on the left side of the testing module, a modification that would substantially increase the complexity and cost of the system. Although paw preference could affect task performance, it is unlikely that preference would be systematically different between WT and HD mice, as differences in handedness have not been described in HD patients. Interestingly, in a group of right-handed HD patients, striatal gray matter loss was found to have a leftward bias (Mühlau et al., 2007), and so if a similar pattern was seen in HD mice, this task could have increased sensitivity as compared to bilateral tasks.

Another potential caveat of this research is the use of HD model mice on the FVB/N genetic background. These mice suffer from retinal degeneration and blindness from ~2 months-old (Farley et al., 2011), and this could influence the circadian rhythmicity of these animals and contribute to the differences in activity levels we observed. However, retinal degeneration should not have affected the ability of animals to perform the PiPaw task, as the sensory feedback required for performance of the task was solely proprioceptive. Indeed, visual feedback during performance of the task was not possible due to the configuration of the testing module and the requirement that mice nose-poke before pulling the lever. The main reason for our use of FVB/N mice in this study is that these animals show increased susceptibility to excitotoxic neurodegeneration (McLin & Steward, 2006). In addition, HD mice bred on this background show a more rapid onset of neuropathology and behavioural abnormalities as compared to those on other backgrounds (Southwell et al., 2016; Van Raamsdonk et al., 2007). This faster onset allows for the assessment of models that have good construct validity, such as heterozygous YAC128 and Q175-FDN mice, without having to age animals past one year. A possible disadvantage of using mice on the FVB/N background is that most commercially available transgenic mouse lines that express fluorescent reporter proteins are bred on the C57BL/6 strain, although this was not an issue for this study.

Regarding the original home-cage study presented in Chapter 2, a variety of methodological limitations were found with this system, including inconsistent performance of the task with the forelimb, and issues with trial structure and data recording. However, the majority of these issues were dealt with in the modifications made to the home-cage task during the development of PiPaw. Still, the data presented in Chapter 2 comes with the caveat that some animals may have been using an alternative strategy to pull the lever (e.g. with both forelimbs or

with their mouth). The PiDose system also has a number of limitations, as discussed previously (Chapter 4.4). These include the requirement that drugs administered using the system must be water soluble and stable at room temperature, and the caveat that the specific timing of dosage cannot be effectively controlled. However, as an alternative to studies where the drug is simply mixed into the home-cage drinking water, PiDose is a substantial improvement, providing much better control of dosing volume and allowing for different treatment conditions within the same cage. A final important caveat of the PiDose study is that we did not confirm the effectiveness of our dosing protocol by measuring the blood or plasma concentration of drug following treatment, although we collected strong evidence that animals were consuming the delivered drug solution.

5.4 Future directions

A key priority for future research is to explore alternative PiPaw testing methodologies that show better sensitivity for motor phenotypes in HD mice. One example of this that I have tested is a version of the task where success is based not on the amplitude of pulls, but the average velocity of the pull. In addition, I have implemented a version of the original home-cage task (i.e. mouse must increase their hold duration over time) in the PiPaw system and have performed some testing of YAC128 mice using this setup. Using this improved system, we plan to repeat our study of 2-month-old YAC128 mice (Chapter 2) to confirm that animals at this age have a motor learning deficit at this version of the task. One advantage of training mice to perform a longer duration movement is that it opens the possibility of applying force perturbations on the lever during the hold period and then assessing the ability to correct for this external force. HD patients have deficits in online error correction during movements (Smith et al., 2000), suggesting that this may be a sensitive behavioural measure in mouse models. As the

lever is directly coupled to a motor in the PiPaw system, force perturbations during the hold period could be implemented without requiring any changes to the system's hardware. Other options could involve changing the structure of testing rather than changing the methodology of the task itself. For instance, mice could be removed from the cage after one week of training, and then re-tested after a break of several days (or longer) to examine long-term motor memory. As a recent study reported deficits in HD mice performing a reaching task after a break in testing (Glangetas et al., 2020), this may reveal deficits not seen with continued daily testing.

One of the limitations of our *ex vivo* patch clamp recordings from DLS-MSNs was that direct and indirect pathway neurons could not be differentiated from one another. As numerous papers have reported pathway-specific alterations of the activity and plasticity of these neurons at baseline in HD mice (André, Fisher, et al., 2011; Sepers et al., 2018), and in response to motor learning in WT animals (Shan et al., 2015; Yin et al., 2009), this would provide more detail about the nature of genotype differences following PiPaw training. One way to do this would be to cross mice that express GFP specifically in D2-expressing neurons (*drd2*-eGFP BAC transgenic mice) with Q175-FDN mice, which would enable identification of iMSNs (GFP-expressing) and putative dMSNs (no GFP expression), as has been done in previous studies (Sepers et al., 2018). Another important direction for future research is to look at neuronal activity *in vivo* during performance of the task. This provides a more direct measure of training-associated plasticity and enables direct correlation of neuronal activity with the animal's task performance. One method for doing this would be to implant a chronic multi-electrode probe into the DLS and track changes in both the baseline activity of individual neurons and the how these neurons are either positively or negatively modulated by task performance over time. Another option would be to inject a fluorescent calcium sensor (e.g. GCaMP) directly into the

DLS and use an implanted optical fiber to record activity from neuronal populations. Although this does not allow for single-neuron resolution, it has the advantage that a virus can be targeted to specific striatal subpopulations (e.g. direct vs. indirect pathway neurons) or even to presynaptic terminals of cortical neurons. Although full-time *in vivo* recording would be technically difficult to perform, especially with group-housed animals, one way to implement this would be to periodically remove animals for imaging sessions in a separate modified test module. This could be done every two to three days to assess longitudinal changes in neuronal activity in WT and Q175-FDN mice. Alternatively, mesoscale cortical activity could be assessed directly in the home-cage by integrating the PiPaw task into a home-cage system which automatically head-fixes and images brain activity through a transcranial window, as has been recently described (T. H. Murphy et al., 2016, 2020).

A final priority is to make the PiPaw system fully open-source and accessible to other labs by creating a set of build instructions and providing all the parts and code online. This has already been done for the PiDose cage, with the hope that other groups will apply this method to their own research. In addition, making these tools open-source allows others to create their own modifications or testing methodologies as needed for their specific research applications. For example, both of these systems could be altered to accommodate testing of rats with relatively minor changes to the dimensions and position of certain components. Making tools and protocols open-source is critical for the transparency of research findings and for ensuring that findings can be replicated by other labs (or that contradictory findings can be accurately compared). It also increases the accessibility of science to research groups that do not have the resources to purchase expensive off-the-shelf behavioural tools.

References

Abada, Y.-S. K., & Ellenbroek, B. (2016). Of rodents and men: understanding the emergence of motor and cognitive symptoms in Huntington disease. *Behavioural Pharmacology*, *27*(5), 403–414. https://doi.org/10.1097/FBP.0000000000000217

Abada, Y.-S. K., Schreiber, R., & Ellenbroek, B. (2013). Motor, emotional and cognitive deficits in adult BACHD mice: a model for Huntington's disease. *Behavioural Brain Research*, *238*, 243–251. https://doi.org/10.1016/j.bbr.2012.10.039

Ahloy-Dallaire, J., Klein, J. D., Davis, J. K., & Garner, J. P. (2019). Automated monitoring of mouse feeding and body weight for continuous health assessment. *Laboratory Animals*, *53*(4), 342–351. https://doi.org/10.1177/0023677218797974

Alaverdashvili, M., & Whishaw, I. Q. (2013). A behavioral method for identifying recovery and compensation: hand use in a preclinical stroke model using the single pellet reaching task. *Neuroscience and Biobehavioral Reviews*, *37*(5), 950–967. https://doi.org/10.1016/j.neubiorev.2013.03.026

Albin, R. L., Reiner, A., Anderson, K. D., Dure, L. S., Handelin, B., Balfour, R., Whetsell, W. O., Penney, J. B., & Young, A. B. (1992). Preferential loss of striato-external pallidal projection neurons in presymptomatic Huntington's disease. *Annals of Neurology*, *31*(4), 425–430. https://doi.org/10.1002/ana.410310412

Alexandrov, V., Brunner, D., Menalled, L. B., Kudwa, A., Watson-Johnson, J., Mazzella, M., Russell, I., Ruiz, M. C., Torello, J., Sabath, E., Sanchez, A., Gomez, M., Filipov, I., Cox, K., Kwan, M., Ghavami, A., Ramboz, S., Lager, B., Wheeler, V. C., … Kwak, S. (2016). Large-scale phenome analysis defines a behavioral signature for Huntington's disease genotype in mice. *Nature Biotechnology*, *34*(8), 838–844. https://doi.org/10.1038/nbt.3587

Allen, W. E., Chen, M. Z., Pichamoorthy, N., Tien, R. H., Pachitariu, M., Luo, L., & Deisseroth, K. (2019). Thirst regulates motivated behavior through modulation of brainwide neural population dynamics. *Science*, *364*. https://doi.org/10.1126/science.aav3932

Almqvist, E. W., Elterman, D. S., MacLeod, P. M., & Hayden, M. R. (2001). High incidence rate and absent family histories in one quarter of patients newly diagnosed with Huntington disease in British Columbia. *Clinical Genetics*, *60*(3), 198–205. https://doi.org/10.1034/j.1399-0004.2001.600305.x

Anca, M. H., Gazit, E., Loewenthal, R., Ostrovsky, O., Frydman, M., & Giladi, N. (2004). Different phenotypic expression in monozygotic twins with Huntington disease. *American Journal of Medical Genetics*, *124A*, 89–91. https://doi.org/10.1002/ajmg.a.20328

André, V. M., Cepeda, C., Fisher, Y. E., Huynh, M., Bardakjian, N., Singh, S., Yang, X. W., & Levine, M. S. (2011). Differential electrophysiological changes in striatal output neurons in

Huntington's disease. *Journal of Neuroscience*, *31*(4), 1170–1182. https://doi.org/10.1523/JNEUROSCI.3539-10.2011

André, V. M., Fisher, Y. E., & Levine, M. S. (2011). Altered balance of activity in the striatal direct and indirect pathways in mouse models of Huntington's disease. *Frontiers in Systems Neuroscience*, *5*(46). https://doi.org/10.3389/fnsys.2011.00046

Andrews, N., & File, S. E. (1993). Handling history of rats modifies behavioural effects of drugs in the elevated plus-maze test of anxiety. *European Journal of Pharmacology*, *235*, 109–112. https://doi.org/https://doi.org/10.1016/0014-2999(93)90827-5

Ariano, M. A., Aronin, N., Difiglia, M., Tagle, D. A., Sibley, D. R., Leavitt, B. R., Hayden, M. R., & Levine, M. S. (2002). Striatal neurochemical changes in transgenic models of Huntington's disease. *Journal of Neuroscience Research*, *68*(6), 716–729. https://doi.org/10.1002/jnr.10272

Arnulf, I., Nielsen, J., Lohmann, E., Schieffer, J., Wild, E., Jennum, P., Konofal, E., Walker, M., Oudiette, D., Tabrizi, S., & Durr, A. (2008). Rapid eye movement sleep disturbances in Huntington disease. *Archives of Neurology*, *65*(4), 482–488. https://doi.org/doi:10.1001/archneur.65.4.482

Atcha, Z., Rourke, C., Neo, A. H. P., Goh, C. W. H., Lim, J. S. K., Aw, C., Browne, E. R., & Pemberton, D. J. (2010). Alternative method of oral dosing for rats. *Journal of the American Association for Laboratory Animal Science*, *49*(3), 335–343.

Aydin, C., Frohmader, K., & Akil, H. (2015). Revealing a latent variable: individual differences in affective response to repeated injections. *Behavioral Neuroscience*, *129*(5), 679–682. https://doi.org/10.1037/bne0000084

Aylward, E. H., Sparks, B. F., Field, K. M., Yallapragada, V., Shpritz, B. D., Rosenblatt, A., Brandt, J., Gourley, L. M., Liang, K., Zhou, H., Margolis, R. L., & Ross, C. A. (2004). Onset and rate of striatal atrophy in preclinical Huntington disease. *Neurology*, *63*(1), 66–72. https://doi.org/10.1212/01.WNL.0000132965.14653.D1

Bains, R. S., Cater, H. L., Sillito, R. R., Chartsias, A., Sneddon, D., Concas, D., Keskivali-Bond, P., Lukins, T. C., Wells, S., Acevedo Arozena, A., Nolan, P. M., & Armstrong, J. D. (2016). Analysis of individual mouse activity in group housed animals of different inbred strains using a novel automated home cage analysis system. *Frontiers in Behavioral Neuroscience*, *10*(106). https://doi.org/10.3389/fnbeh.2016.00106

Balci, F., Oakeshott, S., Shamy, J. L., El-Khodor, B. F., Filippov, I., Mushlin, R., Port, R., Connor, D., Paintdakhi, A., Menalled, L. B., Ramboz, S., Howland, D., Kwak, S., & Brunner, D. (2013). High-throughput automated phenotyping of two genetic mouse models of Huntington's disease. *Plos Currents*, *5*. https://doi.org/10.1371/currents.hd.124aa0d16753f88215776fba102ceb29

Balcombe, J. P., Barnard, N. D., & Sandusky, C. (2004). Laboratory routines cause animal stress. *Journal of the American Association for Laboratory Animal Science*, *43*(6), 42–51.

Barbaro, B. A., Lukacsovich, T., Agrawal, N., Burke, J., Bornemann, D. J., Purcell, J. M., Worthge, S. A., Caricasole, A., Weiss, A., Song, W., Morozova, O. A., Colby, D. W., & Marsh, J. L. (2015). Comparative study of naturally occurring Huntingtin fragments in Drosophila points to exon 1 as the most pathogenic species in Huntington's disease. *Human Molecular Genetics*, *24*(4), 913–925. https://doi.org/10.1093/hmg/ddu504

Barnes, T. D., Kubota, Y., Hu, D., Jin, D. Z., & Graybiel, A. M. (2005). Activity of striatal neurons reflects dynamic encoding and recoding of procedural memories. *Nature*, *437*(7062), 1158–1161. https://doi.org/10.1038/nature04053

Bates, G. P., Dorsey, R., Gusella, J. F., Hayden, M. R., Kay, C., Leavitt, B. R., Nance, M., Ross, C. A., Scahill, R. I., Wetzel, R., Wild, E. J., & Tabrizi, S. J. (2015). Huntington disease. *Nature Reviews Disease Primers*, *1*(1), 1–21. https://doi.org/10.1038/nrdp.2015.5

Batka, R. J., Brown, T. J., Mcmillan, K. P., Meadows, R. M., Jones, K. J., & Haulcomb, M. M. (2014). The need for speed in rodent locomotion analyses. *Anatomical Record*, *297*(10), 1839–1864. https://doi.org/10.1002/ar.22955

Beal, M. F., Kowall, N. W., Ellison, D. W., Mazurek, M. F., Swartz, K. J., & Martin, J. B. (1986). Replication of the neurochemical characteristics of Huntington's disease by quinolinic acid. *Nature*, *321*(May), 168–171. https://doi.org/https://doi.org/10.1038/321168a0

Begeti, F., Schwab, L. C., Mason, S. L., & Barker, R. A. (2016). Hippocampal dysfunction defines disease onset in Huntington's disease. *Journal of Neurology, Neurosurgery and Psychiatry*, *87*(9), 975–981. https://doi.org/10.1136/jnnp-2015-312413

Beglinger, L. J., O'Rourke, J. J. F., Wang, C., Langbehn, D. R., Duff, K., & Paulsen, J. S. (2010). Earliest functional declines in Huntington disease. *Psychiatry Research*, *178*(2), 414–418. https://doi.org/10.1016/j.psychres.2010.04.030

Bekkevold, C. M., Robertson, K. L., Reinhard, M. K., Battles, A. H., & Rowland, N. E. (2013). Dehydration parameters and standards for laboratory mice. *Journal of the American Association for Laboratory Animal Science*, *52*(3), 233–239.

Bolaños, F., LeDue, J. M., & Murphy, T. H. (2017). Cost effective raspberry pi-based radio frequency identification tagging of mice suitable for automated in vivo imaging. *Journal of Neuroscience Methods*, *276*, 79–83. https://doi.org/http://dx.doi.org/10.1016/j.jneumeth.2016.11.011

Bollu, T., Whitehead, S. C., Prasad, N., Walker, J., Shyamkumar, N., Subramaniam, R., Kardon, B., Cohen, I., & Goldberg, J. H. (2019). Automated home cage training of mice in a hold-

still center-out reach task. *Journal of Neurophysiology*, *121*, 500–512. https://doi.org/10.1152/jn.00667.2018

Bonfiglioli, C., Berti, G. De, Nichelli, P., Nicoletti, R., & Castiello, U. (1998). Kinematic analysis of the reach to grasp movement in Parkinson's and Huntington's disease subjects. *Neuropsychologia*, *36*(11), 1203–1208. https://doi.org/10.1016/S0028-3932(97)00171-1

Borlongan, C. V., Koutouzis, T. K., Freeman, T. B., Cahill, D. W., & Sanberg, P. R. (1995). Behavioral pathology induced by repeated systemic injections of 3-nitropropionic acid mimics the motoric symptoms of Huntington's disease. *Brain Research*, *697*, 254–257. https://doi.org/10.1016/0006-8993(95)00901-2

Brandt, J., Bylsma, F. W., Gross, R., Stine, O. C., Ranen, N., & Ross, C. A. (1996). Trinucleotide repeat length and clinical progression in Huntington's disease. *Neurology*, *46*(2), 527–531. https://doi.org/10.1212/WNL.46.2.527

Brinkman, R. R., Mezei, M. M., Theilmann, J., Almqvist, E., & Hayden, M. R. (1997). The likelihood of being affected with Huntington disease by a particular age, for a specific CAG size. *American Journal of Human Genetics*, *60*(5), 1202–1210.

Brooks, S. P. (2011). Neurological evaluation of movement disorders in mice. In E. L. Lane & S. B. Dunnett (Eds.), *Animal Models of Movement Disorders Volume I*. Humana Press.

Brooks, S. P., Betteridge, H., Trueman, R. C., Jones, L., & Dunnett, S. B. (2006). Selective extra-dimensional set shifting deficit in a knock-in mouse model of Huntington's disease. *Brain Research Bulletin*, *69*(4), 452–457. https://doi.org/10.1016/j.brainresbull.2006.02.011

Brooks, S. P., & Dunnett, S. B. (2009). Tests to assess motor phenotype in mice: a user's guide. *Nature Reviews Neuroscience*, *10*(7), 519–529. https://doi.org/10.1038/nrn2652

Brooks, S. P., Higgs, G., Janghra, N., Jones, L., & Dunnett, S. B. (2012). Longitudinal analysis of the behavioural phenotype in YAC128 (C57BL/6J) Huntington's disease transgenic mice. *Brain Research Bulletin*, *88*(2–3), 113–120. https://doi.org/10.1016/j.brainresbull.2010.05.005

Brooks, S. P., Higgs, G., Jones, L., & Dunnett, S. B. (2012). Longitudinal analysis of the behavioural phenotype in Hdh(CAG)150 Huntington's disease knock-in mice. *Brain Research Bulletin*, *88*(2–3), 182–188. https://doi.org/10.1016/j.brainresbull.2010.05.004

Brooks, S. P., Janghra, N., Higgs, G. V., Bayram-Weston, Z., Heuer, A., Jones, L., & Dunnett, S. B. (2012). Selective cognitive impairment in the YAC128 Huntington's disease mouse. *Brain Research Bulletin*, *88*(2–3), 121–129. https://doi.org/10.1016/j.brainresbull.2011.05.010

Brooks, S. P., Jones, L., & Dunnett, S. B. (2012a). Comparative analysis of pathology and

behavioural phenotypes in mouse models of Huntington's disease. *Brain Research Bulletin*, *88*(2–3), 81–93. https://doi.org/10.1016/j.brainresbull.2011.10.002

Brooks, S. P., Jones, L., & Dunnett, S. B. (2012b). Longitudinal analyses of operant performance on the serial implicit learning task (SILT) in the YAC128 Huntington's disease mouse line. *Brain Research Bulletin*, *88*(2–3), 130–136. https://doi.org/10.1016/j.brainresbull.2011.06.008

Brooks, S. P., Pask, T., Jones, L., & Dunnett, S. B. (2004). Behavioural profiles of inbred mouse strains used as transgenic backgrounds. I: motor tests. *Genes, Brain and Behavior*, *3*, 206–215. https://doi.org/10.1111/j.1601-183X.2004.00072.x

Buitrago, M. M., Ringer, T., Schulz, J. B., Dichgans, J., & Luft, A. R. (2004). Characterization of motor skill and instrumental learning time scales in a skilled reaching task in rat. *Behavioural Brain Research*, *155*(2), 249–256. https://doi.org/10.1016/j.bbr.2004.04.025

Buitrago, M. M., Schulz, J. B., Dichgans, J., & Luft, A. R. (2004). Short and long-term motor skill learning in an accelerated rotarod training paradigm. *Neurobiology of Learning and Memory*, *81*(3), 211–216. https://doi.org/10.1016/j.nlm.2004.01.001

Buren, C., Parsons, M. P., Smith-Dijak, A. I., & Raymond, L. A. (2016). Impaired development of cortico-striatal synaptic connectivity in a cell culture model of Huntington's disease. *Neurobiology of Disease*, *87*, 80–90. https://doi.org/10.1016/j.nbd.2015.12.009

Calabresi, P., Picconi, B., Tozzi, A., Ghiglieri, V., & Di Filippo, M. (2014). Direct and indirect pathways of basal ganglia: a critical reappraisal. *Nature Neuroscience*, *17*(8), 1022–1030. https://doi.org/10.1038/nn.3743

Carter, R. J., Lione, L. A., Humby, T., Mangiarini, L., Mahal, A., Bates, G. P., Dunnett, S. B., & Morton, A. J. (1999). Characterization of progressive motor deficits in mice transgenic for the human Huntington's disease mutation. *Journal of Neuroscience*, *19*(8), 3248–3257. https://doi.org/10.1523/jneurosci.19-08-03248.1999

Cayzac, S., Delcasso, S., Paz, V., Jeantet, Y., & Cho, Y. H. (2011). Changes in striatal procedural memory coding correlate with learning deficits in a mouse model of Huntington disease. *Proceedings of the National Academy of Sciences*, *108*(22). https://doi.org/10.1073/pnas.1016190108

Cepeda, C., Galvan, L., Holley, S. M., Rao, S. P., André, V. M., Botelho, E. P., Chen, J. Y., Watson, J. B., Deisseroth, K., & Levine, M. S. (2013). Multiple sources of striatal inhibition are differentially affected in Huntington's disease mouse models. *Journal of Neuroscience*, *33*(17), 7393–7406. https://doi.org/10.1523/JNEUROSCI.2137-12.2013

Cepeda, C., Hurst, R. S., Calvert, C. R., Hernández-Echeagaray, E., Nguyen, O. K., Jocoy, E., Christian, L. J., Ariano, M. A., & Levine, M. S. (2003). Transient and progressive

electrophysiological alterations in the corticostriatal pathway in a mouse model of Huntington's disease. *Journal of Neuroscience*, *23*(3), 961–969. https://doi.org/https://doi.org/10.1523/JNEUROSCI.23-03-00961.2003

Cepeda, C., Starling, A. J., Wu, N., Nguyen, O. K., Uzgil, B., Soda, T., André, V. M., Ariano, M. A., & Levine, M. S. (2004). Increased GABAergic function in mouse models of Huntington's disease: reversal by BDNF. *Journal of Neuroscience Research*, *78*(6), 855–867. https://doi.org/10.1002/jnr.20344

Cerovic, M., D'Isa, R., Tonini, R., & Brambilla, R. (2013). Molecular and cellular mechanisms of dopamine-mediated behavioral plasticity in the striatum. *Neurobiology of Learning and Memory*, *105*, 63–80. https://doi.org/10.1016/j.nlm.2013.06.013

Chang, D. T. W., Rintoul, G. L., Pandipati, S., & Reynolds, I. J. (2006). Mutant huntingtin aggregates impair mitochondrial movement and trafficking in cortical neurons. *Neurobiology of Disease*, *22*(2), 388–400. https://doi.org/10.1016/j.nbd.2005.12.007

Chen, X., Wu, J., Lvovskaya, S., Herndon, E., Supnet, C., & Bezprozvanny, I. (2011). Dantrolene is neuroprotective in Huntington's disease transgenic mouse model. *Molecular Neurodegeneration*, *6*(81). https://doi.org/10.1186/1750-1326-6-81

Chiarlone, A., Bellocchio, L., Blazquez, C., Resel, E., Soria-Gomez, E., Cannich, A., Ferrero, J. J., Sagredo, O., Benito, C., Romero, J., Sanchez-Prieto, J., Lutz, B., Fernandez-Ruiz, J., Galve-Roperh, I., & Guzman, M. (2014). A restricted population of CB1 cannabinoid receptors with neuroprotective activity. *Proceedings of the National Academy of Sciences*, *111*(22), 8257–8262. https://doi.org/10.1073/pnas.1400988111

Chiodi, V., Uchigashima, M., Beggiato, S., Ferrante, A., Armida, M., Martire, A., Luisa, R., Ferraro, L., Tanganelli, S., Watanabe, M., Rosaria, M., & Popoli, P. (2012). Unbalance of CB1 receptors expressed in GABAergic and glutamatergic neurons in a transgenic mouse model of Huntington's disease. *Neurobiology of Disease*, *45*(3), 983–991. https://doi.org/10.1016/j.nbd.2011.12.017

Ciamei, A., Detloff, P. J., & Morton, A. J. (2015). Progression of behavioural despair in R6/2 and Hdh knock-in mouse models recapitulates depression in Huntington's disease. *Behavioural Brain Research*, *291*, 140–146. https://doi.org/10.1016/j.bbr.2015.05.010

Ciamei, A., & Morton, A. J. (2009). Progressive imbalance in the interaction between spatial and procedural memory systems in the R6/2 mouse model of Huntington's disease. *Neurobiology of Learning and Memory*, *92*(3), 417–428. https://doi.org/10.1016/j.nlm.2009.06.002

Consortium, G. M. of H. D. (2015). Identification of genetic factors that modify clinical onset of Huntington's disease. *Cell*, *162*, 516–526. https://doi.org/10.1016/j.cell.2015.07.003

Consortium, G. M. of H. D. (2019). CAG repeat not polyglutamine length determines timing of Huntington's disease onset. *Cell*, *178*, 887–900. https://doi.org/10.1016/j.cell.2019.06.036

Contet, C., Gavériaux-Ruff, C., Matifas, A., Caradec, C., Champy, M. F., & Kieffer, B. L. (2006). Dissociation of analgesic and hormonal responses to forced swim stress using opioid receptor knockout mice. *Neuropsychopharmacology*, *31*(8), 1733–1744. https://doi.org/10.1038/sj.npp.1300934

Corbett, A., McGowin, A., Sieber, S., Flannery, T., & Sibbitt, B. (2012). A method for reliable voluntary oral administration of a fixed dosage (mg/kg) of chronic daily medication to rats. *Laboratory Animals*, *46*, 318–324. https://doi.org/10.1258/la.2012.012018

Cortes, C. J., & La Spada, A. R. (2014). The many faces of autophagy dysfunction in Huntington's disease: from mechanism to therapy. *Drug Discovery Today*, *19*(7), 963–971. https://doi.org/10.1016/j.drudis.2014.02.014

Crabbe, J. C., Wahlsten, D., & Dudek, B. C. (1999). Genetics of mouse behavior: interactions with laboratory environment. *Science*, *284*, 1670–1672. https://doi.org/10.1126/science.284.5420.1670

Crispim Junior, C. F., Pederiva, C. N., Bose, R. C., Garcia, V. A., Lino-de-Oliveira, C., & Marino-Neto, J. (2012). ETHOWATCHER: validation of a tool for behavioral and video-tracking analysis in laboratory animals. *Computers in Biology and Medicine*, *42*, 257–264. https://doi.org/10.1016/j.compbiomed.2011.12.002

Crittenden, J. R., & Graybiel, A. M. (2011). Basal ganglia disorders associated with imbalances in the striatal striosome and matrix compartments. *Frontiers in Neuroanatomy*, *5*(59). https://doi.org/10.3389/fnana.2011.00059

Cui, G., Jun, S. B., Jin, X., Pham, M. D., Vogel, S. S., Lovinger, D. M., & Costa, R. M. (2014). Concurrent activation of striatal direct and indirect pathways during action initiation. *Nature*, *494*(7436), 238–242. https://doi.org/10.1038/nature11846

Cui, L., Jeong, H., Borovecki, F., Parkhurst, C. N., Tanese, N., & Krainc, D. (2006). Transcriptional repression of PGC-1α by mutant huntingtin leads to mitochondrial dysfunction and neurodegeneration. *Cell*, *127*, 59–69. https://doi.org/10.1016/j.cell.2006.09.015

Cummings, D. M., Milnerwood, A. J., Dallérac, G. M., Vatsavayai, S. C., Hirst, M. C., & Murphy, K. P. S. J. (2007). Abnormal cortical synaptic plasticity in a mouse model of Huntington's disease. *Brain Research Bulletin*, *72*, 103–107. https://doi.org/10.1016/j.brainresbull.2006.10.016

Dau, A., Gladding, C. M., Sepers, M. D., & Raymond, L. A. (2014). Chronic blockade of extrasynaptic NMDA receptors ameliorates synaptic dysfunction and pro-death signaling in

Huntington disease transgenic mice. *Neurobiology of Disease*, *62*, 533–542. https://doi.org/10.1016/j.nbd.2013.11.013

Davies, S. W., Turmaine, M., Cozens, B., Difiglia, M., Sharp, A. H., Ross, C. A., Scherzinger, E., Wanker, E. E., Mangiarini, L., & Bates, G. P. (1997). Formation of neuronal intranuclear inclusions underlies the neurological dysfunction in mice transgenic for the HD mutation. *Cell*, *90*(3), 537–548. https://doi.org/https://doi.org/10.1016/S0092-8674(00)80513-9

de Chaumont, F., Ey, E., Torquet, N., Lagache, T., Dallongeville, S., Imbert, A., Legou, T., Le Sourd, A. M., Faure, P., Bourgeron, T., & Olivo-Marin, J. C. (2019). Real-time analysis of the behaviour of groups of mice via a depth-sensing camera and machine learning. *Nature Biomedical Engineering*, *3*(11), 930–942. https://doi.org/10.1038/s41551-019-0396-1

de la Monte, S. M., Vonsattel, J. P., & Richardson, E. P. (1988). Morphometric demonstration of atrophic changes in the cerebral cortex, white matter, and neostriatum in Huntington's disease. *Journal of Neuropathology and Experimental Neurology*, *47*(5), 516–525. https://doi.org/10.1097/00005072-198809000-00003

Deng, Y.-P., Wong, T., Bricker-Anthony, C., Deng, B., & Reiner, A. (2013). Loss of corticostriatal and thalamostriatal synaptic terminals precedes striatal projection neuron pathology in heterozygous Q140 Huntington's disease mice. *Neurobiology of Disease*, *60*, 89–107. https://doi.org/10.1016/j.nbd.2013.08.009

Deng, Y.-P., Wong, T., Wan, J. Y., & Reiner, A. (2014). Differential loss of thalamostriatal and corticostriatal input to striatal projection neuron types prior to overt motor symptoms in the Q140 knock-in mouse model of Huntington's disease. *Frontiers in Systems Neuroscience*, *8*(198). https://doi.org/10.3389/fnsys.2014.00198

Dhawale, A. K., Miyamoto, Y. R., Smith, M. A., & Ölveczky, B. P. (2019). Adaptive regulation of motor variability. *Current Biology*, *29*(21), 3551–3562. https://doi.org/10.1016/j.cub.2019.08.052

Dhawale, A. K., Smith, M. A., & Ölveczky, B. P. (2017). The role of variability in motor learning. *Annual Review of Neuroscience*, *40*, 479–498. https://doi.org/10.1146/annurev-neuro-072116-031548

Dhawan, S. S., Xia, S., Tait, D. S., Bundgaard, C., Bowman, E., & Brown, V. J. (2018). Oral dosing of rodents using a palatable tablet. *Psychopharmacology*, *235*, 1527–1532. https://doi.org/https://doi.org/10.1007/s00213-018-4863-2

Di Pardo, A., Maglione, V., Alpaugh, M., Horkey, M., Atwal, R. S., Sassone, J., Ciammola, A., Steffan, J. S., Fouad, K., Truant, R., & Sipione, S. (2012). Ganglioside GM1 induces phosphorylation of mutant huntingtin and restores normal motor behavior in Huntington disease mice. *Proceedings of the National Academy of Sciences*, *109*(9), 3528–3533.

https://doi.org/10.1073/pnas.1114502109

DiFiglia, M., Sapp, E., Chase, K. O., Davies, S. W., Bates, G. P., Vonsattel, J. P., & Aronin, N. (1997). Aggregation of huntingtin in neuronal intranuclear inclusions and dystrophic neurites in brain. *Science*, *277*(5334), 1990–1993. https://doi.org/10.1126/science.277.5334.1990

DiFiglia, M., Sapp, E., Chase, K., Schwarz, C., Meloni, A., Young, C., Martin, E., Vonsattel, J. P., Carraway, R., Reeves, S. A., Boyce, F. M., & Aronin, N. (1995). Huntingtin is a cytoplasmic protein associated with vesicles in human and rat brain neurons. *Neuron*, *14*(5), 1075–1081. https://doi.org/10.1016/0896-6273(95)90346-1

Doenni, V. M., Gray, J. M., Song, C. M., Patel, S., Hill, M. N., & Pittman, Q. J. (2016). Deficient adolescent social behavior following early-life inflammation is ameliorated by augmentation of anandamide signaling. *Brain Behavior and Immunity*, *58*, 237–247. https://doi.org/10.1016/j.bbi.2016.07.152

Dowie, M. J., Bradshaw, H. B., & Howard, M. L. (2009). Altered CB1 receptor and endocannabinoid levels precede motor symptom onset in a transgenic mouse model of Huntington's disease. *Neuroscience*, *163*, 456–465. https://doi.org/10.1016/j.neuroscience.2009.06.014

Dragatsis, I., Levine, M. S., & Zeitlin, S. (2000). Inactivation of Hdh in the brain and testis results in progressive neurodegeneration and sterility in mice. *Nature Genetics*, *26*(3), 300–306. https://doi.org/10.1038/81593

Dudman, J. T., & Krakauer, J. W. (2016). The basal ganglia: from motor commands to the control of vigor. *Current Opinion in Neurobiology*, *37*, 158–166. https://doi.org/10.1016/j.conb.2016.02.005

Dunnett, S. B., Carter, R. J., Watts, C., Torres, E. M., Mahal, A., Mangiarini, L., Bates, G., & Morton, A. J. (1998). Striatal transplantation in a transgenic mouse model of Huntington's disease. *Experimental Neurology*, *154*(1), 31–40. https://doi.org/10.1006/exnr.1998.6926

Eidelberg, D., & Surmeier, J. (2011). Brain networks in Huntington disease. *Journal of Clinical Investigation*, *121*(2), 484–492. https://doi.org/10.1172/JCI45646.484

Elizalde, N., Gil-Bea, F. J., Ramírez, M. J., Aisa, B., Lasheras, B., Del Rio, J., & Tordera, R. M. (2008). Long-lasting behavioral effects and recognition memory deficit induced by chronic mild stress in mice : effect of antidepressant treatment. *Psychopharmacology*, *199*, 1–14. https://doi.org/10.1007/s00213-007-1035-1

Ellis, N., Tee, A., McAllister, B., Massey, T., McLauchlan, D., Stone, T., Correia, K., Loupe, J., Kim, K. H., Barker, D., Hong, E. P., Chao, M. J., Long, J. D., Lucente, D., Vonsattel, J. P. G., Pinto, R. M., Elneel, K. A., Ramos, E. M., Mysore, J. S., … Holmans, P. (2020). Genetic risk underlying psychiatric and cognitive symptoms in Huntington's disease. *Biological Psychiatry*, *87*(9), 857–865. https://doi.org/10.1016/j.biopsych.2019.12.010

Epping, E. A., Kim, J.-I., Craufurd, D., Brashers-Krug, T. M., Anderson, K. E., McCusker, E., Luther, J., Long, J. D., & Paulsen, J. S. (2016). Longitudinal psychiatric symptoms in prodromal Huntington's disease: a decade of data. *American Journal of Psychiatry*, *173*(2), 184–192. https://doi.org/10.1176/appi.ajp.2015.14121551

Estrada-Sanchez, A. M., Burroughs, C. L., Cavaliere, S., Barton, S. J., Chen, S., Yang, X. W., & Rebec, G. V. (2015). Cortical efferents lacking mutant huntingtin improve striatal neuronal activity and behavior in a conditional mouse model of Huntington's disease. *Journal of Neuroscience*, *35*(10), 4440–4451. https://doi.org/10.1523/JNEUROSCI.2812-14.2015

Farley, S. J., McKay, B. M., Disterhoft, J. F., & Weiss, C. (2011). Reevaluating hippocampus dependent learning in FVB/N mice. *Behavioral Neuroscience*, *125*(6), 871–878. https://doi.org/10.1037/a0026033

Feigin, A., Ghilardi, M. F., Huang, C., Ma, Y., Carbon, M., Guttman, M., Paulsen, J. S., Ghez, C. P., & Eidelberg, D. (2006). Preclinical Huntington's disease: compensatory brain responses during learning. *Annals of Neurology*, *59*(1), 53–59. https://doi.org/10.1002/ana.20684

Fellows, S., Schwarz, M., Schaffrath, C., Dömges, F., & Noth, J. (1997). Disturbances of precision grip in Huntington's disease. *Neuroscience Letters*, *226*(2), 103–106. https://doi.org/10.1016/S0304-3940(97)00264-4

Fenrich, K. K., May, Z., Hurd, C., Boychuk, C. E., Kowalczewski, J., Bennett, D. J., Whishaw, I. Q., & Fouad, K. (2015). Improved single pellet grasping using automated ad libitum full-time training robot. *Behavioural Brain Research*, *281*, 137–148. https://doi.org/10.1016/j.bbr.2014.11.048

Fenrich, K. K., May, Z., Torres-Espin, A., Forero, J., Bennett, D. J., & Fouad, K. (2016). Single pellet grasping following cervical spinal cord injury in adult rat using an automated full-time training robot. *Behavioural Brain Research*, *299*, 59–71. https://doi.org/10.1016/j.bbr.2015.11.020

Fernandez-Garcia, S., Conde-Beriozabal, S., Garcia-Garcia, E., Gort-Paniello, C., Bernal-Casas, D., Barriga, G. G.-D., Lopez-Gil, J., Munoz-Moreno, E., Soria, G., Campa, L., Artigas, F., Rodriguez, M. J., Alberch, J., & Masana, M. (2020). M2 cortex-dorsolateral striatum stimulation reverses motor symptoms and synaptic deficits in Huntington's disease. *BioRxiv*. https://doi.org/https://doi.org/10.1101/2020.04.08.032359

File, S. E., Mahal, A., Mangiarini, L., & Bates, G. P. (1998). Striking changes in anxiety in Huntington ' s disease transgenic mice. *Brain Research*, *805*, 234–240.

Fisher, E. R., & Hayden, M. R. (2014). Multisource ascertainment of Huntington disease in Canada: prevalence and population at risk. *Movement Disorders*, *29*(1), 105–114. https://doi.org/10.1002/mds.25717

Fonio, E., Golani, I., & Benjamini, Y. (2012). Measuring behavior of animal models: faults and remedies. *Nature Methods*, *9*(12), 1167–1170. https://doi.org/10.1038/nmeth.2252

Fowler, S. C., & Muma, N. A. (2015). Use of a force-sensing automated open field apparatus in a longitudinal study of multiple behavioral deficits in CAG140 Huntington's disease model mice. *Behavioural Brain Research*, *294*, 7–16. https://doi.org/10.1016/j.bbr.2015.07.036

Francis, N. A., & Kanold, P. O. (2017). Automated operant conditioning in the mouse home cage. *Frontiers in Neural Circuits*, *11*(10). https://doi.org/10.3389/FNCIR.2017.00010

Freedman, L. P., Cockburn, I. M., & Simcoe, T. S. (2015). The economics of reproducibility in preclinical research. *PLoS Biology*, *13*(6). https://doi.org/10.1371/journal.pbio.1002165

Fricker-Gates, R. A., Smith, R., Muhith, J., & Dunnett, S. B. (2003). The role of pretraining on skilled forelimb use in an animal model of Huntington's disease. *Cell Transplantation*, *12*, 257–264. https://doi.org/https://doi.org/10.3727/000000003108746812

Fusilli, C., Migliore, S., Mazza, T., Consoli, F., De Luca, A., Barbagallo, G., Ciammola, A., Gatto, E. M., Cesarini, M., Etcheverry, J. L., Parisi, V., Al-Oraimi, M., Al-Harrasi, S., Al-Salmi, Q., Marano, M., Vonsattel, J. P. G., Sabatini, U., Landwehrmeyer, G. B., & Squitieri, F. (2018). Biological and clinical manifestations of juvenile Huntington's disease: a retrospective analysis. *The Lancet Neurology*, *17*(11), 986–993. https://doi.org/10.1016/S1474-4422(18)30294-1

Gafni, J., Hermel, E., Young, J. E., Wellington, C. L., Hayden, M. R., & Ellerby, L. M. (2004). Inhibition of calpain cleavage of huntingtin reduces toxicity: accumulation of calpain/caspase fragments in the nucleus. *Journal of Biological Chemistry*, *279*(19), 20211–20220. https://doi.org/10.1074/jbc.M401267200

Garland, H., Wood, N. I., Skillings, E. A., Detloff, P. J., Morton, A. J., & Grant, R. A. (2018). Characterisation of progressive motor deficits in whisker movements in R6/2 , Q175 and Hdh knock-in mouse models of Huntington's disease. *Journal of Neuroscience Methods*, *300*, 103–111. https://doi.org/10.1016/j.jneumeth.2017.04.020

Gauthier, L. R., Charrin, B. C., Borrell-Pagès, M., Dompierre, J. P., Rangone, H., Cordelières, F. P., De Mey, J., MacDonald, M. E., Leßmann, V., Humbert, S., & Saudou, F. (2004). Huntingtin controls neurotrophic support and survival of neurons by enhancing BDNF vesicular transport along microtubules. *Cell*, *118*(1), 127–138. https://doi.org/10.1016/j.cell.2004.06.018

Genewsky, A., Heinz, D. E., Kaplick, P. M., Kilonzo, K., & Wotjak, C. T. (2017). A simplified microwave-based motion detector for home cage activity monitoring in mice. *Journal of Biological Engineering*, *11*(36). https://doi.org/10.1186/s13036-017-0079-y

Ghilardi, M. F., Silvestri, G., Feigin, A., Mattis, P., Zgaljardic, D., Moisello, C., Crupi, D.,

Marinelli, L., DiRocco, A., & Eidelberg, D. (2008). Implicit and explicit aspects of sequence learning in pre-symptomatic Huntington's disease. *Parkinsonism and Related Disorders*, *14*(6), 457–464. https://doi.org/10.1016/j.parkreldis.2007.11.009

Gibson, H. E., Reim, K., Brose, N., Morton, A. J., & Jones, S. (2005). A similar impairment in CA3 mossy fibre LTP in the R6⁄2 mouse model of Huntington's disease and in the complexin II knockout mouse. *European Journal of Neuroscience*, *22*, 1701–1712. https://doi.org/10.1111/j.1460-9568.2005.04349.x

Giordano, N., Iemolo, A., Mancini, M., Cacace, F., De Risi, M., Latagliata, E. C., Ghiglieri, V., Bellenchi, G. C., Puglisi-Allegra, S., Calabresi, P., Picconi, B., & De Leonibus, E. (2018). Motor learning and metaplasticity in striatal neurons: relevance for Parkinson's disease. *Brain*, *141*(2), 505–520. https://doi.org/10.1093/brain/awx351

Giralt, A., Saavedra, A., Carretón, O., Xifró, X., Alberch, J., & Pérez-Navarro, E. (2011). Increased PKA signaling disrupts recognition memory and spatial memory: Role in Huntington's disease. *Human Molecular Genetics*, *20*(21), 4232–4247. https://doi.org/10.1093/hmg/ddr351

Gittis, A. H., & Kreitzer, A. C. (2012). Striatal microcircuitry and movement disorders. *Trends in Neurosciences*, *35*(9), 557–564. https://doi.org/doi:10.1016/j.tins.2012.06.008

Glangetas, C., Espinosa, P., & Bellone, C. (2020). Deficit in Motor Skill Consolidation-Dependent Synaptic Plasticity at Motor Cortex to Dorsolateral Striatum Synapses in a Mouse Model of Huntington's Disease. *ENeuro*, *7*(2). https://doi.org/https://doi.org/10.1523/ENEURO.0297-19.2020

Glass, M., Dragunow, M., & Faull, R. L. M. (2000). The pattern of neurodegeneration in Huntington's disease: a comparative study of cannabinoid, dopamine, adenosine and GABA(A) receptor alterations in the human basal ganglia in Huntington's disease. *Neuroscience*, *97*(3), 505–519. https://doi.org/10.1016/S0306-4522(00)00008-7

Godin, J. D., Colombo, K., Molina-Calavita, M., Keryer, G., Zala, D., Charrin, B. E. C., Dietrich, P., Volvert, M. L., Guillemot, F., Dragatsis, I., Bellaiche, Y., Saudou, F., Nguyen, L., & Humbert, S. (2010). Huntingtin is required for mitotic spindle orientation and mammalian neurogenesis. *Neuron*, *67*(3), 392–406. https://doi.org/10.1016/j.neuron.2010.06.027

Godynyuk, E., Bluitt, M. N., Tooley, J. R., Kravitz, A. V., & Creed, M. C. (2019). An open-source, automated home-cage sipper device for monitoring liquid ingestive behavior in rodents. *ENeuro*, *6*(5). https://doi.org/https://doi.org/10.1523/ENEURO.0292-19.2019 1

Gomez-Tortosa, E., MacDonald, M. E., Friend, J. C., Taylor, S. A. M., Weiler, L. J., Adrienne Cupples, L., Srinidhi, J., Gusella, J. F., Bird, E. D., Vonsattel, J. P., & Myers, R. H. (2001). Quantitative neuropathological changes in presymptomatic Huntington's disease. *Annals of*

Neurology, *49*(1), 29–34. https://doi.org/10.1002/1531-8249(200101)49:1<29::AID-ANA7>3.3.CO;2-2

Gordon, R., Albornoz, E. A., Christie, D. C., Langley, M. R., Kumar, V., Mantovani, S., Robertson, A. A. B., Butler, M. S., Rowe, D. B., Neill, L. A. O., Kanthasamy, A. G., Schroder, K., Cooper, M. A., & Woodruff, T. M. (2018). Inflammasome inhibition prevents alpha-synuclein pathology and dopaminergic neurodegeneration in mice. *Science Translational Medicine*, *10*. https://doi.org/10.1126/scitranslmed.aah4066

Goulding, E. H., Schenk, A. K., Juneja, P., MacKay, A. W., Wade, J. M., & Tecott, L. H. (2008). A robust automated system elucidates mouse home cage behavioral structure. *Proceedings of the National Academy of Sciences*, *105*(52), 20575–20582. https://doi.org/10.1073/pnas.0809053106

Graham, R. K., Deng, Y., Slow, E. J., Haigh, B., Bissada, N., Lu, G., Pearson, J., Shehadeh, J., Bertram, L., Murphy, Z., Warby, S. C., Doty, C. N., Roy, S., Wellington, C. L., Leavitt, B. R., Raymond, L. A., Nicholson, D. W., & Hayden, M. R. (2006). Cleavage at the caspase-6 site is required for neuronal dysfunction and degeneration due to mutant huntingtin. *Cell*, *125*(6), 1179–1191. https://doi.org/10.1016/j.cell.2006.04.026

Gray, M., Shirasaki, D. I., Cepeda, C., André, V. M., Wilburn, B., Lu, X. H., Tao, J., Yamazaki, I., Li, S. H., Sun, Y. E., Li, X. J., Levine, M. S., & Yang, X. W. (2008). Full-length human mutant huntingtin with a stable polyglutamine repeat can elicit progressive and selective neuropathogenesis in BACHD mice. *Journal of Neuroscience*, *28*(24), 6182–6195. https://doi.org/10.1523/JNEUROSCI.0857-08.2008

Graybiel, A. M., & Grafton, S. T. (2015). The striatum: where skills and habits meet. *Cold Spring Harbor Perspectives in Biology*, *7*. https://doi.org/10.1101/cshperspect.a021691

Graybiel, A. M., & Ragsdale Jr., C. W. (1978). Histochemically distinct compartments in the striatum of human, monkey, and cat demonstrated by acetylthiocholinesterase staining. *Proceedings of the National Academy of Sciences*, *75*(11), 5723–5726. https://doi.org/https://doi.org/10.1073/pnas.75.11.5723

Gu, M., Gash, M. T., Mann, V. M., Javoy-Agid, F., Cooper, J. M., & Schapira, A. H. V. (1996). Mitochondrial defect in Huntington's disease caudate nucleus. *Annals of Neurology*, *39*(3), 385–389. https://doi.org/10.1002/ana.410390317

Guedes-Dias, P., Pinho, B. R., Soares, T. R., de Proença, J., Duchen, M. R., & Oliveira, J. M. A. (2016). Mitochondrial dynamics and quality control in Huntington's disease. *Neurobiology of Disease*, *90*, 51–57. https://doi.org/10.1016/j.nbd.2015.09.008

Guo, Z. V., Hires, S. A., Li, N., O'Connor, D. H., Komiyama, T., Ophir, E., Huber, D., Bonardi, C., Morandell, K., Gutnisky, D., Peron, S., Xu, N. L., Cox, J., & Svoboda, K. (2014). Procedures for behavioral experiments in head-fixed mice. *PLoS ONE*, *9*(2).

https://doi.org/10.1371/journal.pone.0088678

Gusella, J. F., Wexler, N. S., Conneally, P. M., Naylor, S. L., Anderson, M. A., Tanzi, R. E., Watkins, P. C., Ottina, K., Wallace, M. R., Sakaguchi, A. Y., Young, A. B., Shoulson, I., Bonilla, E., & Martin, J. B. (1983). A polymorphic DNA marker genetically linked to Huntington's disease. *Nature*, *306*(5940), 234–238. https://doi.org/10.1038/306234a0

Gutekunst, C. A., Li, S. H., Yi, H., Mulroy, J. S., Kuemmerle, S., Jones, R., Rye, D., Ferrante, R. J., Hersch, S. M., & Li, X. J. (1999). Nuclear and neuropil aggregates in Huntington's disease: relationship to neuropathology. *Journal of Neuroscience*, *19*(7), 2522–2534. https://doi.org/10.1523/jneurosci.19-07-02522.1999

Haaker, J., Maren, S., Marta, A., Merz, C. J., Richter, J., Helene, R. S., Drexler, M., Lange, M. D., Jüngling, K., Nees, F., Seidenbecher, T., Fullana, M. A., T, W. C., & Lonsdorf, T. B. (2019). Making translation work: harmonizing cross-species methodology in the behavioural neuroscience of Pavlovian fear conditioning. *Neuroscience and Biobehavioral Reviews*, *107*, 329–345. https://doi.org/10.1016/j.neubiorev.2019.09.020

Halliday, G. M., McRitchie, D. A., Macdonald, V., Double, K. L., Trent, R. J., & McCusker, E. (1998). Regional specificity of brain atrophy in Huntington's disease. *Experimental Neurology*, *154*, 663–672. https://doi.org/https://doi.org/10.1006/exnr.1998.6919

Hånell, A., & Marklund, N. (2014). Structured evaluation of rodent behavioral tests used in drug discovery research. *Frontiers in Behavioral Neuroscience*, *8*(252). https://doi.org/10.3389/fnbeh.2014.00252

Hansson, O., Guatteo, E., Mercuri, N. B., Bernardi, G., Li, X. J., Castilho, R. F., & Brundin, P. (2001). Resistance to NMDA toxicity correlates with appearance of nuclear inclusions, behavioural deficits and changes in calcium homeostasis in mice transgenic for exon 1 of the huntington gene. *European Journal of Neuroscience*, *14*(9), 1492–1504. https://doi.org/10.1046/j.0953-816X.2001.01767.x

Harrison, D. J., Busse, M., Openshaw, R., Rosser, A. E., Dunnett, S. B., & Brooks, S. P. (2013). Exercise attenuates neuropathology and has greater benefit on cognitive than motor deficits in the R6/1 Huntington's disease mouse model. *Experimental Neurology*, *248*, 457–469. https://doi.org/10.1016/j.expneurol.2013.07.014

Hausdorff, J. M., Cudkowicz, M. E., Firtion, R., Wei, J. Y., & Goldberger, A. L. (1998). Gait variability and basal ganglia disorders: stride-to-stride variations of gait cycle timing in Parkinson's disease and Huntington's disease. *Movement Disorders*, *13*(3), 428–437. https://doi.org/https://doi.org/10.1002/mds.870130310

Hedreen, J. C., Peyser, C. E., Folstein, S. E., & Ross, C. A. (1991). Neuronal loss in layers V and VI of cerebral cortex in Huntington's disease. *Neuroscience Letters*, *133*(2), 257–261. https://doi.org/10.1016/0304-3940(91)90583-F

Heikkinen, T., Lehtimaki, K., Vartiainen, N., Puolivali, J., Hendricks, S. J., Glaser, J. R., Bradaia, A., Wadel, K., Touller, C., Kontkanen, O., Yrjanheikki, J. M., Buisson, B., Howland, D., Beaumont, V., Munoz-Sanjuan, I., & Park, L. C. (2012). Characterization of neurophysiological and behavioral changes, MRI brain volumetry and 1H MRS in zQ175 knock-in mouse model of Huntington's disease. *PLoS ONE*, *7*(12). https://doi.org/10.1371/journal.pone.0050717

Hintiryan, H., Foster, N. N., Bowman, I., Bay, M., Song, M. Y., Gou, L., Yamashita, S., Bienkowski, M. S., Zingg, B., Zhu, M., Yang, X. W., Shih, J. C., Toga, A. W., & Dong, H.-W. (2016). The mouse cortico-striatal projectome. *Nature Neuroscience*, *19*(8), 1100–1114. https://doi.org/10.1038/nn.4332

Hipp, M. S., Patel, C. N., Bersuker, K., Riley, B. E., Kaiser, S. E., Shaler, T. A., Brandeis, M., & Kopito, R. R. (2012). Indirect inhibition of 26S proteasome activity in a cellular model of Huntington's disease. *Journal of Cell Biology*, *196*(5), 573–587. https://doi.org/10.1083/jcb.201110093

Ho, A., & Chin, A. (1988). Circadian feeding and drinking patterns of genetically obese mice fed solid chow diet. *Physiology and Behavior*, *43*(5), 651–656. https://doi.org/10.1016/0031-9384(88)90221-1

Ho, A. K., Sahakian, B. J., Brown, R. G., Barker, R. A., Hodges, J. R., Ane, M. N., Snowden, J., Thompson, J., Esmonde, T., Gentry, R., Moore, J. W., & Bodner, T. (2003). Profile of cognitive progression in early Huntington's disease. *Neurology*, *61*(12), 1702–1706. https://doi.org/10.1212/01.WNL.0000098878.47789.BD

Hodges, A., Hughes, G., Brooks, S. P., Elliston, L., Holmans, P., Dunnett, S. B., & Jones, L. (2008). Brain gene expression correlates with changes in behavior in the R6/1 mouse model of Huntington's disease. *Genes, Brain and Behavior*, *7*(3), 288–299. https://doi.org/10.1111/j.1601-183X.2007.00350.x

Hodgson, J. G., Agopyan, N., Gutekunst, C. A., Leavitt, B. R., Lepiane, F., Singaraja, R., Smith, D. J., Bissada, N., McCutcheon, K., Nasir, J., Jamot, L., Xiao-Jiang, L., Stevens, M. E., Rosemond, E., Roder, J. C., Phillips, A. G., Rubin, E. M., Hersch, S. M., & Hayden, M. R. (1999). A YAC mouse model for Huntington's disease with full-length mutant huntingtin, cytoplasmic toxicity, and selective striatal neurodegeneration. *Neuron*, *23*(1), 181–192. https://doi.org/10.1016/S0896-6273(00)80764-3

Hong, W., Kennedy, A., Burgos-Artizzu, X. P., Zelikowsky, M., Navonne, S. G., Perona, P., & Anderson, D. J. (2015). Automated measurement of mouse social behaviors using depth sensing, video tracking, and machine learning. *Proceedings of the National Academy of Sciences*, *112*(38), 5351–5360. https://doi.org/10.1073/pnas.1515982112

Hughes, A. C., Mort, M., Elliston, L., Thomas, R. M., Brooks, S. P., Dunnett, S. B., & Jones, L. (2014). Identification of novel alternative splicing events in the huntingtin gene and

assessment of the functional consequences using structural protein homology modelling. *Journal of Molecular Biology*, *426*(7), 1428–1438. https://doi.org/10.1016/j.jmb.2013.12.028

Hult Lundh, S., Nilsson, N., Soylu, R., Kirik, D., & Petersén, Å. (2013). Hypothalamic expression of mutant huntingtin contributes to the development of depressive-like behavior in the BAC transgenic mouse model of Huntington's disease. *Human Molecular Genetics*, *22*(17), 3485–3497. https://doi.org/10.1093/hmg/ddt203

Huntington, G. (1872). On Chorea. *Medical and Surgical Reporter of Philadelphia*, *26*, 317–326.

Huntington Study Group (1996). Unified Huntington's disease rating scale: reliability and consistency. *Movement Disorders*, *11*(2), 136–142. https://doi.org/https://doi.org/10.1002/mds.870110204

International Organization for Standardization. (2017). *Sterile hypodermic syringes for single use — Part 1: Syringes for manual use (ISO 7886-1:2017)*.

Jacobsen, J. C., Erdin, S., Chiang, C., Hanscom, C., Handley, R. R., Barker, D. D., Stortchevoi, A., Blumenthal, I., Reid, S. J., Snell, R. G., MacDonald, M. E., Morton, A. J., Ernst, C., Gusella, J. F., & Talkowski, M. E. (2017). Potential molecular consequences of transgene integration: the R6/2 mouse example. *Scientific Reports*, *7*(41120). https://doi.org/10.1038/srep41120

Jhuang, H., Garrote, E., Yu, X., Khilnani, V., Poggio, T., Steele, A. D., & Serre, T. (2010). Automated home-cage behavioural phenotyping of mice. *Nature Communications*, *1*(68). https://doi.org/10.1038/ncomms1064

Johnson, E. B., Ziegler, G., Penny, W., Rees, G., Tabrizi, S. J., Scahill, R. I., & Gregory, S. (2019). Dynamics of cortical degeneration over a decade in Huntington's Disease. *BioRxiv*. https://doi.org/10.1101/537977

Jones, C., Busse, M., Quinn, L., Dawes, H., Drew, C., Kelson, M., Hood, K., Rosser, A., & Edwards, R. T. (2016). The societal cost of Huntington's disease: are we underestimating the burden? *European Journal of Neurology*, *23*(10), 1588–1590. https://doi.org/10.1111/ene.13107

Joshi, P. R., Wu, N. P., André, V. M., Cummings, D. M., Cepeda, C., Joyce, J. A., Carroll, J. B., Leavitt, B. R., Hayden, M. R., Levine, M. S., & Bamford, N. S. (2009). Age-dependent alterations of corticostriatal activity in the YAC128 mouse model of Huntington disease. *Journal of Neuroscience*, *29*(8), 2414–2427. https://doi.org/10.1523/JNEUROSCI.5687-08.2009

Karl, J. M., & Whishaw, I. Q. (2011). Rodent skilled reaching for modeling pathological conditions of the human motor system. In E. L. Lane & S. B. Dunnett (Eds.), *Neuromethods*

(Vol. 61, pp. 87–107). Humana Press. https://doi.org/10.1007/978-1-61779-298-4_6

Kaupert, U., Thurley, K., Frei, K., Bagorda, F., Schatz, A., Tocker, G., Rapoport, S., Derdikman, D., & Winter, Y. (2017). Spatial cognition in a virtual reality home-cage extension for freely moving rodents. *Journal of Neurophysiology*, *117*(4), 1736–1748. https://doi.org/10.1152/jn.00630.2016

Kennedy, L., Evans, E., Chen, C. M., Craven, L., Detloff, P. J., Ennis, M., & Shelbourne, P. F. (2003). Dramatic tissue-specific mutation length increases are an early molecular event in Huntington disease pathogenesis. *Human Molecular Genetics*, *12*(24), 3359–3367. https://doi.org/10.1093/hmg/ddg352

Khalil, B., El Fissi, N., Aouane, A., Cabirol-Pol, M. J., Rival, T., & Liévens, J. C. (2015). PINK1-induced mitophagy promotes neuroprotection in Huntington's disease. *Cell Death and Disease, 6*. https://doi.org/10.1038/cddis.2014.581

Kim, H. Y., Kim, H. V, Yoon, J. H., Kang, B. R., Cho, S. M., Lee, S., Kim, J. Y., Kim, J. W., Cho, Y., Woo, J., & Kim, Y. (2014). Taurine in drinking water recovers learning and memory in the adult APP/PS1 mouse model of Alzheimer's disease. *Scientific Reports*, *4*(7467). https://doi.org/10.1038/srep07467

Kirkwood, S. C., Su, J. L., Conneally, P., & Foroud, T. (2001). Progression of symptoms in the early and middle stages of Huntington disease. *Archives of Neurology*, *58*, 273–278. https://doi.org/10.1001/archneur.58.2.273

Kiryk, A., Janusz, A., Zglinicki, B., Turkes, E., Knapska, E., Konopka, W., Lipp, H. P., & Kaczmarek, L. (2020). IntelliCage as a tool for measuring mouse behavior – 20 years perspective. *Behavioural Brain Research*, *388*(112620). https://doi.org/10.1016/j.bbr.2020.112620

Klaus, A., Alves Da Silva, J., & Costa, R. M. (2019). What, if, and when to move: basal ganglia circuits and self-paced action initiation. *Annual Review of Neuroscience*, *42*, 459–483. https://doi.org/10.1146/annurev-neuro-072116-031033

Klein, A., Sacrey, L. A. R., Dunnett, S. B., Whishaw, I. Q., & Nikkhah, G. (2011). Proximal movements compensate for distal forelimb movement impairments in a reach-to-eat task in Huntington's disease: new insights into motor impairments in a real-world skill. *Neurobiology of Disease*, *41*(2), 560–569. https://doi.org/10.1016/j.nbd.2010.11.002

Klein, A., Sacrey, L. R., Whishaw, I. Q., & Dunnett, S. B. (2012). The use of rodent skilled reaching as a translational model for investigating brain damage and disease. *Neuroscience and Biobehavioral Reviews*, *36*(3), 1030–1042. https://doi.org/10.1016/j.neubiorev.2011.12.010

Koch, E. T., & Raymond, L. A. (2019). Dysfunctional striatal dopamine signaling in

Huntington's disease. *Journal of Neuroscience Research*, *97*(12), 1636–1654. https://doi.org/10.1002/jnr.24495

Kolodziejczyk, K., & Raymond, L. A. (2016). Differential changes in thalamic and cortical excitatory synapses onto striatal spiny projection neurons in a Huntington disease mouse model. *Neurobiology of Disease*, *86*, 62–74. https://doi.org/10.1016/j.nbd.2015.11.020

Koralek, A. C., Costa, R. M., & Carmena, J. M. (2013). Temporally precise cell-specific coherence develops in corticostriatal networks during learning. *Neuron*, *79*(5), 865–872. https://doi.org/10.1016/j.neuron.2013.06.047

Kovalenko, M., Milnerwood, A., Giordano, J., Claire, J. S., Guide, J. R., Stromberg, M., Gillis, T., Sapp, E., DiFiglia, M., MacDonald, M. E., Carroll, J. B., Lee, J. M., Tappan, S., Raymond, L. A., & Wheeler, V. C. (2018). HttQ111/+ Huntington's disease knock-in mice exhibit brain region-specific morphological changes and synaptic dysfunction. *Journal of Huntington's Disease*, *7*(1), 17–33. https://doi.org/10.3233/JHD-170282

Krackow, S., Vannoni, E., Codita, A., Mohammed, A. H., Cirulli, F., Branchi, I., Alleva, E., Reichelt, A., Willuweit, A., Voikar, V., Colacicco, G., Wolfer, D. P., Buschmann, J. U. F., Safi, K., & Lipp, H. P. (2010). Consistent behavioral phenotype differences between inbred mouse strains in the IntelliCage. *Genes, Brain and Behavior*, *9*(7), 722–731. https://doi.org/10.1111/j.1601-183X.2010.00606.x

Kravitz, A. V., Freeze, B. S., Parker, P. R. L., Kay, K., Thwin, M. T., Deisseroth, K., & Kreitzer, A. C. (2010). Regulation of parkinsonian motor behaviours by optogenetic control of basal ganglia circuitry. *Nature*, *466*(7306), 622–626. https://doi.org/10.1038/nature09159

Kreitzer, A. C., & Malenka, R. C. (2008). Striatal plasticity and basal ganglia circuit function. *Neuron*, *60*(4), 543–554. https://doi.org/10.1016/j.neuron.2008.11.005

Kudo, T., Schroeder, A., Loh, D. H., Kuljis, D., Jordan, M. C., Roos, K. P., & Colwell, C. S. (2011). Dysfunctions in circadian behavior and physiology in mouse models of Huntington's disease. *Experimental Neurology*, *228*(1), 80–90. https://doi.org/10.1016/j.expneurol.2010.12.011

Kudwa, A. E., Menalled, L. B., Oakeshott, S., Murphy, C., Mushlin, R., Fitzpatrick, J., Miller, S. F., Mcconnell, K., Port, R., Torello, J., Howland, D., Ramboz, S., & Brunner, D. (2013). Increased body weight of the BAC HD transgenic mouse model of Huntington's disease accounts for some but not all of the observed HD-like motor deficits. *PLOS Currents Huntington Disease*, *5*. https://doi.org/10.1371/currents.hd.0ab4f3645aff523c56ecc8ccbe41a198.Revisions

Kung, V. W. S., Hassam, R., Morton, A. J., & Jones, S. (2007). Dopamine-dependent long term potentiation in the dorsal striatum is reduced in the R6/2 mouse model of Huntington's disease. *Neuroscience*, *146*(4), 1571–1580.

https://doi.org/10.1016/j.neuroscience.2007.03.036

Kupferschmidt, D. A., Juczewski, K., Cui, G., Johnson, K. A., & Lovinger, D. M. (2017). Parallel, but dissociable, processing in discrete corticostriatal inputs encodes skill learning. *Neuron*, *96*(2), 476-489.e5. https://doi.org/10.1016/j.neuron.2017.09.040

Labadorf, A. T., & Myers, R. H. (2015). Evidence of extensive alternative splicing in post mortem human brain HTT transcription by mRNA sequencing. *PLoS ONE*, *10*(10). https://doi.org/10.1371/journal.pone.0141298

Labbadia, J., & Morimoto, R. I. (2013). Huntington's disease: underlying molecular mechanisms and emerging concepts. *Trends in Biochemical Sciences*, *38*(8), 378–385. https://doi.org/10.1016/j.tibs.2013.05.003

Labbadia, J., & Morimoto, R. I. (2015). The biology of proteostasis in aging and disease. *Annual Review of Biochemistry*, *84*, 435–464. https://doi.org/10.1146/annurev-biochem-060614-033955

Lambot, L., Rodriguez, E. C., Houtteman, D., Li, Y., Schiffmann, S., Gall, D., & de Kerchove d'Exaerde, A. (2016). Striatopallidal neuron NMDA-receptors control synaptic connectivity, locomotor and goal-directed behaviours. *Journal of Neuroscience*, *36*(18), 4976–4992. https://doi.org/10.1523/JNEUROSCI.2717-15.2016

Langbehn, D. R., Hayden, M. R., & Paulsen, J. S. (2010). CAG-repeat length and the age of onset in Huntington disease (HD): a review and validation study of statistical approaches. *American Journal of Medical Genetics Part B: Neuropsychiatric Genetics*, *153B*(2), 397–408. https://doi.org/doi:10.1002/ajmg.b.30992

Lawhorn, C., Smith, D. M., & Brown, L. L. (2008). Striosome-matrix pathology and motor deficits in the YAC128 mouse model of Huntington's disease. *Neurobiology of Disease*, *32*(3), 471–478. https://doi.org/10.1016/j.nbd.2008.08.006

Lawrence, A. D., Hodges, J. R., Rosser, A. E., Kershaw, A., Rubinsztein, D. C., Robbins, T. W., & Sahakian, B. J. (1998). Evidence for specific cognitive deficits in preclinical Huntington's disease. *Brain*, *121*, 1329–1341.

Lee, A. M., Tai, L. H., Zador, A., & Wilbrecht, L. (2015). Between the primate and "reptilian" brain: rodent models demonstrate the role of corticostriatal circuits in decision making. *Neuroscience*, *296*, 66–74. https://doi.org/10.1016/j.neuroscience.2014.12.042

Lee, J. H., Capan, S., Lacefield, C., Shea, Y. M., & Nautiyal, K. M. (2020). DIY-NAMIC behavior: a high-throughput method to measure complex phenotypes in the homecage. *ENeuro*, *7*(4). https://doi.org/10.1523/ENEURO.0160-20.2020

Li, W., & Pozzo-Miller, L. (2019). Differences in GluN2B-containing NMDA receptors result in

distinct long-term plasticity at ipsilateral versus contralateral cortico-striatal synapses. *ENeuro*, *6*(6). https://doi.org/10.1523/ENEURO.0118-19.2019

Li, X.-J., Li, S.-H., Sharp, A. H., Nucifora Jr., F. C., Schilling, G., Lanahan, A., Worley, P., Snyder, S. H., & Ross, C. A. (1995). A huntingtin-associated protein enriched in brain with implications for pathology. *Nature*, *378*, 398–402. https://doi.org/https://doi.org/10.1038/378398a0

Lin, C. H., Tallaksen-Greene, S., Chien, W. M., Cearley, J. A., Jackson, W. S., Crouse, A. B., Ren, S., Li, X. J., Albin, R. L., & Detloff, P. J. (2001). Neurological abnormalities in a knock-in mouse model of Huntington's disease. *Human Molecular Genetics*, *10*(2), 137–144. https://doi.org/10.1093/hmg/10.2.137

Lione, L. A., Carter, R. J., Hunt, M. J., Bates, G. P., Morton, A. J., & Dunnett, S. B. (1999). Selective discrimination learning impairments in mice expressing the human Huntington's disease mutation. *Journal of Neuroscience*, *19*(23), 10428–10437. https://doi.org/https://doi.org/10.1523/JNEUROSCI.19-23-10428.1999

Loh, D. H., Kudo, T., Truong, D., Wu, Y., & Colwell, C. S. (2013). The Q175 mouse model of Huntington's disease shows gene dosage- and age-related decline in circadian rhythms of activity and sleep. *PLoS ONE*, *8*(7). https://doi.org/10.1371/journal.pone.0069993

Lovinger, D. M. (2010). Neurotransmitter roles in synaptic modulation, plasticity and learning in the dorsal striatum. *Neuropharmacology*, *58*(7), 951–961. https://doi.org/10.1016/j.neuropharm.2010.01.008

MacDonald, M. E., Ambrose, C. M., Duyao, M. P., Myers, R. H., Lin, C., Srinidhi, L., Barnes, G., Taylor, S. A., James, M., Groot, N., MacFarlane, H., Jenkins, B., Anderson, M. A., Wexler, N. S., Gusella, J. F., Bates, G. P., Baxendale, S., Hummerich, H., Kirby, S., … Harper, P. S. (1993). A novel gene containing a trinucleotide repeat that is expanded and unstable on Huntington's disease chromosomes. *Cell*, *72*(6), 971–983. https://doi.org/10.1016/0092-8674(93)90585-E

Machado, A. S., Darmohray, D. M., Fayad, J., Marques, H. G., & Carey, M. R. (2015). A quantitative framework for whole-body coordination reveals specific deficits in freely walking ataxic mice. *ELife*, *4*. https://doi.org/10.7554/eLife.07892

Mandillo, S., Tucci, V., Hölter, S. M., Meziane, H., Banchaabouchi, M. Al, Kallnik, M., Lad, H. V, Nolan, P. M., Ouagazzal, A.-M., Coghill, E. L., Gale, K., Golini, E., Jacquot, S., Krezel, W., Parker, A., Riet, F., Schneider, I., Marazziti, D., Auwerx, J., … Wurst, W. (2008). Reliability, robustness, and reproducibility in mouse behavioral phenotyping: a cross-laboratory study. *Physiological Genomics*, *34*(3), 243–255. https://doi.org/10.1152/physiolgenomics.90207.2008

Mangiarini, L., Sathasivam, K., Seller, M., Cozens, B., Harper, A., Hetherington, C., Lawton,

M., Trottier, Y., Lehrach, H., Davies, S. W., & Bates, G. P. (1996). Exon 1 of the HD gene with an expanded CAG repeat is sufficient to cause a progressive neurological phenotype in transgenic mice. *Cell*, *87*, 493–506. https://doi.org/https://doi.org/10.1016/S0092-8674(00)81369-0

Mantovani, S., Gordon, R., Li, R., Christie, D. C., Kumar, V., & Woodruff, T. M. (2016). Motor deficits associated with Huntington's disease occur in the absence of striatal degeneration in BACHD transgenic mice. *Human Molecular Genetics*, *25*(9), 1780–1791. https://doi.org/10.1093/hmg/ddw050

Markowitz, J. E., Gillis, W. F., Beron, C. C., Neufeld, S. Q., Robertson, K., Bhagat, N. D., Peterson, R. E., Peterson, E., Hyun, M., Linderman, S. W., Sabatini, B. L., & Datta, S. R. (2018). The striatum organizes 3D behavior via moment-to-moment action selection. *Cell*, *174*, 44–58. https://doi.org/10.1016/j.cell.2018.04.019

Marques Sousa, C., & Humbert, S. (2013). Huntingtin: here, there, everywhere! *Journal of Huntington's Disease*, *2*(4), 395–403. https://doi.org/10.3233/JHD-130082

Matikainen-Ankney, B. A., Garmendia-Cedillos, M., Ali, M., Krynitsky, J., Salem, G., Miyazaki, N. L., Pohida, T., & Kravitz, A. V. (2019). Rodent Activity Detector (RAD), an open source device for measuring activity in rodent home cages. *ENeuro*, *6*(4). https://doi.org/https://doi.org/10.1523/ENEURO.0160-19.2019 1

Maywood, E. S., Fraenkel, E., McAllister, C. J., Wood, N., Reddy, A. B., Hastings, M. H., & Morton, A. J. (2010). Disruption of peripheral circadian timekeeping in a mouse model of Huntington's disease and its restoration by temporally scheduled feeding. *Journal of Neuroscience*, *30*(30), 10199–10204. https://doi.org/10.1523/JNEUROSCI.1694-10.2010

Mazarakis, N. K., Cybulska-Klosowicz, A., Grote, H., Pang, T., Dellen, A. Van, Kossut, M., Blakemore, C., Hannan, A. J., & Van Dellen, A. (2005). Deficits in experience-dependent cortical plasticity and sensory-discrimination learning in presymptomatic Huntington's disease mice. *Journal of Neuroscience*, *25*(12), 3059–3066. https://doi.org/10.1523/JNEUROSCI.4320-04.2005

McColgan, P., & Tabrizi, S. J. (2018). Huntington's disease: a clinical review. *European Journal of Neurology*, *25*(1), 24–34. https://doi.org/10.1111/ene.13413

McFadyen, M. P., Kusek, G., Bolivar, V. J., & Flaherty, L. (2003). Differences among eight inbred strains of mice in motor ability and motor learning on a rotorod. *Genes, Brain and Behavior*, *2*(4), 214–219. https://doi.org/10.1034/j.1601-183X.2003.00028.x

McLin, J. P., & Steward, O. (2006). Comparison of seizure phenotype and neurodegeneration induced by systemic kainic acid in inbred, outbred, and hybrid mouse strains. *European Journal of Neuroscience*, *24*(8), 2191–2202. https://doi.org/10.1111/j.1460-9568.2006.05111.x

Meijer, M. K., Spruijt, B. M., van Zutphen, L. F. M., & Baumans, V. (2006). Effect of restraint and injection methods on heart rate and body temperature in mice. *Laboratory Animals*, *40*, 382–391. https://doi.org/https://doi.org/10.1258/002367706778476370

Menalled, L. B., El-Khodor, B. F., Patry, M., Suárez-Fariñas, M., Orenstein, S. J., Zahasky, B., Leahy, C., Wheeler, V., Yang, X. W., Macdonald, M., Morton, A. J., Bates, G., Leeds, J., Park, L., Howland, D., Signer, E., Tobin, A., & Brunner, D. (2009). Systematic behavioral evaluation of Huntington's disease transgenic and knock-in mouse models. *Neurobiology of Disease*, *35*(3), 319–336. https://doi.org/10.1016/j.nbd.2009.05.007

Menalled, L. B., Kudwa, A. E., Miller, S., Fitzpatrick, J., Watson-Johnson, J., Keating, N., Ruiz, M., Mushlin, R., Alosio, W., McConnell, K., Connor, D., Murphy, C., Oakeshott, S., Kwan, M., Beltran, J., Ghavami, A., Brunner, D., Park, L. C., Ramboz, S., & Howland, D. (2012). Comprehensive Behavioral and Molecular Characterization of a New Knock-In Mouse Model of Huntington's Disease: zQ175. *PLoS ONE*, *7*(12). https://doi.org/10.1371/journal.pone.0049838

Menalled, L. B., Lutz, C., Ramboz, S., Brunner, D., Lager, B., Noble, S., Park, L., & Howland, D. (2014). A Field Guid to Working with Mouse Models of Huntington's Disease. *The Jackson Laboratory*.

Menalled, L. B., Sison, J. D., Dragatsis, I., Zeitlin, S., & Chesselet, M. F. (2003). Time course of early motor and neuropathological anomalies in a knock-in mouse model of Huntington's disease with 140 CAG repeats. *Journal of Comparative Neurology*, *465*(1), 11–26. https://doi.org/10.1002/cne.10776

Milnerwood, A. J., Gladding, C. M., Pouladi, M. A., Kaufman, A. M., Hines, R. M., Boyd, J. D., Ko, R. W. Y., Vasuta, O. C., Graham, R. K., Hayden, M. R., Murphy, T. H., & Raymond, L. A. (2010). Early increase in extrasynaptic NMDA receptor signaling and expression contributes to phenotype onset in Huntington's disease mice. *Neuron*, *65*(2), 178–190. https://doi.org/10.1016/j.neuron.2010.01.008

Mineur, Y. S., Belzung, C., & Crusio, W. E. (2006). Effects of unpredictable chronic mild stress on anxiety and depression-like behavior in mice. *Behavioural Brain Research*, *175*, 43–50. https://doi.org/10.1016/j.bbr.2006.07.029

Moreno, C. L., Ehrlich, M. E., & Mobbs, C. V. (2016). Protection by dietary restriction in the YAC128 mouse model of Huntington's disease: relation to genes regulating histone acetylation and HTT. *Neurobiology of Disease*, *85*, 25–34. https://doi.org/10.1016/j.nbd.2015.09.012

Morton, A. J. (2013). Circadian and sleep disorder in Huntington's disease. *Experimental Neurology*, *243*, 34–44. https://doi.org/10.1016/j.expneurol.2012.10.014

Morton, A. J., Glynn, D., Leavens, W., Zheng, Z., Faull, R. L. M., Skepper, J. N., & Wight, J. M.

(2009). Paradoxical delay in the onset of disease caused by super-long CAG repeat expansions in R6/2 mice. *Neurobiology of Disease*, *33*(3), 331–341. https://doi.org/10.1016/j.nbd.2008.11.015

Morton, A. J., Wood, N. I., Hastings, M. H., Hurelbrink, C., Barker, R. A., & Maywood, E. S. (2005). Disintegration of the sleep-wake cycle and circadian timing in Huntington's disease. *Journal of Neuroscience*, *25*(1), 157–163. https://doi.org/10.1523/JNEUROSCI.3842-04.2005

Moss, D. J. H., Tabrizi, S. J., Mead, S., Lo, K., Pardiñas, A. F., Holmans, P., Jones, L., Langbehn, D., Coleman, A., Santos, R. D., Decolongon, J., Sturrock, A., Bardinet, E., Ret, C. J., Justo, D., Lehericy, S., Marelli, C., Nigaud, K., Valabrègue, R., … Tan, L. (2017). Identification of genetic variants associated with Huntington's disease progression: a genome-wide association study. *The Lancet Neurology*, *16*(9), 701–711. https://doi.org/10.1016/S1474-4422(17)30161-8

Moynihan, J., Brenner, G., Koota, D., Breneman, S., Cohen, N., & Ader, R. (1990). The effects of handling on anitbody production, mitogen responses, spleen cell number, and lymphocyte subpopulations. *Life Sciences*, *46*, 1937–1944. https://doi.org/https://doi.org/10.1016/0024-3205(90)90509-P

Mühlau, M., Gaser, C., Wohlschläger, A. M., Weindl, A., Städtler, M., Valet, M., Zimmer, C., Kassubek, J., & Peinemann, A. (2007). Striatal gray matter loss in Huntington's disease is leftward biased. *Movement Disorders*, *22*(8), 1169–1173. https://doi.org/10.1002/mds.21137

Murphy, K. P. S. J., Carter, R. J., Lione, L. A., Mangiarini, L., Mahal, A., Bates, G. P., Dunnett, S. B., & Jennifer Morton, A. (2000). Abnormal synaptic plasticity and impaired spatial cognition in mice transgenic for exon 1 of the human Huntington's disease mutation. *Journal of Neuroscience*, *20*(13), 5115–5123. https://doi.org/10.1523/jneurosci.20-13-05115.2000

Murphy, T. H., Boyd, J. D., Bolaños, F., Vanni, M. P., Silasi, G., Haupt, D., & Ledue, J. M. (2016). High-throughput automated home-cage mesoscopic functional imaging of mouse cortex. *Nature Communications*, *7*. https://doi.org/10.1038/ncomms11611

Murphy, T. H., Michelson, N. J., Boyd, J. D., Fong, T., Bolaños, L. A., Bierbrauer, D., Siu, T., Balbi, M., Bolaños, F., Vanni, M., & Ledue, J. M. (2020). Automated task training and longitudinal monitoring of mouse mesoscale cortical circuits using home cages. *ELife*, *9*. https://doi.org/10.7554/eLife.55964

Nance, M. A., & Myers, R. H. (2001). Juvenile onset Huntington's disease - clinical and research perspectives. *Mental Retardation and Developmental Disabilities Research Reviews*, *7*, 153–157. https://doi.org/https://doi.org/10.1002/mrdd.1022

Nasir, J., Floresco, S. B., O'Kusky, J. R., Diewert, V. M., Richman, J. M., Zeisler, J., Borowski, A., Marth, J. D., Phillips, A. G., & Hayden, M. R. (1995). Targeted disruption of the Huntington's disease gene results in embryonic lethality and behavioral and morphological changes in heterozygotes. *Cell*, *81*(5), 811–823. https://doi.org/10.1016/0092-8674(95)90542-1

Naver, B., Stub, C., Møller, M., Fenger, K., Hansen, A. K., Hasholt, L., & Sørensen, S. A. (2003). Molecular and behavioral analysis of the R6/1 Huntington's disease transgenic mouse. *Neuroscience*, *122*(4), 1049–1057. https://doi.org/10.1016/j.neuroscience.2003.08.053

Naydenov, A. V, Sepers, M. D., Swinney, K., Raymond, L. A., Palmiter, R. D., & Stella, N. (2014). Genetic rescue of CB 1 receptors on medium spiny neurons prevents loss of excitatory striatal synapses but not motor impairment in HD mice. *Neurobiology of Disease*, *71*, 140–150. https://doi.org/10.1016/j.nbd.2014.08.009

Neueder, A., Landles, C., Ghosh, R., Howland, D., Myers, R. H., Faull, R. L. M., Tabrizi, S. J., & Bates, G. P. (2017). The pathogenic exon 1 HTT protein is produced by incomplete splicing in Huntington's disease patients. *Scientific Reports*, *7*(1307). https://doi.org/10.1038/s41598-017-01510-z

Nguyen, K. P., O'Neal, T. J., Bolonduro, O. A., White, E., & Kravitz, A. V. (2016). Feeding Experimentation Device (FED): a flexible open-source device for measuring feeding behavior. *Journal of Neuroscience Methods*, *267*, 108–114. https://doi.org/10.1016/j.jneumeth.2016.04.003

Noorshams, O., Boyd, J. D., & Murphy, T. H. (2017). Automating mouse weighing in group homecages with Raspberry Pi micro-computers. *Journal of Neuroscience Methods*, *285*, 1–5. https://doi.org/10.1016/j.jneumeth.2017.05.002

O'Leary, J. D., O'Leary, O. F., Cryan, J. F., & Nolan, Y. M. (2018). A low-cost touchscreen operant chamber using a Raspberry Pi^{TM}. *Behavior Research Methods*, *50*, 2523–2530. https://doi.org/https://doi.org/10.3758/s13428-018-1030-y

Oakeshott, S., Balci, F., Filippov, I., Murphy, C., Port, R., Connor, D., Paintdakhi, A., Lesauter, J., Menalled, L. B., Ramboz, S., Kwak, S., Howland, D., Silver, R., & Brunner, D. (2011). Circadian abnormalities in motor activity in a BAC transgenic mouse model of Huntington's disease. *PLOS Currents Huntington Disease*, *3*. https://doi.org/doi: 10.1371/currents.RRN1225.

Oakeshott, S., Port, R., Cummins-Sutphen, J., Berger, J., Watson-Johnson, J., Ramboz, S., Paterson, N., Kwak, S., Howland, D., & Brunner, D. (2012). A mixed fixed ratio/progressive ratio procedure reveals an apathy phenotype in the BAC HD and the zQ175 KI mouse models of Huntington's disease. *PLoS Currents*, *4*. https://doi.org/10.1371/4f972cffe82c0

Ondo, W. G., Mejia, N. I., & Hunter, C. B. (2007). A pilot study of the clinical efficacy and safety of memantine for Huntington's disease. *Parkinsonism and Related Disorders*, *13*, 453–454. https://doi.org/10.1016/j.parkreldis.2006.08.005

Orvoen, S., Pla, P., Gardier, A. M., Saudou, F., & David, D. J. (2012). Huntington's disease knock-in male mice show specific anxiety-like behaviour and altered neuronal maturation. *Neuroscience Letters*, *507*, 127–132. https://doi.org/10.1016/j.neulet.2011.11.063

Pacher, P., Batkai, S., & Kunos, G. (2006). The endocannabinoid system as an emerging target of pharmacotherapy. *Pharmacological Reviews*, *58*(3), 389–462. https://doi.org/10.1124/pr.58.3.2

Packard, M. G., & Knowlton, B. J. (2002). Learning and memory functions of the basal ganglia. *Annual Review of Neuroscience*, *25*(1), 563–593. https://doi.org/10.1146/annurev.neuro.25.112701.142937

Pallier, P. N., Drew, C. J. G., & Morton, A. J. (2009). The detection and measurement of locomotor deficits in a transgenic mouse model of Huntington's disease are task- and protocol-dependent: influence of non-motor factors on locomotor function. *Brain Research Bulletin*, *78*(6), 347–355. https://doi.org/10.1016/j.brainresbull.2008.10.007

Pallier, P. N., Maywood, E. S., Zheng, Z., Chesham, J. E., Inyushkin, A. N., Dyball, R., Hastings, M. H., & Morton, A. J. (2007). Pharmacological imposition of sleep slows cognitive decline and reverses dysregulation of circadian gene expression in a transgenic mouse model of Huntington's disease. *Journal of Neuroscience*, *27*(29), 7869–7878. https://doi.org/10.1523/JNEUROSCI.0649-07.2007

Pang, T. Y. C., Du, X., Zajac, M. S., Howard, M. L., & Hannan, A. J. (2009). Altered serotonin receptor expression is associated with depression-related behavior in the R6/1 transgenic mouse model of Huntington's disease. *Human Molecular Genetics*, *18*(4), 753–766. https://doi.org/10.1093/hmg/ddn385

Park, H., Popescu, A., & Poo, M. (2014). Essential role of presynaptic NMDA receptors in activity-dependent BDNF secretion and corticostriatal LTP. *Neuron*, *84*(5), 1009–1022. https://doi.org/10.1016/j.neuron.2014.10.045

Park, S. H., Kukushkin, Y., Gupta, R., Chen, T., Konagai, A., Hipp, M. S., Hayer-Hartl, M., & Hartl, F. U. (2013). PolyQ proteins interfere with nuclear degradation of cytosolic proteins by sequestering the Sis1p chaperone. *Cell*, *154*(1), 134–145. https://doi.org/10.1016/j.cell.2013.06.003

Paulsen, J. S., Langbehn, D. R., Stout, J. C., Aylward, E., Ross, C. A., Nance, M., Guttman, M., Johnson, S., Macdonald, M., Beglinger, L. J., Duff, K., Kayson, E., Biglan, K., Shoulson, I., Oakes, D., & Hayden, M. (2008). Detection of Huntington's disease decades before diagnosis: the Predict-HD study. *Journal of Neurology, Neurosurgery and Psychiatry*, *79*,

874–880. https://doi.org/10.1136/jnnp.2007.128728

Paulsen, J. S., Ready, R. E., Hamilton, J. M., Mega, M. S., & Cummings, J. L. (2001). Neuropsychiatric aspects of Huntington's disease. *Journal of Neurology, Neurosurgery and Psychiatry*, *71*, 310–314. https://doi.org/10.1136/jnnp.71.3.310

Paulsen, J. S., Smith, M. M., & Long, J. D. (2013). Cognitive decline in prodromal Huntington disease: implications for clinical trials. *Journal of Neurology, Neurosurgery and Psychiatry*, *84*, 1233–1239. https://doi.org/10.1136/jnnp-2013-305114

Pekny, S. E., Izawa, J., & Shadmehr, R. (2015). Reward-dependent modulation of movement variability. *Journal of Neuroscience*, *35*(9), 4015–4024. https://doi.org/10.1523/JNEUROSCI.3244-14.2015

Petit-Demouliere, B., Chenu, F., & Bourin, M. (2005). Forced swimming test in mice: a review of antidepressant activity. *Psychopharmacology*, *177*(3), 245–255. https://doi.org/10.1007/s00213-004-2048-7

Plotkin, J. L., Day, M., Peterson, J. D., Xie, Z., Kress, G. J., Rafalovich, I., Kondapalli, J., Gertler, T. S., Flajolet, M., Greengard, P., Stavarache, M., Kaplitt, M. G., Rosinski, J., Chan, C. S., & Surmeier, D. J. (2014). Impaired TrkB receptor signaling underlies corticostriatal dysfunction in Huntington's disease. *Neuron*, *83*(1), 178–188. https://doi.org/10.1016/j.neuron.2014.05.032

Plotkin, J. L., & Surmeier, D. J. (2015). Corticostriatal synaptic adaptations in Huntington's disease. *Current Opinion in Neurobiology*, *33*, 53–62. https://doi.org/10.1016/j.conb.2015.01.020

Poddar, R., Kawai, R., & Ölveczky, B. P. (2013). A fully automated high-throughput training system for rodents. *PLoS ONE*, *8*(12). https://doi.org/10.1371/journal.pone.0083171

Podvin, S., Reardon, H. T., Yin, K., Mosier, C., & Hook, V. (2019). Multiple clinical features of Huntington's disease correlate with mutant HTT gene CAG repeat lengths and neurodegeneration. *Journal of Neurology*, *266*(3), 551–564. https://doi.org/10.1007/s00415-018-8940-6

Poudel, G. R., Stout, J. C., Domínguez D., J. F., Churchyard, A., Chua, P., Egan, G. F., & Georgiou-Karistianis, N. (2015). Longitudinal change in white matter microstructure in Huntington's disease: the IMAGE-HD study. *Neurobiology of Disease*, *74*, 406–412. https://doi.org/10.1016/j.nbd.2014.12.009

Poudel, G. R., Stout, J. C., Domínguez D, J. F., Salmon, L., Churchyard, A., Chua, P., Georgiou-Karistianis, N., & Egan, G. F. (2014). White matter connectivity reflects clinical and cognitive status in Huntington's disease. *Neurobiology of Disease*, *65*, 180–187. https://doi.org/10.1016/j.nbd.2014.01.013

Pouladi, M. A., Graham, R. K., Karasinska, J. M., Xie, Y., Santos, R. D., Petersen, A. & Hayden, M. R. (2009). Prevention of depressive behaviour in the YAC128 mouse model of Huntington disease by mutation at residue 586 of huntingtin. *Brain, 132,* 919-932. https://doi.org/10.1093/brain/awp006

Pouladi, M. A., Morton, A. J., & Hayden, M. R. (2013). Choosing an animal model for the study of Huntington's disease. *Nature Reviews Neuroscience, 14*(10), 708–721. https://doi.org/10.1038/nrn3570

Pouladi, M. A., Stanek, L. M., Xie, Y., Franciosi, S., Southwell, A. L., Deng, Y., Butland, S., Zhang, W., Cheng, S. H., Shihabuddin, L. S., & Hayden, M. R. (2012). Marked differences in neurochemistry and aggregates despite similar behavioural and neuropathological features of Huntington disease in the full-length BACHD and YAC128 mice. *Human Molecular Genetics, 21*(10), 2219–2232. https://doi.org/10.1093/hmg/dds037

Pouladi, M. A., Xie, Y., Skotte, N. H., Ehrnhoefer, D. E., Graham, R. K., Kim, J. E., Bissada, N., Yang, X. W., Paganetti, P., Friedlander, R. M., Leavitt, B. R., & Hayden, M. R. (2010). Full-length huntingtin levels modulate body weight by influencing insulin-like growth factor 1 expression. *Human Molecular Genetics, 19*(8), 1528–1538. https://doi.org/10.1093/hmg/ddq026

Ragozzino, M. E., & Baker, P. M. (2016). Prefrontal cortex and basal ganglia attributes underlying behavioral flexibility. In P. A. Jackson, A. A. Chiba, R. F. Berman, & M. E. Ragozzino (Eds.), *The Neurobiological Basis of Memory*. Springer International Publishing. https://doi.org/10.1007/978-3-319-15759-7

Ranen, N. G., Stine, O. C., Abbott, M. H., Sherr, M., Codori, A. M., Franz, M. L., Chao, N. I., Chung, A. S., Pleasant, N., Callahan, C., Kasch, L. M., Ghaffari, M., Chase, G. A., Kazazian, H. H., Brandt, J., Folstein, S. E., & Ross, C. A. (1995). Anticipation and instability of IT-15 (CAG)N repeats in parent-offspring pairs with Huntington disease. *American Journal of Human Genetics*, *57*(3), 593–602.

Rangel-Barajas, C., & Rebec, G. V. (2018). Overview of Huntington's disease models: neuropathological, molecular, and behavioral differences. *Current Protocols in Neuroscience, 83*. https://doi.org/10.1002/cpns.47

Rattray, I., Smith, E. J., Crum, W. R., Walker, T. A., Gale, R., Bates, G. P., & Modo, M. (2017). Correlations of behavioral deficits with brain pathology assessed through longitudinal MRI and histopathology in the HdhQ150/Q150 mouse model of huntington's disease. *PLoS ONE*, *12*(1). https://doi.org/10.1371/journal.pone.0168556

Rawlins, M. D., Wexler, N. S., Wexler, A. R., Tabrizi, S. J., Douglas, I., Evans, S. J. W., & Smeeth, L. (2016). The prevalence of Huntington's disease. *Neuroepidemiology, 46*, 144–153. https://doi.org/10.1159/000443738

Raymond, L. A. (2017). Striatal synaptic dysfunction and altered calcium regulation in Huntington disease. *Biochemical and Biophysical Research Communications*, *483*(4), 1051–1062. https://doi.org/10.1016/j.bbrc.2016.07.058

Raymond, L. A., André, V. M., Cepeda, C., Gladding, C. M., Milnerwood, A. J., & Levine, M. S. (2011). Pathophysiology of Huntington's disease: time-dependent alterations in synaptic and receptor function. *Neuroscience*, *198*, 252–273. https://doi.org/10.1016/j.neuroscience.2011.08.052

Reilmann, R., Kirsten, F., Quinn, L., Henningsen, H., Marder, K., & Gordon, A. M. (2001). Objective assessment of progression in Huntington's disease: a 3-year follow-up study. *Neurology*, *57*(5), 920–924. https://doi.org/10.1212/WNL.57.5.920

Reiner, A., Albin, R. L., Anderson, K. D., D'Amato, C. J., Penney, J. B., & Young, A. B. (1988). Differential loss of striatal projection neurons in Huntington disease. *Proceedings of the National Academy of Sciences*, *85*(15), 5733–5737. https://doi.org/10.1073/pnas.85.15.5733

Reiner, A., & Deng, Y.-P. (2018). Disrupted striatal neuron inputs and outputs in Huntington's disease. *CNS Neuroscience and Therapeutics*, *24*(4), 250–280. https://doi.org/10.1111/cns.12844

Reiner, A., Shelby, E., Wang, H., Demarch, Z., Deng, Y.-P., Guley, N. H., Hogg, V., Roxburgh, R., Tippett, L. J., Waldvogel, H. J., & Faull, R. L. M. (2013). Striatal parvalbuminergic neurons are lost in Huntington's disease: implications for dystonia. *Movement Disorders*, *28*(12), 1691–1699. https://doi.org/10.1002/mds.25624

Remmelink, E., Chau, U., Smit, A. B., Verhage, M., & Loos, M. (2017). A one-week 5-choice serial reaction time task to measure impulsivity and attention in adult and adolescent mice. *Scientific Reports*, *7*(42519). https://doi.org/10.1038/srep42519

Richter, S. H. (2020). Automated home-cage testing as a tool to improve reproducibility of behavioral research? *Frontiers in Neuroscience*, *14*(383). https://doi.org/10.3389/fnins.2020.00383

Rising, A. C., Xu, J., Carlson, A., Napoli, V. V, Denovan-Wright, E. M., & Mandel, R. J. (2011). Longitudinal behavioral, cross-sectional transcriptional and histopathological characterization of a knock-in mouse model of Huntington's disease with 140 CAG repeats. *Experimental Neurology*, *228*(2), 173–182. https://doi.org/10.1016/j.expneurol.2010.12.017

Rivalan, M., Munawar, H., Fuchs, A., & Winter, Y. (2017). An automated, experimenter-free method for the standardised, operant cognitive testing of rats. *PLoS ONE*, *12*(1). https://doi.org/10.1371/journal.pone.0169476

Robinson, L., & Riedel, G. (2014). Comparison of automated home-cage monitoring systems: Emphasis on feeding behaviour, activity and spatial learning following pharmacological

interventions. *Journal of Neuroscience Methods*, *234*, 13–25. https://doi.org/10.1016/j.jneumeth.2014.06.013

Robinson, L., Spruijt, B., & Riedel, G. (2018). Between and within laboratory reliability of mouse behaviour recorded in home-cage and open-field. *Journal of Neuroscience Methods*, *300*, 10–19. https://doi.org/10.1016/j.jneumeth.2017.11.019

Rosas, H. D., Hevelone, N. D., Zaleta, A. K., Greve, D. N., Salat, D. H., & Fischl, B. (2005). Regional cortical thinning in preclinical Huntington disease and its relationship to cognition. *Neurology*, *65*(5), 745–747. https://doi.org/10.1212/01.wnl.0000174432.87383.87

Rosas, H. D., Liu, A. K., Hersch, S., Glessner, M., Ferrante, R. J., Salat, D. H., Van Der Kouwe, A., Jenkins, B. G., Dale, A. M., & Fischl, B. (2002). Regional and progressive thinning of the cortical ribbon in Huntington's disease. *Neurology*, *58*(5), 695–701. https://doi.org/10.1212/WNL.58.5.695

Rosas, H. D., Salat, D. H., Lee, S. Y., Zaleta, A. K., Pappu, V., Fischl, B., Greve, D., Hevelone, N., & Hersch, S. M. (2008). Cerebral cortex and the clinical expression of Huntington's disease: complexity and heterogeneity. *Brain*, *131*(4), 1057–1068. https://doi.org/10.1093/brain/awn025

Rosenblatt, A., Liang, K. Y., Zhou, H., Abbott, M. H., Gourley, L. M., Margolis, R. L., Brandt, J., & Ross, C. A. (2006). The association of CAG repeat length with clinical progression in Huntington disease. *Neurology*, *66*(7), 1016–1020. https://doi.org/10.1212/01.wnl.0000204230.16619.d9

Ross, C. A., & Tabrizi, S. J. (2011). Huntington's disease: from molecular pathogenesis to clinical treatment. *The Lancet Neurology*, *10*(1), 83–98. https://doi.org/10.1016/S1474-4422(10)70245-3

Rosser, A. E. (2011). Why cannot a rodent be more like a man? A clinical perspective. In E. L. Lane & S. B. Dunnett (Eds.), *Animal Models of Movement Disorders Volume I*. Humana Press.

Rudenko, O., Tkach, V., Berezin, V., & Bock, E. (2009). Detection of early behavioral markers of Huntington's disease in R6/2 mice employing an automated social home cage. *Behavioural Brain Research*, *203*(2), 188–199. https://doi.org/10.1016/j.bbr.2009.04.034

Ryabinin, A. E., Wang, Y., & Finn, D. A. (1999). Different Levels of Fos Immunoreactivity After Repeated Handling and Injection Stress in Two Inbred Strains of Mice. *Pharmacology, Biochemistry and Behavior*, *63*(1), 143–151. https://doi.org/https://doi.org/10.1016/S0091-3057(98)00239-1

Sacrey, L. A. R., Alaverdashvili, M., & Whishaw, I. Q. (2009). Similar hand shaping in

reaching-for-food (skilled reaching) in rats and humans provides evidence of homology in release, collection, and manipulation movements. *Behavioural Brain Research*, *204*(1), 153–161. https://doi.org/10.1016/j.bbr.2009.05.035

Samadi, P., Boutet, A., Rymar, V. V., Rawal, K., Maheux, J., Kvann, J. C., Tomaszewski, M., Beaubien, F., Cloutier, J. F., Levesque, D., & Sadikot, A. F. (2013). Relationship between BDNF expression in major striatal afferents, striatum morphology and motor behavior in the R6/2 mouse model of Huntington's disease. *Genes, Brain and Behavior*, *12*(1), 108–124. https://doi.org/10.1111/j.1601-183X.2012.00858.x

Santos, F. J., Oliveira, R. F., Jin, X., & Costa, R. M. (2015). Corticostriatal dynamics encode the refinement of specific behavioral variability during skill learning. *ELife*, *4*. https://doi.org/10.7554/eLife.09423

Santoso, A., Kaiser, A., & Winter, Y. (2006). Individually dosed oral drug administration to socially-living transponder-tagged mice by a water dispenser under RFID control. *Journal of Neuroscience Methods*, *153*, 208–213. https://doi.org/10.1016/j.jneumeth.2005.10.025

Sathasivam, K., Neueder, A., Gipson, T. A., Landles, C., Benjamin, A. C., Bondulich, M. K., Smith, D. L., Faull, R. L. M., Roos, R. A. C., Howland, D., Detloff, P. J., Housman, D. E., & Bates, G. P. (2013). Aberrant splicing of HTT generates the pathogenic exon 1 protein in Huntington disease. *Proceedings of the National Academy of Sciences*, *110*(6), 2366–2370. https://doi.org/10.1073/pnas.1221891110

Saudou, F., & Humbert, S. (2016). The biology of huntingtin. *Neuron*, *89*(5), 910–926. https://doi.org/10.1016/j.neuron.2016.02.003

Scannell, J. W., & Bosley, J. (2016). When quality beats quantity: decision theory, drug discovery, and the reproducibility crisis. *PLoS ONE*, *11*(2). https://doi.org/10.1371/journal.pone.0147215

Schellinck, H. M., Cyr, D. P., & Brown, R. E. (2010). How many ways can mouse behavioral experiments go wrong? Confounding variables in mouse models of neurodegenerative diseases and how to control them. In *Advances in the Study of Behavior* (Vol. 41). Academic Press. https://doi.org/10.1016/S0065-3454(10)41007-4

Schilling, G., Becher, M. W., Sharp, A. H., Jinnah, H. A., Duan, K., Kotzuk, J. A., Slunt, H. H., Ratovitski, T., Cooper, J. K., Jenkins, N. A., Copeland, N. G., Price, D. L., Ross, C. A., & Borchelt, D. R. (1999). Intranuclear inclusions and neuritic aggregates in transgenic mice expressing a mutant N-terminal fragment of huntingtin. *Human Molecular Genetics*, *8*(3), 397–407. https://doi.org/10.1093/hmg/8.3.397

Sepers, M. D., Smith-Dijak, A. I., Ledue, J., Kolodziejczyk, K., Mackie, K., & Raymond, L. A. (2018). Endocannabinoid-specific impairment in synaptic plasticity in striatum of Huntington's disease mouse model. *Journal of Neuroscience*, *38*(3), 544–554.

Shabbott, B., Ravindran, R., Schumacher, J. W., Wasserman, P. B., Marder, K. S., & Mazzoni, P. (2013). Learning fast accurate movements requires intact frontostriatal circuits. *Frontiers in Human Neuroscience, 7*(752). https://doi.org/10.3389/fnhum.2013.00752

Shan, Q., Christie, M. J., & Balleine, B. W. (2015). Plasticity in striatopallidal projection neurons mediates the acquisition of habitual actions. *European Journal of Neuroscience*, *42*(4), 2097–2104. https://doi.org/10.1111/ejn.12971

Shelbourne, P. F., Keller-McGandy, C., Bi, W. L., Yoon, S. R., Dubeau, L., Veitch, N. J., Vonsattel, J. P., Wexler, N. S., Norman, A., & Augood, S. J. (2007). Triplet repeat mutation length gains correlate with cell-type specific vulnerability in Huntington disease brain. *Human Molecular Genetics*, *16*(10), 1133–1142. https://doi.org/10.1093/hmg/ddm054

Shirasaki, D. I., Greiner, E. R., Al-Ramahi, I., Gray, M., Boontheung, P., Geschwind, D. H., Botas, J., Coppola, G., Horvath, S., Loo, J. A., & Yang, X. W. (2012). Network organization of the huntingtin proteomic interactome in mammalian brain. *Neuron*, *75*(1), 41–57. https://doi.org/10.1016/j.neuron.2012.05.024

Silasi, G., Boyd, J. D., Bolanos, F., LeDue, J. M., Scott, S. H., & Murphy, T. H. (2018). Individualized tracking of self-directed motor learning in group-housed mice performing a skilled lever positioning task in the home cage. *Journal of Neurophysiology*, *119*(1), 337–346. https://doi.org/10.1152/jn.00115.2017

Singh, S., Bermudez-Contreras, E., Nazari, M., Sutherland, R. J., & Mohajerani, M. H. (2019). Low-cost solution for rodent home-cage behaviour monitoring. *PLoS ONE*, *14*(8). https://doi.org/10.1371/journal.pone.0220751

Slow, E. J., Graham, R. K., Osmand, A. P., Devon, R. S., Lu, G., Deng, Y., Pearson, J., Vaid, K., Bissada, N., Wetzel, R., Leavitt, B. R., & Hayden, M. R. (2005). Absence of behavioral abnormalities and neurodegeneration in vivo despite widespread neuronal huntingtin inclusions. *Proceedings of the National Academy of Sciences*, *102*(32), 11402–11407. https://doi.org/10.1073/pnas.0503634102

Slow, E. J., van Raamsdonk, J., Rogers, D., Coleman, S. H., Graham, R. K., Deng, Y., Oh, R., Bissada, N., Hossain, S. M., Yang, Y. Z., Li, X. J., Simpson, E. M., Gutekunst, C. A., Leavitt, B. R., & Hayden, M. R. (2003). Selective striatal neuronal loss in a YAC128 mouse model of Huntington disease. *Human Molecular Genetics*, *12*(13), 1555–1567. https://doi.org/10.1093/hmg/ddg169

Smith-Dijak, A. I., Sepers, M. D., & Raymond, L. A. (2019). Alterations in synaptic function and plasticity in Huntington disease. *Journal of Neurochemistry*, *150*, 346–365. https://doi.org/10.1111/jnc.14723

Smith, M. A., Brandt, J., & Shadmehr, R. (2000). Motor disorder in Huntington's disease begins as a dysfunction in error feedback control. *Nature*, *403*(6769), 544–549.

https://doi.org/10.1038/35000576

Smith, M. A., & Shadmehr, R. (2005). Intact ability to learn internal models of arm dynamics in Huntington's disease but not cerebellar degeneration. *Journal of Neurophysiology*, *93*(5), 2809–2821. https://doi.org/10.1152/jn.00943.2004

Snowden, J. S., Craufurd, D., Thompson, J., & Neary, D. (2002). Psychomotor, executive, and memory function in preclinical Huntington's disease. *Journal of Clinical and Experimental Neuropsychology*, *24*(2), 133–145. https://doi.org/10.1076/jcen.24.2.133.998

Soares, T. R., Reis, S. D., Pinho, B. R., Duchen, M. R., & Oliveira, J. M. A. (2019). Targeting the proteostasis network in Huntington's disease. *Ageing Research Reviews*, *49*, 92–103. https://doi.org/10.1016/j.arr.2018.11.006

Sorge, R. E., Martin, L. J., Isbester, K. A., Sotocinal, S. G., Rosen, S., Tuttle, A. H., Wieskopf, J. S., Acland, E. L., Dokova, A., Kadoura, B., Leger, P., Mapplebeck, J. C. S., Mcphail, M., Delaney, A., Wigerblad, G., Schumann, A. P., Quinn, T., Frasnelli, J., Svensson, C. I., … Mogil, J. S. (2014). Olfactory exposure to males, including men, causes stress and related analgesia in rodents. *Nature Methods*, *11*(6), 629–632. https://doi.org/10.1038/nmeth.2935

Southwell, A. L., Ko, J., & Patterson, P. H. (2009). Intrabody gene therapy ameliorates motor, cognitive, and neuropathological symptoms in multiple mouse models of Huntington's disease. *Journal of Neuroscience*, *29*(43), 13589–13602. https://doi.org/10.1523/JNEUROSCI.4286-09.2009

Southwell, A. L., Smith-Dijak, A. I., Kay, C., Sepers, M. D., Villanueva, E. B., Parsons, M. P., Xie, Y., Anderson, L., Felczak, B., Waltl, S., Ko, S., Cheung, D., Cengio, L. D., Slama, R., Petoukhov, E., Raymond, L. A., & Hayden, M. R. (2016). An enhanced Q175 knock-in mouse model of Huntington disease with higher mutant huntingtin levels and accelerated disease phenotypes. *Human Molecular Genetics*, *25*(17), 3654–3675. https://doi.org/10.1093/hmg/ddw212

Spruijt, B. M., & DeVisser, L. (2006). Advanced behavioural screening: automated home cage ethology. *Drug Discovery Today: Technologies*, *3*(2), 231–237. https://doi.org/10.1016/j.ddtec.2006.06.010

Squitieri, F., Andrew, S. E., Goldberg, Y. P., Kremer, B., Spence, N., Zelsler, J., Nichol, K., Theilmann, J., Greenberg, J., Goto, J., Kanazawa, I., Vesa, J., Peltonen, L., Almqvist, E., Anvret, M., Telenius, H., Lin, B., Napolitano, G., Morgan, K., & Hayden, M. R. (1994). DNA haplotype analysis of huntington disease reveals clues to the origins and mechanisms of CAG expansion and reasons for geographic variations of prevalence. *Human Molecular Genetics*, *3*(12), 2103–2114. https://doi.org/10.1093/hmg/3.12.2103

Steele, A. D., Jackson, W. S., King, O. D., & Lindquist, S. (2007). The power of automated high-resolution behavior analysis revealed by its application to mouse models of Huntington's

and prion diseases. *Proceedings of the National Academy of Sciences*, *104*(6), 1983–1988. https://doi.org/10.1073/pnas.0610779104

Stout, J. C., Paulsen, J. S., Queller, S., Solomon, A. C., Whitlock, K. B., Campbell, J. C., Carlozzi, N., Duff, K., Beglinger, L. J., Langbehn, D. R., Johnson, S. A., Biglan, K. M., & Aylward, E. H. (2011). Neurocognitive signs in prodromal Huntington disease. *Neuropsychology*, *25*(1), 1–14. https://doi.org/10.1037/a0020937

Tabrizi, S. J., Scahill, R. I., Owen, G., Durr, A., Leavitt, B. R., Roos, R. A., Borowsky, B., Landwehrmeyer, B., Frost, C., Johnson, H., Craufurd, D., Reilmann, R., Stout, J. C., & Langbehn, D. R. (2013). Predictors of phenotypic progression and disease onset in premanifest and early-stage Huntington's disease in the TRACK-HD study: analysis of 36-month observational data. *The Lancet Neurology*, *12*(7), 637–649. https://doi.org/10.1016/S1474-4422(13)70088-7

Tecuapetla, F., Jin, X., Lima, S. Q., & Costa, R. M. (2016). Complementary contributions of striatal projection pathways to action initiation and execution. *Cell*, *166*(3), 703–715. https://doi.org/10.1016/j.cell.2016.06.032

Telenius, H., Kremer, B., Goldberg, Y. P., Theilmann, J., Andrew, S. E., Zeisler, J., Adam, S., Greenberg, C., Ives, E. J., Clarke, L. A., & Hayden, M. R. (1994). Somatic and gonadal mosaicism of the Huntington disease gene CAG repeat in brain and sperm. *Nature Genetics*, *6*(4), 409–414. https://doi.org/10.1038/ng0494-409

The Jackson Laboratory. (n.d.). *Body weight information for FVB/NJ (001800)*. Retrieved August 23, 2020, from https://www.jax.org/jax-mice-and-services/strain-data-sheet-pages/body-weight-chart-001800

Thu, D. C. V., Oorschot, D. E., Tippett, L. J., Nana, A. L., Hogg, V. M., Synek, B. J., Luthi-Carter, R., Waldvogel, H. J., & Faull, R. L. M. (2010). Cell loss in the motor and cingulate cortex correlates with symptomatology in Huntington's disease. *Brain*, *133*(4), 1094–1110. https://doi.org/10.1093/brain/awq047

Tippett, L. J., Waldvogel, H. J., Thomas, S. J., Hogg, V. M., Roon-Mom, W. Van, Synek, B. J., Graybiel, A. M., & Faull, R. L. M. (2007). Striosomes and mood dysfunction in Huntington's disease. *Brain*, *130*(1), 206–221. https://doi.org/10.1093/brain/awl243

Todorov, E., & Jordan, M. I. (2002). Optimal feedback control as a theory of motor coordination. *Nature Neuroscience*, *5*(11), 1226–1235. https://doi.org/10.1038/nn963

Trottier, Y., Devys, D., Imbert, G., Saudou, F., An, I., Lutz, Y., Weber, C., Agid, Y., Hirsch, E. C., & Mandel, J. L. (1995). Cellular localization of the Huntington's disease protein and discrimination of the normal and mutated form. *Nature Genetics*, *10*(1), 104–110. https://doi.org/10.1038/ng0595-104

Trueman, R. C., Brooks, S. P., Jones, L., & Dunnett, S. B. (2007). The operant serial implicit learning task reveals early onset motor learning deficits in the HdhQ92 knock-in mouse model of Huntington's disease. *European Journal of Neuroscience*, *25*(2), 551–558. https://doi.org/10.1111/j.1460-9568.2007.05307.x

Trueman, R. C., Brooks, S. P., Jones, L., & Dunnett, S. B. (2008). Time course of choice reaction time deficits in the HdhQ92 knock-in mouse model of Huntington's disease in the operant Serial Implicit Learning Task (SILT). *Behavioural Brain Research*, *189*(2), 317–324. https://doi.org/10.1016/j.bbr.2008.01.020

Trushina, E., Dyer, R. B., Badger II, J. D., Ure, D., Eide, L., Tran, D. D., Vrieze, B. T., Legendre-Guillemin, V., McPherson, P. S., Mandavilli, B. S., Van Houten, B., Zeitlin, S., McNiven, M., Aebersold, R., Hayden, M. R., Parisi, J. E., Seeberg, E., Dragatsis, I., Doyle, K., … McMurray, C. T. (2004). Mutant huntingtin impairs axonal trafficking in mammalian neurons in vivo and in vitro. *Molecular and Cellular Biology*, *24*(18), 8195–8209. https://doi.org/10.1128/MCB.24.18.8195

Tucci, V., Hardy, A., & Nolan, P. M. (2006). A comparison of physiological and behavioural parameters in C57BL/6J mice undergoing food or water restriction regimes. *Behavioural Brain Research*, *173*(1), 22–29. https://doi.org/10.1016/j.bbr.2006.05.031

Turner, P. V, Brabb, T., Pekow, C., & Vasbinder, M. A. (2011). Administration of substances to laboratory animals: routes of administration and factors to consider. *Journal of the American Association for Laboratory Animal Science*, *50*(5), 600–613.

Urai, A. E., Aguillon-Rodriguez, V., Laranjeira, I. C., Cazettes, F., Laboratory, T. I. B., Mainen, Z. F., & Churchland, A. K. (2020). Citric acid water as an alternative to water restriction for high-yield mouse behavior. *BioRxiv*. https://doi.org/https://doi.org/10.1101/2020.03.02.973016

Van De Weerd, H. A., Bulthuis, R. J. A., Bergman, A. F., Schlingmann, F., Tolboom, J., Van Loo, P. L. P., Remie, R., Baumans, V., & Van Zutphen, L. F. M. (2001). Validation of a new system for the automatic registration of behaviour in mice and rats. *Behavioural Processes*, *53*(1–2), 11–20. https://doi.org/10.1016/S0376-6357(00)00135-2

van Dellen, A., Cordery, P. M., Spires, T. L., Blakemore, C., & Hannan, A. J. (2008). Wheel running from a juvenile age delays onset of specific motor deficits but does not alter protein aggregate density in a mouse model of Huntington's disease. *BMC Neuroscience*, *9*(34). https://doi.org/10.1186/1471-2202-9-34

van der Burg, J. M. M., Bacos, K., Wood, N. I., Lindqvist, A., Wierup, N., Woodman, B., Wamsteeker, J. I., Smith, R., Deierborg, T., Kuhar, M. J., Bates, G. P., Mulder, H., Erlanson-Albertsson, C., Morton, A. J., Brundin, P., Petersén, Å., & Björkqvist, M. (2008). Increased metabolism in the R6/2 mouse model of Huntington's disease. *Neurobiology of Disease*, *29*(1), 41–51. https://doi.org/10.1016/j.nbd.2007.07.029

Van Duijn, E., Craufurd, D., Hubers, A. A. M., Giltay, E. J., Bonelli, R., Rickards, H., Anderson, K. E., Van Walsem, M. R., Van Der Mast, R. C., Orth, M., & Landwehrmeyer, G. B. (2014). Neuropsychiatric symptoms in a European Huntington's disease cohort (REGISTRY). *Journal of Neurology, Neurosurgery and Psychiatry*, *85*(12), 1411–1418. https://doi.org/10.1136/jnnp-2013-307343

Van Mastrigt, N. M., Smeets, J. B. J., & Van Der Kooij, K. (2020). Quantifying exploration in reward-based motor learning. *PLoS ONE*, *15*(4). https://doi.org/10.1371/journal.pone.0226789

Van Raamsdonk, J. M., Gibson, W. T., Pearson, J., Murphy, Z., Lu, G., Leavitt, B. R., & Hayden, M. R. (2006). Body weight is modulated by levels of full-length huntingtin. *Human Molecular Genetics*, *15*(9), 1513–1523. https://doi.org/10.1093/hmg/ddl072

Van Raamsdonk, J. M., Metzler, M., Slow, E., Pearson, J., Schwab, C., Carroll, J., Graham, R. K., Leavitt, B. R., & Hayden, M. R. (2007). Phenotypic abnormalities in the YAC128 mouse model of Huntington disease are penetrant on multiple genetic backgrounds and modulated by strain. *Neurobiology of Disease*, *26*(1), 189–200. https://doi.org/10.1016/j.nbd.2006.12.010

Van Raamsdonk, J. M., Pearson, J., Murphy, Z., Hayden, M. R., & Leavitt, B. R. (2006). Wild-type huntingtin ameliorates striatal neuronal atrophy but does not prevent other abnormalities in the YAC128 mouse model of Huntington disease. *BMC Neuroscience*, *7*(80). https://doi.org/10.1186/1471-2202-7-80

Van Raamsdonk, J. M., Pearson, J., Slow, E. J., Hossain, S. M., Leavitt, B. R., & Hayden, M. R. (2005). Cognitive dysfunction precedes neuropathology and motor abnormalities in the YAC128 mouse model of Huntington's disease. *Journal of Neuroscience*, *25*(16), 4169–4180. https://doi.org/10.1523/JNEUROSCI.0590-05.2005

Vetere, G., Kenney, J. W., Tran, L. M., Parkinson, J., Josselyn, S. A., Frankland, P. W., Vetere, G., Kenney, J. W., Tran, L. M., Xia, F., Steadman, P. E., & Parkinson, J. (2017). Chemogenetic interrogation of a brain-wide fear memory network in mice. *Neuron*, *94*(2), 363–374. https://doi.org/10.1016/j.neuron.2017.03.037

Vinkers, C. H., Jong, N. M. De, Kalkman, C. J., Westphal, K. G. C., Oorschot, R. Van, Olivier, B., Korte, S. M., & Groenink, L. (2009). Stress-induced hyperthermia is reduced by rapid-acting anxiolytic drugs independent of injection stress in rats. *Pharmacology, Biochemistry and Behavior*, *93*(4), 413–418. https://doi.org/10.1016/j.pbb.2009.05.017

Vonsattel, J. P., Myers, R. H., Stevens, T. J., Ferrante, R. J., Bird, E. D., & Richardson, E. P. (1985). Neuropathological classification of Huntington's disease. *Journal of Neuropathology and Experimental Neurology*, *44*(6), 559–577. https://doi.org/10.1097/00005072-198511000-00003

Waldvogel, H. J., Kim, E. H., Thu, D. C. V, Tippett, L. J., & Faull, R. L. M. (2012). New perspectives on the neuropathology in Huntington's disease in the human brain and its relation to symptom variation. *Journal of Huntington's Disease*, *1*(2), 143–153. https://doi.org/10.3233/JHD-2012-120018

Walker, F. O. (2007). Huntington's disease. *Lancet*, *369*(9557), 218–228. https://doi.org/10.1016/S0140-6736(07)60111-1

Walker, M. K., Boberg, J. R., Walsh, M. T., Wolf, V., Trujillo, A., Skelton, M., Palme, R., & Felton, L. A. (2012). A less stressful alternative to oral gavage for pharmacological and toxicological studies in mice. *Toxicology and Applied Pharmacology*, *260*(1), 65–69. https://doi.org/10.1016/j.taap.2012.01.025

Walsh, R. N., & Cummins, R. A. (1976). The open-field test: a critical review. *Psychological Bulletin*, *83*(3), 482–504. https://doi.org/10.1037/0033-2909.83.3.482

Wang, G., Liu, X., Gaertig, M. A., Li, S., & Li, X. J. (2016). Ablation of huntingtin in adult neurons is nondeleterious but its depletion in young mice causes acute pancreatitis. *Proceedings of the National Academy of Sciences*, *113*(12), 3359–3364. https://doi.org/10.1073/pnas.1524575113

Weissbrod, A., Shapiro, A., Vasserman, G., Edry, L., Dayan, M., Yitzhaky, A., Hertzberg, L., Feinerman, O., & Kimchi, T. (2013). Automated long-term tracking and social behavioural phenotyping of animal colonies within a semi-natural environment. *Nature Communications*, *4*. https://doi.org/10.1038/ncomms3018

Wellington, C. L., Singaraja, R., Ellerby, L., Savill, J., Roy, S., Leavitt, B., Cattaneo, E., Hackam, A., Sharp, A., Thornberry, N., Nicholson, D. W., Bredesen, D. E., & Hayden, M. R. (2000). Inhibiting caspase cleavage of huntingtin reduces toxicity and aggregate formation in neuronal and nonneuronal cells. *Journal of Biological Chemistry*, *275*(26), 19831–19838. https://doi.org/10.1074/jbc.M001475200

Wexler, N. S. (2004). Venezuelan kindreds reveal that genetic and enviromental factors modulate Huntington's disease age of onset. *Proceedings of the National Academy of Sciences*, *101*(10), 3498–3503.

Wheeler, V. C., Auerbach, W., White, J. K., Srinidhi, J., Auerbach, A., Ryan, A., Duyao, M. P., Vrbanac, V., Weaver, M., Gusella, J. F., Joyner, A. L., & MacDonald, M. E. (1999). Length-dependent gametic CAG repeat instability in the Huntington's disease knock-in mouse. *Human Molecular Genetics*, *8*(1), 115–122. https://doi.org/10.1093/hmg/8.1.115

Wheeler, V. C., Persichetti, F., McNeil, S. M., Mysore, J. S., Mysore, S. S., MacDonald, M. E., Myers, R. H., Gusella, J. F., & Wexler, N. S. (2007). Factors associated with HD CAG repeat instability in Huntington disease. *Journal of Medical Genetics*, *44*(11), 695–701. https://doi.org/10.1136/jmg.2007.050930

Whishaw, I. . Q., Zeeb, F., Erickson, C., & Mcdonald, R. J. (2007). Neurotoxic lesions of the caudate-putamen on a reaching for food task in the rat: acute senorimotor neglect and chronic qualitative motor impairment follow lateral lesions and improved success follows medial lesions. *Neuroscience*, *146*, 86–97. https://doi.org/10.1016/j.neuroscience.2007.01.034

White, S. R., Amarante, L. M., Kravitz, A. V, & Laubach, M. (2019). The future is open: open-source tools for behavioral neuroscience research. *ENeuro*, *6*(4). https://doi.org/https://doi.org/10.1523/ENEURO.0223-19.2019 1

Wijnen, B., Hunt, E. J., Anzalone, G. C., & Pearce, J. M. (2014). Open-source syringe pump library. *PLoS ONE*, *9*(9). https://doi.org/10.1371/journal.pone.0107216

Willingham, D. B., & Koroshetz, W. J. (1993). Evidence for dissociable motor skills in Huntington's disease patients. *Psychobiology*, *21*(3), 173–182. https://doi.org/https://doi.org/10.3758/BF03327132

Wood, N. I., Goodman, A. O. G., van der Burg, J. M. M., Gazeau, V., Brundin, P., Björkqvist, M., Petersén, Å., Tabrizi, S. J., Barker, R. A., & Morton, A. J. (2008). Increased thirst and drinking in Huntington's disease and the R6/2 mouse. *Brain Research Bulletin*, *76*(1–2), 70–79. https://doi.org/10.1016/j.brainresbull.2007.12.007

Woodman, B., Butler, R., Landles, C., Lupton, M. K., Tse, J., Hockly, E., Moffitt, H., Sathasivam, K., & Bates, G. P. (2007). The Hdh Q150/Q150 knock-in mouse model of HD and the R6/2 exon 1 model develop comparable and widespread molecular phenotypes. *Brain Research Bulletin*, *72*, 83–97. https://doi.org/10.1016/j.brainresbull.2006.11.004

Wright, G. E. B., Collins, J. A., Kay, C., McDonald, C., Dolzhenko, E., Xia, Q., Bečanović, K., Drögemöller, B. I., Semaka, A., Nguyen, C. M., Trost, B., Richards, F., Bijlsma, E. K., Squitieri, F., Ross, C. J. D., Scherer, S. W., Eberle, M. A., Yuen, R. K. C., & Hayden, M. R. (2019). Length of uninterrupted CAG, independent of polyglutamine size, results in increased somatic instability, hastening onset of Huntington disease. *American Journal of Human Genetics*, *104*(6), 1116–1126. https://doi.org/10.1016/j.ajhg.2019.04.007

Yamanaka, T., Miyazaki, H., Oyama, F., Kurosawa, M., Washizu, C., Doi, H., & Nukina, N. (2008). Mutant Huntingtin reduces HSP70 expression through the sequestration of NF-Y transcription factor. *EMBO Journal*, *27*(6), 827–839. https://doi.org/10.1038/emboj.2008.23

Yhnell, E., Dunnett, S. B., & Brooks, S. P. (2016a). A longitudinal operant assessment of cognitive and behavioural changes in the HdhQ111 mouse model of huntington's disease. *PLoS ONE*, *11*(10), 1–19. https://doi.org/10.1371/journal.pone.0164072

Yhnell, E., Dunnett, S. B., & Brooks, S. P. (2016b). The utilisation of operant delayed matching and non-matching to position for probing cognitive flexibility and working memory in mouse models of Huntington's disease. *Journal of Neuroscience Methods*, *265*, 72–80.

https://doi.org/10.1016/j.jneumeth.2015.08.022

Yin, H. H., Mulcare, S. P., Hilário, M. R. F., Clouse, E., Holloway, T., Davis, M. I., Hansson, A. C., Lovinger, D. M., & Costa, R. M. (2009). Dynamic reorganization of striatal circuits during the acquisition and consolidation of a skill. *Nature Neuroscience*, *12*(3), 333–341. https://doi.org/10.1038/nn.2261

Yu, A., Shibata, Y., Shah, B., Calamini, B., Lo, D. C., & Morimoto, R. I. (2014). Protein aggregation can inhibit clathrin-mediated endocytosis by chaperone competition. *Proceedings of the National Academy of Sciences*, *111*(15). https://doi.org/10.1073/pnas.1321811111

Zarringhalam, K., Ka, M., Kook, Y. H., Terranova, J. I., Suh, Y., King, O. D., & Um, M. (2012). An open system for automatic home-cage behavioral analysis and its application to male and female mouse models of Huntington's disease. *Behavioural Brain Research*, *229*(1), 216–225. https://doi.org/10.1016/j.bbr.2012.01.015

Zuccato, C., Ciammola, A., Rigamonti, D., Leavitt, B. R., Goffredo, D., Conti, L., MacDonald, M. E., Friedlander, R. M., Silani, V., Hayden, M. R., Timmusk, T., Sipione, S., & Cattaneo, E. (2001). Loss of huntingtin-mediated BDNF gene transcription in Huntington's disease. *Science*, *293*(5529), 493–498. https://doi.org/10.1126/science.1059581

Zuccato, C., Tartari, M., Crotti, A., Goffredo, D., Valenza, M., Conti, L., Cataudella, T., Leavitt, B. R., Hayden, M. R., Timmusk, T., Rigamonti, D., & Cattaneo, E. (2003). Huntingtin interacts with REST/NRSF to modulate the transcription of NRSE-controlled neuronal genes. *Nature Genetics*, *35*(1), 76–83. https://doi.org/10.1038/ng1219